Electrochemical Society

HELP

... on any customer's operating problem has top priority on the schedule of our technical service personnel. Your call triggers action—focuses attention on the answers you seek. For fast, effective, superior technical assistance, you can rely on GLC every time.

ELECTRODE GLC DIVISION

GREAT LAKES CARBON CORPORATION

18 EAST 48TH STREET, NEW YORK 17, N. Y. OFFICES IN PRINCIPAL CITIES

EDITORIAL STAFF

H. H. Uhlig, Chairman, Publication Committee

Cecil V. King, Editor

Norman Hackerman, Technical Editor

Ruth G. Sterns, Managing Editor

U. B. Thomas, News Editor

H. W. Salzberg, Book Review Editor

Natalie Michalski, Assistant Editor

DIVISIONAL EDITORS

W. C. Vosburgh, Battery

Milton Stern, Corrosion, I

R. T. Foley, Corrosion, II

T. D. Callinan, Electric Insulation

Seymour Senderoff, Electrodeposition

H. C. Froelich, Electronics

Ernest Paskell, Electronics—Semiconductors

Sherlock Swann, Jr., Electro-Organic, I

Stanley Wawzonek, Electro-Organic, II

John M. Blocher, Jr., Electrothermics and Metallurgy, I

A. U. Seybolt, Electrothermics and Metallurgy, II

N. J. Johnson, Industrial Electrolytic

C. W. Tobias, Theoretical Electrochemistry, I

A. J. deBethune, Theoretical Electrochemistry, II

ADVERTISING OFFICE

ECS
1860 Broadway, New York 23, N. Y.

ECS OFFICERS

W. C. Gardiner, President
Olin Mathieson Chemical Corp., Niagara Falls, N. Y.

R. A. Schaefer, Vice-President
The Bunting Brass and Bronze Co., Toledo, Ohio

Henry B. Linford, Vice-President
Columbia University, New York, N. Y.

F. L. LaQue, Vice-President
International Nickel Co., Inc., New York, N. Y.

Lyle I. Gilbertson, Treasurer
Air Reduction Co., Murray Hill, N. J.

I. E. Campbell, Secretary
National Steel Corp., Weirton, W. Va.

Robert K. Shannon, Executive Secretary
National Headquarters, The ECS, 1860 Broadway, New York 23, N. Y.

Manuscripts submitted to the Journal should be sent, in triplicate, to the Editorial Office at 1860 Broadway, New York 23, N. Y. They should conform to the Instructions to Authors, last published in the August 1959 issue, pp. 232C-233C. Manuscripts so submitted become the property of The Electrochemical Society and may not be published elsewhere, in whole or in part, unless permission is requested and granted by the Editor.

Journal of the Electrochemical Society

SEPTEMBER 1959 **VOL. 106 • NO. 9**

CONTENTS

Editorial

National Goals 238C

Technical Papers

Titanium and Zirconium as Primary Cell Anodes. *M. A. Thompson, A. B. Scott, D. Chittick, and P. M. Gruzensky* 737

Investigation of the Electrochemical Characteristics of Organic Compounds, IV. Quinone Compounds. *R. Glicksman and C. K. Morehouse* 741

The Cathodic Reduction of Manganese Dioxide in Alkaline Electrolyte. *N. C. Cahoon and M. P. Korver* 745

High-Temperature Reaction Rates of Several Metals with Hydrogen Chloride and Water Vapor. *M. Farber* 751

The Electrochemical Behavior and Passivity of Titanium. *M. Stern and H. Wissenberg* 755

The Influence of Noble Metal Alloy Additions on the Electrochemical and Corrosion Behavior of Titanium. *M. Stern and H. Wissenberg* 759

High-Temperature Sulfiding of Iron Alloys in Hydrogen Sulfide-Hydrogen Mixtures. *E. W. Haycock* 764

Transitions from Parabolic to Linear Kinetics in Scaling of Metals. *E. W. Haycock* 771

The Effect of Halides on the Capacity and Resistance of the Magnesium Electrode in Aqueous Solutions. *G. R. Hoey and M. Cohen* 776

Use of Nickel-Aluminum Alloy Coatings for the Protection of Molybdenum from Oxidation. *W. Beck* 783

Electroplating Metal Contacts on Germanium and Silicon. *D. R. Turner* 786

On the Research and Development of Electron Emitting Substances for Gas Discharges. *D. M. Speros* 791

The Calcium Silicate Mn + Pb Phosphor Phase Relationships and Preparation. *D. E. Harrison and M. V. Hoffman* 800

The Dielectric Behavior of Solids Embedded in a Homogeneous Medium. *B. R. Eichbaum* 804

Growth of Whiskers by Reduction of Halogenides. *H. Wiedersich* 810

Electrolytic Production of Boron. *G. T. Miller* 815

Overvoltage and Catalysis. *P. Rüetschi* 819

On the Conductivity of Dispersions. *R. E. De La Rue and C. W. Tobias* 827

Effect of Gas Evolution on Current Distribution and Ohmic Resistance in Electrolyzers. *C. W. Tobias* 833

Technical Note

Preparation and Properties of ZnS-Type Crystals from the Melt. *A. G. Fischer* 838

Technical Review

The Manganese Dioxide Electrode. *W. C. Vosburgh* 839

Brief Communication

Investigations on the Silver-Zinc Alkaline Storage Battery by the Aid of Radioactive Isotopes. *T. Z. Palágyi* 846

Current Affairs 244C-259C

Published monthly by The Electrochemical Society, Inc., from Manchester, N. H., **Executive Offices, Editorial Office** and **Circulation Dept.,** and **Advertising Office** at 1860 Broadway, New York 23, N. Y., combining the JOURNAL and TRANSACTIONS OF THE ELECTROCHEMICAL SOCIETY. Statements and opinions given in articles and papers in the JOURNAL OF THE ELECTROCHEMICAL SOCIETY are those of the contributors, and The Electrochemical Society assumes no responsibility for them. Nondeductible subscription to members $5.00; subscription to nonmembers $18.00. Single copies $1.25 to members, $1.75 to nonmembers.

Copyright 1959 by The Electrochemical Society, Inc.

Entered as second-class matter at the Post Office at Manchester, N. H., under the act of August 24, 1912.

KEITHLEY MODEL 150 MICRO VOLT-AMMETER

MEASURES DOWN TO 0.03 μv AND 2 x 10⁻¹² AMPERE

The Keithley 150 sets new standards in sensitivity, stability and noise figure for dc microvoltmeters. It also serves as an amplifier, null detector, micro-microammeter, and (with an external voltage supply) meg-megohmmeter. Functions and measurement spans include:

DC Voltmeter, 1 microvolt to 1 volt full scale
Ammeter, 10^{-10} to 10^{-3} ampere full scale
DC Amplifier, gains of 10 to 10,000,000
Null Detector, with 0.5 to 2 second period.

OTHER FEATURES of the 150 include zero suppression of up to 100 times full scale; optional floating or grounded input; high input resistance; zero stability as a voltmeter within ±0.1 microvolt per day, and within $\pm 2 \times 10^{-11}$ ampere per day as an ammeter; short term noise within 0.03 microvolt peak to peak (0.006 microvolt RMS). The 150 is rugged, relatively insensitive to vibration, 60-cycle fields, or thermal EMF's. It is available in either rack or cabinet packaging.

USES of the 150 encompass nearly every branch of research and engineering. Examples include measuring the outputs from strain gages, thermopiles, thermocouples, bolometers, phototubes, ionization chambers, scintillation counters, and barrier layer cells. Other applications are found in cell studies, electrochemical potentials, corrosion work, molecular-weight analysis, Hall effect studies.

DETAILED DATA about the 150 Micro Voltammeter are now available in Keithley Engineering Notes, Vol. 7 No 1. A request will bring your copy promptly.

BRIEF SPECIFICATIONS

dc voltage: 13 ranges in 1X and 3X steps from ±1 microvolt to ±1 volt full scale.

current: 17 ranges in 1X and 3X steps from $\pm 10^{-10}$ to $\pm 10^{-3}$ ampere full scale.

zero stability: within 0.1 microvolt per day, or 2×10^{-11} ampere per day.

noise: less than 0.006 microvolt RMS as a voltmeter; less than 2×10^{-12} ampere as an ammeter.

accuracy: voltage, ±2% of full scale on all ranges; current, ±3% on all ranges.

zero suppression: up to 100 times full scale.

response speed: 0.5 to 2 seconds.

gain: 10,000,000 maximum.

output: ±10 v and 5 ma for full scale deflections

price: $675.00

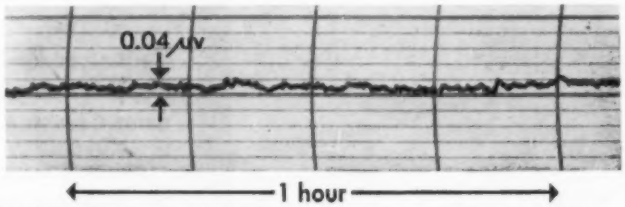

Long-term drift of the Model 150 is shown in the above recording. A 1000-ohm resistance was connected across the input. Note the very low peak to peak noise, even at this slow paper speed.

KEITHLEY INSTRUMENTS, INC.
12415 EUCLID AVENUE CLEVELAND 6, OHIO

Electronics progress through chemistry and metallurgy

New look in Crystals...

Sylvania develops a new optical instrument for easy, accurate alignment of single-crystal germanium and silicon

Semiconductor manufacturers and research laboratories can now orient monocrystalline germanium and silicon quickly and easily without the use of X ray, microscope or other methods requiring skilled operators or extensive processing.

Sylvania has developed a versatile new Crystal Orientation Instrument that is especially adaptable to the preparation of germanium and silicon single-crystal slabs for dicing, to seed crystal preparation, and many other uses. The device reveals the symmetry and orientation of a crystal through the light pattern it reflects from the facets in the etched surface of the crystal.

Here are some of the advantages of the Sylvania Crystal Orientation Instrument:

SPEED—Cutting, preparation, etching and evaluation of a crystal in as little as 15 minutes.

SIMPLICITY—Clean design allows easy operation by unskilled personnel.

ACCURACY—to $\pm$ 12 minutes of arc.

ECONOMY—Lower initial and operational costs than X ray and other techniques.

SAFETY—Non-hazardous operation—no radiation risk.

VERSATILITY—Can be used on any monocrystalline material in which etch pits can be produced.

FLEXIBILITY—Top mount can be rotated or removed. It can be set up on duplicate base units in other locations.

The Sylvania Crystal Orientation Instrument is available as a complete assembly or in individual parts. For complete particulars on this newest aid to the semiconductor industry from the Chemical & Metallurgical Division, contact your Sylvania representative or write the division directly in Towanda, Pa.

SYLVANIA

Subsidiary of
GENERAL TELEPHONE & ELECTRONICS

Sylvania Electric Products Inc.
Chemical & Metallurgical Div.
Towanda, Penna.

Editorial

National Goals

IN his State of the Union Message last winter, President Eisenhower declared that the country needed national goals, which should extend for five or even ten years in the future. A national magazine (*This Week*) published an article in which readers were asked to "Help the President" by voting on a list of goals which the nation should strive for. The response was prompt and enthusiastic, with replies from some 45,000 readers. The results have been tabulated and sent in bound form to the White House as "A Report to the President."

The ten goals which received the most votes are as follows: 1. Control inflation, 2. Raise human standards, 3. Reduce crime and labor racketeering, 4. Improve international relations, 5. Reduce taxes, 6. Provide stronger national defense, 7. Improve interfaith and interracial relations, 8. Provide college education for all gifted students, 9. Stabilize population, 10. Conserve natural resources.

This is, indeed, a worthy list of goals to study and to work toward, and it is especially gratifying to know that a great many people are concerned with national plans for the future and are not content with a policy of improvising from day to day. To be sure, most of the goals should receive life-time as well as immediate attention; and some of them are probably not mutually compatible at present. Is it possible to control inflation, reduce taxes, and provide stronger national defense? Many people seem to feel that "control inflation" is synonymous with "reduce government spending." In the early summer, there was a widespread campaign urging every voter to write to his congressmen, asking them to vote for only the necessary amount of spending. This is praiseworthy and important; high taxes are endurable only if they are necessary and if they are used wisely. But, to balance the budget is not enough. The experts say that the way to control inflation is to start paying off the national debt, and that the way to do this is to *raise* taxes. Not a popular program at all; but actually the "austerity" necessary to put our Treasury in a much sounder position would be mild compared to what we have seen in other countries.

The President is well aware of the dangers of drifting. During the past year, he set up a Committee on National Goals, called on government leaders to study the problems of inflation, called on Congress to allow the interest rate on long-term Treasury bonds to rise, vetoed inflationary bills, asked Congress not to undertake new spending without providing new funds. Certainly very strong leadership is needed at the present time, and the widest publicity should be given to every action of Congress and of the Administration. A well-informed public will insist on sound government action, and nothing can be of more help in striving toward the important humanitarian goals than a healthy economy.

—CVK

Edwin Felch, project director in charge of developing the Titan guidance system, holds the "voice" of the ICBM.

VOICE OF A GUIDED MISSILE

This is a missile-borne transmitter. It is the "voice" of a missile in flight . . . part of a new radio-inertial guidance system developed by Bell Telephone Laboratories for the Ballistic Missile Division of the Air Force.

This versatile system helped deliver the nose cone of a Thor-Able test missile precisely to its South Atlantic target area—5000 miles from Cape Canaveral, Florida. So accurately was the nose cone placed that a waiting group of ships and planes retrieved it in a matter of hours. It was the first nose cone ever to be recovered after so long a flight.

The command guidance system which made such accuracy possible combines precision tracking radar with a special Remington Rand Univac computer. Fed a steady stream of signals from the missile-borne transmitter, the ground-based equipment compares the missile's flight path with the preselected path. Corrective steering orders are computed and transmitted automatically to the missile. The ground station monitors the progress of the flight continuously and obtains immediate evaluation of mission success. And since the principal control equipment is kept on the ground, expendable hardware in the missile itself is minimized.

This radio-inertial guidance system is a product of the Bell Laboratories-Western Electric development-production team. It is in production at Western Electric for the first operational squadrons of the Titan intercontinental ballistic missile.

Bell Labs scientists and engineers developed the world's most versatile telephone network and much of our nation's radar. They have constantly pioneered in missile systems. From their storehouse of knowledge and experience comes this new achievement in missile guidance.

BELL TELEPHONE LABORATORIES

World center of communications research and development

FUTURE MEETINGS OF
The Electrochemical Society

Columbus, Ohio, October 18, 19, 20, 21, and 22, 1959

Headquarters at the Deshler Hilton Hotel

Sessions will be scheduled on

Batteries, Corrosion (including a joint Corrosion–Electronics-Semiconductors session), Electrodeposition (including symposia on "Electrodeposition from Organic Solvents" and "Electro- and Chemical-Polishing"), Electronics (Semiconductors), Electro-Organics, and Electrothermics and Metallurgy

★ ★ ★

Chicago, Ill., May 1, 2, 3, 4, and 5, 1960

Headquarters at the Lasalle Hotel

Sessions probably will be scheduled on

Electric Insulation (including a symposium on "Electrolytic Capacitors"), Electronics (including Luminescence and Semiconductors), Electrothermics and Metallurgy (including a symposium on "High-Purity Vanadium" and a round table on "Methods of Reducing Iron Ores"), Industrial Electrolytics, and Theoretical Electrochemistry

★ ★ ★

Houston, Texas, October 9, 10, 11, 12, and 13, 1960

Headquarters at the Shamrock Hotel

★ ★ ★

Indianapolis, Ind., April 30, May 1, 2, 3, and 4, 1961

Headquarters at the Claypool Hotel

★ ★ ★

Detroit, Mich., October 1, 2, 3, 4, and 5, 1961

Headquarters at the Statler Hotel

Papers are now being solicited for the meeting to be held in Chicago, Ill., May 1-5, 1960. Triplicate copies of each abstract (*not exceeding 75 words in length*) are due at Society Headquarters, 1860 Broadway, New York 23, N. Y., *not later than January 4, 1960* in order to be included in the program. *Please indicate on abstract for which Division's symposium the paper is to be scheduled, and underline the name of the author who will present the paper.* Complete manuscripts should be sent in triplicate to the Managing Editor of the JOURNAL at 1860 Broadway, New York 23, N.Y.

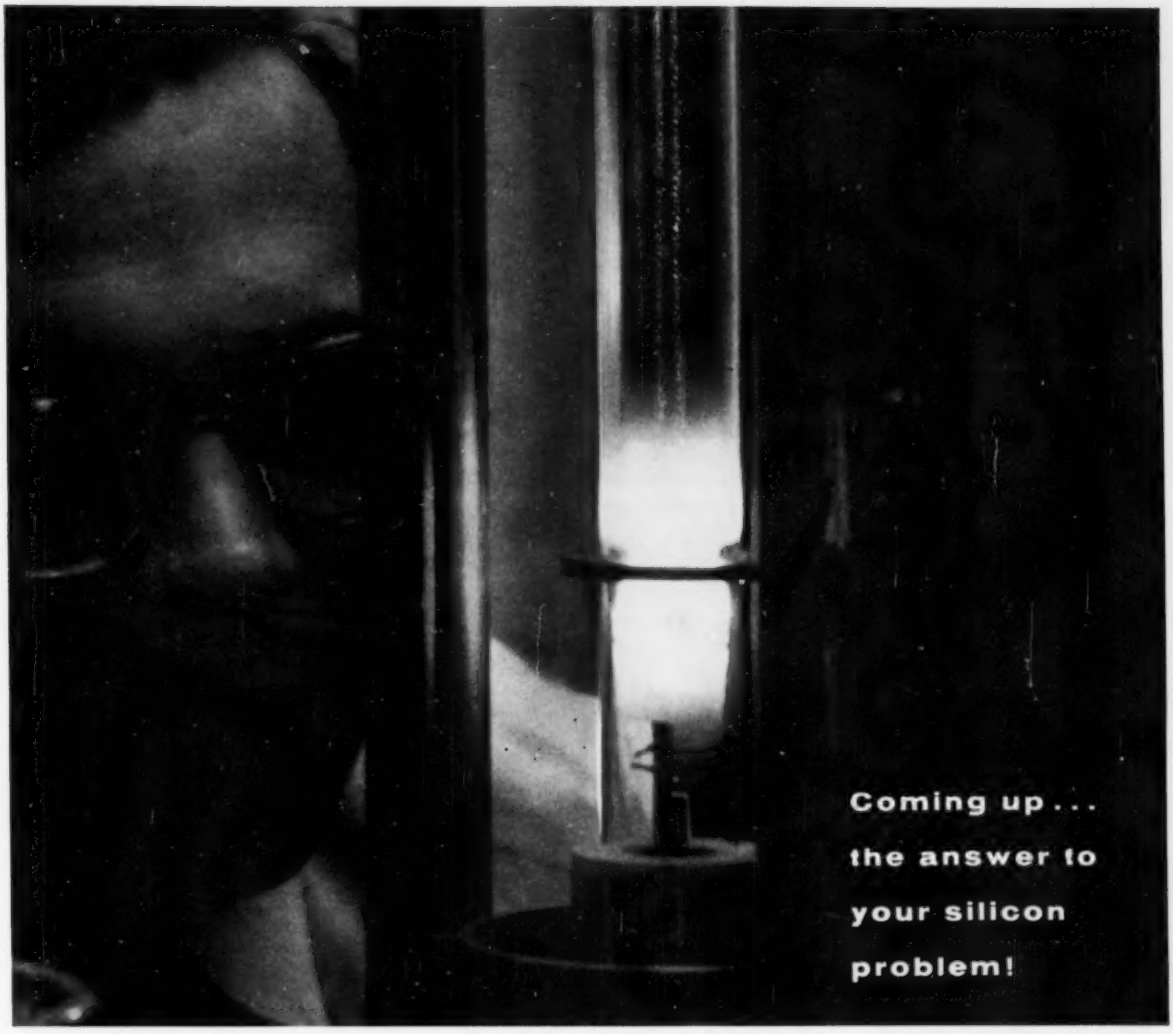

Du Pont . . . manufacturer of Hyperpure Silicon offers the services of technical specialists

When you specify Du Pont HYPERPURE Silicon, you get a product of highest dependability as well as expert technical assistance, when needed. Experienced Du Pont Technical Specialists will gladly discuss techniques of crystal growing and materials processing with you. What's more, you can take advantage of Du Pont's new $3,000,000 Technical-Service Laboratory designed for researching customer problems.

Floating zone single crystals of Du Pont HYPERPURE Silicon are available in a wide range of resistivities. Du Pont HYPERPURE Silicon is also supplied in densified cut rods . . . and rods suitable for float zone refining. They're offered in several grades with carefully controlled purity levels.

Here's more news: Du Pont's new Brevard, N. C., plant has a capacity of 70,000 lbs. of HYPERPURE Silicon per year. That means you're assured of a prompt supply of high-purity silicon in the form you need. For more information, write Du Pont . . . pioneer producer of semiconductor-grade silicon.

Free booklet is available upon request. It describes the manufacture, properties and uses of HYPERPURE Silicon. E. I. du Pont de Nemours & Co. (Inc.), Pigments Dept., Silicon Development Group, Wilmington 98, Delaware.

HYPERPURE SILICON

DU PONT

BETTER THINGS FOR BETTER LIVING
. . . THROUGH CHEMISTRY

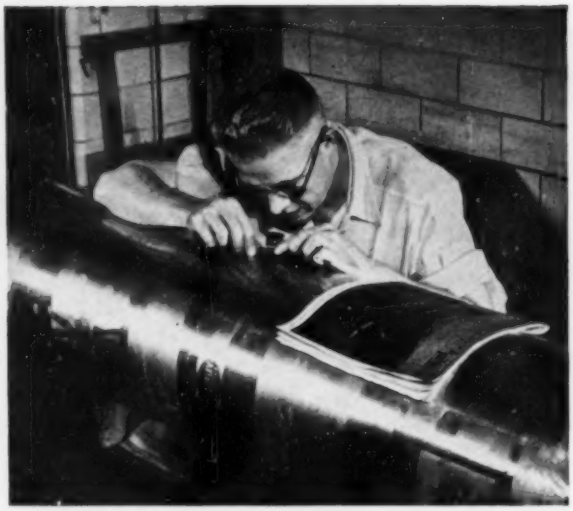

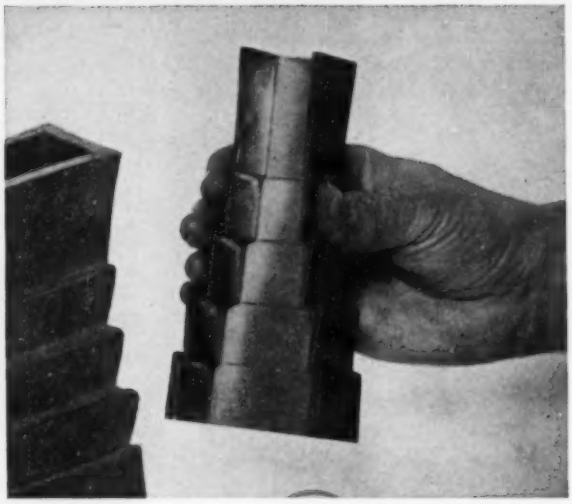

In electrotyping, plating rotogravure rolls, electroforming, "Plus-4" Copper Anodes cut plating costs

ELECTROTYPERS have discovered that, in addition to eliminating the use of bags and diaphragms, they can place "Plus-4" (Phosphorized Copper) Anodes closer to the cathodes to speed up the plating cycle 30% or more with the same power input – and still obtain a smooth deposit. As an alternate, power can be reduced by one-third with an equal reduction in resistance and generation of heat to obtain finished electros in the same plating time. This is an important advantage when thermoplastic plates or molds are used and tanks must run no higher than 95F.

MAKERS OF ROTOGRAVURE ROLLS have found that "Plus-4" Anodes provide a much finer, smoother surface for polishing and etching, and retain the quality of the light tones in runs of over one million impressions on a single set of design cylinders.

In addition, they report significant reductions in cost. One publisher found that he produces superior rolls with less labor and a reduction of 18 to 20% for materials required in the plating process. Another reports he gets a dividend of eight extra rolls for each tank load of "Plus-4" Anodes. And still another has found a 15% saving in over-all costs.

IN ELECTROFORMING operations, "Plus-4" Anodes – by eliminating the most prevalent acid-copper plating difficulties – have made it practical to produce many new products. Their ability to provide a smooth, dense deposit relatively free from growths and blemishes made possible relatively thick shells for molds used in making rubber and plastic articles, and in intricate precision parts for electronic use. Electroformers report operating economies similar to those found in the graphic arts field.

WRITE FOR INFORMATION on how you can obtain a test quantity to supply one tank. Address: The American Brass Company, Waterbury 20, Conn. In Canada: Anaconda American Brass, Ltd., New Toronto, Toronto 14, Ontario. B9106

ANACONDA®

"PLUS-4"® ANODES Phosphorized Copper

Made by The American Brass Company

Titanium and Zirconium As Primary Cell Anodes

Milton A. Thompson, Allen B. Scott, Donald Chittick, and Paul M. Gruzensky

Department of Chemistry, Oregon State College, Corvallis, Oregon

ABSTRACT

Polarization, chemical corrosion rates, and the anodic electrochemical equivalence for titanium and zirconium were measured in several electrolytes, chiefly fluoride solutions. Titanium exhibited satisfactory electrode characteristics in dilute HF, containing added NH_4F, except for somewhat excessive chemical corrosion. Zirconium was corroded severely by fluoride solutions in which its electrode characteristics were otherwise satisfactory and was somewhat less suitable as an electrode in H_2SO_4 solutions in which chemical corrosion was not serious. The Ti-HF, NH_4F-MnO_2 cell operated stably during discharge with good anode utilization but is probably limited to use as a reserve cell chiefly because of the deleterious effects of fluoride upon the MnO_2 electrode.

The experiments described in this paper were undertaken in order to determine the suitability of titanium and zirconium as negative electrodes in primary cells. Both metals are characterized by large negative electrode potential, corrosion resistance in many electrolytes, galvanic corrodibility in some of these solutions, and relatively low equivalent weight and equivalent volume. On the other hand, both may be rendered passive by oxide films when anodized under certain conditions. While the cost of the metals is still high compared to that of zinc, magnesium, and aluminum, it is decreasing rapidly and continually, and even now an amount of Ti electrochemically equivalent to the Zn contained in a flashlight D cell costs only 4.5 cents.

Electrochemical data for Ti and Zr are given in Table I; data for Zn are also given as a comparison.

Considerable information is available concerning the corrodibility of Ti and Zr in the more common electrolytes (3). Both metals are highly resistant to corrosion under a variety of conditions; however, Ti is attacked by H_2SO_4 above 5% concentration, HCl above 5%, H_3PO_4 above 30%, certain organic acids and HF at all concentrations. Zirconium is corroded by H_2SO_4 above 80%, $FeCl_3$ and $CuCl_2$ solutions, and HF at all concentrations. Straumanis and Gill (4) reported that the addition of NH_4F increased the dissolution rate of Ti in HCl and H_2SO_4 up to a concentration of 4M NH_4F, above which the metal was rendered practically passive. In HF, the effect of NH_4F was to reduce the dissolution rate at all NH_4F concentrations.

Table I. Comparison of Ti, Zr, and Zn as anode materials

	Ti	Zr	Zn
Eq. wt[a]	11.97	22.8	32.69
Eq. vol, cm^3	2.66	3.50	4.59
Amp min/g	134.	70.6	49.4
Cost (1), \$/lb	2.05	7.50	0.10
Standard oxidation potential,[b] (2) v	1.19	1.53	0.76

[a] Based on oxidation to tetravalent Ti and Zr.
[b] For couples: Ti-$TiF_6^{=}$, Zr-ZrO^{++}, and Zn-Zn^{++}, respectively.

Schlain and co-workers (5) studied galvanic corrosion of Ti and Zr. When coupled with several other metals in a variety of electrolytes, both were usually cathodic; however, Ti was anodic to stainless steel in H_2SO_4 and to Al after several days in a deaerated H_2SO_4 solution.

Several studies of electrode potentials of Ti and Zr have been reported. Botts and Krauskopf (6) and more recently Sato and Yamane (7) attempted to obtain the standard electrode potential of Ti in $Ti_2(SO_4)_3$ solutions. The values obtained, e.g., −0.355 v in the latter experiment, were far different from the value −1.30 v calculated from thermodynamic data (2), showing that the electrode was not reversible. Other experiments (5, 8) generally support the conclusion that potentials of these electrodes in many electrolytes are variable with time, sensitive to degree of aeration, and that the electrodes are highly irreversible. Straumanis and Chen (8) found that the Ti electrode potential in HF becomes more negative with increasing HF concentration up to 0.20*N*, beyond which it was constant at −0.768 v. Addition of NH_4F resulted in a potential of −0.95 v.

Anodic polarization and oxide film growth during anodization of Ti and Zr have been extensively investigated (9). Passivity is usually attributed to a layer of TiO_2 or ZrO_2.

The only application of either Ti or Zr in a primary cell, to our knowledge, involves a positive electrode of porous Ti coated with depolarizer (10). Schlain (5) obtained a current as high as 11 ma from a Mg-Ti couple in which Ti was cathodic.

In the course of this investigation the following quantities were determined: (*a*) electrode potentials for Ti and Zr as a function of anodic current density in a variety of electrolytes; (*b*) average charge of the ion produced by the anode reaction in several electrolytes and at several current densities; (*c*) characteristics of more than a hundred primary cells having either a Ti or Zr anode and either a Pb-PbO_2 or C-MnO_2 cathode.

Experimental

Titanium sheet,[1] 0.25 mm thick, was cut to the desired size and polished with emery paper for use as electrodes. Titanium tubing,[2] 3.17 cm O.D., was used for the construction of dry cells. Zirconium sheet, 0.25 mm thick, was either Iodide Process[3] or Kroll Process.[4] No significant differences were observed in the behavior of the two types of Zr. All reagents were C.P. or Analytical Reagent grade.

Single electrode potentials were measured by means of a L&N Type K potentiometer. Cell voltages were measured either potentiometrically or by means of a vacuum-tube voltmeter. Current densities were computed from the measured area of electrodes without application of a roughness factor. The electrode area was regulated by coating the entire electrode with paraffin and cleaning off the desired area on one side of the electrode, finally polishing the exposed area with emery paper.

C-MnO_2 electrodes were of the commercial D-cell type.[5]

In order to select an electrolyte and a usable cathode for detailed tests, the behavior of Ti and Zr coupled to other electrodes in about 40 electrolytes was studied. The open-circuit voltage and the voltage of the couples connected by a 12-ohm resistor were measured. The electrolytes were principally solutions of H_3PO_4, HF, H_2SO_4, $FeCl_3$, NH_4F, and combinations of these. The other electrodes were Cu, Al, Pb, stainless steel, and MnO_2. Most of the couples exhibited either a low open-circuit voltage or severe polarization under load; however, Ti coupled with the MnO_2 electrode in 1*N* HF gave 1.37 v open circuit and 0.600 v under load. A Zr-MnO_2 couple, with 0.1*N* HF, gave 1.60 v open circuit and 0.89 v under load. The highest current drawn was 75 ma, using an anode area of 2 cm^2.

It is evident that acid fluoride solutions are the most effective in reducing polarization under load in the case of both Ti and Zr. The C-MnO_2 electrode, although undoubtedly adversely affected by fluoride, was selected for detailed investigation because of the high voltage observed when coupled with Ti and Zr in many different acid fluoride solutions.

Polarization Measurements

Titanium or zirconium was made the anode in electrolytes composed chiefly of HF, NH_4F, KCl, and in some cases H_2SO_4. The single electrode potential was measured by means of a reference normal calomel electrode, as a function of current density. The single electrode potentials of replications agreed within 1% at current densities less than 1 ma cm^{-2} and within 5% at the highest current densities. Representative curves are presented in Fig. 1 and 2. Potentials are taken with respect to the standard hydrogen electrode.

In the case of Ti (Fig. 1), as the current density was increased, a point was attained at which the electrode potential suddenly became strongly positive. The current density at which this occurred is indicated by the broken vertical portion of the polarization curve, and electrodes which have undergone the sudden positive change in potential will be referred to as passive. In this condition, oxygen is evolved and the electrode is presumably covered by a protective film. The current density for passivation, i_p, was not very reproducible, even though the electrode potentials prior to passivation were quite so. This arose from the fact that i_p depended markedly on the rate at which the current was increased. The curves were selected to show typical passivity behavior.

Zirconium electrodes generally showed less tendency to become passive. However, in solutions containing only HF, or dilute mixed solutions of HF and NH_4F, i_p was lower for Zr than for Ti, as shown in Fig. 2. NH_4F was very effective in eliminating passivation of Zr, even in the absence of HF.

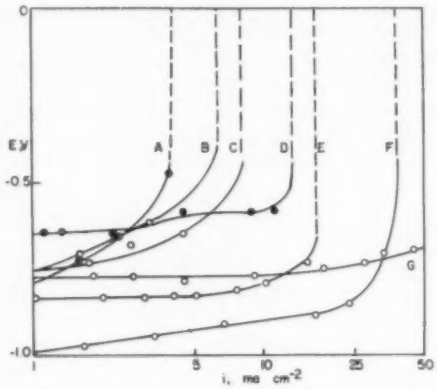

Fig. 1. Polarization and passivation of Ti in fluoride solutions. Curve A, 0.05N HF; B, 0.075N HF; C, 0.1N HF; D, 1N HF, 20% NH_4F; E, 0.2N HF; F, 0.075N HF, 0.1N KCl, 6% NH_4F; G, 1N HF. i_p for 1N HF was 110 ma cm^{-2}.

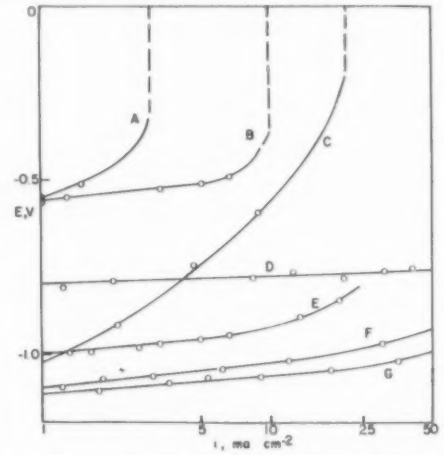

Fig. 2. Polarization and passivation of Zr in fluoride solutions, and Zn in Leclanche electrolyte (curve D). Curve A, 0.1N HF; B, 1N HF; C, 0.1N HF, 1% NH_4F; E, 8% NH_4F; F, 0.075N HF, 4% NH_4F; G, 0.075N HF, 8% NH_4F. Passivity did not occur in E, F, or G, even though in G i was taken as high as 180 ma cm^{-2}.

[1] Supplied by Titanium Metals Corp. as Ti-75A.

[2] Supplied by Superior Tube Co.

[3] Supplied by Foote Mineral Co.

[4] Supplied by the Carborundum Metals Co.

[5] Supplied by the National Carbon Co.

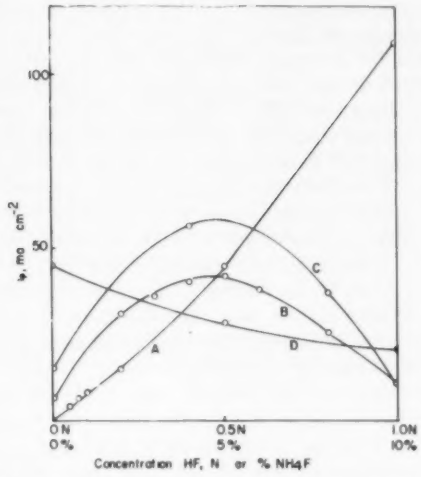

Fig. 3. Dependence of the passivation current density of Ti on HF and NH_4F concentration. A, HF only; B, 0.075N HF, added NH_4F; C, 0.2N HF, added NH_4F; D, 0.5N HF, added NH_4F.

Returning to Fig. 1, we note in particular the effect of HF concentration on the slope of the E vs. i curve for Ti and on the value of i_p. Even more important is the beneficial effect of added NH_4F in dilute HF solutions on the potential, polarization, and passivation current density for Ti, as illustrated by the difference between curves B and F. (KCl had a very minor effect on electrode behavior and was added to several electrolytes for the purpose of increasing conductivity.) Although i_p was somewhat uncertain, enough values were at hand to allow an approximate evaluation to be made of its dependence on electrolyte composition. In Fig. 3, the passivation current density is plotted against the concentration of HF (with no NH_4F), or against % NH_4F at fixed HF concentration. NH_4F exerts a beneficial influence up to about 5% in dilute HF (0.2N) but a deleterious effect at higher HF concentrations. This is also clearly shown by curves D and G of Fig. 1. In 1N HF i_p was reduced from 110 ma cm^{-2} to 8.1 ma cm^{-2} by the addition of 20% NH_4F. In NH_4F solutions with no HF (except that arising from hydrolysis), i_p was very low, e.g., 2.6 ma cm^{-2} in 8% NH_4F.

Considering also the chemical corrosion of Ti which increases rapidly with HF concentration and is inhibited by NH_4F, we conclude that the best electrolyte to be used with Ti is 0.075N HF containing 5-6% NH_4Cl and about 0.1N KCl. For brevity this solution is designated solution A. The potential of Ti in solution A is −1.02 v (about 0.2 v more negative than Zn in the usual dry-cell electrolyte) and remains below −0.8 v up to a current density of 28 ma cm^{-2}.

This current density may be compared with typical values at the Zn electrode in the Leclanché cell. During discharge of a fresh D-cell under 4-ohm load the anodic current density is about 6 ma cm^{-2}, and during operation of an ordinary 2-cell flashlight it is about 20 ma cm^{-2}.

There were too few cases of passivity for Zr to permit the same kind of correlation between i_p and electrolyte composition. Curve G of Fig. 2 shows, however, that the most satisfactory electrolyte for Zr from the standpoint of polarization was 0.075N HF with 8% NH_4F. The addition of KCl caused no significant difference. In this electrolyte the potential of Zr is superior to that of Zn (curve D, Fig. 2) in a solution containing 26% NH_4Cl, 8.8% $ZnCl_2$, and a trace of $HgCl_2$ (a common dry-cell electrolyte) at all current densities up to 200 ma cm^{-2}.

Corrosion

The corrosion rates of Ti and Zr were measured in electrolytes which appeared promising from polarization studies and in several other solutions used in the experimental cells described later. Solutions were in contact with air at room temperature, but not stirred. The favorable effect of added NH_4F on the corrosion of Ti by HF, previously reported (4), was confirmed. The rate for Ti in electrolyte A was 22 mdd, which, while not excessive, sets an upper limit of about six months on the life of a 0.25-mm sheet anode in this electrolyte.

On the other hand, Zr corroded rapidly in all acid fluoride solutions investigated, and the addition of NH_4F was of no benefit. The rate was 6000 mdd in electrolyte A and 800 mdd in 8% NH_4F alone. Small concentrations of Pb, Zr, and chromate ions reduced the corrosion rate in 0.1N HF, but not to a useful level. $Na_2Cr_2O_7$ reduced significantly the corrosiveness of H_2SO_4 on Zr, the rate in the case of 80% H_2SO_4, 1% $Na_2Cr_2O_7$ being only 2.3 mdd.

Anode Reaction

The number of faradays to dissolve a mole of metal, z, when Ti or Zr was made the anode was measured over a series of current densities and with varying electrolyte composition.

Electrolytes used with Ti were all mixtures of NH_4F, KCl, and HF, containing from 4 to 8% NH_4F, 0.1N KCl, and from 0.075 to 0.1N HF. Current densities ranged from 1 to 20 ma cm^{-2}. There was no observable dependence of z on either composition or current density. The average of 16 measurements of z which lay between 3.93 and 4.18 was 4.04.

Electrolytes used with Zr included 0.05 to 0.2N HF, 5 to 10% NH_4F, mixtures of HF and NH_4F, $CuCl_2$, $FeCl_3$, NH_4Cl, and HCl of several concentrations each. Current densities were higher than in the case of Ti in order to reduce the time required and thus the error due to chemical corrosion, ranging from 50 to 140 ma cm^{-2}. At 100 ma cm^{-2}, the anodic corrosion rate is 2 x 10^5 mdd. z did not depend on either composition or current density. The average of 14 measurements of z, which lay between 3.25 and 4.44 was 3.90.

It is clear that the only reaction of significance in these cases is oxidation of the metal to the tetravalent state. Chemical corrosion during the measurements has the effect of reducing z below the actual value; this may account for the somewhat smaller average value for Zr, since in some electrolytes the chemical corrosion rate was in the neigh-

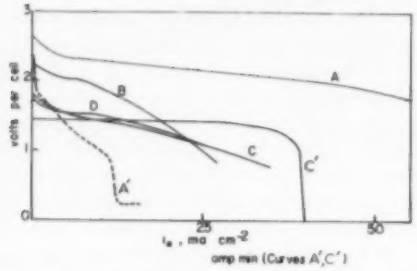

Fig. 4. Characteristics of primary cells. Curve A, A', Ti-0.07N HF, 0.1N KCl, 9% NH_4F, 1.6% H_2SO_4-PbO_2; B, Zr-90% H_2SO_4, 1% $Na_2Cr_2O_7$-PbO_2; C, C', Ti-soln. A-MnO_2; D, Zr-soln. A-MnO_2. Soln. A = 0.075N HF, 0.1N KCl, 6% NH_4F.

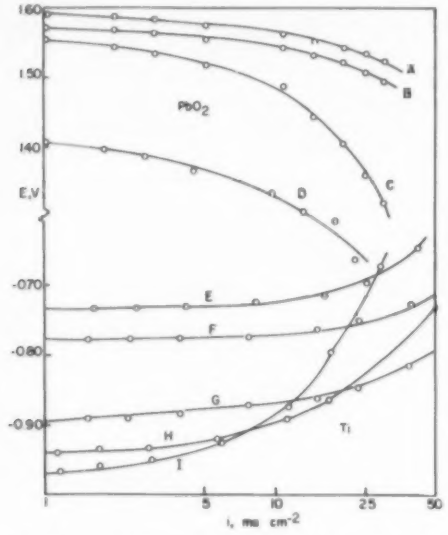

Fig. 5. Effect of H_2SO_4 on Ti and PbO_2 electrodes. Composition given as ratio: vol. soln. A/vol. of 15% H_2SO_4. Curve A, 1/99; B, E, 25/75; C, F, 50/50; D, G, 75/75; H, 90/10; I, 99/1.

borhood of 3% of the anodic corrosion rate. Oxygen was evidently not produced in a significant quantity.

Primary Cells

Cells were made in open beakers using Ti or Zr anodes and either PbO_2 or MnO_2 cathodes. The principal electrolytes used were solution A (0.075*N* HF, 6% NH_4F, 0.1*N* KCl), mixtures of A with H_2SO_4 and additional NH_4F, H_2SO_4, and H_2SO_4 containing $Cr_2O_7^{--}$. Th PbO_2 electrodes were made with commercial positive grids, pasted and formed in the laboratory according to the method described by Vinal (11). Representative data for four types of cells are shown in Fig. 4. Curves A through D were obtained by measuring the cell voltage during very short periods of discharge through a variable load. The drain is given by i_a, the anodic current density. In all cases the cathode was of much greater area than was the anode.

Curves C and C' represent the behavior of a Ti-MnO_2 cell containing solution A. The open-circuit voltage was 1.75. When discharged at $i_a = 10$ ma cm^{-2} the voltage remained about 1.4 for delivery of 25 amp min, and dropped to 1.0 v at 39 amp min. This corresponded to 81% utilization of the anode. The behavior of these cells was not very reproducible, and the example cited here was representative of several of the best cells studied. Unfortunately, fluoride solutions affect MnO_2 electrodes deleteriously, so that even the open-circuit voltage of such cells would fall to zero after 2 or 3 days.

The use of PbO_2 in place of MnO_2 resulted in a much higher initial open-circuit voltage (2.2 to 2.7 v). The addition of a small concentration of H_2SO_4 to the electrolyte increased the PbO_2 potential. Titanium became more positive with increasing H_2SO_4 concentration, but the polarization characteristics were improved. These effects are illustrated by Fig. 5. However, the polarization of Ti with time during continuous discharge was more severe in solutions containing H_2SO_4. Thus we find that, although the voltage remained high for high drain of short duration (curve A, Fig. 4), the discharge characteristics were disappointing (curve A'). Much of the decrease in voltage during discharge was due to failure of the PbO_2 electrode in fluoride solution. At the end of the discharge, the PbO_2 single electrode potential had fallen from an original value of 1.4 v to 0.6 v.

Zr-MnO_2 cells containing solution A were similar (see curve D, Fig. 4) to the Ti cells except for the much greater chemical corrosion of the anode. Many cells of the type Zr-H_2SO_4-PbO_2 were tested, to several of which chromate was added to reduce corrosion. The performance of the best of these is illustrated by curve B, Fig. 4. Discharge characteristics were generally inferior to the Ti-PbO_2 cells.

"Dry" cells were constructed from Ti tubing or Zr sheet, commercial MnO_2 electrodes, and a starch paste containing solution A. These cells polarized completely at low current density, probably because the polarization product was held mechanically in contact with the electrode, while in the open-beaker cells it was allowed to drop off.

Other electrolytes used in experimental cells were chosen with the purpose of eliminating water or reducing its activity markedly in the hopes of avoiding the formation of oxide layers on the Ti or Zr electrodes. Fused hydrates of NaOAc, $FeCl_3$, $CaCl_2$, and KF, and the nonaqueous solvents glacial acetic acid, fused alkali halides, fused KI_3 methanol, diethyl ether, nitrobenzene, SCl_2, S_2Cl_2, formamide, acetone, acetic anhydride, and dioxane all gave unsatisfactory results. Cells containing H_2SiF_6 in aqueous solution were moderately successful but corrosion was severe.

Polarization Product

The nature of the product responsible for polarization of Ti in solution of HF and NH_4F was not ascertained. Colors commonly observed on polarized electrodes were black, blue, or white and were due to material which could be readily scraped off. X-ray diffraction photographs of four products obtained under different conditions showed that no two were identical, nor were any to be identified with compounds for which data are tabulated by ASTM (12). While TiO_2 is undoubtedly a major

component of the polarization product under many conditions, in no case studied did it appear as a pure product.

Acknowledgments

The work described here was supported by contract with W. J. Kroll, whose generosity and technical advice are gratefully acknowledged. We wish to thank the National Carbon Company, the Carborundum Metals Company, the Titanium Metals Corporation of America, the Foote Mineral Company, and the Burgess Battery Company for gifts of materials used in this study. Thanks are also due N. C. Cahoon and Miss M. P. Korver, with whom valuable discussions were held, Miss Judith Skow and Mrs. Celia Rockholt, who made many of the measurements.

Manuscript received March 2, 1959. This paper was taken, in part, from the Ph.D. Thesis of one of the authors (M.A.T.), Oregon State College (1957).

Any discussion of this paper will appear in a Discussion Section to be published in the June 1960 JOURNAL.

REFERENCES

1. *Chem. Eng. News*, **36**, No. 40, 92 (1958).
2. W. Latimer, "Oxidation Potentials," Prentice-Hall, New York (1953).
3. W. J. Kroll, "Corrosion Handbook," H. H. Uhlig, Editor, p. 347, John Wiley & Sons, Inc., New York (1948); L. B. Golden, I. R. Lane, and W. L. Acherman, *Ind. Eng. Chem.*, **44**, 1930 (1952); J. Schmets and M. Pourbaix, "Proceedings of Sixth Meeting, C.I.T.C.E.," p. 167, Butterworths, London (1955); T. Smith and G. R. Hill, *This Journal*, **105**, 117 (1958).
4. M. E. Straumanis and C. Gill, *This Journal*, **101**, 10 (1951).
5. D. Schlain, *U. S. Bur. Mines Repts. Invest. 4965* (1953); D. Schlain, C. Kenahan, and D. Steele, *This Journal*, **102**, 102 (1955); *U. S. Bur. Mines Repts. Invest. 5189* (1956); *ibid., 5201* (1956).
6. E. Botts and F. Krauskopf, *J. Phys. Chem.*, **31**, 1404 (1927).
7. S. Sato and K. Yamane, *Repts. Sci. Research Inst. (Japan)*, **32**, 8 (1956).
8. M. E. Straumanis and P. Chen, *Z. Technik, Industrie, U. Handel*, **7**, 85 (1953).
9. C. D. Hall and N. Hackerman, *J. Phys. Chem.*, **57**, 262 (1953); G. B. Adams, Jr., P. Van Rysselberghe, and M. Maraghini, *This Journal*, **102**, 502 (1955).
10. A. L. Fox (to Manganese Battery Corp.), U.S. Pat. 2,631,115, Mar. 10, 1953.
11. G. W. Vinal, "Storage Batteries," p. 27-46, John Wiley & Sons, Inc., New York (1950).
12. "Numerical Index of X-ray Diffraction Data," American Society for Testing Materials, Philadelphia (1950).

Investigation of the Electrochemical Characteristics of Organic Compounds IV. Quinone Compounds

R. Glicksman and C. K. Morehouse

Semiconductor and Materials Division, Radio Corporation of America, Somerville, New Jersey

ABSTRACT

A study of the electrochemical characteristics of various quinone compounds shows that the cathode potential of these compounds during current flow is dependent on the type and position of substituent groups in the molecule, the pH of the electrolyte, and the nature of the quinone itself. Experimental data are presented for dry cells containing 2,5-dichloro-p-quinone and p-quinonedioxime as cathodes coupled with a magnesium anode.

Most oxidation and reduction reactions in organic chemistry are irreversible. An exception to this is the group of reactions involving quinoid-benzenoid equilibria. One of the best known of these is the quinone-hydroquinone system, whose potential has been reported by Hovorka and Dearing (1) to be

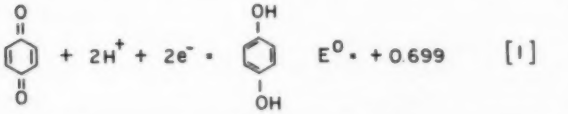

[1]

In this paper the effect of such factors as group substitution, aromaticity, and pH on the operating potential and coulombic capacity of various quinone compounds are presented and their use as cathode materials in primary cells is considered.

Experimental Data and Discussion of Results

Apparatus and Technique

A technique, previously described (2), has been used to measure the operating potential during current flow and the coulombic capacity of the various quinone-type compounds. This technique consists in discharging at a constant current drain of 0.005 amp/g, in a large volume of electrolyte, a 0.5-g sample of the quinone-type cathode material mixed with 0.05 g of Shawinigan acetylene black. The change in cathode potential with time was measured with a L&N type K potentiometer using a saturated calomel reference electrode. The measured potentials were corrected for the *IR* drop associated with the apparatus and electrolyte by means of an oscillographic technique (3).

All half-cell potential data reported in this paper are referred to the normal hydrogen electrode and include a liquid junction potential, which in most cases is small and can be neglected. For most of the measurements an aqueous magnesium bromide electrolyte and a magnesium anode were used, while in studying the effect of pH on potential, a zinc anode was employed with the acidic NH_4Cl-$ZnCl_2$-H_2O and basic NaOH-H_2O electrolytes.

Half-Cell Potential Studies

Effect of aromaticity.—Figure 1 gives half-cell discharge curves for a series of quinones derived from benzene and other polynuclear hydrocarbons. The ortho quinones have higher operating potentials than their corresponding para quinone compounds. In addition, both the ortho- and para quinones show a marked dimunition in cathode potential as one goes to the bicyclic and tricyclic quinone compounds. For example, a comparison of p-quinone with its corresponding naphthoquinone indicates a difference in potential of 200-300 mv, in agreement with standard potential measurements. Fieser and Fieser (4) attribute the markedly diminished energy content of the bicyclic compounds to the fact that the quinoid double bond is incorporated in the aromatic nucleus and hence is relatively inert. In anthraquinone both the otherwise reactive quinoid double bonds participate in benzenoid ring systems and the potential of the quinone is lower yet. Similarly, because of the higher energy content of the orthoquinones as compared to the isomeric paraquinones the standard potentials of the ortho compounds are 85-95 mv higher.

If the standard potentials of a series of quinones are compared, the change in potential will be dependent on the change in free energy in going from the quinone-hydrogen system to the hydroquinone, according to the following equation

$$E^\circ = -\frac{\Delta F^\circ}{nF} = -\frac{\Delta H^\circ}{nF} + \frac{T\Delta S^\circ}{nF} \qquad [2]$$

It has been found that the temperature coefficient of the standard potential is approximately the same for a large number of quinones and is equal to about 0.7 mv/deg. This temperature coefficient, which corresponds to an entropy change of −32 cal/deg for the hydrogenation of a quinone, corresponds roughly to the entropy of the mole of hydrogen lost in the reaction. Thus the change in potential in a series of quinones will represent the change in the relative heat contents of the quinone and hydroquinone through the series (5). The change in bond energies in the reduction represented by Eq. [1] is the same for all quinones and is small compared to the benzene resonance energy gained on the hydroquinone side. Thus it would be expected that resonance effects would be a controlling factor in the magnitude of the potential. Since the largest contribution to the resonance energy is due to the equivalent Kekule forms, the relative numbers of such equivalent forms may be used as a quantitative estimate of the relative energy of the oxidized and reduced forms.

The relationship between the number of contributing resonance forms in the quinone and hydroquinone and the standard potential of the system has been demonstrated by Branch and Calvin (5). They obtained a straight line relationship between the standard potential of para quinones and the ratio of the contributing forms n_q/n_h.[1] A still better relationship was obtained when the expression $(n_h - n_q)/(n_h + n_q)$ was used instead of the simple ratio and when allowance was made for steric and ortho effects in quinones of polynuclear structure. Similarly, Berliner (6) computed the difference in empirical resonance energies of a number of quinones and their respective hydroquinones from known experimental data and found a linear relationship exists between the oxidation-reduction potential and the difference in resonance energies of the quinones and the respective hydroquinones.

To test the above relationship for electrodes undergoing discharge, the cathode potentials of the quinones after 1 amp-min of discharge were plotted vs. $(n_h - n_q)/(n_h + n_q)$, as shown in Fig. 2. In agreement with the results of Branch and Calvin a straight line relationship was found between the potential and the ratio of the number of resonance forms in the quinone and hydroquinone compounds. In addition a similar line is obtained for the orthoquinones but displaced upward about 0.1 v and parallel to the paraquinone line.

[1] n_q and n_h are the number of forms of the quinone and hydroquinone. For p-quinone there is only one such form, while in hydroquinone there are two Kekule forms. In 1, 4-naphthoquinone there are two, while in the corresponding hydroquinone there are three.

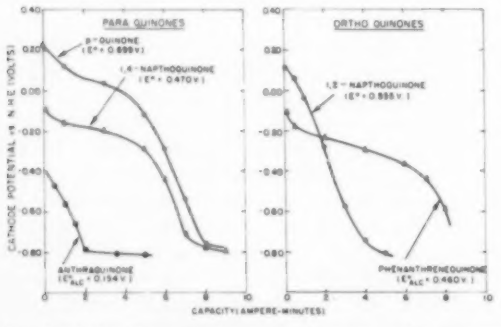

Fig. 1. Half-cell potential studies of various ortho and para-quinone compounds discharged at a rate of 0.005 amp/g in 250 g/l $MgBr_2 \cdot 6H_2O$ electrolyte.

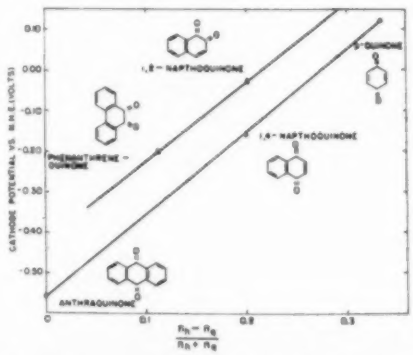

Fig. 2. Relationship between the number of contributing resonance forms in the quinone and hydroquinone and the half-cell potential as measured at a rate of 0.005 amp/g in 250 g/l $MgBr_2 \cdot 6H_2O$ electrolyte.

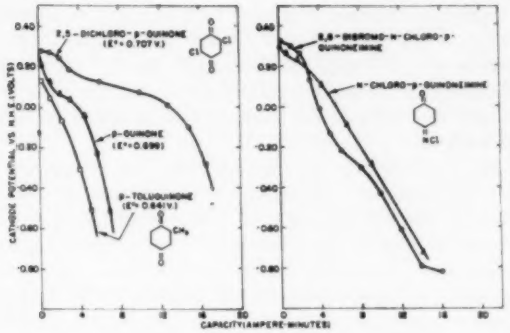

Fig. 3. Effect of group substitution on the cathode potential of p-quinone and N-chloro-p-quinoneimine discharged at a rate of 0.005 amp/g in 250 g/l $MgBr_2 \cdot 6H_2O$ electrolyte.

Effect of group substitution.—Presented in Fig. 3 are discharge curves for various para quinone and chloroimide compounds illustrating the effect of substituent groups on the operating potential of these compounds. It is seen that an electron-attracting halogen group raises the potential while an electron-repelling methyl group lowers the potential of the parent compound. This type of effect closely parallels the effect of these constituents on the standard potentials of quinones, as well as on the operating potential of aromatic nitro compounds (7).

The effect of substituent groups on the standard potentials of quinone compounds has been studied extensively by Fieser (8, 9). Most of the determinations were carried out in alcoholic solution, but the results would be expected to apply closely to aqueous solutions. In general, it was found that electron-attracting groups, such as $-NO_2$, -CN, -COOH, and halogens, raise the potential of the parent quinone, whereas a potential-lowering effect is exerted by electron-repelling groups such as $-NH_2$, -OH, and $-CH_3$. This is in agreement with the data presented in Fig. 3. These relationships are those expected from the course of aromatic substitutions. Electron-attracting groups tend to decrease the electron density in the vicinity of the oxygen atoms and thus to increase the attractive power of the system for external electrons, rendering the compound a stronger oxidizing agent. Conversely electron-repelling substituents decrease the affinity for electrons and hence lower the potential.

When the substituent is not in the quinoid ring its effect is much smaller and depends to a large extent on its position with respect to the quinoid ring. For example, Fieser (8) has shown that substituents in the 1 or 3 position of phenanthrenequinone have a considerable effect on the potential of phenanthrenequinone while in the 2 or 4 positions they are practically ineffective. The importance of the position of substituent group on the electrode potential of an organic compound has also been shown for both aromatic nitro (7) and nitroalkane compounds (10), and it depends essentially on its effect in altering the electron density in the vicinity of the reducible group.

Effect of electrolyte pH.—For the quinone-hydroquinone system the variation of the oxidation-reduction potential with hydrogen ion concentration is relatively simple in acidic electrolytes, but in alkaline solutions allowance must be made for the ionization of hydroquinone, which can function as a dibasic acid. Thus in acidic electrolyte $dE/d(pH) = 0.059$ for this system, while at pH's higher than about 8 the slope of the potential-pH curve becomes 0.030 to a pH of approximately 11 and is zero in more alkaline solutions (11).

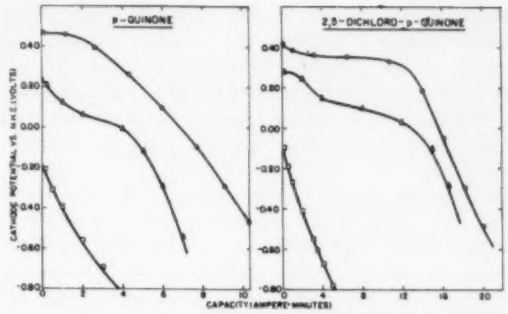

Fig. 4. Effect of pH on the cathode potential of p-quinone and 2, 5-dichloro-p-quinone when discharged at a rate of 0.005 amp/g in various electrolytes. ○—25% NH_4Cl, 20% $ZnCl_2$, 55% H_2O; △—14% $MgBr_2$, 86% H_2O; □—30% NaOH, 70% H_2O, saturated with ZnO.

Taking into account the effect of pH on potential, it is seen from Fig. 4 that both p-quinone and 2,5-dichloro-p-quinone have initial operating potentials close to their reversible values in the NH_4Cl-$ZnCl_2$ ($pH = 4.5$) and $MgBr_2$ ($pH = 8.2$) electrolytes. Similarly, the initial operating potentials of the quinone compounds previously presented in Fig. 1 and 3 are also reasonably close to their reversible values in the magnesium bromide electrolyte. However, in the strongly alkaline sodium hydroxide electrolyte, the operating potentials of p-quinone and 2,5-dichloro-p-quinone show a considerable deviation from their reversible values. This is attributed to the decomposition of both the quinone and hydroquinone by atmospheric oxygen in this alkaline electrolyte (12).

Various N-analogues of quinone.—In addition to the various quinone compounds discussed above there are a number of analogous organic compounds containing quinoid structures which are of scientific interest. Many of these compounds are employed as oxidation-reduction indicators in biological applications. Presented in Fig. 5 are discharge curves of

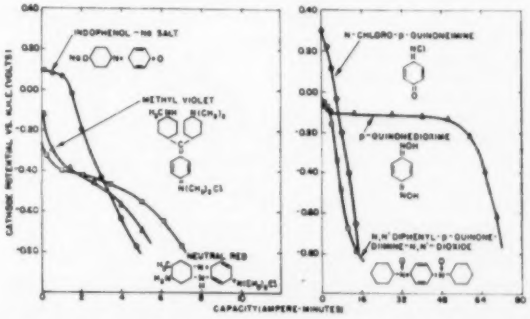

Fig. 5. Half-cell potential studies of various quinone-type compounds discharged at a rate of 0.005 amp/g in 250 g/l $MgBr_2 \cdot 6H_2O$ electrolyte.

three typical indicators, indophenol-Na salt (indophenol group), neutral red (azine group), and methyl violet (triphenylmethane group). As with the other quinones both indophenol-Na salt and neutral red operate at potentials close to their theoretical values (13) after corrections are made for the pH of the solution.

Also shown in Fig. 5 are discharge curves of three other N-analogues of p-quinone, which contain in addition to the quinoid structure additional reducible groups in the molecule. Of the three, N-chloro-p-quinoneimine which contains a positive halogen and p-quinonedioxime with two reducible oxime groups are of the most interest, as the amine oxides in N,N′-diphenyl-p-quinonediimine-N,N′-dioxide are reduced very difficultly (14, 15). Only the N-chloro-p-quinoneimine compound has a higher operating potential than p-quinone and, as evidenced by the data in Fig. 3 for 2,6-dibromo-N-chloro-p-quinoneimine, it would appear that the effect of substituent groups on the operating potential of chloroimides is similar to that of the quinones.

Capacities of Quinone Compounds

Presented in Table I are theoretical capacities and electrode efficiencies of various quinone-type compounds as calculated from the half-cell discharge data in Fig. 1, 3, and 5. It is seen that on the basis of theoretical capacity in ampere-minutes per gram the quinone compounds are superior to manganese dioxide, the cathode material now used in conventional Leclanché dry cells. However, because of the low densities and poor electrode efficiencies of these organic compounds a manganese dioxide cathode would give markedly superior performance when rated on the basis of ampere-minute output per cubic centimeter. As seen from the half-cell potential data in Fig. 4 the use of a more acidic NH_4Cl-$ZnCl_2$ electrolyte has no appreciable effect on the electrode efficiency of the quinones, and no advantage could be gained for the organic compounds in going to this electrolyte.

Table I. Theoretical capacities and electrode efficiencies of various quinone compounds discharged in 250 g/l $MgBr_2 \cdot 6H_2O$ electrolyte at a rate of 0.005 amp/g

Compound	Capacity, amp-min/g		Efficiency, %
	Theoretical	Actual*	
Manganese dioxide†	18.5	10.3	65.6
p-quinones			
p-quinone	29.8	6.4	21.5
1, 4-naphthoquinone	20.4	5.8	28.4
anthraquinone	15.5	—	—
p-toluquinone	26.4	4.6	17.4
2, 5-dichloro-p-quinone	18.2	17.2	94.5
o-quinones			
1, 2-naphthoquinone	20.4	2.3	11.3
phenanthrenequinone	15.5	6.5	41.9
N-Analogues			
N-chloro-p-quinoneimine	45.5(4)‡	10.4	22.9
N-chloro-p-quinoneimine	22.8(2)	10.4	45.6
2, 6-dibromo-N-Chloro-p-quinoneimine	21.5(4)	9.6	44.7
2, 6-dibromo-N-Chloro-p-quinoneimine	10.8(2)	9.6	88.9
p-quinonedioxime	69.9(6)	65.2	93.3
N, N′-diphenyl-p-quinone-diimine-N, N′-dioxide	11.1(2)	6.6	59.5
indophenol-Na salt	14.6	2.8	19.2

* Capacities calculated on basis of an end voltage of −0.40 v.
† Electrolytic manganese dioxide (85% MnO_2 content).
‡ Values in parentheses indicate the electron change.

More promising for use as cathodes in primary cell applications are some of the quinones which contain reducible groups in addition to the quinoid structure. These compounds not only have higher theoretical capacities than the quinones but also operate at higher electrode efficiencies. Of particular interest is p-quinonedioxime which has a theoretical capacity of 69.9 amp-min/g and which operates under these conditions of discharge at an electrode efficiency of 93.3%. On the basis of these results and the polarographic data of Elofson and Atkinson (16) it is believed the over-all reduction of p-quinonedioxime takes place with a 6 electron change, the actual reduction probably proceeding through the intermediate diimino stage as shown here:

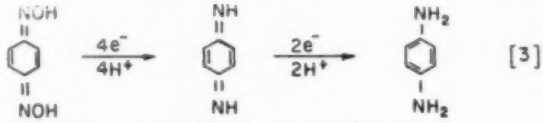

[3]

Experimental Dry Cell Data

The use of quinone compounds in primary batteries was suggested previously by Arsem (17) who referred to the coupling of a zinc anode with an organic oxidizing agent such as quinone. More recently Tripler and McGraw (18) evaluated tetrachloroquinone as a cathode material in both acid and basic electrolyte using zinc and lead anodes. In the present study the quinones were coupled with a magnesium anode to take advantage of the higher potential of this electrode.

Experimental dry cells containing 2,5-dichloro-p-quinone and p-quinonedioxime cathodes were assembled in the usual manner using an impact extruded magnesium AZ10A alloy AA-size can as anode, and a 500 g/l $MgBr_2 \cdot 6H_2O$ electrolyte. The cathode mix (weighing approximately 4.5 g) consisted of one part by weight of the quinone compound to two parts by weight of Darco carbon black G-60.

Performance characteristics of these cells on a 4- and 50-ohm continuous discharge test are shown in Fig. 6. Included for comparison are performance

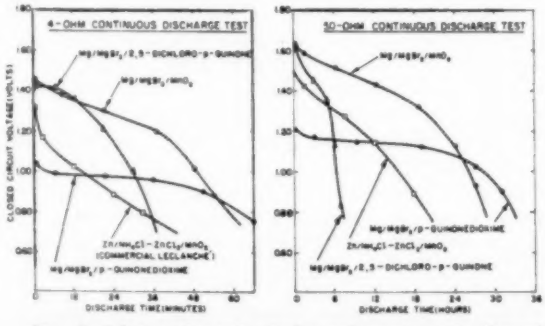

Fig. 6. AA-size dry cells discharged continuously through 4- and 50-ohm resistances at 70° ±2°F. (50% RH).

data for comparable-size commercial Leclanché and magnesium-manganese dioxide dry cells (19) of the type being developed by the Dow Chemical Company. It is seen that the performance of the magnesium-p-quinonedioxime cell is superior to the Leclanché cell on both these tests, while the magnesium-2,5-dichloro-p-quinone cell performs better only on the higher current drain test. Compared to the magnesium-manganese dioxide cell, the quinone cells give inferior performance on these tests. However, the flat voltage discharge curve of the p-quinonedioxime cell is advantageous for some applications.

Summary

An investigation of the electrochemical characteristics of various quinone-type compounds show these compounds to operate close to their reversible values during current flow. The operating potential of these compounds has been found to be dependent on the type and position of the substituent groups in the molecule as well as the pH of the electrolyte, electron-attracting groups and low pH's favoring higher potentials. The operating potential of the quinones is also dependent on the nature of the compound; for example, the ortho quinones operate at potentials approximately 0.1 v higher than their isomeric para quinones, while a decrease in potential is found as one goes to bicyclic and tricyclic members in any given series.

Compared to the conventional inorganic cathode materials the quinone compounds, in general, are not as good. However certain quinone-type compounds containing other reducible groups in the molecule, such as p-quinonedioxime, show some advantages when coupled with a magnesium anode in a magnesium bromide electrolyte.

Manuscript received Feb. 13, 1959. This paper was prepared for delivery before the Ottawa Meeting, Sept. 28-Oct. 2, 1958.

Any discussion of this paper will appear in a Discussion Section to be published in the June 1960 JOURNAL.

REFERENCES

1. F. Hovorka and W. C. Dearing, *J. Am. Chem. Soc.*, **57**, 446 (1935).
2. C. K. Morehouse and R. Glicksman, *This Journal*, **103**, 94 (1956).
3. R. Glicksman and C. K. Morehouse, *ibid.*, **102**, 273 (1955).
4. L. F. Fieser and M. Fieser, "Organic Chemistry," 3rd ed., p. 712, Reinhold Publishing Corp., New York (1956).
5. G. E. K. Branch and M. Calvin, "The Theory of Organic Chemistry," pp. 303-314, Prentice-Hall, Inc., New York (1941).
6. E. Berliner, *J. Am. Chem. Soc.*, **68**, 49 (1946).
7. R. Glicksman and C. K. Morehouse, *This Journal*, **105**, 299 (1958).
8. L. F. Fieser, *J. Am. Chem. Soc.*, **51**, 3101 (1929).
9. L. F. Fieser and M. Fieser, *ibid.*, **57**, 491 (1935).
10. R. Glicksman and C. K. Morehouse, *This Journal*, **106**, 288 (1959).
11. S. Glasstone, "Introduction to Electrochemistry," pp. 291-295, D. Van Nostrand Co., Inc., New York (1942).
12. G. Kortum and J. O'M. Bockris, "Textbook of Electrochemistry," Vol. I, p. 291, Elsevier Publishing Co., New York (1951).
13. W. M. Clark, *J. Appl. Phys.*, **9**, 97 (1938).
14. E. Ochiai, *J. Pharm. Soc. Japan*, **69**, 1 (1949).
15. R. Glicksman and C. K. Morehouse, *This Journal*, **105**, 613 (1958).
16. R. M. Elofson and J. G. Atkinson, *Can. J. Chem.*, **34**, 4 (1956).
17. W. C. Arsem, U. S. Pat. 2,306,927, Dec. 29, 1942.
18. A. B. Tripler, Jr., and L. D. McGraw, *This Journal*, **105**, 179, (1958).
19. R. C. Kirk, P. F. George, and A. B. Fry, *ibid.*, **99**, 323 (1952).

The Cathodic Reduction of Manganese Dioxide in Alkaline Electrolyte

N. C. Cahoon[1] and M. P. Korver

Research Laboratories, National Carbon Company, Division of Union Carbide Corporation, Cleveland, Ohio

ABSTRACT

A study of the mechanism of the reduction of manganese dioxide in strongly alkaline electrolytes has shown that the rather complex process may be considered as occurring in three steps. The first is the simultaneous reduction to form a divalent manganese compound, presumably, $Mn(OH)_2$ and an intermediate oxide tentatively identified as Mn_4O_7; the second step is the electrochemical reduction of Mn_4O_7 to form both Mn_3O_4 and $Mn(OH)_2$; the final step is the electrochemical reduction of Mn_3O_4 to $Mn(OH)_2$. Both chemical and x-ray diffraction analyses of cathodes at various stages of reduction are presented.

The cathodic reduction of manganese dioxide in Leclanché cells (1) has been examined previously and a mechanism proposed to account for the experimental observations. The need of a similar examination of the cathodic reduction of MnO_2 in alkaline electrolytes was recognized some years ago. Accordingly, a study was undertaken to determine the mechanism of the reaction when MnO_2 is used as the cathodic depolarizer in an alkaline cell. The approach to this problem followed the lines of earlier studies in that the products of the cathodic reductions were separated into two fractions by a differ-

[1] Edgewater Development Laboratories, National Carbon Company, Cleveland, Ohio.

Table I. Extent of reaction of cathodes of experimental alkaline cells during the course of discharge

Cell No.	Initial free MnO_2 content, g	Theoretical* capacity, amp min	Actual electrical output, amp min	Output equivalent to Mn^{III}		Output associated with insoluble cathode product, amp min	Last cell reading, v
				Amount present, amp min	% of total output		
1	0.5938	14.64	2.22	1.16	52.3	1.06	1.26
2	0.5174	12.78	4.14	2.41	58.2	1.73	1.19
2a	0.6029	14.88	4.20	1.71	40.3	2.49	1.20
3	0.4642	11.46	6.12	3.79	61.9	2.33	1.09
4	0.5292	13.08	8.09	5.06	63.7	3.03	1.03
5	0.5342	13.20	9.39	5.11	54.5	4.28	0.96
6	0.3949	9.78	8.87	3.25	37.6	5.62	0.63

* The theoretical capacity is calculated on the basis of the reduction of the free MnO_2 to Mn_3O_4.

ence in solubility. The soluble and insoluble fractions were studied separately by both chemical and physical methods. This paper presents some significant results obtained in the course of the work.

Experimental

A series of experimental cells was prepared from electrolytic grade MnO_2, acetylene black, and an electrolyte containing 7.6*N* KOH. An excess of amalgamated powdered Zn was used in a compressed pellet as the anode, and an adequate supply of electrolyte was provided so that the cathodic depolarizer would be the only service limiting factor. The composition of a representative cell follows: electrolytic MnO_2 0.5128 g, acetylene black 0.1923, KOH (7.6*N*) 0.2949, amalgamated Zn 4.0 (approximately). The parts of the cells were assembled in a bench-type cell of a circular cross section with a cross-sectional area of 2.58 cm^2 (0.40 $in.^2$). A cellulosic separator 0.0208 cm (0.0082 in.) thick was employed. The cell was closed with a close-fitting plunger and throughout the test the unit was maintained under a mechanical pressure equivalent to 4.32 kg/cm^2 (61.5 $lb/in.^2$) of cell area. A continuous load of 30 ohms was placed across the cell, and cell voltage readings were taken periodically with a recording voltmeter.

One cell was removed after each of the following service levels had been reached: 2.20, 4.14, 4.19, 6.12, 8.09, 8.87, and 9.39 amp min. Immediately following the removal from test, the cell was quickly dismantled and the cathode mix was suspended in 500 cc of an aqueous solution of 25% NH_4Cl. The pH of this suspension was quickly measured and ½*N* HCl added with adequate stirring to reduce the pH to 5.4. The suspension was stirred mechanically for 2 hr at room temperature to permit the solution of any divalent manganese that may have been formed in the cell discharge. Previous studies had shown that MnO_2, $Mn_2O_3 \cdot H_2O$, and Mn_3O_4 are all stable under these conditions and that substantially no complicating reactions would occur at this pH. Following the leaching operation, the residue was separated from the filtrate and thoroughly washed. The combined washings and filtrate were made up to one liter and aliquot samples of 100 ml were analyzed for manganese content by the method of Lingane and Karplus.(2)

The residue was dried at 100°-110°C and then subjected to examination by standard x-ray diffraction techniques to identify the solid phases remaining in the cathode. Another portion of the residue was analyzed for available oxygen and total manganese contents by conventional analytical methods.

Discussion

The discharge curve characteristic of this group of cells is shown in Fig. 1. Cells 1 to 5 gave substantially the same discharge curve as shown by the upper line in Fig. 1, while cell 6, which had a somewhat smaller cathode but was otherwise the same as cells 1 to 5, gave a discharge curve shown by the lower line in the same figure. Data obtained from the discharge of the cells and analyses of the soluble portion of the depolarizers are given in Table I. The conditions used for leaching the discharged cathodes were chosen so that any divalent manganese, presumably present as manganous hydroxide, would be dissolved. The amounts of divalent manganese leached from the cathodes in this manner have been calculated to equivalent ampere minutes on the basis of the following reaction:

$$MnO_2 + 2e + 2K^+ + 2H_2O \rightarrow Mn(OH)_2 + 2KOH \quad [1]$$

From this reaction 1 amp min of energy results from the reduction of 0.027 g MnO_2 to form 0.0173 g of

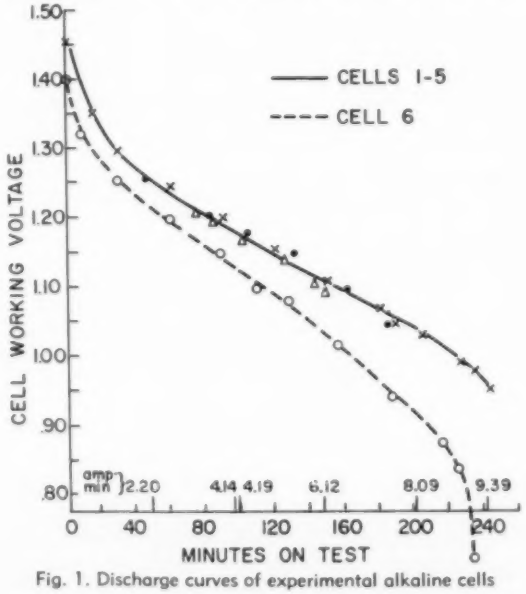

Fig. 1. Discharge curves of experimental alkaline cells

Table II. Composition of the insoluble cathode products during discharge of experimental alkaline cells

Cell No.	Initial depolarizer content: Weight, g	Initial depolarizer content: Free MnO_2, g	Amount free MnO_2 converted to $Mn(OH)_2$, g	Amount free MnO_2 in insoluble cathode product, g	Chemical composition of insoluble cathode product: MnO_2, %	Mn, %	x in $MnOx$	Free MnO_2, %
1	0.7056	0.5938	0.0313	0.5625	55.33	40.21	1.879	47.04
2	0.6148	0.5174	0.0651	0.4523	55.04	39.83	1.883	47.05
2a	0.7164	0.6029	0.0461	0.5568	55.52	39.88	1.888	47.94
3	0.5516	0.4642	0.1023	0.3619	51.42	39.62	1.819	40.16
4	0.6288	0.5292	0.1365	0.3927	—	—	—	—
5	0.6348	0.5342	0.1380	0.3962	42.79	36.66	1.738	27.57
6	0.4692	0.3949	0.0878	0.3071	26.55	42.91	1.391	None

Note: The electrolytic MnO_2 used in these tests contained 86.36% total MnO_2, 55.89% total Mn which can be calculated to 84.16% free MnO_2.

Table III. Relationship between the insoluble reaction product and the electrical output

Cell No.	Initial depolarizer weight, g	Free MnO_2 converted to $Mn(OH)_2$, g	Remaining depolarizer: Weight, g	Remaining depolarizer: Percent free MnO_2	Remaining depolarizer: Free MnO_2 content, g
1	0.7056	0.0313	0.6743	47.04	0.3172
2	0.6148	0.0651	0.5497	47.05	0.2586
2a	0.7164	0.0462	0.6702	47.94	0.3213
3	0.5516	0.1023	0.4493	40.16	0.1804
4	0.6288	0.1365	0.4923	—	—
5	0.6348	0.1380	0.4968	27.57	0.1370
6	0.4692	0.0878	0.3814	—	—

Cell No.	Amount free MnO_2 in insoluble cathode product, g	Free MnO_2 present at end of test, g	Free MnO_2 consumed in test, g	Output obtained, amp min	Free MnO_2 consumed per amp min, g
1	0.5625	0.3172	0.2453	1.06	0.2314
2	0.4523	0.2586	0.1937	1.73	0.1120
2a	0.5568	0.3213	0.2355	2.49	0.0946
3	0.3619	0.1804	0.1815	2.33	0.0779
4	—	—	—	—	—
5	0.3962	0.1370	0.2592	4.28	0.0606
6	0.3071	—	0.3071	5.62	0.0546

manganese as manganous hydroxide. The proportion of the total output in ampere minutes represented by the manganous hydroxide found and calculated on the above basis is shown in Fig. 2. It is evident from these data that while about half the reaction product is in this form, a sudden decrease in the proportion occurs between 8.09 and 9.39 amp min output. However, the finding that $Mn(OH)_2$ constitutes a large proportion of the cathodic reduction product is not in accord with previously published data (3) which indicate that the product is an orange-red Mn_2O_3.[2]

[2] We are unable to rationalize these earlier data with our findings.

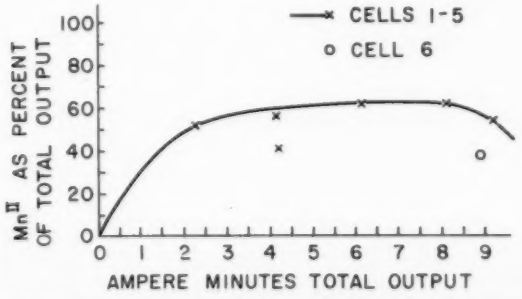

Fig. 2. Proportion of divalent manganese found in the cathodic reaction product as a percentage of the total cell output throughout the test.

Table I shows the depolarizer contents of the five experimental cells in terms of the free MnO_2[3] content and the equivalent theoretical cell output if all this MnO_2 were converted to Mn_3O_4 according to the following cathodic reaction:

$$3MnO_2 + 4K^+ + 4e + 2H_2O \rightarrow Mn_3O_4 + 4KOH \quad [2]$$

In this way 0.0405 g of MnO_2 provides 1 amp min of energy. This basis has been used for general calculation of cell output since work in this laboratory had previously shown that a variety of MnO_2 types was, at least in part, reduced to this compound. Table I also shows the actual electrical output of each cell as well as that portion of the output in equivalent ampere minutes that can be accounted for by the formation of $Mn(OH)_2$. The ampere minute output which must therefore be associated with a change in composition of the insoluble residue is listed. Table II also shows the compositions of these cathode residues. Table III combines the data of Tables I and II and shows the amount of free MnO_2 consumed per ampere minute for that portion of the output associated with the formation of the insoluble cathodic product. The values obtained are calculated on the assumption that only a single insoluble reaction product is formed in each case. By comparison of these values with the amounts of MnO_2 consumed per ampere minute for the reduction to the various lower oxides, some helpful correlations may be found. Thus, in reaction [2] 0.0405 g MnO_2 is required per ampere minute to form Mn_3O_4. Similarly 0.027 g MnO_2 (reaction [1]) and 0.054 g MnO_2 are needed per ampere minute to form $Mn(OH)_2$ and Mn_2O_3, respectively.

Figure 3 shows the ampere minutes per gram of free MnO_2 lost by the residue plotted against the ampere minute output associated with this residue taken from the last two columns in the second part of Table III. The values fall on a smooth curve which approaches the value of 0.0405 characteristic of reaction [2]. However, the three intermediate values for cells 2, 2a, and 3 fall too close to one another to attribute to experimental error. One possible cathodic reaction that gives a value approaching these points is the following:

$$4MnO_2 + 2K + 2e + H_2O \rightarrow Mn_4O_7 + 2KOH \quad [3]$$

This reaction consumes 0.108 g MnO_2/amp min which is not too far from the 0.112 g/amp min obtained from cell 2.

[3] Free MnO_2 is the amount of MnO_2 in the depolarizer available to react electrochemically.

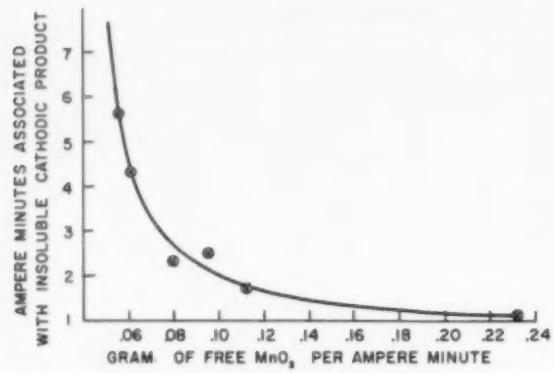

Fig. 3. Relationship between free MnO_2 consumed per ampere minute in the insoluble cathodic product and the extent of discharge.

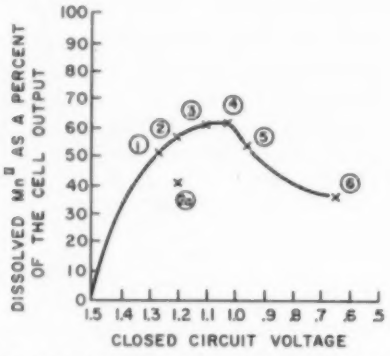

Fig. 4. Relationship between the proportion of divalent manganese found in the cathodic reaction product and the last cell voltage reading.

Data for cell 6, shown in Tables I, II, and III, differ somewhat from that for cells 1 to 5. A lower discharge curve for cell 6 is shown in Fig. 1, and it will be noted that the closed circuit voltage of this unit fell to 0.63 v at the time the test was terminated. The lower voltage of cell 6 probably is the result of the smaller quantity of depolarizer contained in the unit as shown in the tables. When the amount of the cell output represented by the divalent manganese removed from the cathode is plotted on Fig. 3, the point is somewhat lower than the curve given by the data of cells 1 to 5. At this time it appears that the fact that the discharge progressed relatively so much farther in cell 6 than in cells 1 to 5 is probably responsible for this situation. Added evidence to this viewpoint is given by Fig. 4 where there is a sharp break in the curve relating Mn^{II} as a per cent of total output to the last closed circuit voltage reading.

From a consideration of the results of these analyses of the cathode residues, it is concluded that the intermediate oxide is probably Mn_4O_7. However, the evidence we have presented for the existence of this manganese oxide needs further confirmation. The fact that it is cathodically reduced to Mn_2O_3 is not unknown with other manganese oxides. For example, $Mn_2O_3 \cdot H_2O$ when used as the sole depolarizer in experimental cells similar to those used in these tests is electrochemically reduced to $Mn(OH)_2$ and Mn_2O_3 simultaneously. On the other hand, Mn_2O_3 on reduction yields only $Mn(OH)_2$.

The identification of the insoluble cathodic product may also be studied by x-ray diffraction methods since many oxides of manganese possess characteristic patterns. The difficulties inherent in a precise comparison of a possible mixture of manganese oxides are well recognized. However, the results of such a study often yield valuable primary and confirmatory evidence for the existence of a particular solid phase and thereby indicate the reaction by which it may have been formed. A close examination of Fig. 5 showing the actual diffraction patterns of the insoluble residues from the experimental cells shows some rather startling differences. The original electrolytic MnO_2 is a typical gamma structure with the characteristic gamma "hump" and additional characteristic lines. From Fig. 5 it is evident that the shape of the gamma hump changes during the cell discharge from a rounded to a nearer square shape with a wider base and in the last pattern it almost disappears. The charts given in Fig. 5 indicate that each of the so-called gamma humps are topped by a number of small peaks located at specific "d" values. It could be interpreted that the gamma hump itself is only the result of the near coincidence of these specific peaks and many peaks of lesser intensity which are interspersed among them. Attention is drawn to a comparison of the "d" values from 3.0 to 6.0 for the six diffraction patterns. In trying to compare such patterns, considerable care must be taken to avoid misinterpreting random variations in the background counting rate or instrumental hunting as actual but small individual peaks. However, the remarkable regularity shown in the "d" values of the specific lines which occur in several of the gamma hump patterns in Fig. 5 strongly suggest the predominant peaks could represent true diffraction lines.

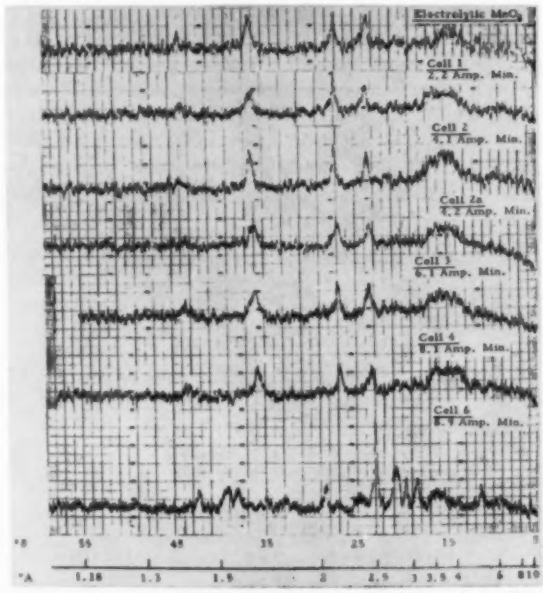

Fig. 5. X-ray diffraction patterns of insoluble cathode products at various levels of discharge.

Table IV. D values of x-ray diffraction patterns of MnO_2 shown in Fig. 5

Electrolytic MnO_2		Cell 1		Cell 2		Cell 3		Cell 4		Cell 6	
d	I	d	I	d	I	d	I	d	I	d	I
5.03	6	4.77	5	6.00	7	4.69	3	4.62	5	4.90	13
4.90	6	4.44	4	5.41	5	4.47	6-7	4.51	7	4.58	6
4.86	8	4.30	4-5	5.12	5	4.44	5	4.21	9	4.12	6
4.25	8	4.24	5	4.98	5	4.15	3	4.11	7	4.06	5
4.07	8	4.12	5-6	4.54	7	4.12	10	4.09	5	4.00	6
3.97	6	4.07	8	4.30	6-7	4.09	5-6	3.97	4	3.81	6
3.89	5	4.02	5	4.12	4-5	4.00	4	3.81	4	3.74	6
3.81	6	3.92	5	4.07	10	3.95	4	3.74	7	3.65	8
3.79	8	3.82	4	3.97	10-11	3.79	7	3.51	7	3.58	7
3.69	4	3.74	3	3.92	10	3.76	11	3.49	8	3.51	8
3.55	5	3.65	9	3.84	8-9	3.69	7	3.45	9	3.49	8
3.37	6	3.62	3	3.76	5	3.65	6	3.35	4	3.45	7
3.29	3	3.60	3	3.67	6	3.58	6	3.26	7	3.37	4
3.09	4	3.53	5	3.65	6	3.51	6	3.13	5	3.31	3
2.91	4	3.51	7	3.60	7	3.49	5	3.02	7	3.27	7
2.78	5	3.49	7	3.51	5	3.41	4	2.84	4	3.08	14
2.55	4	3.45	6	3.49	5	3.37	3	2.75	6	3.03	14
2.49	3	3.43	7	3.41	5	3.29	6	2.71	4	2.97	4
2.43	15	3.35	2	3.29	5	3.17	5	2.69	4	2.87	15
2.41	14	3.29	6-7	3.24	6	3.03	4	2.65	4	2.78	18
2.35	5	3.24	5	3.20	4	2.97	4	2.58	5	2.69	18
2.32	3	3.13	6	3.12	5	2.84	4	2.54	5	2.48	47
2.22	4	3.02	3	3.00	4	2.76	6	2.49	9	2.35	5
2.13	18	3.00	3	2.86	5	2.71	4	2.46	14	2.31	5
2.12	18	2.91	3	2.84	5	2.61	5-6	2.44	15	2.27	7
		2.79	5	2.76	6	2.60	5-6	2.39	8	2.19	7
		2.71	6	2.73	5-6	2.48	7-8	2.33	5	2.14	7
		2.69	2-3	2.68	5	2.44	17	2.28	5	2.11	7
		2.55	5	2.63	8	2.43	17	2.15	18	2.04	16
		2.51	3	2.42	16	2.41	15			2.02	14
		2.42	13	2.33	5	2.28	5				
		2.40	13	2.18	5	2.18	7				
		2.35	7	2.13	16	2.15	15				
		2.28	5	2.12	21	2.14	18				
		2.22	5			2.10	5				
		2.18	5			2.04	7				
		2.15	7								
		2.13	18								

Note: I indicates the relative intensity of the lines and is a measure of the height of divisions above the background.

It seems clear from Fig. 5 that the relatively simple diffraction pattern of the original electrolytic MnO_2 becomes much more complex as the discharge proceeds. It is quite easy to identify the major new component in cell 6, which was discharged to the lowest voltage, as Mn_3O_4. There is some evidence of the characteristic diffraction pattern lines of this material in the chart for cell 4 also, thus indicating that Mn_3O_4 begins to form after the cell reaches the 0.9-1.0 v level. However, it is in the intermediate range of discharge that the real question arises as to what insoluble cathodic product is present.

In view of the crystallographic difficulties involved in interpreting the significance of the gamma band in the pattern of electrolytic MnO_2, it seems unwise to attempt to assign exact diffraction spacings to the new phase which developed during the cell discharge. More extensive data would be required to establish the presence of such a new phase. Therefore, attention is drawn to the fact that a group of diffraction lines appears in the "d" value region of 3.7 to 3.3 which could be associated with the presence of the intermediate oxide tentatively designated Mn_2O_3. Added emphasis to this general point of view is furnished by the fact that some of these diffraction lines become reduced in intensity as the discharge proceeds and Mn_3O_4 is formed. An alternative explanation of these new diffraction lines would be that they might represent a solid solution of certain reduced manganese compounds in manganese dioxide. No conclusive evidence for solid solutions of manganese oxides in Leclanché dry cells has been published although the concept of a solid solution has been suggested in the absence of definitive data.

Perhaps the most complete analysis of the x-ray diffraction patterns of gamma MnO_2 is that of Cole, Wadsley, and Walkley (4) who postulate gamma, gamma I, and gamma II varieties. Their analysis of the gamma I type, electrolytic MnO_2, gives only the 3.94, 2.57, 2.41, 2.33, 2.11, 1.62, 1.41, and 1.37 lines. The 3.94 line apparently refers to the peak of the gamma band mentioned earlier in this paper. From the data presented in Fig. 5 and Table IV, there seems to be no indication that a change from the electrolytic MnO_2 to either of the other phases described by Cole, Wadsley, and Walkley occurs in the discharge of the experimental cells. The diffraction spacings presented in this paper do not conform with any of the patterns of reduced manganese

Table V. X-ray diffraction patterns for MnO_2 reduction by-products

Mn_2O_3		γ-Mn_2O_3		$Mn_2O_3H_2O$		$Mn_2O_3H_2O$		$MnO_{1.88}$		Mn_3O_4		Mn_3O_4		Mn_xO_y		$HMnO_2$	
d	I/I_1	d	I/I_1	d	I/I_1	d	I/I_1	d	I/I_1	d	I/I_1	d	I/I_1	d	I/I_1	d	I/I_1
3.86	10	4.93	40	3.40	100	3.40	100	6.99	25	4.86	70	5.10	80	5.1	20	5.36	10
2.72	100	3.08	60	2.64	60	2.63	60	4.91	25D	3.05	50	3.09	20	4.39	100	4.17	100
2.35	10	2.74	70	2.53	5	2.53	40	3.99	10D	2.87	20	2.63	100	4.12	100	3.462	10-20
2.01	20	2.48	100	2.41	20	2.41	70	3.502	10D	2.74	90	2.51	15	3.34	20	2.798	60
1.84	30	2.39	40	2.28	50	2.26	40	3.132	75D	2.47	100	2.17	15	2.46	100	2.675	60
1.66	90	2.03	20	2.23	5N	1.77	50	2.755	10D	2.34	50	1.77	10	2.35	50	2.524	10
1.45	20	1.83	30	2.20	5	1.71	40	2.392	100	2.02	60	1.67	20	2.06	35	2.369	60
1.42	60	1.79	20	1.783	20	1.68	70	2.152	75D	1.812	10	1.53	18	1.74	50	2.303	50
1.39	20	1.59	30	1.708	40	1.64	20	2.086	10D	1.779	50			1.62	50	2.210	20
1.35	10	1.55	60	1.672	30	1.50	40	1.633	25	1.689	20			1.58	35	2.008	10
1.28	10			1.636	40	1.44	40	1.542	50D	1.629	15			1.50	20	1.957	5
1.19	5			1.502	20			1.425	50	1.571	60			1.30	20	1.932	10
1.18	10			1.437	30			1.368	25D	1.537	80			1.27	35	1.798	5
1.16	10			1.326	10			1.358	25D	1.462	10					1.763	20
1.14	10			1.297	10			1.348	25D	1.434	50					1.732	10
				1.256	5					1.405	10					1.692	50
				1.24	20S					1.378	10					1.603	40
				1.21	20S					1.340	20					1.559	0
				1.183	10					1.323	30					1.515	30
				1.162	10					1.238	10					1.465	10
				1.139	40					1.226	30					1.448	10
				1.116	20					1.215	10					1.435	20
				1.10	20S					1.189	30					1.398	10
				1.08	20S					1.175	30					1.367	5-10
				1.029	30					1.142	10					1.345	10
				1.01	—S					1.128	40					1.304	5
				0.993	10					1.095	10					1.286	10
				0.932	20S					1.075	50					1.281	10
				0.890	20S					1.053	30					1.267	10
				0.878	20S											1.258	10
				0.867	20S											1.220	10
				0.860	20S											1.212	10
				0.835	20S											1.202	10
																1.153	20
																1.134	10-20
																1.107	10
																1.086	5
																1.077	5
																1.068	30
Mineralogical designation		Bixbyite		Manganite						Hausmannite						Groutite	

Ref: McMurdie & Golovato, J. Res. Nat. Bur. Stds., 41, 589 (1948)

Ref: Cowley & Walkley, Nature, 161, 173 (1948)

Ref: Gruener, Am. Min., 32, 654 (1947)

compounds as shown in Table V which are possible products under the conditions used for testing. These compounds include manganite, $Mn_2O_3H_2O$, bixbyite, Mn_2O_3, and groutite, MnOOH (5).

Conclusion

A mechanism for the electrochemical reduction of electrolytic manganese dioxide in strongly alkaline electrolytes is proposed which consists of the several steps listed below.

Step 1.—The manganese dioxide is electrochemically reduced according to the two following reactions which occur simultaneously:

$$4MnO_2 + 2K^+ + 2e + H_2O \rightarrow Mn_4O_7 + 2KOH$$

$$MnO_2 + 2K^+ + 2e + 2H_2O \rightarrow Mn(OH)_2 + 2KOH$$

Step 2.—The intermediate insoluble oxide product formed in Step 1 then becomes the depolarizer which is electrochemically reduced by the following two reactions:

$$3Mn_4O_7 + 10K^+ + 10e + 5H_2O \rightarrow 4Mn_3O_4 + 10KOH$$

$$Mn_4O_7 + 6K^+ + 6e + 7H_2O \rightarrow 4Mn(OH)_2 + 6KOH$$

Step 3.—The insoluble product of the second step then becomes the depolarizer and is electrochemically reduced in this manner:

$$Mn_3O_4 + 2K^+ + 2e + 4H_2O \rightarrow 3Mn(OH)_2 + 2KOH$$

Step 1 occurs during the first part of the discharge while the working voltage falls from the initial value of 1.46 to 1.20. Step 2 apparently operates in the working voltage range of from 1.20 to 0.95. Step 3 occurs in the range below 0.95 v to the complete reduction of the oxide to $Mn(OH)_2$. Much of this last part of the discharge often occurs at a working voltage of 0.4-0.5 v or lower.

Manuscript received March 10, 1959. This paper was prepared for delivery before the Ottawa Meeting, Sept. 28-Oct. 2, 1958.

Any discussion of this paper will appear in a Discussion Section to be published in the June 1960 JOURNAL.

REFERENCES

1. N. C. Cahoon, R. S. Johnson, and M. P. Korver, *This Journal*, **105**, 295 (1958).
2. J. J. Lingane and Robert Karplus, *Ind. Eng. Chem., Anal. Ed.*, **18**, 191 (1946).
3. W. S. Herbert, *This Journal*, **99**, 190C (1952).
4. W. F. Cole, A. D. Wadsley, and Allan Walkley, *Trans. Electrochem. Soc.*, **92**, 133 (1947).
5. J. W. Gruener, *Am. Min.*, **32**, 654 (1947); Cyrus Klingsberg, "The System Mn-O-OH," Ph.D. Thesis, Pennsylvania State University, 1958.

High-Temperature Reaction Rates of Several Metals with Hydrogen Chloride and Water Vapor

Milton Farber

Research Laboratories, Rocket Power Inc., Pasadena, California

ABSTRACT

An experimental study has been made of the high-temperature reaction rates of various metal filaments with HCl and H_2O vapors and mixtures of the two. Measurements were made by an electrical method in which the change in resistance of the metal filament was related to the loss in pure metal due to the vapor-metal reaction. Measurable reaction rates were determined for both nickel and iron in a temperature range from 1000° to 1600°K. Specific reaction rate constants and apparent activation energies are presented. The reaction rates of tungsten with H_2O vapor were measured in a temperature range from 1600° to 2000°K. The reaction rates of chromium, Inconel, stainless steel 18-8, and tungsten did not proceed at a measurable rate in either pure HCl or in mixtures of HCl and H_2O. Nickel, copper, Inconel, and stainless steel 18-8 did not react appreciably with water vapor at temperatures approaching the melting points. The reaction rates for iron in pure HCl varied from 0.03 to 0.04% area loss per second over the temperature range investigated with an apparent activation energy of 10.5 kcal/mole. The reaction rates of iron in mixtures of HCl and H_2O varied from 0.08 to 0.17% area loss per second in the same temperature range with an apparent activation energy of 8.5 kcal/mole. Reaction rates of nickel in pure HCl varied from 0.005 to 0.03% area loss per second in the temperature range of 1000° to 1600°K with an apparent activation energy of 13 kcal/mole. The reaction rates of nickel in the HCl and H_2O mixtures varied from 0.004 to 0.03% area loss per second in the same temperature range with an apparent activation energy of 22 kcal/mole below 1300°K and 13 kcal/mole above this temperature. Reaction rates of iron in H_2O vapor varied from 0.002 to 0.05% area loss per second from 1120° to 1415°K with an activation energy of 28 kcal/mole. Reaction rates of tungsten in H_2O vapor varied from 0.02 to 0.03% area loss per second from 1700° to 2000°K with an activation energy of 14.5 kcal/mole.

In the field of high-temperature reactions of gases and metals, reaction rates are measured in terms of seconds as compared to days and years for reactions between metals and gases at conventional temperatures. This paper is the third in a series of investigations of the reaction rates of several metals with the combustion products of chemical propellants. Previous papers (1, 2) include the study of several metals with H_2S, SO_2, and NO at a temperature range from 1000°-2000°K.

Concerning the reactions of metals with HCl some previous work of a qualitative nature has been reported. A few investigators have studied this reaction by allowing the metal to remain in the HCl atmosphere for a period of time and obtaining the corrosion rate by the loss in weight of the metal (3, 4). Brown, DeLong, and Auld (5) studied the corrosion rates of nickel, platinum, gold, Inconel, stainless steel, Monel, copper, iron, and several nickel and chromium alloys in dry HCl and also in a mixture of HCl containing 0.2% H_2O. They found that nearly all the metals, with the exception of gold and platinum, are corroded quite readily at fairly low temperatures and that the addition of the water vapor increases the corrosion rate only slightly.

When a metal is corroded in an atmosphere of either dry or wet hydrogen chloride, the reaction products are usually the metal chloride and hydrogen as:

$$M + HCl = MCl + \tfrac{1}{2}H_2$$

In the presence of water vapor the reaction can become quite complicated because of the possible formation of other compounds of the metal besides the chloride.

The dissociation of water to H_2 and OH radicals is less than 1% at temperatures below 2000°K, while

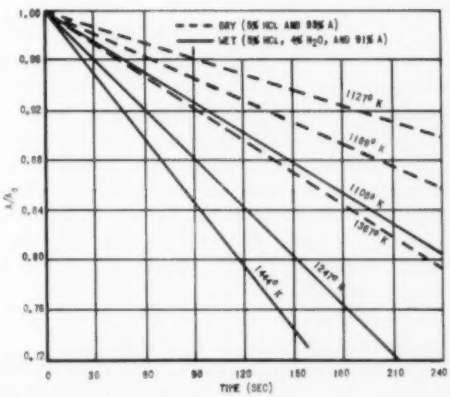

Fig. 1. Corrosion rate of Fe with dry and wet HCl vs. time

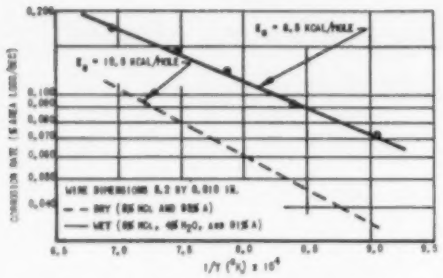

Fig. 2. Corrosion rate of Fe with dry and wet HCl as function of 1/T.

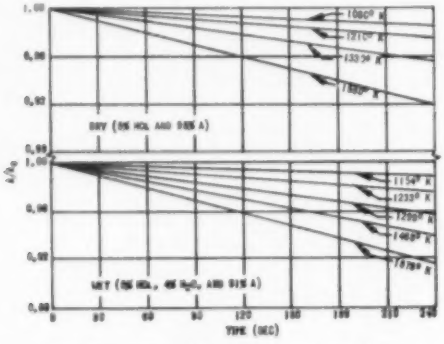

Fig. 3. Corrosion rate of Ni with dry and wet HCl vs. time

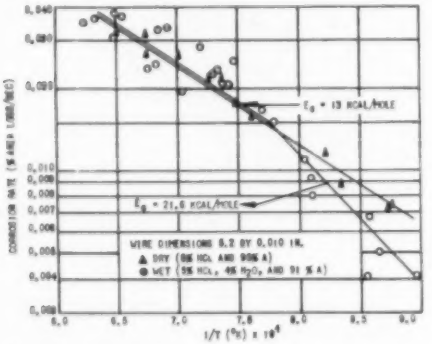

Fig. 4. Corrosion rate of Ni with dry and wet HCl as function of 1/T.

the dissociation of water to O_2 and H_2 does not become appreciable below 3000°K.

Experimental Procedure

The author (1, 2) has previously employed the method presented in this paper for measuring the reaction rates of various metals with H_2S, SO_2, and NO and the apparatus has been described. Garner, Gray, and Stone (6) studied the reaction rate of copper with oxygen by measuring the increase in resistance of a copper film which was plated on the walls of a glass bulb. Wilson (7) and Hudson (8) studied corrosion rates by measuring the change in electrical conductivity of flat metal strips. The method employed here and described in detail earlier (1) is concerned with the measurement of the change in resistance of a metal filament (hot wire) of 0.010 in. diameter in a corrosive medium. Since the corrosion rate is obtained directly from the resistance change, a recording mechanism is necessary to indicate the current and voltage across the filament. The arrangement of the equipment used to conduct rate experiments has been described previously (2).

In order to obtain uniform corrosion of the wire, it is necessary to use filaments which have been accurately machine-drawn. Thus, hot spots can be eliminated and consistent burnout times obtained, justifying the resistance method for measuring corrosion rates.

Theoretical corrosion rate laws have been derived (2) for these cylindrical wires. These resulted in the following rate laws for

Table I. Initial reaction rates of Fe and Ni with dry and wet HCl

Metal	T, °K	(1/T) x 10⁴	k, % area loss/sec
	Gas mixture: 95% argon and 5% HCl		
Iron	1127	8.87	0.037
	1184	8.44	0.042
	1198	8.34	0.053
	1222	8.18	0.064
	1300	7.69	0.068
	1305	7.66	0.083
	1388	7.20	0.087
Nickel	1060	9.44	0.0053
	1140	8.76	0.0073
	1146	8.73	0.0073
	1195	8.37	0.0087
	1210	8.27	0.0113
	1313	7.61	0.0153
	1330	7.52	0.0173
	1355	7.38	0.0213
	1373	7.28	0.0213
	1419	7.07	0.0260
	1486	6.73	0.0260
	1550	6.48	0.0320
	Gas mixture: 91% argon, 5% HCl, and 4% H_2O		
Iron	1105	9.05	0.075
	1186	8.43	0.092
	1274	7.84	0.122
	1335	7.49	0.142
	1444	6.93	0.172
Nickel	1115	8.97	0.0042
	1154	8.67	0.0050
	1162	8.60	0.0067
	1167	8.57	0.0042
	1231	8.12	0.0080
	1233	8.11	0.0092
	1241	8.05	0.0108
	1255	7.97	0.0075
	1283	7.80	0.0150
	1299	7.70	0.0167
	1333	7.50	0.0233
	1340	7.47	0.0250
	1347	7.42	0.0208
	1354	7.38	0.0192
	1355	7.38	0.0208
	1360	7.35	0.0233
	1391	7.19	0.0283
	1445	6.92	0.0333
	1460	6.85	0.0325
	1528	6.55	0.0367
	1543	6.48	0.0308
	1543	6.48	0.0375
	1578	6.33	0.0358
	1608	6.22	0.0341

parabolic

$$A/A_o = 1 - 2\sqrt{\frac{2\pi kt}{A_o}} + \frac{2\pi kt}{A_o} \qquad [1]$$

rectilinear

$$A/A_o = 1 - 2(\pi/A_o)^{1/2}\, kt + \pi/A_o k^2 t^2 \qquad [2]$$

logarithmic

$$A/A_o = 1 - 2(\pi/A_o)^{1/2} \ln (1+kt) + \pi/A_o \ln (1+kt)^2 \qquad [3]$$

The results obtained for the metals studied yield an experimental rate law of

$$A/A_o = 1 - k/100\, t$$

where: A is the cross-sectional area of wire remaining at time t, A_o is the initial area of wire, and k is per cent area change per second.

This expression is similar to the logarithmic rate law for thin coatings and also to the rectilinear rate law for initial corrosion, wherein the third term is small compared to the second.

It was shown in the previous papers (1, 2) that the conductivity of oxide coatings was negligible in comparison to that of the pure metal even at high temperatures (9). However, in the case of the chlorides, metal chlorides are usually in the vapor phase at the temperatures in question and the surface remains essentially clean during the course of the experiment.

The effect of the solubility of the gases on the resistance of the metal filaments investigated was negligible since there was no discernible change in their resistance at temperatures just below the point of corrosion. However, it was not possible to study the corrosion rates of metals such as zirconium or titanium because the solubility of oxygen and nitrogen changed their resistivities to such an extent that the change in resistance due to corrosion could not be measured.

Results

Reaction Rates of Metals with HCl

Reaction rates of iron with HCl.—Corrosion rates of iron were investigated in both dry HCl (95% A-5% HCl) and wet HCl (91% A-5% HCl-4% H_2O) over a range of temperature from 1100° to 1450°K. The results of the corrosion rates are shown as a function of time in Fig. 1. As may be seen from this figure, the corrosion rate of iron in the wet HCl is slightly faster than in the dry HCl. This fact would tend to indicate that the presence of water speeds up the reaction. In Fig. 2, the logarithm of the rate is plotted against the reciprocal of the absolute temperature. The activation energies are 8.5 and 10.5 kcal for the wet and the dry HCl, respectively. The rate constants as functions of the temperature are given in Table I.

Reaction rates of nickel with HCl.—The corrosion rate of nickel was also investigated in both dry and wet HCl mixtures over a temperature range from 1050° to 1600°K. The rates are given in Fig. 3. The corrosion of nickel with dry HCl shows a slightly higher rate than with wet HCl, particularly in the lower temperature range, as can be seen from the plot of the logarithm of the corrosion rate as a function of the reciprocal of the absolute temperature shown in Fig. 4.

The activation energy for the wet HCl is of the order of 22 kcal/mole for temperatures below 1300°K and decreases to 13 kcal/mole above this temperature. This latter value is approximately the same as for the dry HCl over the entire temperature range covered. The rate constants for the corrosion rates of nickel in both dry and wet HCl are given in Table I. The rates are of the order of approximately 20% of those for iron in the same gas mixtures.

Table II. Initial reaction rates of Fe and W with H_2O

Metal	T, °K	(1/T) x 10^4	k, % area loss/sec
Gas mixture: 95% argon and 5% H_2O			
Iron	1122	8.91	0.0020
	1195	8.36	0.0070
	1202	8.31	0.0085
	1253	7.98	0.0105
	1280	7.81	0.0195
	1314	7.46	0.0260
	1415	7.06	0.0475
Tungsten	1685	5.93	0.0170
	1780	5.61	0.0233
	1800	5.55	0.0185
	1860	5.37	0.0200
	1870	5.34	0.0194
	1965	5.08	0.0313
	1995	5.01	0.0313

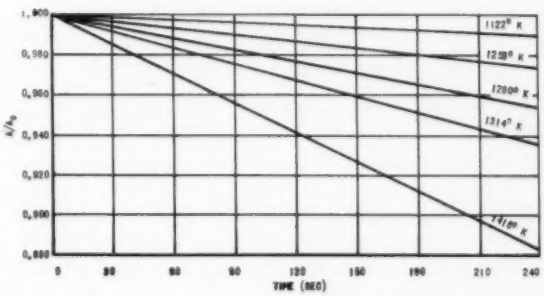

Fig. 5. Corrosion rate of Fe with H_2O vs. time

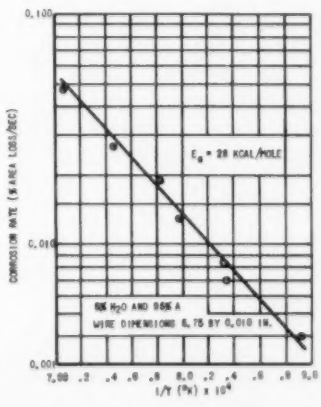

Fig. 6. Corrosion rate of Fe with H_2O as function of 1/T

Table III. Activation energies and rate constants of several metals with reactive gases[a]

Metal	Gas (Pressure = 1 atm) 5% HCl-95% A E_a (kcal/mole)	a	5% HCl-4% H_2O-91% A E_a (kcal/mole)	a	4% H_2O-96% A E_a (kcal/mole)	a
Fe	10.5 (1120 to 1400°K)	4.14	8.5 (1180 to 1430°K)	3.46	28 (1030 to 1400°K)	9.98×10^2
Ni	13.0 (1140 to 1540°K)	2.34	21.6 (1140 to 1300°K)	69.4	—	—
	—	—	13.0 (1300 to 1560°K)	2.41	—	—
W	—	—	—	—	14.5 (1700 to 2000°K)	1.25

[a] E_a = activation energy; a = exponential constant; $k = ae^{-E_a/RT}$.

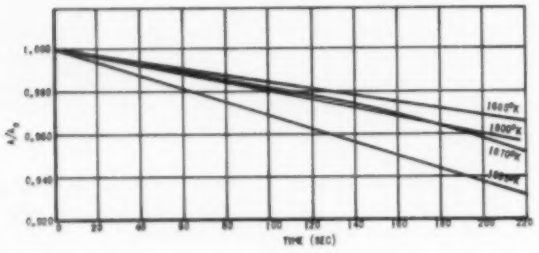

Fig. 7. Corrosion rate of W with H_2O vs. time

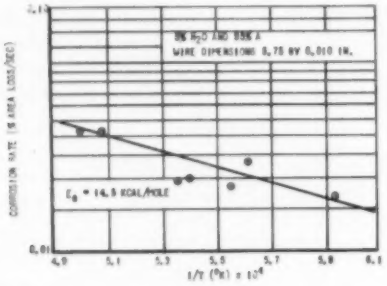

Fig. 8. Corrosion rate of W with H_2O as function of 1/T

Reaction Rates of Several Metals with Water Vapor

Several metals including iron, tungsten, nickel, copper, Inconel, and stainless steel 18-8 were tested in a gas mixture containing 95% A and 5% H_2O vapor. Iron and tungsten were the only metals of the group that corroded at a measurable rate at temperatures approaching the melting points.

Reaction rates of iron with water vapor.—Corrosion rates of iron in a mixture of 95% A and 5% H_2O vapor were measured in a temperature range of 1100° to 1400°K. Corrosion rates are plotted against time in Fig. 5. A plot of the logarithm of the corrosion rate against the reciprocal of the absolute temperature gives an activation energy of 28 kcal/mole (Fig. 6). The rate constants k, which are listed in Table II, vary from 0.0020 (% area loss/sec) at 1120°K to 0.047 at 1415°K.

Reaction rates of tungsten with water vapor.—The corrosion of W in H_2O does not become appreciable until temperature of 1600°K is attained. The corrosion rates of tungsten in a gas mixture of 95% A and 5% H_2O vapor were measured in the temperature range from 1685° to 1995°K. At the higher temperatures the dissociation of H_2O to H_2 and OH is in the neighborhood of 0.1%. The curves of corrosion rate vs. time are shown in Fig. 7. The plot of the logarithm of the rate vs. $1/T$ gives an activation energy of 14.5 kcal/mole (Fig. 8). The rate constants listed in Table III vary from 0.0170 (% area loss/sec) at 1685°K to 0.0313 at 1995°K.

Manuscript received Aug. 9, 1957. Some of the laboratory work for this paper was performed at the Jet Propulsion Laboratory, California Institute of Technology under Contract No. DA-04-495-ORD 18, sponsored by the Department of the Army, Ordnance Corps.

Any discussion of this paper will appear in a Discussion Section to be published in the June 1960 JOURNAL.

REFERENCES

1. M. Farber and D. M. Ehrenberg, *This Journal*, **99**, 427 (1952).
2. M. Farber, A. J. Darnell, and D. M. Ehrenberg, *ibid.*, **102**, 446 (1955).
3. W. Z. Friend and B. B. Knapp, *Trans. Am. Inst. Chem. Engrs.*, **39**, 731 (1943).
4. B. Pershke and L. Pecherkin, *Khimstroi*, **6**, 140 (1934).
5. M. H. Brown, W. B. DeLong, and J. R. Auld, *Ind. Eng. Chem.*, **39**, No. 7, 839 (1947).
6. W. E. Garner, T. J. Gray, and F. S. Stone, *Proc. Roy. Soc. London*, **A197**, 294 (1949).
7. E. Wilson, *Proc. Phys. Soc. London*, **39**, 15 (1926).
8. J. C. Hudson, *ibid.*, **40**, 107 (1928).
9. S. Veil, Thesis, Paris (1920); International Critical Tables, 4, p. 153.

The Electrochemical Behavior and Passivity of Titanium

Milton Stern and Herman Wissenberg

Metals Research Laboratories, Union Carbide Metals Company, Division of Union Carbide Corporation, Niagara Falls, New York

ABSTRACT

In the active condition, corrosion of titanium is controlled by activation polarization. The metal presents a surface with a low exchange current for a variety of electrochemical reactions. Low exchange currents are not conducive to establishment of passivity. However, this is overcome by unusually active critical potentials for passivity. This accounts for the ease with which titanium is passivated by many substances which are only slightly oxidizing. It also explains the ease with which the metal can be protected anodically by galvanic coupling to other metals and alloys. Anodic deposition of thick titanium oxide films is observed under some experimental conditions.

The mechanism of passivating-type inhibitors has been described (1) solely in terms of the kinetics of the various electrochemical processes which occur, without the necessity for reference to the nature of the passive film. The environmental parameters which are pertinent to the achievement of passivity are the exchange current, Tafel slope, and limiting diffusion current for cathodic processes. Passivity is favored by high values of exchange current and limiting diffusion current and by low values for the Tafel slope. The important parameters related to the metal are the critical anodic current and the critical potential for passivity. A low value of critical anodic current and a relatively active critical potential favor passivity.

Titanium shows active-passive behavior similar to stainless steel except that it is not affected adversely by chloride ion and does not exhibit transpassive behavior. This work was done to obtain data which would relate the anodic behavior of Ti to the parameters of temperature and acid concentration. Such information should help in understanding passivity of Ti and permit more efficient use of passivating inhibitors.

Experimental Procedure

Electrodes, glass cells, and methods for measuring potential were generally the same as those reported elsewhere (2) except that anodic polarization measurements were conducted with an Analytical Instruments Company[1] potentiostat, an electromechanical device. It was necessary to use the same material for the test electrode and for a potentiostat reference electrode and to place the two electrodes in the same solution, since the potentiostat does not operate properly if a high impedance exists between these electrodes. Auxiliary electrodes of the same material as the test electrode were placed directly in the cell. All electrodes were aged for about 30 min in the solution before the first measurement. Potentials were measured by means of a Luggin probe to minimize errors caused by *IR* drop. Potentials were measured against a saturated calomel electrode external to the cell at room temperature. No effort was made to correct for liquid junction potentials or temperature effects when the solution was hot.

In systems where hydrogen was used, the gas was purified with Cu at 500°C followed by Pt and Pd catalysts. The solution was further purified by preelectrolysis for 3 hr on a Ti cathode held at −1.0 v vs. saturated calomel with the potentiostat. The current density during pre-electrolysis was greater than 80 ma/cm^2. In this case, auxiliary electrodes were external to the cell and connected to it by salt bridges.

The Ti metal was of commercial purity containing 0.032% C and 0.13% oxygen.

Behavior of Hydrogen-Saturated H_2SO_4

Figure 1 shows anodic and cathodic polarization curves for Ti in hydrogen-saturated 20% H_2SO_4 at

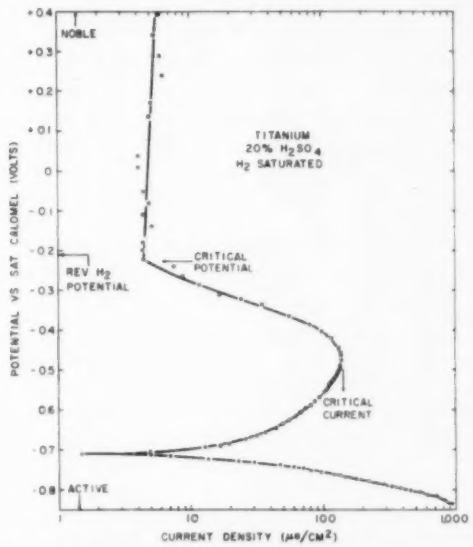

Fig. 1. Anodic and cathodic behavior of Ti in room-temperature, hydrogen-saturated 20% H_2SO_4.

[1] Bristol, Connecticut.

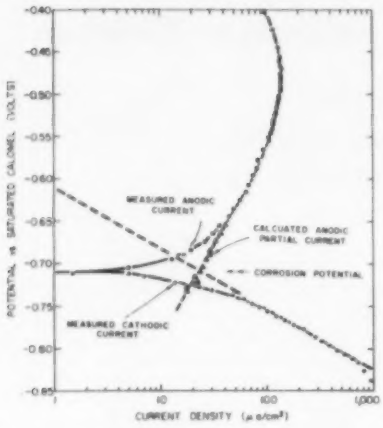

Fig. 2. Expanded view of Fig. 1 showing the calculated anodic polarization curve of Ti.

room temperature. The reversible hydrogen potential of this solution, measured with platinized Pt, is −0.21 v vs. saturated calomel. Polarization data were obtained with the potentiostat by starting at a potential of −0.85 v and gradually increasing the potential in the noble direction. The cathodic curve exhibits a Tafel slope of 0.07 v and an exchange current of only 1.9 (10^{-12}) amp/cm². Relatively small changes in Tafel slope will have a marked effect on exchange current, since extrapolation to the reversible hydrogen potential is made over a potential range of about 0.6 v. Thus, the measured exchange current could be in considerable error. It is evident, however, that the hydrogen ion reduction reaction on Ti is accompanied by a high overvoltage (approaching that of Hg) because of the extremely small exchange current. This agrees with other observations (3, 4).

The anodic data show a critical current for passivity of 140 μa/cm². The critical potential for passivity is about −0.23 v vs. saturated calomel which is 20 mv more active than the potential of Pt in the hydrogen-saturated 20% H_2SO_4 solution. If one defines passivity as the state where the potential of a metal is more noble than the critical potential shown in Fig. 1, then it becomes evident that Ti can show stable passive behavior in solutions which contain a redox system no more oxidizing than the hydrogen ion-hydrogen gas system. Passivity in hydrogen-saturated solutions is an unusual phenomenon which is not observed in Fe- or Ni-base alloy systems. The relatively active critical potential exhibited by Ti explains, in part, the ease with which this metal is passivated by many oxidizing inhibitors.

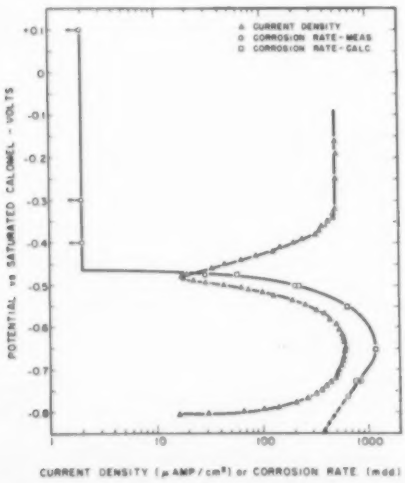
Δ CURRENT DENSITY
○ CORROSION RATE - MEAS
□ CORROSION RATE - CALC
POTENTIAL vs SATURATED CALOMEL - VOLTS
CURRENT DENSITY (μ AMP/cm²) or CORROSION RATE (mdd)

Fig. 3. Current density and corrosion rate at controlled potentials for Ti in boiling 2% H_2SO_4 containing 5% Na_2SO_4.

The data of Fig. 1 permit an examination of the dissolution kinetics of Ti in the active potential region to determine if they are consistent with presently accepted views on electrode kinetics involving activation overvoltage. Figure 2 shows an expanded view of the data close to the corrosion potential. Calculated values of the dissolution rate of Ti as a function of potential are shown as triangles. The methods used for this calculation are similar to those already described (2). The points more noble than the corrosion potential were obtained by summing the extrapolated rate of hydrogen reduction and applied anodic current at any given potential. The points on the active side of the corrosion potential were obtained by subtracting the applied cathodic current from the extrapolated rate of hydrogen reduction at any given potential.

It is evident that in this potential region the dissolution kinetics are controlled by activation polarization with a Tafel slope of 0.22 v. While this value is high, the kinetics near the corrosion potential cannot be considered unusual. Thus, the phenomena associated with passivity are not evident near the corrosion potential but become significant near the potential region associated with the critical current for passivity.

Correlation of Polarization Data with Weight Loss Measurements

An anodic polarization curve, such as that shown in Fig. 1, is expected to represent the dissolution rate of Ti as a function of potential, except in the region close to the corrosion potential where the measured current is significantly less than the dissolution rate as illustrated in Fig. 2. To check this, data were obtained with Ti in boiling 2% H_2SO_4 containing 5% Na_2SO_4, where corrosion rates are higher than at room temperature and more easily measured.

Figure 3 shows the anodic polarization curve obtained. The portion below the critical potential for passivity is as expected. The current rises to some maximum value (the critical current for passivity) and then falls to a low value at the critical potential for passivity. Weight loss measurements in the same environment utilized separate electrodes, each held at a controlled potential for 18-24 hr. Continuous recording during these measurements revealed long-time current variations. These are attributed to changes in the environment caused by accumulating corrosion products from the sample, the auxil-

iary electrodes, and the potentiostat reference electrode. Assuming that Ti corrodes to form trivalent ions, integration of each current-time curve leads to a calculated corrosion weight loss which is also plotted on Fig. 3 (squares) along with the measured weight loss (circles).

It is evident from Fig. 3 that dissolution rate as a function of potential closely parallels the anodic polarization curve in the potential region more active than the critical potential for passivity. Quantitative agreement between the measured corrosion rates and the anodic polarization curve is precluded by differences in experimental procedure. For example, each point on the polarization curve represents only 3 min at that potential contrasted to a minimum of 18 hr for a weight loss measurement.

Unexpected behavior is found in the anodic polarization curve above the critical potential for passivity. Rather than remaining relatively constant with increasing potential as shown in Fig. 1, the current again rises and finally reaches a limiting value. This does not represent the anodic behavior of Ti, but is an artifact resulting from the experimental procedure used. This can be shown in the following manner. Electrodes held at constant potential in this region show a considerable weight gain and develop a thick oxide coating which is not particularly adherent. Scraping the oxide off accounts for all of the weight gain within the error of the technique, and the final sample shows a corrosion rate of less than 2 mdd. Therefore, anodic current measured in this region does not represent oxidation of metal but rather represents a different oxidation process. The most likely process is electrodeposition of oxide in accordance with a reaction of the type $Ti^{+3} + 2H_2O \rightarrow TiO_2 + 4H^+ + e$. It is quite possible that this is not the specific reaction which occurs, since lower oxides could also have been produced. In any event, it is clear that corrosion products are plated onto the anode surface in the form of oxides. The vertical line on the polarization curve probably represents the limiting diffusion current for the process.

The current associated with oxide deposition may obscure the true value of the critical potential for passivity. The critical potential shown in Fig. 3 could be slightly more active than the true value. This error is probably not significant as evidenced by the weight loss data.

Since the corrosion rate of Ti in the potential region of oxide deposition was less than 2 mdd (the experimental error in weight change), the points on Fig. 3 are shown at 2 mdd with arrows indicating the rate is less than this value. Thus, above the critical potential for passivity, the dissolution rate is very slow.

Cotton (5) has measured corrosion rate as a function of potential for Ti in 40% H_2SO_4 at 60°C. His data are similar to those shown here and extend to 2 v more noble than the saturated calomel electrode.

Anodic Polarization by Galvanic Coupling

Anodic passivation of Ti by means of an externally applied potential is described above. Titanium can also be passivated by galvanic coupling (5-7) with some metal or alloy whose potential is more noble than the critical potential for passivity of Ti in the given environment. The mixed potential of the resulting couple must also be more noble than the critical potential. Since the couple mixed potential is dependent on cathodic polarization, large cathode areas should favor passivation of Ti.

Table I. Effect of galvanically coupling titanium to various cathodic materials in boiling H_2SO_4 solutions

Couple	Area ratio A (Ti) / A (Cathode)	Weight loss of titanium (mdd) Boiling* 1% H_2SO_4	Boiling† 3% H_2SO_4 + 5% Na_2SO_4	Boiling‡ 5% H_2SO_4 + 5% Na_2SO_4
Ti		1400	1800	2900
Ti-(18-8)	1	0		
	2	10		
	6.6	6		
Ti-(Hastelloy alloy F)	1	0		
	12	2		
Ti-C	0.2	0	0	3600
	0.5		0	
	1		1200	
Ti-Pt	0.25			21
	1			65
	2			65
	4			108
	35			1700

* Critical potential for passivity of Ti is −0.45 v vs. saturated calomel.
† Critical potential for passivity of Ti is −0.42 v vs. saturated calomel.
‡ Critical potential for passivity of Ti is −0.34 v vs. saturated calomel.

Table I shows the effect of coupling Ti to Pt, C, 18-8 stainless steel, and Hastelloy alloy F in several environments as a function of the ratio of Ti area to cathode area. All the above materials exhibit potentials in these environments which are more noble than the critical potentials for passivity of Ti. In these experiments, no effort was made to estimate surface roughness factors, and all areas are calculated from geometric measurements assuming smooth surfaces. Results show that all of these materials can passivate Ti if sufficient cathode area is present. The more aggressive the environment, the greater the cathode area necessary to passivate. It is important to note that stainless steel and Hastelloy alloy F are both electrochemically active in boiling 1% H_2SO_4. However, their active mixed potentials are still sufficiently more noble than the critical potential for passivity of Ti to produce passivity when galvanically coupled to this metal.

Effect of Temperature on Dissolution Kinetics

Since temperature is known to affect the behavior of passivating inhibitors, it is important to establish how temperature affects those metal dissolution parameters which determine when stable passivity can be achieved.

Figure 4 shows the anodic polarization behavior of Ti in hydrogen-saturated 5% H_2SO_4 containing 5% Na_2SO_4. The critical current for passivity increases considerably as temperature is increased from 50° to 95°C. The critical potential for passivity is not significantly affected. In general, temperature

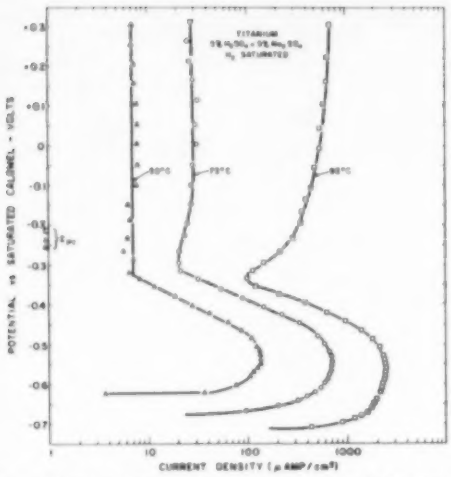

Fig. 4. Effect of temperature on the anodic behavior of Ti in hydrogen-saturated 5% H_2SO_4 containing 5% Na_2SO_4.

serves only to increase reaction rates, shifting the curves to higher current values with an increase in temperature.

At 95°C, where corrosion product build-up is faster, oxide deposition is again observed as evidenced by the shape of the polarization curve in the passive region. At 50° and 75°C, the oxidation rate of corrosion products is probably not significant, and passive currents represent the dissolution rate which also increases with temperature.

The measured potential of platinized Pt as a function of temperature is also shown on Fig. 4. It is important to note for subsequent discussion that the critical potential for passivity of Ti is again more active than the reversible hydrogen potential for this system.

Effect of Acid Concentration on Dissolution Kinetics

Figure 5 shows the anodic polarization behavior of Ti in various concentrations of boiling H_2SO_4 containing 5% Na_2SO_4. Paralleling the effect of temperature, increasing acid concentration markedly increases the critical current for passivity. However, the critical potential for passivity and the potential at the critical current are shifted in the noble direction.

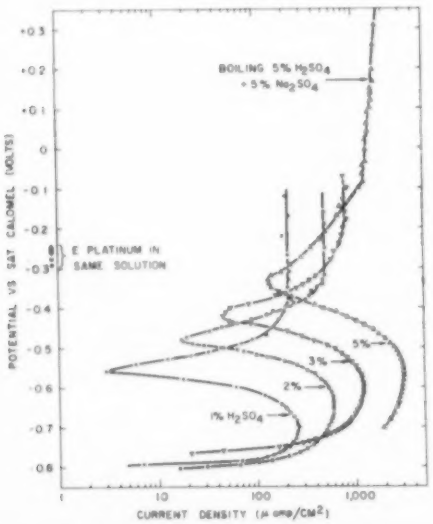

Fig. 5. Anodic behavior of Ti in boiling H_2SO_4 solutions containing 5% Na_2SO_4.

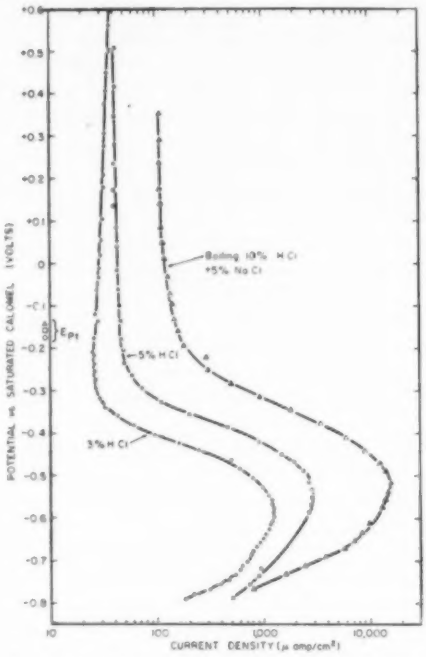

Fig. 6. Anodic behavior of Ti in boiling HCl solutions containing 5% NaCl.

Corrosion product build-up in the solution is sufficiently fast at the boiling point to cause oxide deposition in the passive region. Thus, as described above, anodic current in the passive region does not represent the effect of acid concentration on passive corrosion rate. Rather, the vertical section probably represents the limiting diffusion current for the deposition process which increases with acid concentration because corrosion product build-up increases.

Oxide deposition is not observed in HCl as shown in Fig. 6, where it is evident that the passive corrosion rate increases with acid concentration.

Discussion and Conclusions

In the active condition, corrosion of Ti is controlled by activation polarization. The metal exhibits a particularly high hydrogen overvoltage (low exchange current). In general, it presents a surface with a low exchange current for a variety of electrochemical reactions as evidenced by measurements of rates of ferric ion reduction and oxygen evolution (8). Low exchange currents are not conducive to establishment of passivity. However, this is overcome by unusually active critical potentials for passivity. The critical potential for passivity of Ti is about 0.6 v more active than the corresponding value for Fe and about 0.1-0.2 v more active than the value for stainless steel. The exact differences, of course, are dependent on the environment used

for comparison. This, in large part, accounts for the ease with which Ti is passivated by many substances which are only slightly oxidizing. It also explains the ease with which the metal can be protected anodically by galvanic coupling to other metals and alloys.

Potentiostatic measurements in H_2SO_4 containing corrosion products of Ti show that increasing anodic polarization of Ti in the passive potential region results in an increasing current. This current is caused by anodic deposition of titanium oxide rather than an increasing Ti corrosion rate.

Data presented here show that, as temperature increases, the concentration of inhibitor required to passivate increases. Since the inhibitor concentration must provide a limiting diffusion current greater than the critical current for passivity (1), measurements of the type presented here permit an estimate of the minimum concentration of inhibitor required to attain passivity of a given system as temperature is raised.

The situation is similar for an increase in acid concentration except that, since the critical potential for passivity becomes more noble, the inhibitor must exhibit a greater oxidizing character (more noble reversible potential) for more acid environments.

For anodic protection of Ti by galvanic coupling to a cathodic metal or alloy, data presented here assist in the determination of the couple area ratio required to produce passivity of Ti. The cathodic polarization behavior of the cathode member of the couple also must be known and its area made sufficiently large so that the mixed potential of the couple is more noble than the critical potential of Ti in the environment.

Acknowledgment

The authors acknowledge the skillful assistance of E. J. Bartolomei who obtained much of the data presented here.

Manuscript received April 6, 1959. This paper was prepared for delivery before the Columbus Meeting, Oct. 18-22, 1959.

Any discussion of this paper will appear in a Discussion Section to be published in the June 1960 JOURNAL.

REFERENCES

1. M. Stern, *This Journal*, **105**, 638 (1958).
2. M. Stern, *ibid.*, **102**, 609 (1955); **104**, 391, 559 (1957).
3. S. Tajima, Y. Nakamura, and T. Mori, *J. Electrochem. Soc. Japan*, **22**, 513 (1954).
4. M. E. Straumanis, S. T. Shih, and A. W. Schlechten, *J. Phys. Chem.*, **59**, 317 (1955).
5. J. B. Cotton, *Chemistry & Industry*, p. 68, Jan. 18, 1958.
6. W. R. Buck, III and H. Leidheiser, *Nature*, **181**, 1681 (1958).
7. N. D. Tomashov, *Z. Elektrochem.*, **62**, 717 (1958).
8. M. Stern, *This Journal*, **104**, 600 (1957).

The Influence of Noble Metal Alloy Additions on the Electrochemical and Corrosion Behavior of Titanium

Milton Stern and Herman Wissenberg

Metals Research Laboratories, Union Carbide Metals Company, Division of Union Carbide Corporation, Niagara Falls, New York

ABSTRACT

Alloying of titanium with small amounts of noble metals markedly improves its corrosion resistance in reducing-type acids without any impairment of its high resistance to oxidizing media. The mixed potentials of titanium noble metal alloys are more noble than the critical potential for passivity of titanium in the same environment. Passivity is observed in hydrogen-saturated systems without the presence of a redox system more oxidizing than the hydrogen electrode. The mixed potential of titanium noble metal alloys is much more sensitive to traces of oxidizing agents than unalloyed metal.

Previous work (1) proposed that passivating-type inhibitors function primarily by creating a mixed potential more noble than the critical potential for passivity of the metal involved. The establishment of a potential more noble than some critical value is a basic concept which applies not only to inhibitors but also to the phenomenon of anodic protection (2) and prevention of corrosion by galvanic coupling to suitable cathode materials (3-5).

Anodic polarization under a variety of conditions shows that Ti exhibits unusually active values of critical anodic potential (5). Often, this potential is even more active than the reversible hydrogen potential of the solution. This permits establishment of passivity by alloying with elements having low overvoltage characteristics.

The purpose of this work is to describe the corrosion and electrochemical characteristics of these alloys.

Theory of Noble Metal Alloying to Obtain Passivity

According to what has already been described, passivity is obtained by producing a condition which results in a potential more noble than the critical potential for passivity. Without an externally applied potential, a metal in solution can attain a passive mixed potential only if the solution contains a redox system with a reversible potential more

noble than the critical potential for passivity of the metal. This is a necessary, but not sufficient, condition for stable passivity (1).

Alloying can contribute to the passivation of metals by two distinctly different principles:

1. Alloy addition may affect those metal dissolution parameters (the critical anodic current and the critical anodic potential) which, in turn, determine the ease of passivation. This is the effect which Cr has on Fe in the stainless steels. Increasing Cr content decreases the critical anodic current (6) and moves the critical anodic potential in the active direction (7,8).

2. Alloy addition may influence the reduction kinetics of the cathodic process. Mixed potentials in the passive potential region are favored by an increase in exchange current and a decrease in the cathodic Tafel slope (1).

An example of cathodic process influence was described by Tomashov (9). Alloying of 18% Cr-8% Ni stainless steel or 27% Cr stainless steel with Pt or Pd markedly improves corrosion resistance in room-temperature H_2SO_4 by facilitating the cathodic reaction. While it is not clear whether these experiments were done with intentional aeration of the acid, oxygen was most likely present in solution.

Passivation by alteration of cathodic process kinetics is of special interest when the critical anodic potential of the metal is more active than the reversible hydrogen potential of the solution. Under these circumstances, passivity theoretically can be achieved with the presence of a redox system no more oxidizing than the hydrogen electrode. Under conditions where the metal exhibits a relatively high hydrogen overvoltage, a passive mixed potential may not be obtained directly. However, passivity can be accomplished by alloying such a metal with an element which is essentially insoluble in the environment and which exhibits a high exchange current for the hydrogen ion reduction process. A small amount of corrosion should leave the alloy addition essentially in elemental form on the surface. The surface is now a bi-electrode, or galvanic couple, with one of the constitutents presenting a low-hydrogen overvoltage surface. This is shown schematically in Fig. 1 which may be considered typical of the behavior of Ti. The exchange current for the hydrogen reduction reaction of Ti is very small (5) resulting in an active mixed potential. When alloyed with a metal like Pt, regions with very high exchange currents are produced on the surface creating a mixed potential in the passive potential range. This results in a markedly reduced dissolution rate. Evidence for this is presented below.

Procedures

In general, electrochemical techniques and procedures were similar to those reported previously (5). Alloy buttons were prepared in an argon atmosphere by nonconsumable arc melting on a water-cooled Cu hearth. The buttons, weighing approximately 50 g, were melted three times, reduced in thickness about 50% by cold-rolling, and heat-treated at 1000°C in vacuum for 18-24 hr followed by furnace-cooling.

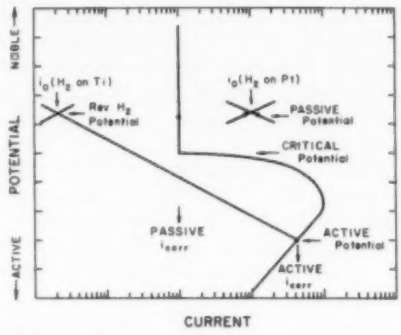

Fig. 1. Schematic diagram showing how alloying with a noble metal produces a passive mixed potential and a marked reduction in corrosion rate.

Corrosion Behavior

Table I shows the effect of ten alloy additions on the corrosion rate of Ti in boiling H_2SO_4 and HCl. Corrosion resistance is markedly improved in many cases. The best results are produced by Pt, Pd, Rh, and Ru; Os, Ir, and Re are intermediate in effect; Au is beneficial only in higher concentrations, while Ag and Cu are detrimental. As expected, the effectiveness of the various additions is roughly in the same order as their hydrogen overvoltage. Generally, Pt and Pd exhibit very low-hydrogen overvoltages, whereas Au, Ag, and Cu may be considered the relatively high-hydrogen overvoltage elements of those evaluated. The approximate exchange current densities (10) in HCl for the various metals are Pt (10^{-4}), Pd(10^{-5}), Rh(10^{-4}), Au(10^{-5} to 10^{-4}), Ag (10^{-7}), Cu(10^{-7}) amp/cm^2.

Table I. Effect of various alloy additions on corrosion resistance of Ti

Composition	Weight loss in 24 hr* (mil/yr)			
	Boiling H_2SO_4		Boiling HCl	
	1%	10%	3%	10%
Titanium	460	3950	242	4500
Ti + 0.064% Pt	<2	145	<2	128
Ti + 0.54% Pt	<2	48	3	120
Ti + 0.08% Pd	<2	166	3	100
Ti + 0.44% Pd	<2	45	<2	67
Ti + 0.1% Rh	<2	26	5	96
Ti + 0.5% Rh	3	48	<2	55
Ti + 0.1% Ru	3	187	5	280
Ti + 0.5% Ru	<2	48	<2	113
Ti + 0.11% Ir	<2	359	3	120
Ti + 0.60% Ir	<2	45	3	88
Ti + 0.10% Os	5	480	3	1820
Ti + 0.48% Os	<2	82	3	208
Ti + 0.11% Re	235	—	345	—
Ti + 0.36% Re	9	—	30	—
Ti + 0.11% Au	1050	—	1500	—
Ti + 0.48% Au	3	—	9	146
Ti + 0.04% Ag	500	—	334	—
Ti + 0.34% Ag	—	—	—	4850
Ti + 0.17% Cu	470	—	340	—
Ti + 0.44% Cu	660	—	550	—

* The possible weighing error of these tests is ±2 mil/yr.

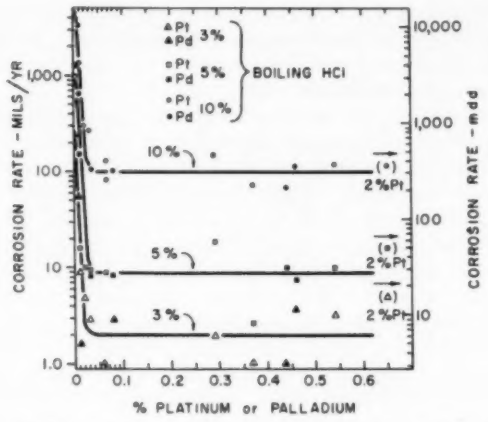

Fig. 2 Effect of Pt and Pd additions on corrosion rate of Ti in boiling HCl solutions.

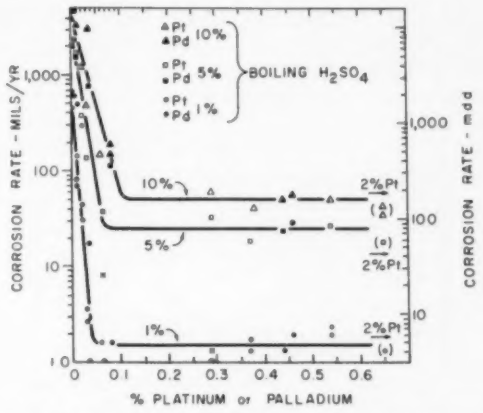

Fig. 3. Effect of Pt and Pd additions on corrosion rate of Ti in boiling H_2SO_4 solutions.

The qualitative theory of noble metal alloy additions described above does not permit an estimate of the alloy concentration required to produce a maximum effect. However, one would predict that, in a given environment, increasing the alloy concentration and noting the effect on corrosion rate should reveal a composition above which no additional benefit is produced. This is the concentration sufficient to produce a mixed potential more noble than the critical potential for passivity. One would also expect that insufficient alloy addition would be detrimental, since the mixed potential would move in the noble direction, yet remain in the active potential region.

Figure 2 shows the effect of Pt and Pd additions to Ti on corrosion rate in boiling HCl solutions. Both of these alloying elements apparently behave in a similar manner, and this observation was used to combine the data on one plot. It is evident that about 0.05% Pt or Pd reduces the corrosion rate by a factor of from 50 to 100. Increased concentrations of noble metals are not additionally beneficial. These data are the results of 24-hr corrosion tests. The sample size was such that a corrosion rate of about 2 mil/yr is within the possible weighing error of the test.

Figure 3 shows similar data in boiling H_2SO_4. In this case, it appears that more noble metal is required to achieve the maximum beneficial effect. Also, in this environment, Pd appears to be not quite as effective as Pt, although only one line is drawn through the points in each H_2SO_4 concentration.

As expected, alloy additions above some critical concentration do not further reduce corrosion rate. However, contrary to expectations, very small alloy additions do not increase the observed corrosion rate. This is because the observed corrosion rate is an average value for a 24-hr test. As will be shown below, these alloys are initially active and probably corrode at an accelerated rate. However, they become passive during the test so that the average corrosion rate is between that of active and passive Ti.

Data not presented here show that such alloying is not detrimental to behavior in highly oxidizing media, such as concentrated HNO_3 or ferric chloride. This is expected since Ti does not exhibit a transpassive potential region where the dissolution rate increases at quite noble potential values. Similar alloying in the case of stainless steels (9) is expected to be detrimental under highly oxidizing conditions because of the transpassive behavior of such alloys.

Electrochemical Behavior

Figure 4 shows potential-time data in boiling 1% H_2SO_4 for Ti and a series of Ti alloys containing various amounts of Pt. The data were recorded continuously using high impedance instrumentation. Note that all Pt-bearing alloys reach the passive potential region during the 24-hr test period. Those alloys containing the higher concentrations of Pt are passive from the very beginning of test, whereas the more dilute alloys remain active for some time prior to becoming passive. It is believed that during this active period the surface concentration of Pt is increasing as a result of corrosion until the area ratio is sufficient to produce a noble mixed potential. Anodic polarization of Ti in this environment, Fig. 5, shows a critical current of about 1000 μamp/cm^2

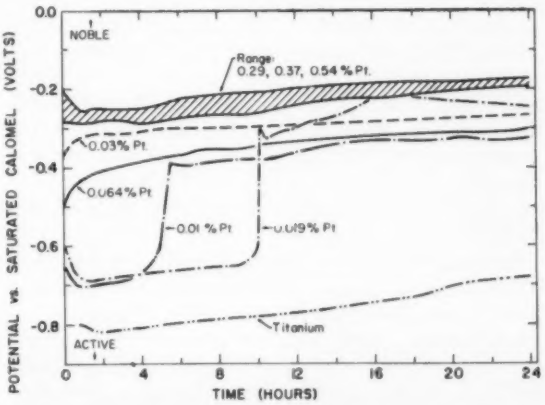

Fig. 4 Potential as a function of time for Ti alloyed with various concentrations of Pt in boiling 1% H_2SO_4.

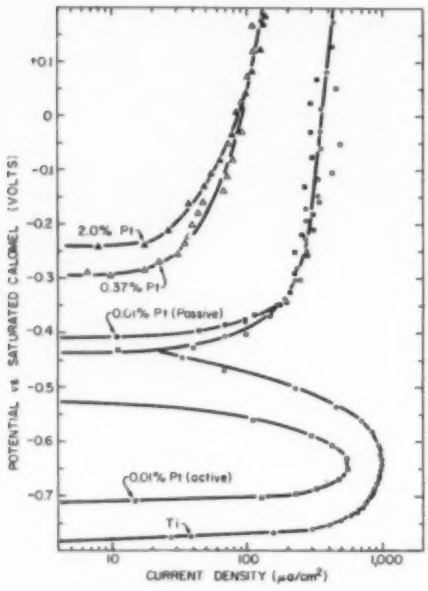

Fig. 5. Anodic polarization of Ti and Ti-Pt alloys in boiling 1% H_2SO_4.

at a potential of −0.64 v vs. saturated calomel. The critical anodic potential is about −0.44 v on the same scale. It is interesting to note in Fig. 4 that the two dilute alloys, 0.01% Pt and 0.019% Pt, which are active for a relatively long period, rapidly pass through the potential region where the polarization curve of Ti has a negative slope. Also, the rapid change in potential occurs when the electrodes have reached values of about −0.64 v. This indicates that this potential region is unstable for these alloys.

Figure 5 shows anodic polarization data for three alloys in boiling 1% H_2SO_4 compared with that of unalloyed Ti. If such measurements are conducted with the 0.01% Pt alloy soon after it is immersed in solution while its potential is still relatively active (see Fig. 4), the polarization curve (open squares) is essentially that of a typical active metal. However, if this alloy is immersed in solution overnight prior to anodic measurements, the data (solid squares) closely parallel the behavior of unalloyed Ti in the passive region. The 0.01% Pt alloy, initially in the active condition, shows negative (cathodic currents) in the potential region between about −0.53 and −0.44 v. This phenomenon has been described adequately by Edeleanu (2), and this observation is consistent with his explanation, since this alloy is expected to exhibit a higher exchange current for the hydrogen ion reduction reaction than unalloyed Ti.

Titanium alloys containing 0.37% or 2% Pt are passive very soon after immersion. Anodic polarization shows only passive behavior as expected. As shown earlier (5) in H_2SO_4 solutions containing appreciable quantities of corrosion products, measured currents in the passive potential region represent the rate of titanium oxide deposition rather than metal oxidation. Thus, currents observed for the 0.37% and 2% Pt alloy are less than that for Ti or the 0.01% Pt alloy because corrosion product build-up in solution (from the sample and the auxiliary electrodes) is slower.

According to the mechanism of protection obtained by noble metal alloying described above, one would expect that cathodic polarization of a Pt-containing alloy would cause a marked increase in corrosion rate. This was found with the 0.37% Pt alloy in boiling 1% H_2SO_4. The potential of this alloy is normally in the passive range between about −0.2 and −0.3 v. It was held at a potential of −0.55 ±0.05 v (see Fig. 5) for 19 hr with a potentiostat. The cathodic current required to accomplish this was very high (0.2-0.3 amp/cm²), presumably because of the high Pt content of the surface. The corrosion rate for this period was 110 mil/yr compared with normal corrosion rate of less than 2 mil/yr in this environment. This supports the mechanism proposed.

Ease of Passivation

Titanium alloyed with noble metals should show another particularly beneficial property. Such alloys should become passive in aggressive environments with concentrations of oxidizing agent insufficient to passivate unalloyed Ti.

A schematic polarization diagram which illustrates this property is shown in Fig. 6. The solid cathodic curve originating from i_{c_1} represents hydrogen ion reduction on Ti and produces an active mixed potential E_1. The solid cathodic curve originating from i_{ox} represents reduction of an oxidizing agent on Ti which produces either a passive potential at E_2' or an active potential E_2. Oxidation and reduction of the oxidizing agent on the alloy surface, where the noble metal content markedly raises the exchange current, are shown at i_{ox}. In this case, only one passive mixed potential, E_3, is obtained (1). Evidence for this behavior was obtained in the following experiments.

Corrosion measurements were obtained in H_2SO_4 and HCl at 190°C (374°F). Samples with areas of 2-3 cm² were sealed in heavy wall Pyrex tubes containing 40 ml acid solution. Prior to sealing the tubes, a stream of nitrogen was bubbled through the acid for about 2 hr and continued while the tube

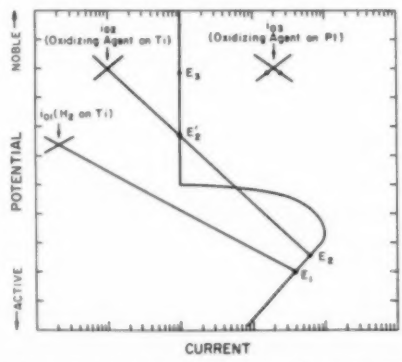

Fig. 6 Schematic polarization diagram showing influence of an oxidizing agent on the potential of Ti and Ti alloyed with a noble metal.

Table II. Effect of Pt and Pd alloy additions on the corrosion resistance of Ti in oxygen-free H_2SO_4 and HCl at 190°C (374°F)

Composition	Weight Loss,* mil/yr						
	H_2SO_4				HCl		
	1%	5%	10%	20%	3%	5%	10%
Ti	515	—	—	—	2250	—	—
Ti + 0.03% Pt	<2	<2	3.4	Diss	—	—	—
Ti + 0.29% Pt	<2	<2	3.3	11.5	<2	<2	890
Ti + 0.08% Pd	<2	<2	3.5	Diss	—	—	—
Ti + 0.44% Pd	<2	<2	5.0	12.0	<2	<2	1120

* One-period tests, 44-64 hr duration. The possible weighing error in these tests is ±2 mil/yr.

was being necked down. Although the gas inlet tube was removed just prior to sealing, the solutions cannot be considered completely oxygen-free. The tubes then were heated in a pressurized autoclave. The weight loss results for Ti and Ti alloyed with Pt and Pd are shown in Table II. Unalloyed Ti corrodes at very high rates, whereas Pt and Pd additions are quite effective in rather high concentrations of acid. The persistence of the noble metal effect at this high temperature is in itself quite important and can be explained in view of evidence (5) showing that temperature does not markedly affect the critical potential for passivity of Ti. What is most significant about these data is that the corrosion rates observed are considerably less than those obtained at the boiling point of the acids. Small quantities of oxygen present during the test are believed responsible for the lower corrosion rate at the higher temperature.

These data alone are probably not sufficient evidence for the general conclusion that noble metal alloying improves the susceptibility to passivation by oxidizing agents. More direct evidence was obtained by a combination of electrochemical and corrosion data. It was observed that in 20% H_2SO_4 at room temperature, unalloyed Ti shows unstable passivity when the solution is oxygen-saturated. This is shown in Fig. 7A. The potential oscillates in an unpredictable manner from a value only slightly more noble than the critical potential for passivity (shown in Fig. 7B) to an active value. The relatively active value of the passive potential of unalloyed Ti is due primarily to a particularly small

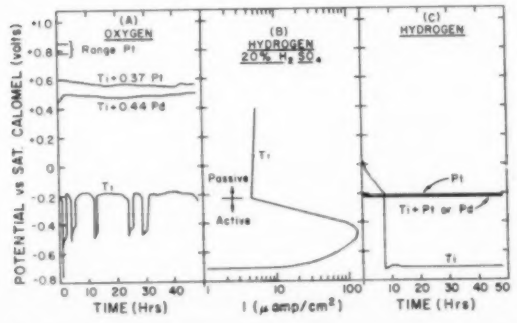

Fig. 7. Anodic behavior of Ti and electrode potential of Ti and Ti alloyed with Pt or Pd in 20% H_2SO_4 at room temperature.

value of exchange current for oxygen reduction on the Ti surface. Alloys containing Pt and Pd are 0.7-0.8 v more noble than unalloyed Ti and only about 0.3 v more active than Pt in the same solution. These data are an ideal illustration of the mechanism shown in Fig. 6.

Figure 7C shows potential-time behavior in hydrogen-saturated solution. Platinum exhibits the reversible hydrogen potential. Potentials of Ti containing Pt and Pd are within 25 mv of this value. The potential of unalloyed Ti, which initially had an air-formed film, is active. This illustrates the basic mechanism of noble metal alloy additions shown in Fig. 1.

Note in Fig. 7 that relatively stable potentials are not observed in the potential region where the anodic polarization curve has a negative slope. When the potential of passive Ti reaches the critical potential, it moves rapidly to active values. When active Ti reaches potentials close to that at the critical current, it moves rapidly to passive values. Also note that the potential of active Ti in oxygen-saturated solution is more noble than active Ti in hydrogen-saturated acid because of the combined cathodic reduction of oxygen and hydrogen ions.

Weight loss data for the electrodes whose behavior is described in Fig. 7A and C are shown in Table III. Alloys containing Pt or Pd are passive and exhibit negligible corrosion rates in either hydrogen- or oxygen-saturated acid. Unalloyed Ti is active in hydrogen-saturated solution and is intermittently active in oxygen-saturated solution. In the latter case, the weight loss is between that observed for the active and passive conditions.

These experiments in 20% H_2SO_4 support the concept that Ti containing noble metal alloy additions is much more sensitive to oxidizing agents than unalloyed metal. Data, which show that this extends to trace concentrations of oxidizing agents, were obtained by measuring the mixed potential of Ti and Ti alloys containing Pt as a function of ferric ion concentration in boiling 1% H_2SO_4. Measurements which were conducted in the manner described previously (1) are shown in Fig. 8. Titanium, which is initially active, requires a ferric ion concentration of about 0.2 mg/ml to passivate. Platinum-containing alloys which are already electrochemically passive in this environment (see Fig. 5) without ferric ion additions respond markedly to concentrations of the oxidizing agent which

Table III. Effect of O_2 and H_2 on corrosion resistance of Ti and Ti alloys in room temperature 20% H_2SO_4

Alloy	Gas	Weight loss, mil/yr
Ti	O_2	4*
	H_2	29
Ti + 0.37% Pt	O_2	<2†
	H_2	<2
Ti + 0.44% Pd	O_2	<2
	H_2	<2

* Passive during most of test. See Fig. 7A.
† The possible weighing error of these tests is ±2 mil/yr.

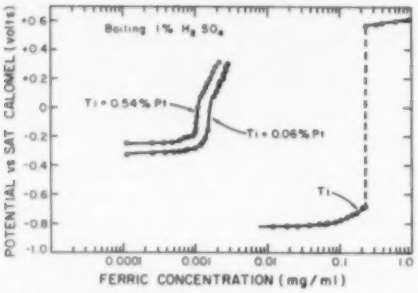

Fig. 8 Effect of ferric ion concentration in boiling 1% H_2SO_4 on the potential of Ti and Ti-Pt alloys.

are less than one-hundredth of that necessary to passivate Ti.

Conclusions

1. Alloying Ti with small amounts of Pt, Pd, Re, Ru, Ir, Os, Rh, and Au markedly improves corrosion resistance to H_2SO_4, HCl, and other reducing-type media.

2. The mixed potentials of Ti-noble metal alloys which exhibit low corrosion rates are more noble than the critical potential for passivity of Ti in the same environment. Anodic polarization of these alloys shows only passive behavior, whereas cathodic polarization into the active potential region produces an increase in corrosion rate.

3. Electrochemical passivity is observed in hydrogen-saturated systems without the presence of a redox system more oxidizing than the hydrogen electrode.

4. The mixed potential of Ti-noble metal alloys is much more sensitive to traces of oxidizing agents than unalloyed metal.

5. The above observations are consistent with the theory of noble metal alloying proposed. Titanium is particularly susceptible to improvement by alloying because it exhibits unusually active values of critical potential for passivity in a variety of media.

6. Alloying Ti with noble metals is not detrimental to behavior in oxidizing media, such as HNO_3 or ferric chloride. This is expected since Ti does not exhibit a transpassive potential region where the dissolution rate increases at quite noble potential values. Similar alloying in the case of stainless steels is expected to be detrimental under highly oxidizing conditions because of the transpassive behavior of Fe-Cr-Ni-type alloys. Thus, the addition of small amounts of noble metals to Ti produces a material with unusually broad corrosion resistance to both oxidizing and reducing-type media.

Manuscript received April 6, 1959. This paper was prepared for delivery before the Columbus Meeting, Oct. 18-22, 1959.

Any discussion of this paper will appear in a Discussion Section to be published in the June 1960 JOURNAL.

REFERENCES

1. M. Stern, *This Journal*, **105**, 638 (1958).
2. C. Edeleanu, *Metallurgia*, **50**, 113 (1954); *J. Iron Steel Inst.*, **186**, 122 (1958).
3. W. R. Buck, III, and H. Leidheiser, *Nature*, **181**, 1681 (1958).
4. N. D. Tomashov, *Z. Electrochem.*, **62**, 717 (1958).
5. M. Stern and H. Wissenberg, *This Journal*, **106**, 755 (1959).
6. H. H. Uhlig and G. E. Woodside, *J. Phys. Chem.*, **57**, 280 (1953).
7. T. Heumann, "Passivierende Filme und Deckschichten," p. 276, H. Fischer, K. Hauffe, and W. Wiederholt, Editors, Springer-Verlag, Berlin (1956).
8. M. Prazak, V. Prazak, and V. L. Cihal, *Z. Elektrochem.*, **61**, 739 (1958).
9. N. D. Tomashov, *Uspekhi Khim.*, **24**, 453 (1955); *Corrosion*, **14**, 229t (1958).
10. J. O'M. Bockris, "Modern Aspects of Electrochemistry," p. 180, Butterworth Scientific Publication, London (1954).

High-Temperature Sulfiding of Iron Alloys in Hydrogen Sulfide-Hydrogen Mixtures

E. W. Haycock

Shell Development Company, Emeryville, California

ABSTRACT

Rates of sulfide scale formation on pure iron and a series of chromium steels have been measured over the temperature range 400°-550°C in H_2S-H_2 mixtures at a total pressure of 600 psi with an H_2S partial pressure of 0.6 psi for exposure periods up to 500 hr. A mechanism of scaling, involving the depletion of a barrier scale layer by recrystallization and grain growth processes, is proposed and substantiated by laboratory studies of the structural properties and mode of formation of scales grown on the various materials studied. A single kinetic equation, based on this mechanism, is shown to satisfy the rate curves over the complete range of conditions studied. A solid defect structure, protons trapped at metal ion vacancies, is suggested to explain the effect of hydrogen on the scaling process. The term "E" center is suggested to describe such a lattice irregularity.

Interest in the high-temperature steel-hydrogen sulfide reaction has been stimulated in recent years by scaling problems experienced in high-temperature refining operations of the petroleum industry. Corrosion due to presence of H_2S in hydrorefining processes has been unexpectedly severe, chromium steels containing up to 9% chromium scaling equally as rapid as carbon steel. Several investigations of

this reaction have been reported (1). Of these investigations, those carried out under well-controlled conditions have, for the most part, involved relatively short duration exposures and have been performed at or near atmospheric pressure. The primary objective of the investigation reported here was to study the kinetics and mechanism of scaling under conditions similar to those experienced in refinery operations. This has involved scaling experiments at elevated pressures and with exposure times beyond the range reported by previous investigators. In the present investigation, corrosion rates of pure iron and iron-chromium alloys have been compared with those of commercial steels and scaling rates studied as a function of chromium content.

Dravnieks and Samans (2) recently have suggested a mechanism for the steel-hydrogen sulfide reaction. Mechanistic studies of the iron-H_2S reaction have been reported by Delahay and coworkers (3). The interpretation of kinetic data in these studies is complicated by the thermodynamic possibility that FeS_2 could be formed as well as FeS. In the present work the H_2S/H_2 mole ratio has been maintained at a sufficiently low value to insure that over the entire range of conditions studied FeS was the only stable product phase. As a result of the present kinetic and mechanistic studies a new mechanism of the reaction is proposed. Although the present studies confirm certain hypothetical features of the Dravnieks-Samans mechanism, our kinetics analysis differs significantly from that of the above authors and allows the experimental data to be explained by a single rate equation over the entire range of conditions studied.

Experimental Rate Measurements

The rates of scaling of pure iron, ½% Mo steel, and a series of chromium steels were measured over the temperature range 400°-550°C in H_2S-H_2 mixtures at a total pressure of 600 psi with an H_2S partial pressure of 0.6 psi. On the basis of thermodynamic data published by Rosenqvist (4), FeS is the stable product under these conditions. The compositions of the alloys studied are given in Table I. Two pure irons, Armco and Ferrovac E, were used, and no significant differences were observed in the relatively long exposure scaling rates studied. Commercial ½% Mo steel was used rather than carbon steel to avoid hydrogen attack of the metal.

The experiments were made in the apparatus shown schematically in Fig. 1. Metal specimens were

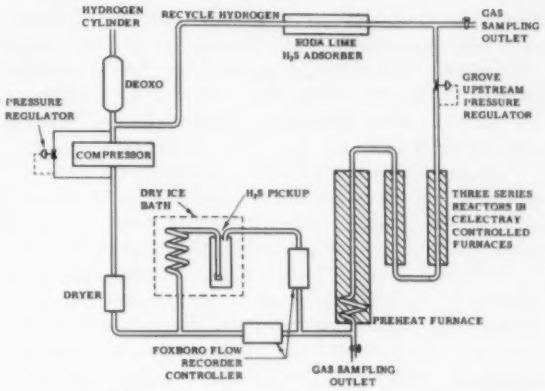

Fig. 1. Schematic diagram of apparatus used to measure metal scaling rate in H_2S/H_2 mixtures at 600 psi.

exposed in three stainless steel reactor tubes heated by electric furnaces which were maintained at chosen temperatures ±2°C by a Celectray indicator-controller. The temperature controller was actuated by iron-constantan thermocouples situated in thermowells close to the metal specimens.

Cylinder hydrogen (99.8% H_2, 0.15% O_2, 0.05% N_2) was led through a Deoxo catalytic cartridge and drying column to remove oxygen. The desired H_2S-H_2 mixture was obtained by dividing the hydrogen stream and passing part of it through liquid H_2S in a dry ice bath. The divided gas stream then was remixed and passed through a preheat column into the reactors. Division of the hydrogen stream to the desired extent was achieved by the use of Foxboro flow recorder-controllers. The total flow of gas over the scaling specimens was maintained at a sufficiently high rate to keep the effluent H_2S concentration to within 10% of the inlet concentration. The gas composition at both the inlet and outlet was checked at frequent intervals, and in many experiments the difference in inlet and outlet composition was considerably less than this amount. For ease in long term continuous operation, H_2S was removed from the effluent gas in soda lime towers and the hydrogen recycled.

The metal specimens studied were in the form of cylindrical rings approximately ½ in. long, ⅝ in. O.D., with 3/32 in. wall thickness. Ring specimens were chosen primarily to insure that scale samples would be obtained *in situ* on the metal surface for subsequent examination by metallurgical microscopic techniques. The scales formed under com-

Table I. Alloy compositions

Nominal alloy composition	Weight % constituents								
	Cr	Ni	Mo	C	Mn	P	S	Si	Cu
Armco iron	—	—	—	0.03	0.02	0.003	0.02	0.01	—
Ferrovac E*	<0.02	—	—	0.01	<0.02	0.004	0.001	<0.03	<0.01
½% Mo steel	—	—	0.55	0.20	0.56	0.018	0.025	0.22	—
5% Cr, ½% Mo steel	4.76	—	0.54	0.10	0.35	0.002	0.011	0.33	—
9% Cr, 1% Mo steel	8.44	—	1.01	0.09	0.42	0.012	0.015	0.36	—
12% Cr, type 410	12.31	0.50	0.11	0.13	0.65	0.010	0.009	0.55	0.03
18% Cr, 8% Ni, type 304	18.43	10.36	—	0.054	1.71	0.014	0.010	0.48	—

* Vacuum melted pure iron.

pression on the inside of the rings remained intact, whereas in many cases the scales on the outer surfaces of ring specimens or on flat specimens would spall on cooling from the reactor temperatures. Up to ten specimens could be supported in each reactor tube.

The experimental procedure adopted was as follows. Prior to exposure, specimens were ground smooth and sharp edges removed with 180 grit abrasive followed by soft rubber erasing. Specimens then were washed with acetone, weighed, and loaded into preheated reactor tubes under nitrogen. Final temperature adjustments were made as the nitrogen was swept out with hydrogen and the pressure brought up to 600 psi. The hydrogen sulfide-hydrogen stream then was introduced and scaling allowed to proceed for various exposure times up to 500 hr. Experiments were terminated by stopping flows to the reactors, venting, and purging with nitrogen. To determine the extent of metal consumption after each exposure, the specimens were descaled in an electrolytic cleaner in 5% w sulfuric acid, dried, soft rubber erased, and weighed. Duplication of alloy specimens allowed additional sampes for scale analyses and microscopic examination.

Experimental Results and Discussion

The rate curves obtained were similar in form to those obtained for carbon steel by Dravnieks and Samans (2). For all of the alloys studied, the rate of scaling was observed to be high initially and gradually decrease over the first 20-30 hr to approach an essentially constant value.

The scaling rate curves for pure iron, ½% Mo steel, and 5% Cr, ½% Mo steel are illustrated in Fig. 2, 3, and 4 for exposures up to 500 hr. The shapes of these curves are typical of all of the alloys studied including 18-8 stainless steel. Several experiments with pure iron-chromium alloys, made by vacuum melting "Ferrovac E" pure iron with electrolytic chromium, showed no significant difference in scaling properties between these materials and the corresponding commercial alloys. A large number of scaling experiments, which will not be reported in detail here, have been made under varying partial pressures of H_2S and H_2. These experiments have confirmed previously reported (1) observations that, within the thermodynamic limits of FeS stability, the over-all scaling rate depends on the partial pressure of H_2S and is not affected by changes in the partial pressure of H_2.

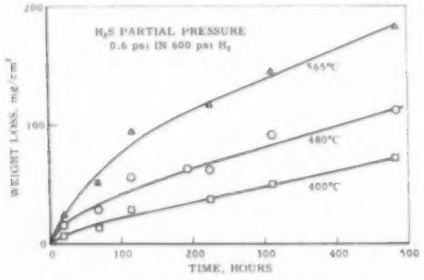

Fig. 2. Sulfiding rate curves for pure iron

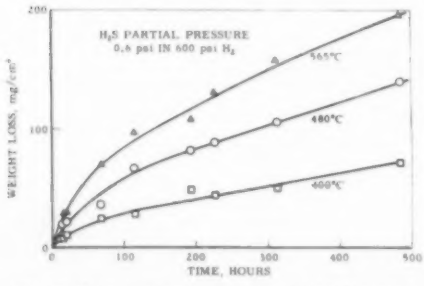

Fig. 3. Sulfiding rate curves for ½% Mo steel

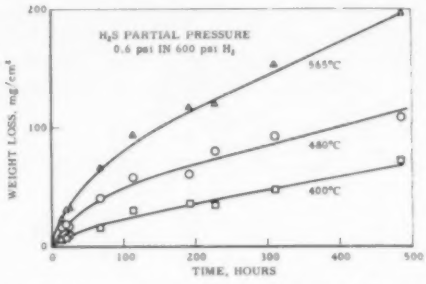

Fig. 4 Sulfiding rate curves for 5% Cr-½% Mo steel. Curves are plots of Eq. 1 with the following rate constants

Temp, °C	K_p	K_L
400	1.1	0.14
480	5	0.23
565	18	0.31

Scale structure and composition.—Scales formed on all of the materials investigated consisted of two well-defined layers. The scales resembled those described by Delahay (3) for the pure iron-H_2S product and by Dravnieks (2) for the carbon steel corrosion product. The layer next to the metal consisted of small disorganized crystallites and was coherent and adherent. The second layer adjacent to the gaseous environment consisted of a columnar array of relatively large crystals with pores extending from the gas interface to the surface of the adherent sulfide layer. The scale structure illustrated by the photomicrograph shown in Fig. 5 is typical of that obtained on all of the materials studied.

Chemical analyses of the individual scale layers showed that, for pure iron and the low chromium steels, the main constituent of both layers was metal deficient ferrous sulfide. Similar results for pure iron have been reported by Delahay (3). This was confirmed by power x-ray analyses, the iron sulfide

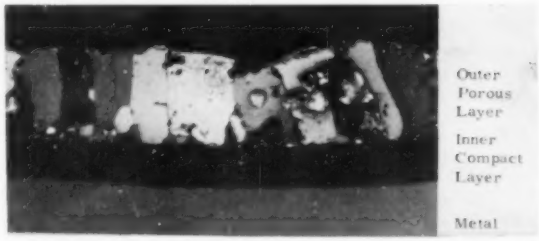

Fig. 5. Sulfide scale formed on 12% Cr steel. Specimen scaled 400 hr at 565°C, partial pressure, H_2S 0.3 psi in 600 psi H_2. Magnification 100X before reduction for publication.

super lattice (α') pattern being obtained in all cases. This structure is associated with the FeS composition range 50-50.74 at. % sulfur. Similar x-ray patterns have been reported by Bruns (5). For the chromium alloys, chemical analyses showed that chromium and molybdenum were retained in the scale layer next to the metal. Other trace metals present such as nickel and manganese were found to be distributed throughout both layers, although some tendency to retain nickel in the inner layer was observed. Silicon and carbon were found to accumulate in the inner layer. For the higher chromium steels and for low chromium steels which had been exposed sufficiently long to allow a significant concentration of chromium to be built up in the inner scale layer, an x-ray pattern corresponding to the spinel structure $FeCr_2S_4$ was observed. Although no thermodynamic data are available for this compound, by comparison with the analogous oxygen compound, it would be expected to have a high negative free energy of formation and its occurrence accounts for the retention of chromium in the inner scale layer.

Mechanism of scale formation.—Microscopic study of scale structure strongly suggests that the outer porous scale layer is formed at the expense of the inner layer by a recrystallization and grain growth mechanism. This is indicated by the sharpness of the interface between the scale layers and the change in crystal size and orientation from one layer to the other. It is also in keeping with the observation that for pure iron both layers are identical within the limits determinable by chemical and x-ray analyses.

To obtain confirmation of this general model, inert marker experiments were performed on 1% Cr, ½% Mo steel, and ½% Mo steel scaled under the conditions previously described for the rate measurements. Three marking materials were used: chromium oxide, aluminum oxide, and platinum metal dust. The positions of the chromium oxide and platinum markers were studied by metallographic techniques and aluminum oxide by chemical analyses of the scale layers. In all cases markers were found distributed throughout the outer scale layers and on the outermost scale surface. Some markers, particularly in the case of chromium oxide, were found at the interface between the scale layers, and the relative number and appearance of these markers suggested that the chromium oxide was not entirely inert and that some inhibition of the processes taking place at the interface between the two scale layers was occurring. The fact that no markers were found in the inner layer or at the metal surface clearly indicates that the inner scale layer was formed by sulfide ion diffusion to the metal surface. The general scattering of markers through the outer layer suggests that continuous rearrangement takes place in this layer, and this is in keeping with the proposed model of its formation by recrystallization and grain growth processes.

The growth of the inner layer by sulfide ion diffusion to the metal surface necessitates that this layer be formed under high compressive stress. The molar volume of ferrous sulfide is considerably greater than that of the parent metal and, except for some relief due to slight plastic deformation, the product sulfide is confined beneath existing scale to the same volume as that initially occupied by the parent metal. It seems probable that the stress in the inner scale layer is the main driving force for nucleation and growth of the outer scale layer. The phenomenon of stress induced recrystallization is well known, particularly in metal systems. A pertinent example of this is the observation that the growth of single crystal tin "whiskers" from polycrystalline tin is greatly enhanced by the application of a compressive stress (6).

The difference in the mechanism of scale formation in hydrogen sulfide environments as compared to sulfide formation in sulfur vapor studied by Birchenall (7) is dealt with later when interaction of hydrogen with metal deficient ferrous sulfide is discussed.

Kinetic analysis of rate data.—Microscopic examination of sulfide scales formed in hydrogen sulfide environments indicates that the porosity of the outer scale layer is sufficiently high to render it ineffective as a solid diffusion barrier between the metal and the gas phase. The main resistance to reaction appears to reside in the inner barrier layer scale. The simplest kinetic model which adequately explains the experimental observations is one to which a combination parabolic-linear law may be applied in which the linear component of the rate is associated with the process occurring at the interface between the compact and the porous scale layers. By comparison with other solid-state interface transformations, the proposed recrystallization process for the formation of the porous layer would be expected to occur at a linear rate and the interfacial area will remain sensibly constant throughout the reaction. The barrier layer scale therefore will grow by the diffusion of sulfide ions to the metal surface and be depleted at a constant rate by the process forming the porous outer scale layer. If it is assumed that diffusion across the inner scale layer determines the rate of metal consumption, then this rate will be inversely proportional to the inner scale thickness. The rate of scaling will start therefore at a high value and decline as the inner scale thickens. When the rate of metal consumption approaches the rate of recrystallization, the inner scale layer will approach a constant thickness and the scaling rate will approach a constant value. This model leads to the expression

$$x = \frac{K_p}{K_l} \ln \frac{K_p}{K_p - K_l(x - K_l t)} \qquad [1]$$

for the metal weight loss as a function of time, where x equals metal weight loss, t, time, K_p is a rate constant associated with the parabolic diffusion process by which the barrier layer is formed, and K_l a rate constant associated with the linear recrystallization rate by which it is depleted.

Equation [1] is a general expression for the rate of scaling of any system in which a diffusion barrier, which would normally be formed parabolically,

is depleted at a constant rate by any secondary process. Its derivation, which is an extension of the work of Loriers (8) and Wagner (9), will be given in more detail in the following paper (10) where it is applied to systems other than sulfiding.

The close correspondence between the present experimental data and the theoretical rate curves obtained from Eq. [1] for the range of conditions studied is shown in Fig. 4 for 5% Cr, ½% Mo steel. Similar agreement has been found for the other alloys studied.

Equation [1] is based on a model of an ideal system. The assumptions made in its derivation are: (*a*) the consumption of metal is controlled solely by diffusion processes in the compact layer, i.e., no surface or interface reaction influences the primary reaction; (*b*) the diffusion coefficient of the rate-determining species is constant throughout the reaction; (*c*) the secondary interface reaction giving the porous scale layer depletes the diffusion barrier at a uniform rate; and (*d*) both scale layers begin to grow at $t = 0$ and have constant density throughout the reaction. For the early stages of scaling on pure iron and the low chromium steels, these requirements apparently are obeyed reasonably well. However, at long exposure times deviations are to be expected and the results of some of these are apparent in scales formed in long term experiments in both laboratory and refinery plant equipment. The presence of nonmetallic materials (carbon and silicon) in the steels may introduce a changing additional resistance to the consumption of metal at the metal-scale interface. The enrichment of certain alloy constituents in various locations in the scale gradually will effect the diffusion coefficient of other constituents. The outer scale layer, as it thickens, may offer a gradually increasing resistance to gas flow to the interface between the two scale layers. Thus, at the base of pores of the outer scales, the ratio of H_2 to H_2S may increase as the porous scale grows and gaseous diffusion paths to the reaction zone become longer. The compact diffusion barrier may develop stress cracks as the reaction proceeds. The scale interface reaction, which is thought of basically as a recrystallization process, could be affected by changes in concentration of foreign materials at the interface.

Experimental observations of scale layer thicknesses made in the present study indicate that the inner scale layer thickens over the first 24-hr exposure to a value which remains essentially constant for 70-100 hr. A slight but continuous thickening of the inner layer takes place for 100-500 hr exposure and this is accompanied by a slight decrease in the rate of thickening of the outer porous layer. These deviations from the theoretical model do not appear to be of sufficient magnitude to prevent the experimental rate curves being fitted adequately by Eq. [1].

Values of K_p and K_l, plotted as a function of temperature according to the Arrhenius equation, are shown in Fig. 6 and 7. Straight lines were obtained in all cases, which adds support of internal consistency to the proposed mechanism and kinetic

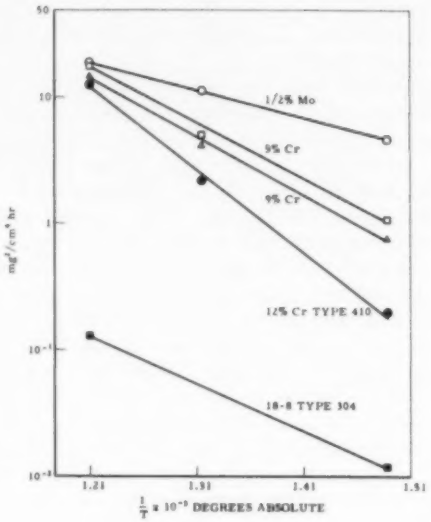

Fig. 6 Arrhenius plots for K_p

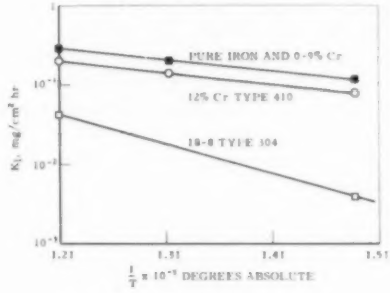

Fig. 7. Arrhenius plots for K_l

analysis. For the purpose of clarity, the pure iron K_p plot has been omitted from Fig. 6 and the lines for various alloys have been grouped in Fig. 7. Activation energies and pre-exponential factors determined from the data for each individual metal are given in Table II for the diffusion and recrystallization processes. The accuracy with which weight losses could be determined and the deviations of individual points from the theoretical curves obtained from Eq. [1] set a limit of accuracy of ±1 kcal on the reported activation energies for all alloys except 18-8 stainless steel. In this case weight losses were very small and the experimental data more widely scattered. The data given for 18-8

Table II. Activation energies and pre-exponential factors for parabolic and linear processes
$K = Ae^{-E/RT}$

Alloy	Parabolic rate constant, K_p		Linear rate constant, K_l	
	Activation energy, E, kcal/mole	Pre-exp. factor, A, mg^2/cm^4 hr	Activation energy, E, kcal/mole	Pre-exp. factor, A, mg/cm^2 hr
Iron	12.5	2.1×10^4	7	10
½% Mo	10	7.7×10^3	7	10
5% Cr, ½% Mo	19	1.6×10^9	7	10
9% Cr, 1% Mo	20	2.4×10^9	7	10
12% Cr, type 410	28	2.9×10^9	7	22
18-8, type 304	17	3.7×10^7	16	7×10^3

stainless steel therefore could be considerably in error and should be taken for comparison in a qualitative rather than quantitative sense. It will be seen that, with the chromium alloys, the activation energy for the diffusion process increases as the chromium content of the steel increases. The activation energy of the recrystallization process, however, stays essentially constant until the 12% chromium alloy is reached and then increases sharply for the 18% Cr, 8% Ni stainless steel.

These activation energy data serve to illustrate several practical features of the scaling process. Since, on the basis of the proposed model, the ultimate rate of scale formation is determined by the recrystallization rather than the diffusion process, the constancy of the activation energies and preexponential factors for the recrystallization process are to be expected since practical experience has shown that chromium additions of less than 12% to steel are not beneficial in lowering the long-term scaling rate (1). The fact that the activation energies for the diffusion process increase with chromium content implies that, if the scaling process involved the diffusion-controlled formation of the barrier scale only, then low percentage chromium additions would be beneficial in reducing scaling. This is in keeping with experience in oxidation of chromium steels where no porous scale layer is produced and low percentage additions of chromium lower the scaling rate. It is anticipated that additions of chromium would be beneficial in the pure sulfur vapor scaling system.

Effect of Hydrogen on Ferrous Sulfide Scale Formation

The effect of hydrogen in high-temperature sulfiding of iron can be appreciated best by comparison of the scaling processes in hydrogen sulfide and in pure sulfur vapor. In hydrogen sulfide environments the rate of scaling is high initially and falls to an essentially constant value. A two-layer scale is formed, the inner layer growing by sulfide ion diffusion to the metal surface. In contrast to this, the iron-sulfur vapor reaction follows a parabolic rate law (7). A single layer scale is formed and has been shown by Birchenall to grow by iron ion diffusion from the metal surface to the scale-gas interface. Since the product in both cases is iron deficient ferrous sulfide, it is evident that hydrogen plays an important role in the mechanism of scale formation in hydrogen sulfide environments.

To obtain a quantitative measure of the interaction of hydrogen with ferrous sulfide, the all glass apparatus shown schematically in Fig. 8 has been used. In a typical experiment a sample of ferrous sulfide in bulb A was equilibrated with a reservoir mixture of approximately 6% hydrogen sulfide in hydrogen at atmospheric pressure for 15 hr at 500°C. This gas composition was suitable to maintain ferrous sulfide thermodynamically stable against bulk reduction at this temperature. The adsorption chamber A was then evacuated to 10^{-4} mm Hg at 500°C for 8 hr. A known amount of H_2S-H_2 mixture was introduced into the system from the reservoir, and the adsorption of gases followed by the reduction in pressure measured with a glass capillary bourdon gauge (11). At any stage of the adsorption a part of the ambient gas could be isolated in section B of the apparatus and the H_2S condensed out in the ampoule C. This allowed a measurement of the H_2S/H_2 volume ratio existing above the adsorbent at any given time. The volumes of the various sections of the apparatus were calibrated with helium. Furnace temperatures were controlled to ±2°C. The surface area of the sulfide was determined after each experiment to allow for any sintering which might occur. Surface areas were measured by the B.E.T. method using nitrogen. A typical adsorption isotherm is shown in Fig. 9 with the pertinent primary and calculated data for the experiment. It will be seen that the system had not reached equilibrium even after 12 hr. Even if it is assumed that the evacuation treatment before adsorption removed all of the hydrogen associated with the ferrous sulfide, the total measured amount of hydrogen adsorbed after 12 hr exceeds the value expected for a monolayer. The slow, essentially linear, adsorption observed after 1 hr is attributed to the solution of hydrogen into the bulk sulfide.

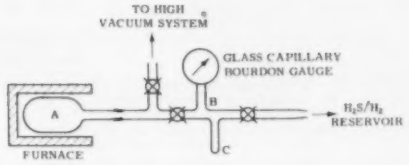

Fig. 8. Schematic diagram of apparatus used to measure absorption of hydrogen by ferrous sulfide.

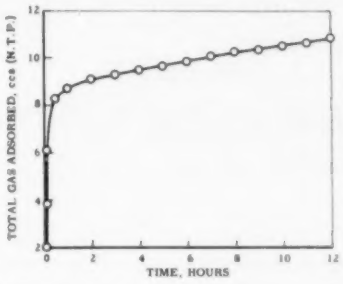

Fig. 9. Adsorption of H_2S/H_2 mixture on ferrous sulfide at 500°C. Weight of ferrous sulfide, 75.6 g; surface area (after experiment), 0.11 m^2/g; gas pressure at zero time, 40.8 cm Hg; gas pressure after 12 hr, 15.8 cm Hg; initial composition of H_2S/H_2 mixture, 6.15% H_2S; gas composition after 12 hr, 10.9% H_2S; hydrogen adsorbed after 12 hr, 10.4 ccs (N.T.P.); hydrogen sulfide adsorbed after 12 hr, 0.34 ccs (N.T.P).

The adsorption of hydrogen by metal deficient oxides, materials known as p-type semiconductors, has been studied extensively and it is known that the adsorption of hydrogen is accompanied by a decrease in electrical conductivity (12). It is anticipated therefore that the adsorption of hydrogen by ferrous sulfide and incorporation into the lattice would be accompanied by a decrease in the concentration of positive holes. From a chemical point of view this is equivalent to adsorbed hydrogen reducing the number of ferric ions in the metal deficient ferrous sulfide lattice. Assuming this to be

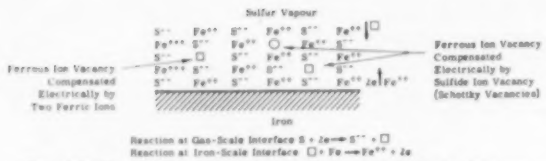
Sulfur Vapour
Ferrous Ion Vacancy Compensated Electrically by Two Ferric Ions
Ferrous Ion Vacancy Compensated Electrically by Sulfide Ion Vacancies (Schottky Vacancies)
Iron
Reaction at Gas-Scale Interface S + 2e⟶ S⁻⁻ + □
Reaction at Iron-Scale Interface □ + Fe ⟶ Fe⁺⁺ + 2e

Fig. 10. Growth of iron-deficient ferrous sulfide in the iron-sulfur system.

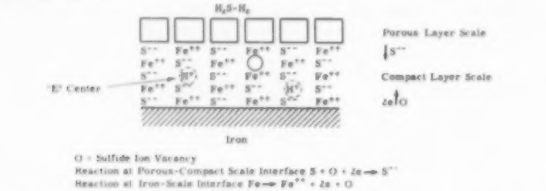
H₂S-H₂
Porous Layer Scale
Compact Layer Scale
"E" Center
Iron
O = Sulfide Ion Vacancy
Reaction at Porous-Compact Scale Interface S + O + 2e⟶ S⁻⁻
Reaction at Iron-Scale Interface Fe⟶ Fe⁺⁺ + 2e + O

Fig. 11. Growth of iron-deficient ferrous sulfide modified by hydrogen.

the case, and recognizing the difference in scaling mechanism observed in hydrogen sulfide and sulfur vapor, i.e., scale formation by diffusion of sulfide rather than iron ions, it appears that hydrogen is incorporated in the ferrous sulfide lattice as protons associated with metal ion vacancies. As illustrated schematically in Fig. 10, iron deficient ferrous sulfide formed by the reaction of iron with sulfur vapor would be expected to contain metal ion vacancies, of which a part are compensated for electrically by sulfide ion vacancies and a part by the existence of ferric ions. It is suggested that interaction of hydrogen with this system results in a structure shown in the reaction scheme illustrated in Fig. 11. In addition to chemisorbed hydrogen at the surface, protons will be incorporated into the lattice reducing the number of ferric ions. This structure can be regarded as equivalent to a number of HS^- ions incorporated in the lattice, these ions being dissociated to an extent dependent on temperature. Since metal ion vacancies carry an effective negative charge, they would be expected to be efficient traps for protons in the lattice. It is proposed to name the defect structure of a proton trapped at a metal ion vacancy an "E" center. A previous suggestion of such a structure has been made by Caplan and Cohen (13) to explain the inhibiting effect of water in the high temperature oxidation of iron-chromium alloys. An "E" center would be expected to have certain properties similar to those of the well-established "f" center, i.e., an electron trapped at an anionic vacancy. The effective diameter of protons trapped at metal ion vacancies would increase with temperature and, under the scaling conditions studied, an "E" center could be expected to present an effective barrier to the migration of metal ions.

The recrystallization phenomena observed with sulfide scaling in the presence of hydrogen suggest that, in addition to blocking iron ion diffusion, the interaction of hydrogen enhances the mobility of the relatively bulky sulfide ions. This is readily understood on the basis of the above model since the presence of singly charged HS^- ions will tend to loosen the close packed sulfide ion lattice. Surface mobility of sulfide ions would be expected to increase since the energy required to transfer an HS^- ion from the bulk sulfide to a surface adsorbed state would be considerably less than for a S^{--} ion. Such surface mobility is the process considered to be important in recrystallization and grain growth processes.

The enhanced surface ionic mobility in the presence of hydrogen has been demonstrated by sintering experiments. Powdered ferrous sulfide with an initial B.E.T. surface area of 0.5 sq meter/g was maintained in a vacuum of 10^{-6} mm Hg for 5 hr at 500°C. No detectable change in surface area occurred. Heating the powder at the same temperature in a hydrogen-7% H_2S atmosphere for 2 hr reduced the surface area to a half of its initial value, and the powder had visibly sintered to a porous plug.

On the basis of hydrogen interacting with the ferrous sulfide product to (*a*) retard metal ion diffusion, and (*b*) accelerate surface and bulk diffusion of sulfide ions, it is possible to account for the difference in mechanisms observed when steel is scaled in hydrogen sulfide and in sulfur vapor.

The general similarity in oxide and sulfide systems suggests that the effects of hydrogen interaction discussed here for iron sulfide would also apply to metals oxidized in water vapor, although similar effects might be expected to occur over different temperature ranges due to the difference in stability of OH^- and SH^- ions. The study by Gulbransen (14) of the orientation of oxide crystals formed on iron lends support to the suggestion that the interaction of hydrogen with iron oxides will enhance the mobility of oxide ions. It was shown that iron scaled in pure oxygen produced a poorly oriented surface oxide. However, iron scaled in water vapor was found to form a highly oriented film. The bulky anions in the presence of hydrogen apparently possessed sufficient mobility to achieve a desired orientation in the time of oxide formation. The system Fe-H_2O-H_2 has been studied by Chaudron and co-workers (15), and these authors describe a double scale formation similar to that observed in the iron-hydrogen sulfide reaction. Further experimental work will be required, involving measurement of cation and anion diffusion rates in metal deficient oxides and sulfides in the presence of hydrogen, to firmly establish the effects suggested by the present study.

Acknowledgment

The author is indebted to Mr. W. H. Sharp for obtaining the rate data used in this article and to Mr. H. S. MacKinnon for his assistance in the remainder of the experimental work. Helpful discussions by Mr. R. S. Treseder and Dr. A. Wachter are also gratefully acknowledged.

Manuscript received Oct. 13, 1958. This paper was prepared for delivery before the Ottawa Meeting, Sept. 28-Oct. 2, 1958.

Any discussion of this paper will appear in a Discussion Section to be published in the June 1960 JOURNAL.

REFERENCES

1. G. Sorel, *Corrosion*, **14**, 33 (1958).
2. A. Dravnieks and C. H. Samans, *This Journal*, **105**, 183 (1958).

3. F. Hügli, C. M. Hudgins, Jr., and P. Delahay, Paper presented API Division of Refining, Los Angeles, California, May 1958.
4. T. Rosenqvist, *J. Iron Steel Inst., London*, **176**, 37 (1954).
5. F. J. Bruns, *Corrosion*, **13**, 27t (January 1957).
6. R. M. Fisher, L. S. Darken, and K. G. Carroll, *Acta Met.*, **2**, 370 (1954).
7. R. A. Meussner and C. E. Birchenall, *Corrosion*, **13**, 79 (1957).
8. J. Loriers, *C. R. Acad. Sci., Paris*, **231**, 522 (1950).
9. W. W. Webb, J. T. Norton, and C. Wagner, *This Journal*, **103**, 107 (1956).
10. E. W. Haycock, *This Journal*, **106**, 771 (1959).
11. Constructed by S. G. Yorke, The University, Bristol, England.
12. F. S. Stone, "Chemistry of Solid State," Ch. 15, W. E. Garner, Editor, Academic Press, Inc. New York, Butterworths Scientific Publications, London (1955).
13. D. Caplan and M. Cohen, *J. Metals*, **4**, 1057 (1952).
14. E. A. Gulbransen and R. Ruka, *This Journal*, **99**, 360 (1952).
15. R. Collongues, R. Sifferlen, and G. Chaudron, *Rev. Met.*, **50**, No. 10, 727 (1953).

Transitions from Parabolic to Linear Kinetics in Scaling of Metals

E. W. Haycock

Shell Development Company, Emeryville, California

ABSTRACT

A general rate equation is derived for a model of a barrier scale layer being formed by a diffusion process and simultaneously being depleted at a constant rate by a secondary process. The equation, derived to satisfy rate curves for sulfide scaling of iron in hydrogen sulfide, is shown to be applicable to the oxidation of aluminum and hafnium over ranges of conditions where two or three rate equations have been used previously to explain the experimental data. The validity of this equation emphasizes the importance of secondary processes, such as scale recrystallization, in determining the over-all rate of high-temperature corrosion reactions.

An important part of fundamental studies of the mechanism of high-temperature corrosion is the fitting of theoretical rate equations, derived from mechanistic models, to experimental scaling data. The basis of nearly all kinetic treatments of scaling processes, beyond the thin film range, is the simple, diffusion-controlled formation of a barrier product layer. The accepted mechanism by which the barrier scale grows according to a parabolic rate equation is attributed mainly to Wagner (1) and has been described exhaustively in recent review texts (2, 3). Many scaling systems, however, do not follow a parabolic equation except over limited ranges of temperature. Other rate equations such as linear, cubic, exponential, or combinations of these have been shown to fit experimental rate data for various systems, and a number of mechanisms have been suggested to account for these deviations from parabolic behavior (2, 3).

For the oxidation of most metals, an intermediate temperature range has been observed over which a parabolic rate law is reasonably well obeyed. At low temperatures a tendency toward logarithmic laws has been noted, while linear kinetics are favored at elevated temperatures. The apparent need for more than one theoretical rate equation to satisfy experimental data over a range of temperatures usually has been ascribed to transitions in the mechansim of scaling.

Systems which have not received an adequate quantitative treatment are those whose rates begin at a high value and then decrease over a certain time period to follow linear kinetics for the remainder of the scaling reaction. In these systems the linear portion of the rate curve may begin close to the origin or may not be apparent until the scaling reaction is well advanced, depending on the temperature of reaction. The purpose of this paper is to develop a quantitative approach which yields an equation capable of satisfying rate curves of this type over a wide range of conditions.

Mechanisms Associated with Linear Kinetics

Linear rate laws generally are associated with one of two mechanistic features. Surface reactions occurring at either the metal-scale or scale-gas interface can be considered in some cases to be slow and therefore rate determining. If the interface has a constant area throughout the reaction, then an overall linear rate law would be expected. The second mechanism giving rise to linear kinetics depends on the formation of an "open" or porous scale structure. This includes systems where volatile products are formed. Early investigators of oxidation systems associated a porous scale with metals, such as the alkaline earth metals, whose oxides have a smaller molar volume than the parent metal. The oxides of these systems were supposed to be formed under tension, and hence crack and shear as the scale thickened to give access of reactant gas to the metal surface at a constant rate. This is the basis of the well-known Pilling-Bedworth (4) rule. An improved understanding of the mechanism of oxide formation, however, has shown that the Pilling-Bedworth rule is without theoretical foundation (5, 6) for scales formed by metal ion diffusion. A more reasonable explanation, discussed by Evans (7), is that cracking, shearing, etc., can occur as a result of stresses

in the product scale but that the rate of metal consumption is determined by diffusion across a thin barrier layer on the metal surface which builds up to and then maintains a constant thickness. Such a mechanism can apply equally well to systems whose oxides have a molar volume greater or less than that of the parent metal.

Following a study of the oxidation of cerium, Loriers (8) suggested that the observed linear kinetics could be explained by the formation of a porous CeO_2 layer on top of a nonporous Ce_2O_3 barrier layer. The outer scale layer was observed to grow at the expense of the barrier layer at a constant rate while the consumption of metal was controlled by a diffusion process in the barrier layer. The barrier layer approached a constant thickness as the rate of its formation became equal to the rate of formation of the outer porous layer. The over-all rate of reaction therefore was high initially and decreased to approach a constant value. Similar reasoning has been applied by Wagner (9) to the oxidation of tungsten, and it appears that the same mechanistic approach can be used for the oxidation of uranium (10) and thorium (11). In all of these cases a two-layer scale is formed. The outer layer is porous and is a higher oxide of the metal than the compact inner barrier scale. In these systems it is reasonable to assume that the porous layer is formed at the expense of the barrier layer by nucleation and growth of a different chemical phase.

There are other scaling systems, such as iron-H_2S (12), and the oxidation of aluminum (13, 14), hafnium (15), calcium (16), and magnesium (17), where linear rate curves are obtained over certain temperature ranges. In these cases, however, where two scale layers have been observed, both layers have been found to be chemically the same material. In these systems it seems logical to extend the kinetics described qualitatively by Loriers (8) and to attribute the formation of the porous second layer to recrystallization and grain growth processes. Such a mechanism is treated in the following section.

Proposed Scaling Mechanism

By extending the qualitative arguments of Evans (7) and Loriers (8), the mechanistic model illustrated in Fig. 1 can be described in a quantitative manner.

A barrier layer scale AB is formed on the metal surface, its rate of formation being governed by ionic diffusion. Simultaneously, a secondary process is superimposed upon this primary process which depletes the barrier layer at a constant rate. In Fig. 1 this secondary process is shown to give the scale layer BC which is assumed to be sufficiently porous so that it offers no significant barrier to the availability of reactive gas at the interface B. The rate of metal consumption will be inversely proportional to the thickness of the compact barrier layer and will be given by the standard parabolic equation (18).

$$dx/dt = ak_p/2\mu \qquad [1]$$

where x is metal weight loss at time t; μ, thickness of compact layer at time t; k_p, parabolic rate constant;

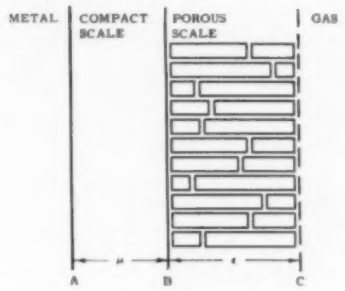

Fig. 1. Schematic model for derivation of rate equation

and a, a conversion factor relating the thickness of metal reacted to the thickness of the compact scale produced. In an unhindered, single scale forming reaction governed entirely by a parabolic kinetic law, a would be defined by $x = a\mu$. In addition to the usual assumptions of constant diffusion coefficient and uniform area at interface A, Eq. [1] assumes that layer AB has a constant uniform density.

Let ϵ be the thickness of the porous layer at time t. As a first approximation we assume the recrystallization process to begin at $t = 0$. Then

$$\epsilon = k_i t \qquad [2]$$

where k_i = linear rate constant of the interface reaction forming BC. We write

$$x = a\mu + b\epsilon \qquad [3]$$

where a and b are the density conversion factors from metal to the two scale types. This introduces the assumption that the porous layer has a constant density throughout the reaction. Substituting in Eq. [3] from Eq. [1] and [2], μ and ϵ in terms of x and t, we obtain

$$\frac{dx}{dt} = \frac{K_p}{x - K_i t} \qquad [4]$$

where

$$K_p = a^2 k_p/2$$

$$K_i = bk_i$$

Integration of Eq. [4] yields the equation giving metal weight loss as a function of time

$$x = \frac{K_p}{K_i} \ln \frac{K_p}{K_p - K_i(x - K_i t)} \qquad [5]$$

In the general case, the process which depletes the barrier layer may be either vaporization of the primary reaction product or, as in the case illustrated, the formation of a solid second scale layer. If a solid second layer is formed, it must either be porous and offer negligible resistance to the availability of reactive gases at the interface between the two-scale layers or it must have a structure such that solid diffusion rates in it are very rapid compared to those in the barrier layer. Mechanical processes such as cracking, spalling, etc., can be considered as possible mechanisms of porous second layer scale formation. However, the general smoothness of linear rate curves and conformance with the Arrhenius

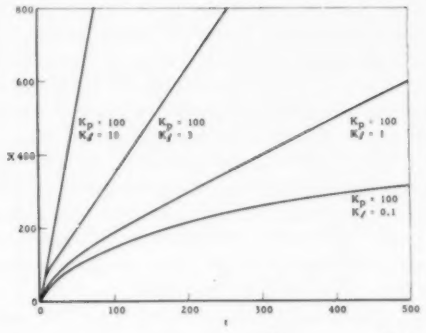

Fig. 2. Theoretical rate curves. $X = \frac{K_p}{K_l} \ln \frac{K_p}{K_p - K_l(X - K_l t)}$

equation as a function of temperature are considered evidence against such an unpredictable process as mechanical cracking being important in more than a few cases. In instances where the porous and barrier layers are chemically identical, the most reasonable mechanism of porous scale formation appears to be recrystallization and grain growth.

If we eliminate x and ϵ from Eq. [1], [2], and [3] we obtain

$$\frac{d\mu}{dt} = \frac{K_p}{a^2\mu} - \frac{K_l}{a} \qquad [6]$$

The inner scale grows, i.e., $d\mu/dt$ is positive, as long as $K_p/a^2\mu > K_l/a$. As μ approaches a thickness given by $K_p/a^2\mu = k_l/a$, then $d\mu/dt$ approaches zero. The inner layer, therefore, approaches a constant thickness $\mu = K_p/aK_l$. It should be pointed out that mathematically this occurs at infinity. However, for practical purposes, the inner scale layer can be considered to become essentially constant after it has achieved 95% of its ultimate thickness. Equation [6] has been derived by Wagner and co-workers (9) for the oxidation of tungsten.

A plot of Eq. [5] yields a curve which approaches the straight line $K_p - K_l(x - K_l t) = 0$. The general shape characteristics of the curve are determined by the relative values of K_p and K_l. When K_p is large compared with K_l, the parabolic features of the equation are emphasized and the plot is considerably curved for short exposure time. As K_l increases relative to K_p, the linear portion of the plot begins closer to the origin of reaction. These variations are illustrated by the theoretical rate curves shown in Fig. 2.

In the following sections, Equation [5] is applied to systems where scale recrystallization appears to be the mechanism of porous second layer scale formation, and sufficient data are available to test the equation. The K_p and K_l values reported for these systems were obtained from the experimental data in the following way. A trial asymptote was drawn to the final stages of the rate curve. As stated above, this line should follow the equation $K_p - K_l(x - K_l t) = 0$, and hence the gradient was an approximate value of K_l and the intercept on the x axis an approximate value of K_p/K_l. The approximate values of K_p and K_l obtained in this way were then adjusted slightly to give the best coincidence with the experimental data. The number of significant figures to which values of K_p and K_l are reported is an indication of the sensitivity with which the experimental rate curves could be fitted.

Application of Proposed Mechanism and General Rate Equation

Iron-hydrogen sulfide reaction.—In the preceding paper (19), Eq. [5] was shown to satisfy sulfiding rates of iron and a series of chromium steels over a range of environmental conditions. For this system two scale layers are formed. Both layers consist of iron deficient ferrous sulfide. The inner barrier layer is formed by the diffusion of sulfide ions to the metal-scale interface. Since this involves the formation of ferrous sulfide beneath existing scale, it is expected that the barrier layer would be formed under high compressive stresses. The formation of the porous layer is attributed to stress induced recrystallization of the inner scale layer.

Oxidation of aluminum.—An apparent kinetic transition from parabolic to linear oxidation of aluminum has been observed at 475° to 500°C by Gulbransen (13) and Smeltzer (14). Hunter and Fowle (20) have shown that oxide films on aluminum consist of two layers, a barrier layer and a porous outer layer. Vermilyea (6) has suggested that recrystallization qualitatively could account for the formation of the porous layer and explain the transition to linear kinetics.

Equation [5] is fitted to the experimental data of Gulbransen (13) in Fig. 3. The three lower curves in this figure have been fitted with a parabolic equation by Gulbransen, while no attempt was made to satisfy the upper curve. It can be seen that Eq. [5] is capable of fitting all the curves over the apparent transition range. The rate constants K_p and K_l obtained from Fig. 3 have been plotted according to the Arrhenius equation in Fig. 4. Straight lines are obtained, and this is an indication of internal consistency in the application of Eq. [5] to the aluminum system. The experimental activation energy of 23 kcal for K_p is identical to that obtained by Gulbransen from parabolic rate constants of the lower temperature curves and is of the order of magnitude expected for the movement of metal ions in an oxide system. The activation energy of 49 kcal for K_l is similar to the value of 50.5 kcal obtained by Leontis and Rhines (17) for the linear high tem-

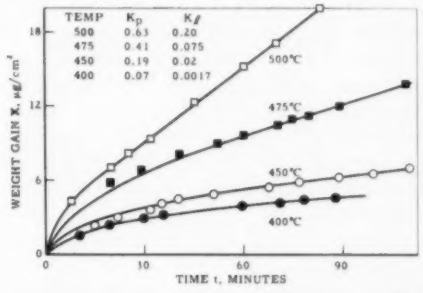

Fig. 3. Application of equation $X = \frac{K_p}{K_l} \ln \frac{K_p}{K_p - K_l(X - K_l t)}$ to aluminum oxidation rate data. Experimental data taken from Ref. (13).

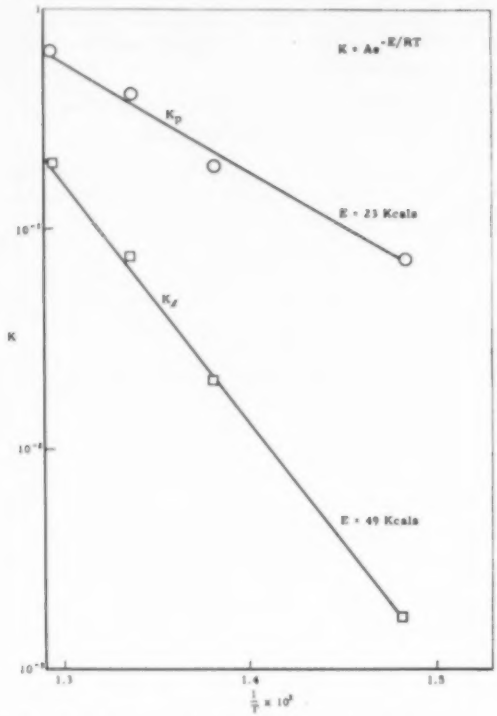

Fig. 4. Arrhenius plots for the oxidation of aluminum

perature oxidation of magnesium. It would be expected that the rate of recrystallization in aluminum oxide would be controlled by the surface mobility of the relatively bulky oxide ions. A high activation energy for this process would be expected for refractory oxides such as alumina and magnesia which are known to be difficult to sinter even at very high temperatures.

On the basis of our previous discussion of the effects of the relative values of K_p and K_l on the shape of the plot of Eq. [5], it would be expected that the apparent transition from parabolic to linear kinetics would occur over a small range of temperature for systems in which K_l has a high temperature coefficient compared with K_p. This effect is well illustrated by the oxidation of aluminum.

The successful application of Eq. [5] to the oxidation curves shown in Fig. 3 emphasizes that short term experiments can be misleading in mechanistic studies. If the mechanism associated with Eq. [5] is correct, then the low temperature curves in Fig. 3 would become straight lines if the experiments were continued for sufficient time. The application of parabolic equations to these curves is misleading, especially if a particular mechanism is associated with the parabolic law. It is important that the correct mechanism and kinetic equations be established if the kinetic data are to be used for theoretical absolute rate calculations such as those attempted by Gulbransen (21).

Oxidation of hafnium.—The oxidation of hafnium from 350° to 1200°C has been studied recently by Smeltzer and Simnad (15). The mechanism appears to be very similar to that of the iron-H_2S system. A two-layer scale is formed. Both layers consist of HfO_2, and the outer layer is very porous. Inert marker experiments indicate that the barrier layer is formed by diffusion of oxygen from the gas-scale interface to the metal surface and hence would be formed under a high compressive stress. The above authors have used an exponential, parabolic, and linear law successively to satisfy empirically the experimental data over the temperature range studied. The scale thickness measurements reported by Smeltzer and Simnad support the mechanism used to derive Eq. [5]. They have shown that the barrier layer approaches a constant thickness which can be expressed in terms of the rate constants K_p and K_l.

The application of Eq. [5] to the experimental results of Smeltzer and Simnad is shown in Fig. 5. It can be seen that the equation explains the data previously fitted by three equations. There is no theoretical evidence therefore of "transitions" occurring over the temperature range studied. As a further test of internal consistency, the straight-line Arrhenius plots, for values of K_p and K_l obtained from Fig. 5, are shown in Fig. 6. The activation energy of 36 kcal obtained for K_p is identical to the value reported by Smeltzer and Simnad from parabolic rate constants obtained by approximating portions of the experiment rate curves to parabolas over the temperature range 470°-1200°C. The activation energy of 18 kcal for K_l is somewhat lower than the value of 26 kcal reported by the above authors from linear rate constants obtained from portions of the experimental rate curves in the temperature range 900°-1200°C. This difference results because, in our analysis of the experimental rate curves, only the 1200°C curve was considered to have reached the final linear stage. The curves presented by Smeltzer and Simnad for 900° and 1000°C were considered not to have reached the final linear rate of reaction in the exposure time studied. Since Smeltzer and Simnad illustrated the growth of the barrier layer oxide by oxide ion diffusion, the activation energy of 36 kcal is associated with the bulk mobility of oxide ions in polycrystalline hafnia. On the basis of a recrystallization process determining the rate of formation of the outer porous scale layer, the activation energy of 18 kcal is associated with the surface mobility of ions. Since, in this case, the temperature coefficient of K_p is greater than that of K_l, apparent transitions in short term exposures are spread over a wide temperature

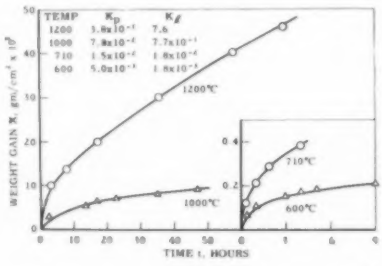

Fig. 5. Application of equation $X = \frac{K_p}{K_l} \ln \frac{K_p}{K_p - K_l(X - K_l t)}$ to hafnium oxidation rate data. Experimental data taken from Ref. (15).

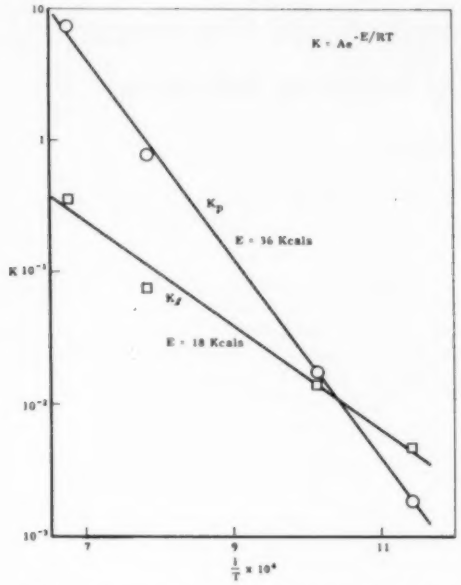

Fig. 6. Arrhenius plots for the oxidation of hafnium

range. The closest approximation of the rate curves to parabolas occurs at the highest temperatures.

A possible extension of the proposed kinetic treatment is that Eq. [5] will be modified in some cases to include the possibility that the secondary process does not begin at $t = 0$. In cases similar to those discussed, this would correspond to the requirement that a minimum stress level be reached before formation of the porous layer begins. This modification yields a rate equation of the form

$$\frac{dx}{dt} = \frac{K_p}{x - K_l(t + t_o)} \qquad [7]$$

where t_o is the time at which the secondary process begins. Such an equation would be expected to apply to systems such as the oxidation of niobium studied recently by Cathcart, Campbell, and Smith (22).

Conclusions

It has been shown that a single rate equation can replace the need for multiple equations in several systems for which sufficient experimental data are available to test its validity. It is probable that, when more data are available, it will be possible to show its general applicability to other scaling reactions. For the systems discussed, the concept of transitions in mechanism occurring over certain temperature ranges has been shown to be an unnecessary complication of previous kinetic treatments. The present analysis emphasizes the fact that short duration experiments can be misleading in studies of scaling mechanisms.

The general validity of Eq. [5] for the systems discussed indicates that secondary processes, such as scale recrystallization, can be of considerable importance in determining the rate of scaling processes. The application of Eq. [5] in future studies, and further development of the mechanistic concept associated with it, should be helpful in improving our understanding of the mechanism of corrosion at high temperature.

Acknowledgment

The author is indebted to Mr. H. S. MacKinnon for valuable assistance in the analysis of the rate data reported and to Mr. R. S. Treseder and Dr. A. Wachter for encouragement and helpful discussions.

Manuscript received Oct. 13, 1958. This paper was prepared for delivery before the Ottawa Meeting, Sept. 28-Oct. 2, 1958.

Any discussion of this paper will appear in a Discussion Section to be published in the June 1960 JOURNAL.

REFERENCES

1. C. Wagner, *Z. physik. Chem.*, **B21**, 25 (1933); *ibid.*, **B32**, 447 (1936).
2. T. B. Grimley, "The Chemistry of the Solid State," Ch. 14, Editor, W. E. Garner, Academic Press, Inc., New York, Butterworths Scientific Publications, London (1955).
3. O. Kubaschewski and B. E. Hopkins, "Oxidation of Metals and Alloys," Butterworths Scientific Publications, London (1953).
4. N. B. Pilling and R. E. Bedworth, *J. Inst. Metals*, **29**, 529 (1923).
5. E. A. Gulbransen, *Ind. Eng. Chem.*, **41**, 1385 (1949).
6. D. A. Vermilyea, *Acta Met.*, **5**, 492 (1957).
7. U. R. Evans, *This Journal*, **91**, 547 (1947).
8. J. Loriers, *C. R. Acad Sci., Paris*, **231**, 522 (1950).
9. W. W. Webb, J. T. Norton, and C. Wagner, *This Journal*, **103**, 107 (1956).
10. J. Loriers, *C. R. Acad. Sci., Paris*, **234**, 91 (1952).
11. P. Levesque and D. Cubicciotti, *Am. Chem. Soc.*, **73**, 2028 (1951).
12. A. Dravnieks and C. H. Samans, *This Journal*, **105**, 183 (1958); F. Hügli, C. M. Hudgins, Jr., and P. Delahay, Paper presented API Div. of Refining, Los Angeles, California, May 1958.
13. E. A. Gulbransen and W. S. Wysong, *J. Physik. chem.*, **51**, 1087 (1947).
14. W. W. Smeltzer, *This Journal*, **103**, 209 (1956).
15. W. W. Smeltzer and M. T. Simnad, *Acta Met.*, **5**, 320 (1957).
16. D. Cubicciotti, *J. Am. Chem. Soc.*, **74**, 557 (1952).
17. T. E. Leontis and F. N. Rhines, *Trans. Am. Inst. Mining Met. Engrs.*, **166**, 265 (1946).
18. Reference (3), p. 41.
19. E. W. Haycock, *This Journal*, **106**, 764 (1959).
20. M. S. Hunter and P. Fowle, *This Journal*, **103**, 482 (1956).
21. E. A. Gulbransen, *Annals. N. Y. Acad. Sci.*, **58**, 830 (1954).
22. J. V. Cathcart, J. J. Campbell, and G. P. Smith, *This Journal*, **105**, 442 (1958).

The Effect of Halides on the Capacity and Resistance of the Magnesium Electrode in Aqueous Solutions

G. R. Hoey and M. Cohen

Division of Applied Chemistry, National Research Council, Ottawa, Ontario, Canada

ABSTRACT

A study of potential-time decay curves at anodically and cathodically polarized magnesium by the d-c current interrupter method is presented. Potential-time oscillograms and polarization curves were determined for magnesium electrodes in buffered and unbuffered aqueous solutions containing chloride, bromide, iodide, and fluoride. Film capacity, solution double layer capacity, and resistance data determined from the oscillograms using the electrical analog

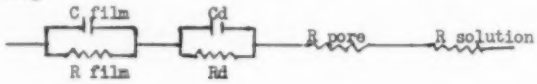

is presented where Cd and Rd are the capacity and resistance of the Helmholtz-Gouy double layer. The effect of specific adsorption of anions and the physical nature of the film on the magnesium electrode are discussed.

Local corrosion (1-3) and electrochemical formation of Mg^{+} (4-10), Mg_2^{++} (11), and $Mg \cdot Mg^{++}$ (3) have been suggested to explain the negative difference effect observed for magnesium. The existence of the ions Mg^{+}, Mg_2^{++}, and $Mg \cdot Mg^{++}$ has not been definitely established, and the negative difference effect of Mg may, in fact, be explained solely on the basis of local corrosion. It can be stated with certainty, however, that even if Mg^{+} is formed, local corrosion must also occur. This conclusion follows from the experimental facts: (*a*) values of the apparent Mg valency (determined coulometrically) less than unity as well as greater than unity have been observed; (*b*) a positive difference effect is observed for Mg at low anodic current densities in solutions containing HCl or NH_4Cl (9, 12). Observed Mg valencies greater than unity may be explained by electrochemical formation of Mg^{++}, either directly or via the reaction, $Mg^{+} \rightarrow Mg^{++} + e$ (5).

From the above considerations it may be concluded: (*a*) the potential of Mg is a mixed anodic-cathodic potential, and (*b*) although the mechanism of the local anodic reaction is uncertain it consists, in part, of the electrochemical formation of Mg^{++}, either directly or via monovalent Mg. The local cathodic reaction is generally the hydrogen evolution reaction but may under some experimental conditions consist both of the h.e.r. and the oxygen adsorption reaction (13, 14).

The potential of the Mg electrode may be under anodic, cathodic, or mixed control depending on the experimental conditions. In acid solutions (pH's < 3 in unbuffered solutions) the corrosion reaction is probably under cathodic control; the potential becomes more noble with increasing hydrogen ion concentration (15) and the corrosion proceeds under H_3O^{+} diffusion control (16, 17). At high pH's (pH $>$ 11 in unbuffered solutions), the potential increases sharply in the more noble direction with increasing pH and anodization causes passivation (15) which indicates that at high pH's the reaction is under anodic control. In the intermediate pH range the potential of Mg is practically independent of pH and a transition from cathodic to anodic control probably occurs. Film formation at high pH's undoubtedly plays a major role in the transition from cathodic to anodic control and there are indications that transport phenomena through surface film may be partly rate controlling even at low pH's (18). Although the chemical composition of the surface film is reasonably well established (19-23), little is known concerning such important factors as the conductivity and porosity of the film. The Mg electrode potential is dependent on the nature and concentration of inactive anions in solution (24) which suggests that specific adsorption effects of anions on the electrode might also be important.

This study was undertaken in order to gain further information on the roles of specific adsorption of anions and film formation in the electrochemical behavior of Mg. It was felt that a comparison of the effect of halide ions on the Mg electrode capacity, resistance, and polarization curves would provide information on specific adsorption and film effects. A limited amount of data exists in the literature which might be used for predicting the adsorption behavior of halide ions on Mg. Cl^{-1}, Br^{-1}, and I^{-1} form soluble salts with Mg, whereas MgF_2 is insoluble leading to passive films. The order of increasing adsorption of these ions on mercury are $F^{-1} < Cl^{-1} < Br^{-1} < I^{-1}$ (25). The fluoride ion is not considered to be specifically adsorbed on mercury. On platinum, I^{-1} is probably more strongly adsorbed than Cl^{-1}; the minimum in the Pt electrode capacity vs. potential curve for solutions containing I^{-1} is more cathodic than that for solutions containing Cl^{-1} (26). The same order of

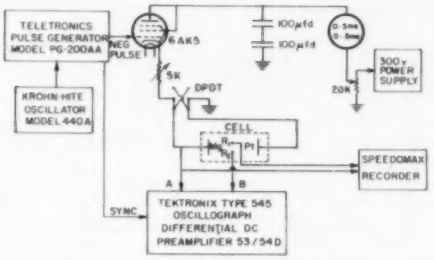

Fig. 1. D-C current interrupter apparatus

adsorbability of Cl^{-1}, Br^{-1}, and I^{-1} might be expected for Mg as for Hg and Pt.

Experimental

Polarization capacity and resistance was determined by the d-c current interrupter method. The current interrupter technique used was similar to that of Shuldiner and White (27). The circuit is given in Fig. 1. The cell was polarized by means of a constant current supplied in the plate circuit of the pentode 6AK5. The pentode was hooked up as a triode. By reversing the DPDT switch the Mg electrode could be made anodic or cathodic. The potential of the Mg electrode was continuously recorded on a Speedomax recorder. Potential-time oscillograms were determined as follows. A negative pulse with a rise time of 0.1 μsec was supplied to the grid of the pentode which shuts off the tube for the pulse interval; the Teletronics pulse generator was used to give interruption times from 1 μsec to 1 msec, and a Tektronix type 161 pulse generator was used for pulse widths from 1 msec to 0.1 sec. The pulse generator could be triggered by the oscillator to give from 0.1 pulses/sec to 5000 pulses/sec; repetition rates less than 0.1 pulses/sec could not be recorded on the oscilloscope. The pulse generator was triggered to a Tektronix type 545 oscilloscope which recorded the potential-time changes occurring at the Mg electrode during the current interruption. The maximum sensitivity of the Tektronix type 53/54D preamplifier was 1 mv/cm. Oscilloscope traces were photographed with a type 299 Dumas oscilloscope recording camera.

Potential-current polarization curves were determined using the constant current method. The Mg electrode was anodically polarized at 0.4 ma/cm² for 12 hr during which time the potential reaches a steady value. The current was then changed in steps lasting about ½ hr from 0.4 ma/cm² anodic to 0.4 ma/cm² cathodic and back again to 0.4 ma/cm² anodic in steps. At each setting of the current the potential was recorded on the Speedomax recorder and potential-time oscillograms were taken. The electrolytic cell was machined from Lucite, cylindrical in shape, with a slit along the top through which the reference electrodes could be immersed in the solution. The distance of the reference electrode from the Mg electrode could be varied along the length of the cell. The working electrode was platinized platinum; the reference electrode (R_1) was a silver-silver halide electrode; and R_2 was a Mg wire reference electrode (Fig. 1).

The Mg test electrode (area = 5 cm²) was machined from commercially distilled pure Mg. This material was supplied to have a minimum purity of 99.96% with a total Fe, Ni, and Cu content not greater than 0.005%. The Mg electrode surface was prepared by polishing on silicon carbide papers followed by a 1 min etch in 10% HNO_3 acid solution. The optical and electron microscopes revealed a clean surface preparation. By electron diffraction examination the film remaining on the Mg electrode after the chemical etch was shown to be MgO and $Mg(OH)_2$.

Solutions were prepared from reagent grade salts. During a run fresh solution was continuously supplied to the cell solution by means of an overflow system.

Results

Typical potential-time decay curves are given in Fig. 2, 3, and 4. The potential-time curves are interpreted in terms of the equivalent electrical circuit:

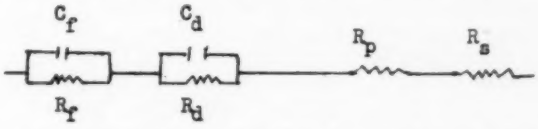

C_f is the capacity of the electrical double layer with the film as dielectric and R_f is the polarization resistance of the film; C_d and R_d are the capacity and polarization resistance of the solution electrical double layer; R_p is that part of the pore resistance of the film which is noncapacitive; and R_s is the resistance of the solution between the reference electrode and the magnesium electrode.

The equivalent electrical circuit is based on the model of the metal electrode given in Fig. 11 which

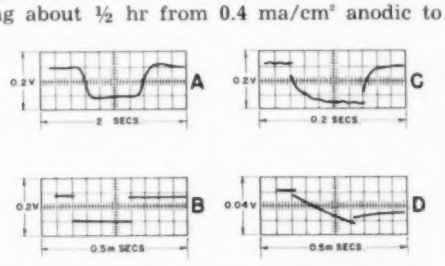

Fig. 2. Potential-time decay curves of anodically polarized Mg; A, B, and C; solution, 0.05M NaOH, 0.186N H_3BO_3; 0.1M NaCl; pH = 8.9; 0.4 ma/cm². D; solution 0.1M NaF; 0.035 ma/cm².

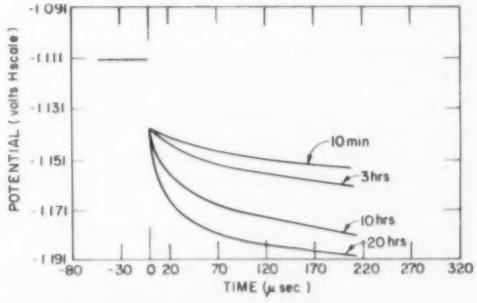

Fig. 3. Potential-time decay curves of anodically polarized Mg after various polarization times in a solution containing 0.1M NaOH; 0.1M H_3BO_3, and 0.1M NaBr; 0.4 ma/cm²; pH = 11.

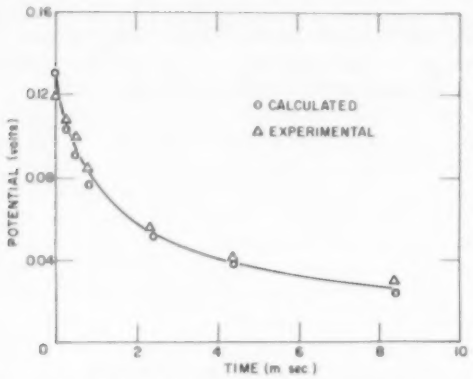

Fig. 4. Calculated and experimental potential-time decay curves of anodically polarized Mg in solution containing 0.05M NaOH, 0.186 H_3BO_3, and 0.1M NaCl; 0.4 ma/cm²; pH = 8.9.

is described in the Discussion. The solution double layer (Fig. 11) is considered to be in a pore of a nonconducting type film. The comparison of the electrical double layer of the electrode with an equivalent circuit is not strictly correct, but it is a simple and convenient manner in which to express the results of this type of experiment.

The components of the equivalent circuit are determined from the potential-time oscillograms. The potential drop which occurs in the first 0.3 μsec of the interruption in Fig. 2A, which will be called the series polarization, is the sum of the potential drops across elements of the equivalent circuit with time constants < 0.3 μsec; the series resistance (R_s) is equal to the series polarization divided by the value of the current before interruption. R_s is equal to the sum of R_p and R_r and will also include R_f and R_d if R_fC_f and C_dR_d is < 0.3 μsec. The residual series resistance exclusive of the solution resistance is obtained by measuring the series polarization at various points from the Mg electrode; R_r is a function of the distance of the reference electrode from the Mg electrode whereas R_f and R_p are not. Typical plots of the series resistance vs. the distance of the reference electrode from the Mg electrode are given in Fig. 5; the residual series resistance for both cases is 25 ohm-cm². For the experimental conditions studied in this work the contribution of the residual series resistance to the overpotential of the Mg electrode is less than 5% in active solutions and less than 1% in passive solutions.

The capacity of the Mg electrode (C) is defined by the expression:

$$C = -i^\circ/(dE/dt)_{t=0} \qquad [1]$$

where i° is the current at the moment of interruption and $(dE/dt)_{t=0}$ is the slope of the potential-time decay curve taken at $t = 0$.

The rate of potential decay across the capacitive part of the equivalent circuit is

$$dE/dt = -(E_f/R_fC_f + E_d/R_dC_d) \qquad [2]$$

where E_f and E_d are the potentials across the film and solution double layer circuits, respectively. At $t = 0$, $E_f/R_f = E_d/R_d = i^\circ$

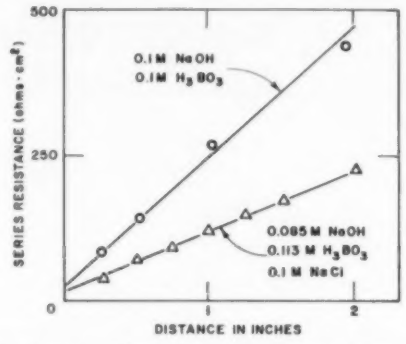

Fig. 5. Series resistance as a function of distance of the reference electrode from the Mg electrode: 0.4 ma/cm².

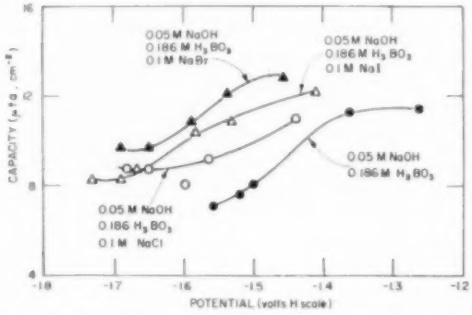

Fig. 6. Magnesium electrode capacity as a function of polarization potential; pH = 8.9.

$$(dE/dt)_{t=0} = -i^\circ(C_f + C_d)/C_fC_d \qquad [3]$$

and

$$C = C_fC_d/(C_f + C_d) \qquad [4]$$

Equation [3] is simplified when the time constants R_fC_f and R_dC_d are quite different, and then

$$(dE/dt)_{t=0} = -i^\circ/C_f \qquad [5a]$$

$$\text{or} \qquad = -i^\circ/C_d \qquad [5b]$$

depending on the time range studied by the oscilloscope. Magnesium electrode capacity data are given in Fig. 6 and Table I. The experimental capacities are correlated with the components of the equivalent electrical circuit in the discussion.

The parallel polarization resistance is obtained from the potential time oscillograms using the equation:

$$R_{f,d} = -\frac{|\Delta E|_{t=0}^{t=t}}{C} \Big/ |dE/dt|_{t=0}^{t=t} \qquad [6]$$

where $R_{f,d}$ is the parallel polarization resistance of either the film or the solution double layer; $|\Delta E|_{t=0}^{t=t}$ is the difference in potential and $|\Delta dE/dt|_{t=0}^{t=t}$ is the difference in rate of potential decay at times $t = t$ and $t = 0$. Equation [6] is valid when the time constants for decay across the film and solution double layers are equal or when one of the two decay rates is small compared to the other. Resistance data for the solutions studied are given in Table I. The reproducibility of $R_{f,d}$ determinations using Eq. [6] is about ±50%.

Potential-current polarization curves of Mg in buffered and unbuffered solutions with halide addi-

Table I

Solution	pH	Current ma/cm²	Polarization potential, v-H scale	Rest potential (E_c), v-H scale	Series polarization, v	Parallel resistance, ohm-cm²	Capacity, μf/cm²
0.05M NaOH, 0.186M H_3BO_3	8.9	0.39(a)	−1.40	−1.61	0.038	40	11.2
0.1M NaCl		0.40(c)	−1.72	−1.61	0.038	55	8.8
0.05M NaOH, 0.186M H_3BO_3	8.9	0.40(a)	−1.18	−1.48	0.125	60	11.0
0.0002M NaCl		0.40(c)	−1.72	−1.48	0.150	85	7.2
0.05M NaOH, 0.186M H_3BO_3	8.9	0.40(a)	−1.37	−1.63	0.038	40	12.2
0.1M NaI		0.19(c)	−1.70	−1.63	0.016	25	8.2
0.05M NaOH, 0.186M H_3BO_3	8.9	0.40(a)	−1.41	−1.63	0.052	70	12.8
0.1M NaBr		0.40(c)	−1.75	−1.63	0.040	135	9.4
0.05M NaOH, 0.186M H_3BO_3	8.9	0.40(a)	−1.15	−1.48	0.12	50	11.2
		0.42(c)	−1.70	−1.48	0.14	80	7.0
0.05M NaOH, 0.186M H_3BO_3	8.9	0.21(a)	4.5	−1.5	0.030	2500	0.30
0.1M NaF		0.28(c)	−2.4	−1.5	0.040	1150	0.36
0.085M NaOH, 0.113M H_3BO_3	10.0	0.40(a)	−1.35	−1.62	0.033	90	10.0
0.1M NaCl		0.40(c)	−1.79	−1.62	0.036	300	7.4
0.10M NaOH, 0.10M H_3BO_3	11.2	0.37(a)	2.42	−1.38	0.065	110	0.2
0.10M NaOH, 0.10M H_3BO_3 0.1M NaCl	11.1	0.36(a)	−1.23	−1.41	0.028	65	0.5
0.10M NaOH, 0.10M H_3BO_3 0.1M NaI	11.0	0.35(a)	−0.86	−1.45	0.030	250	0.2
0.10M NaOH, 0.10M H_3BO_3 0.1M NaBr	11.0	0.38(a)	−1.12	−1.40	0.036	75	0.4
0.10M NaOH, 0.10M H_3BO_3	10.9	0.14(a)	9.0	−1.42	0.012	600	0.32
0.1M NaF		0.20(c)	−2.27	−1.42	0.020	850	0.53
0.1M NaCl	10.6	0.36(a)	−1.21	−1.44	0.090	55	9.0
0.1M NaBr	10.5	0.38(a)	−1.32	−1.50	0.040	70	5.6
0.1M NaI	10.5	0.4(a)	−1.34	−1.45	0.038	55	6.0
0.1M NaF	9.9	0.14(a)	13.7	−1.63	0.004	3250	0.28
		0.50(c)	−2.29	−1.63	0.018	1500	0.44

(a) Anodic polarization; (c) Cathodic polarization.

tions are given in Fig. 7, 8, 9, and 10. The reproducibility of potential measurements for the experimental conditions of Fig. 7, 8, and 9 is 30 mv and for Fig. 10 the reproducibility is 0.2 v. Cathodic polarization measurements of Mg in solutions buffered at pH = 11 containing NaCl, NaBr, or NaI and unbuffered solutions containing NaCl, NaBr, or NaI are nonreproducible and are not presented.

Discusssion

An exact theoretical treatment of the potential time curves observed in this work is not possible; the current density is probably nonuniform over the electrode surface and the electrochemical mechanism is complicated and uncertain. However, a semiquantitative and perhaps fortuitous agreement between the current interrupter theory and experiment was found.

An equation for the potential-time decay curves is derived in the following manner. Assume the rate-controlling reaction is:

$$Mg = Mg^{n+} + ne \qquad [7]$$

The forward current ($\vec{i}$) and the reverse current ($\overleftarrow{i}$) of reaction [7] are given by the equations (28),

$$\vec{i} = i_o \exp(\alpha n\mathbf{F}\,\Delta E_c/RT) \exp(\alpha n\mathbf{F}\,\Delta E/RT) \qquad [8]$$

$$\overleftarrow{i} = i_o \exp(-(1-\alpha)n\mathbf{F}\Delta E_c/RT) \exp(-(1-\alpha)n\mathbf{F}\Delta E/RT) \qquad [9]$$

$$i = \vec{i} - \overleftarrow{i} - i_{corr} \qquad [10]$$

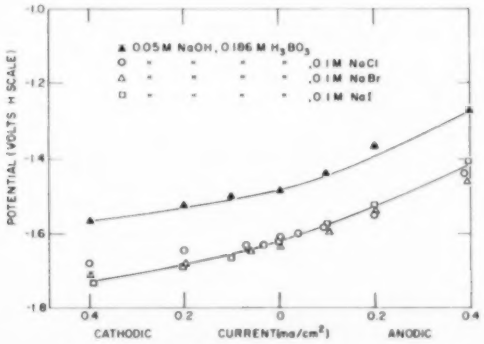

Fig. 7. Anodic and cathodic polarization curves of Mg corrected for series polarization; pH = 8.9.

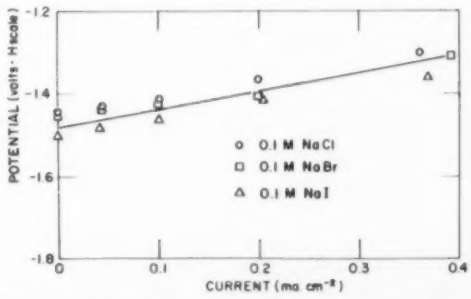

Fig. 8. Anodic polarization curve of Mg corrected for series polarization; pH = 10.5.

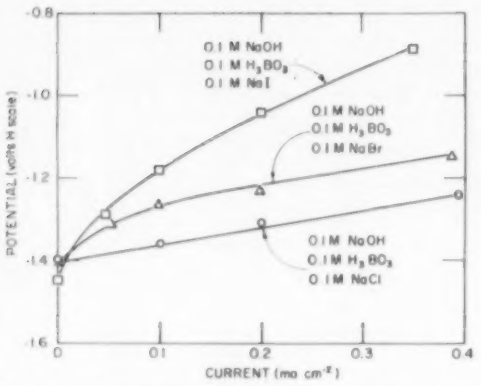

Fig. 9. Anodic polarization curve of Mg corrected for series polarization; pH = 11.

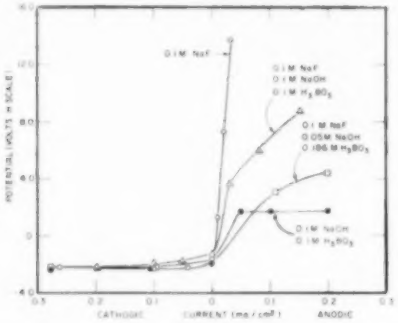

Fig. 10. Anodic and cathodic polarization curves of Mg corrected for series polarization; ●, pH = 11; □, pH = 8.9; △, pH = 11; ○, pH = 10.

where $\Delta E = E - E_c$, and $\Delta E_c = E_c - E_e$; i_o is the exchange current and α is the transfer coefficient for reaction [7]; **F** is the Faraday; R is the gas constant; T is the absolute temperature; E is the polarization potential; E_c is the corrosion potential at zero applied current; E_e is the equilibrium potential for reaction [7]; i is the applied current and i_{corr} is the corrosion current. The current efficiency for the anodic dissolution of Mg assuming $n = 2$ (3) is independent of current density at high current densities ($i > 0.05$ ma/cm^2) which indicates that the corrosion current is directly proportional to the applied current. Thus, it may be assumed that $i_{corr} = (K - 1)\, i$ where K is a constant ($K > 1$) which is independent of the applied current.

Since

$$dE/dt = -\, i/C \qquad [11]$$

then

$$\int \frac{d\,\Delta E}{\overrightarrow{i} - \overleftarrow{i}} = -\int (1/CK)\,dt \qquad [12]$$

where it is assumed that E_c and E_e are independent of applied current. Integration of Eq. [12] by Grahame's method (29) using the assumptions $\alpha = \frac{1}{2}$, $\exp\,(\alpha n\mathbf{F}\Delta E_c/RT) \gg 1$, and C is independent of ΔE yields the equation

$$\Delta E = \frac{2RT}{n\mathbf{F}} \ln \frac{1 + \exp\,(-n\mathbf{F}i_o(t + t')/RTCK)}{1 - \exp\,(-n\mathbf{F}i_o(t + t')/RTCK)} \qquad [13]$$

t is measured from the moment of interruption and t' has the meaning that ΔE would be infinite at $t = -t'$. The assumption that $\exp\,(\alpha n\mathbf{F}\Delta E_c/RT) \gg 1$ may set a fictitious value to the equilibrium potential for reaction [7], i.e., $E_e \approx E_c$, when Eq. [13] is applied to a corroding Mg electrode; the simultaneous occurrence of the cathodic and anodic reactions on anodically polarized Mg could have the effect of displacing the experimental potential of the electrode from the potential of the anodic reaction toward the potential of the cathodic reaction if an appreciable ohmic potential drop exists between the reaction paths of the cathodic and anodic reactions.

Equation [13] was derived for an electrode with a uniform current density over the surface. In active solutions at pH = 8.9 a uniform attack occurs on Mg which indicates a uniform current density. The general form of the potential-time decay curves for Mg in this type of solution is represented by Eq. [13]. In Fig. 4 the potential-time decay curve for anodically polarized Mg calculated from Eq. [13] using assumed values of n, t', K, and i_o ($n = 2$, $t' = 0.1$ msec, $K = 2$, and $i_o = 0.024$ ma/cm^2), and $C = 10\ \mu$ f/cm^2 from initial slope compares well with the experimental potential-time decay curve. The rate of reaction [7] calculated from Eq. [10] is within an order of magnitude of the rate of dissolution of Mg in this particular solution at the same current (10^{-5} moles/cm^2/sec).

In view of the many simplifying assumptions necessary for the derivation of Eq. [13] further interpretation of the results in terms of this equation would be unwarranted. The remainder of the discussion will be concerned with qualitative interpretation of the capacity and potential data in terms of the equivalent electrical circuit previously given and the following concept of the structure of the Mg electrode interface.

The structure of the Mg electrode interface will be assumed to be of the form schematically represented in Fig. 11. Positive and negative polarization refers to polarization relative to the potential of the zero point of charge. The anodic and cathodic reactions are assumed to occur at the barrier film-solution interface. In Fig. (11B) the electrode is considered to be sufficiently polarized to completely suppress the anodic reaction. The nature of the film is pH dependent. A thin nonporous barrier film is assumed to be present at all pH's. In active solutions, at pH's $\lesssim 10.5$, thick white films (10^{-4} cm) are formed on Mg; at pH's < 10.5 thin films ($< 10^{-5}$ cm) are formed. The discontinuity in film formation is due to precipi-

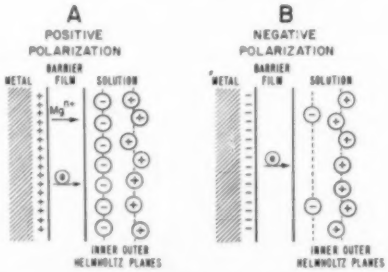

Fig. 11. Schematic diagrams of the electrical double layer of positively and negatively polarized Mg.

tation on the Mg at pH's ≥ 10.5 of $Mg(OH)_2$ from solution (3). At the low field strength used in this work transport of ions and electrons through the thick film would not occur for nonpassive films.

The capacity of the barrier film is a decreasing function of pH and polarization current since these factors would tend to increase the barrier film thickness. The polarization resistance of the barrier film is dependent on thickness and chemical and physical structure of the film; the latter factor controls the type of transport (ionic or electronic). The capacity of the solution double layer which includes the fixed double layer and the diffuse double layer is a complex function of potential; several maxima and minima are sometimes observed (25). In the simplest case the capacity of the solution double layer reaches a minimum at the potential of the zero point of charge and increased polarization increases the capacity due to the decrease in effective distance between the outer Helmholtz plane and the barrier film. The electrode capacity per unit of apparent area is directly related to the pore area and the polarization resistance of the electrode is inversely proportional to the pore area.

Specific adsorption of anions on Mg would have the effect of increasing the capacity of the solution double layer and displacing the potential of the zero point of charge to more cathodic potentials. Specific adsorption of anions provides a means of explaining the negative difference effect of Mg. Increased anodic polarization causes increased adsorption on the barrier film which results in an increased positive charge on the diffuse double layer and a closer proximity of the diffuse double layer to the barrier film. Hydrogen ions in the diffuse double layer are therefore more easily discharged at the barrier film by increased anodic polarization.

In the following sections a satisfactory explanation of the experimental results is presented in terms of the pore theory.

Buffered Solutions at pH = 8.9

The halide additions affect the polarization curves of the buffer solutions but no specific effect of the anions Cl^{-1}, Br^{-1}, or I^{-1} are apparent (Fig. 7). The shift in potential observed in solutions without halide additions is probably due to higher Helmholtz-Gouy double layer impedance corresponding to the lower conductivity of the buffer solution. The Mg electrode capacity is probably the solution double layer capacity (C_d) since the capacity increases as the anodic polarization is increased (Fig. 6). Thus, it appears that the time constant for decay across the barrier film at pH = 8.9 is less than 0.3 μsec. Specific effects of each of the halides on the capacity are not evident within the reproducibility of the experiments. The borate ion is apparently preferentially adsorbed on Mg in these solutions.

Cathodic polarization in the range studied does not effect a change in sign of the charge on the metal surface from positive to negative (Fig. 11) since the capacity did not go through a minimum on cathodic polarization. The rate of dissolution of cathodically polarized Mg in these solutions is quite large which serves to maintain the Mg metal surface positively charged or perhaps neutral (there is the possibility that the minimum in the capacity vs. potential curves was reached at the most cathodic potentials studied).

Buffered Solutions at pH = 11

The capacity of the Mg electrode at pH = 11 is considerably lower than the capacity at pH = 8.9 (Table I). A decrease in capacity of both the barrier film and the solution double layer is expected due to the decreased reacting area of the electrode and increased barrier film thickness. The formation of the porous film or barrier film is a slow process; the Mg electrode capacity changes from 2 $\mu f/cm^2$ at 10 min polarization to 0.4 $\mu f/cm^2$ at 20 hr polarization (Fig. 3). Trends of the observed capacity at pH = 11 with specific halide ion or potential may be hidden due to the low reproducibility of capacity measurements in these solutions. Therefore, it is not possible to decide whether the experimental capacity is C_f,C_d, or the series capacity, $C_fC_d/(C_f + C_d)$:

Buffered solutions at pH = 11 without a halide additive exhibit passive potentials on anodic polarization in contrast to solutions buffered at pH = 8.9 (Fig. 10). Halide additions destroy this passivity (Fig. 9). The order of increasing effectiveness of the halide ions as depassivating ions is $I^{-1} < Br^{-1} < Cl^{-1}$. The depassivating effect of halide additions on the passivity of Mg at pH = 11 is explicable in terms of the pore theory if it is assumed that the pore size is large enough for penetration by halide ions and too small for penetration by BO_3^{-3} ions. The relative depassivating effect of the halide ions may be due to the relative mobilities of the halide ions which follow this same order, i.e., $I^{-1} < Br^{-1} < Cl^{-1}$.

Unbuffered Solutions

The film formed on Mg in unbuffered solutions of NaCl, NaBr, and NaI is similar to that at pH = 11 but the pH in the pores is probably lower than the bulk pH of the unbuffered solution. The reacting area of the Mg metal surface is increased over that in buffered solutions at pH = 8.9 by a change in type of attack from general to pitting and film formation in unbuffered solutions tends to decrease the reacting area of the barrier film. Without a knowledge of relative roughness factors of the electrode it is impossible to compare observed capacities in unbuffered solutions with those in buffered solutions. The capacity of the Mg electrode in NaCl solution is significantly greater than for solutions of NaBr and NaI, which indicates that the Cl^{-1} ion is more strongly adsorbed on Mg than either the Br^{-1} ion or I^{-1} ion which is the reverse of what might be expected from data on Pt and Hg (25, 26). If this is true specific adsorption of anions does not produce significant changes in the potential of Mg (Fig. 8). The capacity of the Mg electrode in 0.1M NaCl solution determined by Tomashov, *et al.* (13) using the a-c bridge method (500-5000 cps) is 7-8 $\mu f/cm^2$ which is in good agreement with this work (9 $\mu f/cm^2$).

Sodium Fluoride Solutions

Magnesium in NaF solutions exhibits high anodic polarization (Fig. 10); the rest potential is active yet the corrosion rate is small. These facts may be ex-

plained by a pore theory with the following assumptions: the barrier film is nonporous MgF_2 with inclusions of porous film; the area of the porous film is small compared with the area of the nonporous film; and the nonporous film becomes charged on anodic polarization, but electrochemical reaction both cathodic and anodic occurs only at the porous areas. Thus, at zero applied polarization the corrosion of Mg occurs at a slow rate at the pores which explains the active rest potential observed; anodic polarization would partially fill up the pores with MgF_2 at a rate proportional to the applied polarization current and raise the potential in the pores to passive potentials. The anodic overpotential of Mg is less in buffered solution of NaF than in unbuffered solutions. Evidently the BO_3^{-3} ion has a similar effect on the passivity of Mg in NaF solution as Cl^{-1}, Br^{-1}, and I^{-1} have on the passivity of Mg in the buffer solution at pH = 11 but to a much lesser degree. Partial filling up of the pores with $Mg(OH)_2$ explains the fact that the anodic overpotential is higher for NaF solutions buffered at pH = 11 than at pH = 8.9. The relatively lower overpotential for the cathodic polarization indicates that cathodic polarization does not reduce the pore area.

The capacity in buffered and unbuffered solutions of NaF varied from 0.3 to 0.5 $\mu f/cm^2$ over the entire potential range studied. The invariance of the capacity over the large range of potentials suggest that the capacity is due to the nonporous areas of the film, the effective thickness of which is independent of potential. The double layer with the nonporous areas of the film as dielectric discharges through the pores in the film.

Resistance Measurements

In solutions containing fluoride the parallel polarization resistance ($R_{p,a}$) varied from 600 ohm-cm^2 to 3200 ohm-cm^2; in all other solutions the parallel resistance varied from 25 ohm-cm^2 to 250 ohm-cm^2. Little significance can be given to the values of $R_{p,a}$ due to the poor reproducibility except to state that the relative magnitude of $R_{p,a}$ for Mg in NaF solution indicates that the pore area is smaller than for the other solutions.

The contribution of the ohmic potential drop to the total overpotential of Mg in the passivating solutions studied in this work is less than 1% which is in general agreement with the work of Epelboin, *et al.* (30). By application of a circuit breaking technique Epelboin, *et al.* (30) have shown that the high potentials observed in passivating, anodic oxidation, and electrolytic polishing experiments are not due to diffusion overvoltage or ohmic drop but are probably due to adsorption effects of anions at the metal surface.

Acknowledgment

The authors wish to express their appreciation to Mr. L. T. Bradley for assistance in the design of the d-c current interrupter apparatus, and to Dr. P. B. Sewell and Mr. E. G. Brewer for examination of the magnesium surface preparation used in this work by electron diffraction and the electron microscope.

Manuscript received Jan. 23, 1959. This paper was prepared for delivery before the Ottawa Meeting, Sept. 28-Oct. 2, 1958.

Any discussion of this paper will appear in a Discussion Section to be published in the June 1960 JOURNAL.

REFERENCES

1. H. A. Robinson, *Trans. Electrochem. Soc.*, **90**, 485 (1946); "Cathodic Protection, A Symposium" p. 104, N.A.C.E. Houston (1949).
2. N. D. Tomashov, V. S. Komissarova, and M. A. Timonova, *Trudy Inst. Fiz. Khim., Akad. Nauk S.S.S.R.*, **4**, 172 (1955).
3. G. R. Hoey and M. Cohen, *This Journal*, **105**, 245 (1958).
4. M. D. Rausch, W. E. McEwen, and J. Kleinberg, *J. Am. Chem. Soc.*, **76**, 363, 3622 (1954); **77**, 2093 (1955).
5. W. E. McEwen, J. Kleinberg, D. L. Burdick, W. D. Hoffman, and J. Y. Yang, *ibid.*, **78**, 4587 (1956).
6. J. H. Greenblatt, *This Journal*, **103**, 539 (1956).
7. W. Beetz, *Pogg. Ann.*, **27**, 115 (1866).
8. P. Brouillet, I. Epelboin, and M. Froment, *Compt. rend.*, **239**, 1795 (1954).
9. D. V. Kokoulina and B. N. Kabanov, *Doklady Akad. Nauk. S.S.S.R.*, **112**, 692 (1957).
10. B. N. Kabanov and D. V. Kokoulina, *ibid.*, **120**, 558 (1958).
11. S. Bodforss, *Z. Physik Chem.*, **153**, 83 (1931).
12. B. Roald and W. Beck, *This Journal*, **98**, 277 (1951).
13. E. N. Paleolog, G. V. Akimov, N. P. Tomashov, and K. S. Korotkova, "Problemy Korozii i Zashchity Metallov," *Inst. Fiz. Khim., Akad. Nauk S.S.S.R.*, 237 (1956).
14. N. D. Tomashov and T. V. Matveeva, *Trudy Inst. Fiz. Khim., Akad. Nauk S.S.S.R.*, **2**, Zssledovaniza po Korrozii Metal No. 1, 146 (1951).
15. G. V. Akimov and I. L. Rozenfeld, *Compt. rend. acad. sci. U.R.S.S.*, **44**, 193; *Doklady Akad. Nauk. S.S.S.R.*, **44**, 211 (1944).
16. C. V. King and W. H. Cathcart, *J. Am. Chem. Soc.*, **59**, 63 (1937).
17. G. E. Coates, *J. Inst. Metals*, **71**, 457 (1945).
18. E. J. Casey and R. E. Bergeron, *Can. J. Chem.*, **31**, 849 (1953).
19. R. Faivre and A. Michel, *Compt. rend.*, **208**, 1008 (1939).
20. C. Brouchere, *J. Inst. Metals*, **71**, 131 (1943).
21. K. Huber, *This Journal*, **100**, 376 (1953).
22. N. A. Shishakov, *Zhur. Fiz. Khim.*, **26**, 358 (1952).
23. S. Yamaguchi, *J. Appl. Phys.*, **25**, 1437 (1954); *J. Chem. Soc. Japan*, **61**, 887 (1940).
24. J. Van Muylder and M. Pourbaix, Centre Belge D'Etude De La Corrosion Rappt. Tech. No. 39 (1956).
25. D. C. Grahame, *Chem. Revs.*, **41**, 441 (1947).
26. J. N. Sarmousakis and M. J. Prager, *This Journal*, **104**, 454 (1957).
27. S. Shuldiner and R. E. White, *ibid.*, **97**, 433 (1950).
28. M. Stern, *ibid.*, **104**, 56 (1957).
29. D. C. Grahame, *J. Phys. Chem.*, **57**, 257 (1953).
30. I. Epelboin, P. Brouillett, and M. Froment, *Proc. Intern. Comm. Electrochem. Thermodynam. and Kinet.*, 7th Lindau 26 (1957).

Use of Nickel-Aluminum Alloy Coatings for the Protection of Molybdenum from Oxidation

W. Beck[1]

American Electrometal Corporation, Yonkers, New York

ABSTRACT

Coatings produced by electrodeposition of aluminum on nickel-plated molybdenum protect this metal effectively against high-temperature oxidation. Information about composition and distribution of the Ni-Al phases formed in the coating was obtained from a metallographic analysis of a layer created by deposition of aluminum from the cryolite bath on a sheet of high-purity nickel.

Effective protection of molybdenum against high-temperature oxidation by a coating consisting of nickel aluminides has been reported recently by Couch, Shapiro, and Brenner (1). The coating was produced in an unorthodox fashion by electrodeposition (1, 2) of aluminum from a fused cryolite bath onto nickel, which had been plated from an aqueous solution onto chromium-plated molybdenum. Some years ago, the author of this report (3) succeeded in imparting to Mo, protection against high-temperature oxidation by converting its surface into a Mo-Al alloy, created during electrodeposition of Al from the cryolite bath.

This paper is concerned with the production of Ni-Al coatings on Mo, removal of bath salts from the coating, testing of the effectiveness of the alloy layer to protect Mo against high-temperature oxidation, and the metallographic studies of a Ni-Al diffusion couple.

These investigations were completed some years ago but were not published until now.

Experimental Procedures and Results

Specimens and pretreatment.—The specimens consisted of rods of Mo of 99.9% purity, ¼ in. in diameter and 6 in. long. The ends were rounded in order to avoid sharp angles, ground with a green wheel, and finally polished on a hard rubber wheel.

Various pretreatments were used to achieve satisfactory adhesion of the Ni plate to the Mo surface, including an anodic treatment in HF-HCl mixture and immersion in aqua regia. The latter method, which gave the best results, consisted of a 1-min dip in the acid mixture, followed by cleaning the specimen with cotton under streaming water. This procedure was repeated several times. Immediately following the last immersion and cleaning, the specimen was Ni plated.

Nickel plating.—Nickel was electrodeposited from a Watts-type bath. The average plating thickness was 0.8 mil.

Aluminum plating.—Aluminum was deposited on the Ni plating from a eutectic mixture of 75% cryolite with 25% NaF at a temperature of 1005° ± 5°C. A uniform coating was obtained only when the total concentration of Al in the bath was kept above a minimum value. The Al used up during plating was replaced when necessary by recharging the crucible containing the bath with Al_2O_3 (saturated concentration of Al_2O_3 in the eutectic mixture at 982°C is 15%).

After keeping the rods in the bath for 1 min, Al was plated at a current density of 0.15 amp/cm^2. The approximate total thickness of the aluminide layer, after a plating time of 15 min, was 1.8 mil.

All coatings were produced in a graphite crucible which served as the anode. Bath components were fused by means of high-frequency heating.

Leaching of excess Al *and bath salts and testing for protection against high-temperature oxidation.*—To avoid premature breakdown of the coatings in the blast burner test to be described below, it is of the utmost importance to remove from the surface excess Al and cryolite without attacking the coating itself.

Numerous attempts were made to solve this problem; some of the results are reproduced in Table I. Most effective and least damaging is apparently a 20% HCl solution when used at room temperature.

After leaching, the rods were fastened securely in holders and about 1 in., measured from the tip of the rod, was inserted in the oxidizing cone of an air-gas blast burner. The temperature of the specimens in the flame was determined by optical measurements to be approximately 800°C. They were kept in the flame until the coating broke down and the Mo began to oxidize, evidenced by a change in color of the flame from reddish orange to bright yellow, which is caused by the oxidation products of Mo. The times to breakdown recorded on specimens leached in different solutions are listed in Table I.

Microscopic examination of the nickel-aluminide coating, as plated and after breakdown.—Two sections were taken through each rod after breakdown had occurred, section A about ¼ in. from the tip of the rod, section B approximately 1 in. from section A.

The specimens were mounted in a mixture of amber Bakelite and phenolic resin which has been found to be particularly suitable for coated material,

[1] Present address: Aeronautical Materials Laboratory, Naval Air Material Center, Philadelphia 12, Pennsylvania.

Table I. Time to breakdown of coated Mo specimens exposed to blast burner after leaching of excess Al and bath salts

Composition of coating	Average thickness of alloy coating, 1.8 mil Leaching solution	Appearance of solution or coating after leaching	Time to breakdown in hours in blast burner, Temp. of specimens about 800°C
Ni-Aluminide	Specimen quenched without delay in 20% HCl	Solution showed in all cases green color [1]	Max. 435 Min. 208[2]
Ni-Aluminide	Specimen cooled to room temperature and leached in 20% HCl	In some cases, solution showed slight green color	Max. 1100 Min. 100[2]
Ni-Aluminide	Specimen cooled to room temperature and leached in 37% (conc.) HCl	No change in color became visible	Max. 200
Ni-Aluminide	Specimen cooled to room temperature and leached in 20% NaOH[3]	Coating changed color from dark to black	Max. 100
Mo-Aluminide	Dip in alkali melt[4] followed by leaching in 20% HCl	No change in color became visible	Max. 600
Ni plated from aqueous solution	—	—	Max. 24

Notes:
[1] Leaching time in HCl in all cases was 2 hr; leaching solution was frequently renewed.
[2] Total number of leached specimens was in all cases 10; 80% of specimens had maximum lifetime.
[3] Leaching time was at least 4 hr.
[4] Alkali melt consisted of 60% NaOH and 40% Na_2CO_3 and was used at 540°C.

polished in the conventional manner, etched with Kellers (4) reagent, and then repolished. Subsequently, photomicrographs were taken.

Figures 1 to 3 are photomicrographs of section A. Figure 1 pictures a specimen in the as plated condition. Micrographs shown in Fig. 2 and 3 are taken on specimens after 100- and 540-hr exposure to the blast burner. The coatings represent single phase systems and a number of breakdowns can be distinguished. The coating thickness decreases slightly with increasing oxidation time.

Fig. 1. Ni-aluminide coating. Aluminum electrodeposited from eutectic NaF-cryolite bath on Ni plated on Mo; as plated; leaching in 20% HCl; Keller's etch. Magnification 500X before reduction for publication.

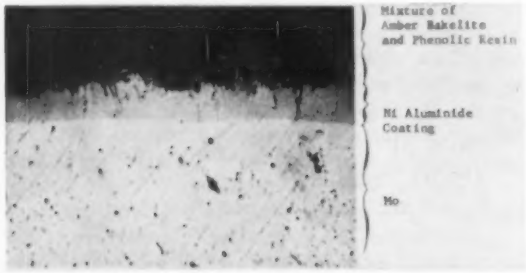

Fig. 2. Ni-aluminide coating. Breakdown after 100-hr exposure to oxidizing flame at approx. 800°C; leaching in 20% HCl; Keller's etch. Magnification 500X before reduction for publication.

Figure 4 exhibits the characteristic "oxidation fingers" which are formed after the coating has broken down and the unprotected Mo is exposed to oxidation. There were no startling differences between the A and B sections.

Phase identification in a Ni-Al *diffusion layer.*— Various attempts to identify the phases formed in the nickel aluminide layer on Mo were not successful, therefore, a different approach was used. Aluminum was electrodeposited from the cryolite bath saturated with Al_2O_3 onto a sheet of A nickel (5),

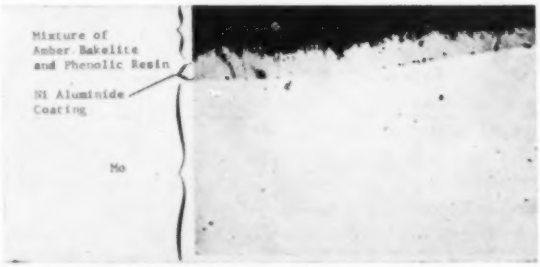

Fig. 3. Ni-aluminide coating. Breakdown after 540-hr exposure to oxidizing flame at approx. 800°C; leaching in 20% HCl; Keller's etch. Magnification 500X before reduction for publication.

Fig. 4. Type of oxidation fingers formed by oxidation of Mo on breakdown points of Ni-aluminide coating at 800°C. Magnification 500X before reduction for publication.

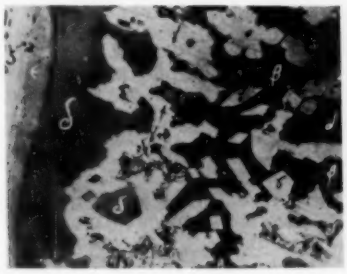

Fig. 5. Phases and phase distribution in Ni-Al diffusion layer produced by electrodeposition of Al from a eutectic NaF-cryolite bath (saturated with Al_2O_3) on a sheet of A Ni. Excess Al was removed in 20% HCl, anodic etch in 1 part conc. HCl with 3-5 parts ethyl alcohol, 1 v, 0.5 amp/in.^{2}, 10 sec. Magnification 1000X before reduction for publication.

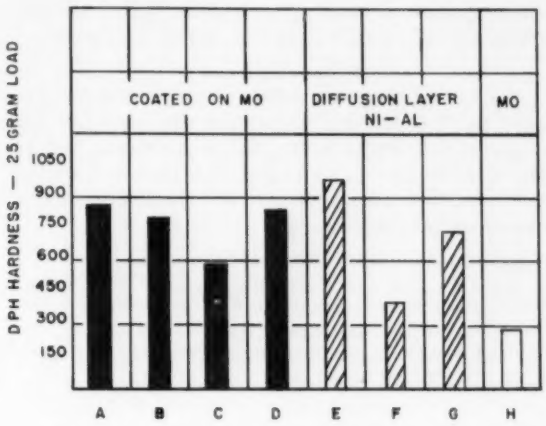

Fig. 6. Hardness measurements made at room temperature: A, Al on Ni, as coated; B, Al on Ni, exposed for 540 hr at 800°C; C, Ni on Al, as plated; D, Ni on Al, exposed for 540 and 1000 hr at 800°C; E, δ phase; F, γ phase; G, β phase; H, Mo.

which was polished to a mirror finish and degreased prior to plating.

The longest time of electrolysis was 5 hr. A number of experiments were made with shorter exposures; however, this did not produce any essential change in the phase distribution shown in Fig. 5. The current density was the same as that used to deposit Al on Ni-plated Mo. After removal from the cryolite bath, the specimen was cooled in ambient air and the coating etched anodically (6).

At the current density and plating time employed, it has to be inferred that the Al diffuses essentially from the liquid phase into the solid Ni after being formed at the cathode, by "direct" electrochemical reduction of an Al donor (7, 8). The Ni is thus in contact with superheated molten Al at a temperature a little above two-thirds of its melting point. By reference to the phase diagram (9), it may be ascertained that Ni may take upwards of about 6 w/o (or 12 a/o) approximately of Al to form the solid solution phase zeta (ζ). This may be assumed to take place by the simple dissolving action of molten Al on Ni, a mutually interpenetrating action between the Al and Ni caused by their comparatively equal atomic sizes, unit cell structure, high temperature, and driving force of the current in the electrolytic cell.

The intermediate phases or secondary solid solutions ϵ, δ, and γ (10), occur in sequence as the distance from the surface of the Ni is increased. These may be assumed to have been nucleated by a diffusion process dependent on the operation of Fick's law at the environmental conditions obtained in the cryolite cell. The basis of the identification of these various secondary solid solution phases lies in their proximity, or lack of it, to the surface of the Ni cathode, their comparative hardness determined by microhardness tests (to be presented in the next section), and their obviously different etching characteristics.

On removal of the Ni cathode from the cryolite bath, an interface between the γ secondary solid solution and molten Al would be formed. On cooling, as may be seen from the phase diagram (9), the incongruently melting phase β would be formed by the peritectic reaction of the γ and molten Al.

This is believed to be the origin of the mixed black and white areas which appear as islands interspersed in the γ secondary phase. A peritectic reaction would also explain the proximity of the free β phase to these areas. The β phase was also identified by its comparative hardness.

Hardness measurements.—Hardness measurements were made with the Bergsman hardness tester and are presented in Fig. 6. These values are the averages of 3 determinations. Nickel aluminides of three different compositions, Ni_2Al_3, NiAl, and $NiAl_3$, were made by casting (11) and their hardnesses determined. Hardness values of some of the phases formed when Al was deposited on the Ni sheet were determined also. Comparison of these values with those of the cast nickel aluminides was then used as one method of identifying the γ, δ, and β phases in the diffusion coating.

As may be seen from Fig. 6, the hardness values determined on the coatings on Mo did not correspond directly to any Ni-Al system. However, the hardness of the coatings in the as-plated condition and after oxidation periods of 540 and 1000 hr was close to that of the very hard, high melting δ phase.

That the coatings contained ample Ni and Al was proven by chemical analysis of a strong HCl solution in which the coatings had been stripped anodically.

Coatings of Ni *on diffused* Al.—The adhesion of Ni plated on Mo covered with a molybdenum aluminide coating produced by electrodeposition of Al from the cryolite bath was excellent. The molybdenum aluminides are characterized by good electrical conductivity and, therefore, Ni can be plated on them easily from an aqueous solution. The author has succeeded in identifying by x-ray diffraction (3) the two brittle intermetallic systems, Al_3Mo and Al_5Mo, in the coating and, as could be expected, the oxidation life of specimens covered with a molybdenum aluminide layer, overplated with nickel, was rather limited.

Further work to improve the effectiveness of the protection of Mo against high-temperature oxidation by coatings containing Ni and Al, the latter being

electrodeposited from the cryolite bath, should, therefore, be restricted to the nickel aluminides.

Acknowledgment

The author is much indebted to Dr. Paul Schwarzkopf and Dr. Robert Steinitz for the great interest taken in this study, to Mr. Larry Kaufman, and to Mr. William Sipes (Aeronautical Materials Laboratory) for their assistance with the metallurgical and metallographic evaluations.

Manuscript received Feb. 2, 1959.

Any discussion of this paper will appear in a Discussion Section to be published in the June 1960 JOURNAL.

REFERENCES

1. D. E. Couch, H. Shapiro, and A. Brenner, *This Journal*, **105**, 485 (1958).
2. D. E. Couch and J. H. Connor, WADC Tech. Report 58-5, Part I, March 1958, NBS Report 5894, May 1, 1958.
3. W. Beck, *Metal Ind.*, **86** (Jan. 21) 43 (1955).
4. "Metals Handbook," ASM, 1948 Ed., p. 800.
5. *Ibid.*, p. 1047.
6. R. L. Wachtell, WADC Tech. Report 52-291 (1952).
7. M. Feinleib and B. Potter, *This Journal*, **103**, 235 (1956).
8. J. O'Mara Bockris, Liquid Metals and Solidification, p. 172, A Seminar held during the 39th Metal Congress, Chicago, 1957, published by ASM (1958).
9. "Metals Handbook," 1948 Ed., p. 1164.
10. L. S. Castleman and L. L. Seigle, *Trans. Met. Soc. AIME*, **212**, No. 5, 589 (1958).
11. W. A. Alexander and N. B. Vaughan, *J. Inst. Metals*, No. 2, **61**, 248 (1937).

Electroplating Metal Contacts on Germanium and Silicon

Dennis R. Turner

Bell Telephone Laboratories, Incorporated, Murray Hill, New Jersey

ABSTRACT

Various metals have been plated on germanium and silicon. These semiconductors usually have oxide layers on them which could interfere with the intimate contact required between metal and semiconductor for good adhesion and the desired electrical properties. Oxide films and residues from chemical etching on germanium can be removed by cathodic reduction prior to metal deposition in many plating solutions. Sixteen different metals were plated on n- and p-type germanium. Since oxide films on silicon are difficult to reduce cathodically, other methods of removing the oxide film are employed to produce adherent electrodeposits on silicon.

Solid-state electronic devices made from semiconducting materials require some kind of electrical contact to the semiconductor. Electroplating techniques have been used to make ohmic contacts to semiconductors for many years. More recently, good rectifying contacts have been made by electroplating small metal spots ($\sim 10^{-5}$ cm^2) on germanium and silicon (1-4). Much of this work was carried out using a jet plating technique. One of the best types of plating baths, cyanide solutions, was avoided completely. This paper discusses the results of experiments which sought to determine the solutions and conditions that give high quality, large area deposits with maximum adhesion on Ge and Si. Either ohmic or rectifying contacts can be obtained by electroplating the proper metal on Ge and Si.

Germanium

Semiconducting materials usually have oxide layers on them which could interfere with making an intimate contact between plated metal and the semiconductor. Some oxides on metals can be removed by electrochemical reduction. For example, Linford and Feder (5) have shown that copper oxide layers up to about 650Å thick are completely reduced electrochemically prior to nickel deposition. Turner (6) demonstrated that the continuous monolayer of oxide formed on Ge during anodic dissolution is reduced cathodically in acid solutions prior to hydrogen gas evolution. Many residues from chemical etching and oxide films thicker than a monolayer on Ge can also be reduced electrolytically. This is demonstrated in Fig. 1. If a Ge electrode is chemically polished in C.P.-4 solution,[1] rinsed in distilled water and then subjected to a cathodic treatment in 0.1*N* H_2SO_4, a cathodic reduction curve is obtained. The number of coulombs in the potential arrest stage corresponds to about 2 atom layers of oxide.[2] The cathodic reduction curve obtained on a Ge electrode previously anodized in a fused salt bath (34% $LiNO_3$ + 66% KNO_3, mp ~ 155°C) to produce a thicker oxide layer

[1] Composition of C.P.-4 etch: 5 parts by vol. conc. HNO_3, 3 parts by vol. 48% HF, 3 parts by vol. glacial acetic acid, and 10 drops liquid bromine/50 cc of acid mixture.

[2] Acid fluoride solutions may actually leave a fluoride film on the surface.

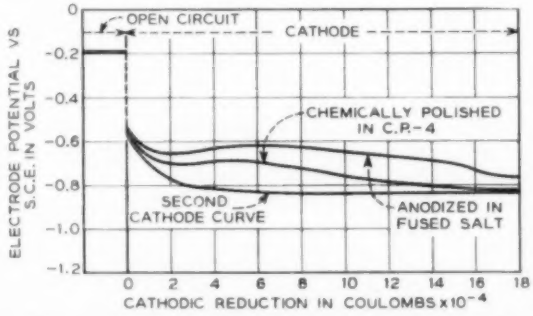

Fig. 1. Cathodic reduction curves of chemically polished and anodized Ge in 0.1N H_2SO_4.

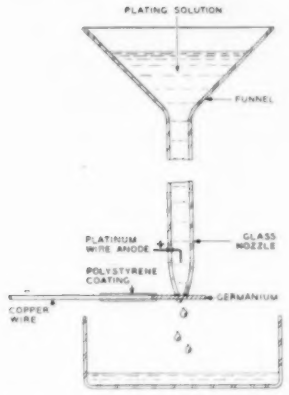

Fig. 2. Experimental arrangement for plating metal spots on Ge.

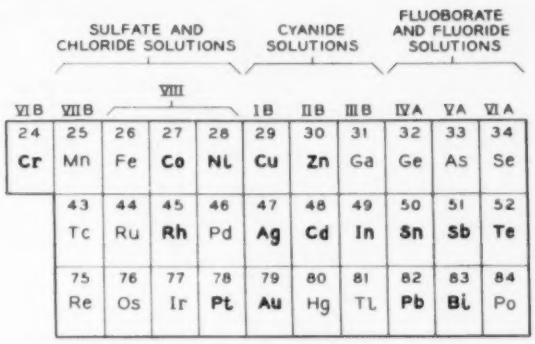
SULFATE AND CHLORIDE SOLUTIONS
CYANIDE SOLUTIONS
FLUOBORATE AND FLUORIDE SOLUTIONS
VIII
VI B VII B 1B IIB IIIB IVA VA VI A
24 Cr 25 Mn 26 Fe 27 Co 28 Ni 29 Cu 30 Zn 31 Ga 32 Ge 33 As 34 Se
43 Tc 44 Ru 45 Rh 46 Pd 47 Ag 48 Cd 49 In 50 Sn 51 Sb 52 Te
75 Re 76 Os 77 Ir 78 Pt 79 Au 80 Hg 81 Tl 82 Pb 83 Bi 84 Po

Fig. 3. Metals plateable from aqueous solutions. Bold lettered metals were plated on Ge. Preferred plating solutions are indicated above table.

is also included in Fig. 1. The length of the potential arrest corresponds to about 4 atom layers of oxide. The second cathodic curve obtained in each experiment is included to show that all reducible material is removed in the first cathodic treatment and that the reduced material in the initial curve is not due to some solution impurity. Schmidt (7) has found that thick layers of GeO_2, formed anodically in N-methylacetamide, can be reduced in the same solvent.

These results suggest that the best choice of metals and solutions for electroplating intimate metal contacts on Ge are those which deposit metal only after all oxide films or residues from chemical polishing are removed by cathodic reduction.

Experimental

The experiments were carried out with Ge electrodes about 1 cm square by 1 mm thick. These were cut from two single crystals, one 4-ohm cm n-type Ge and the other 3-ohm cm p-type Ge. An ohmic contact was made to the Ge by abrading one edge and soldering it to a 1.3 mm (0.050 in.) diameter copper wire using a standard lead-tin solder and an acid zinc chloride flux. The solder joint and about 2 cm of the copper wire were coated with polystyrene cement to protect them from the acid etches used later. Prior to plating, the surface of the germanium was chemically polished in the C.P.-4 solution. After a thorough water rinse the Ge was placed against a glass nozzle as shown in Fig. 2. This procedure confined the area of metal plated mainly to the inside diameter of the nozzle tip. A Pt wire sealed into the glass about 2.5 cm above the nozzle tip served as the anode. A glass or polyethylene funnel served as the solution reservoir. Plating solutions that work best above room temperature were preheated prior to filling the funnel. A section of Tygon tubing connected the funnel to the nozzle. Relatively high plating current densities were possible since the solution flowed continuously during plating. About 0.025 mm (0.001 in.) of metal was plated for the contact studies. After plating, the samples were water rinsed and given a brief etch in a suitable acid solution to remove the feather edge around the main spot of metal. This acid etch after plating was often essential for good rectifying contacts.

Sixteen different metals were plated on n- and p-type Ge. They represent practically all of the readily plated metals. The section of the periodic table containing all the elements plateable from aqueous solutions is shown in Fig. 3. The bold lettered metals were plated in this study. The preferred solutions, with a few exceptions, are indicated above the chart. A sulfate solution was used to plate indium instead of the cyanide bath because it was more stable chemically. As a rule the cyanide solutions are to be preferred in this application since metals deposit in them at potentials considerably more negative than that required to reduce oxide films on Ge. Electrodeposits from cyanide baths also are usually of good quality, i.e., smooth and dense. The chromium spots were plated from a standard chromic acid sulfate bath. Bismuth was plated from a perchlorate solution (8) while the tellurium deposits were obtained from a fluoride-sulfate solution (9).

Only technical grade chemicals were available for some of the plating baths. These solutions were purified electrolytically to remove metallic impurities. Overnight electrolysis with a dummy Pt cathode at 2 ma/cm^2 current density was usually sufficient.

Electrical contact to the plated metal spot was made by touching it with a loop of gold wire. Measurements of the electrical properties of the metal-germanium junction consisted first of observing the E-I pattern on an oscilloscope screen using a conventional display circuit and then making a point by point plot of both the forward and reverse E-I characteristic using d. c.

Results of Plated Metal Contacts on Ge

All the plated metals tested except antimony produced rectifying contacts on n-type Ge and ohmic contacts on p-type Ge. Electroplated Sb contacts behaved just the opposite, i.e., they were ohmic on n- and rectifying on p-type Ge. Borneman, *et al.* (3) reported that all plated metals gave rectifying contacts on n- and ohmic contacts on p-type Ge. The reverse voltage-current curves of the sixteen metals plated on n-type Ge are shown in Fig. 4. These results were obtained with circular metal spots about 2 mm in diameter. Most of the curves have the same general shape but are displaced from one another along the current axis. The large differences in the

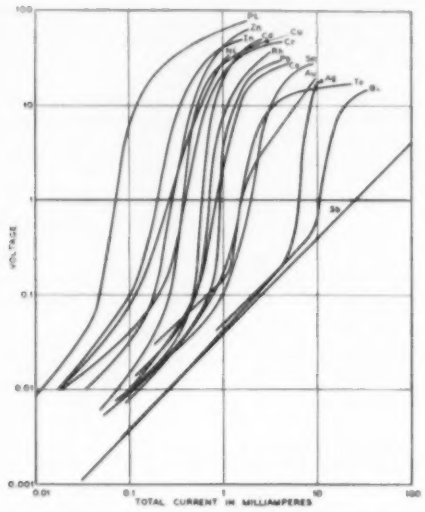

Fig. 4. Reverse curves for 2 mm diameter plated metal contacts on n-type Ge (measured in room air).

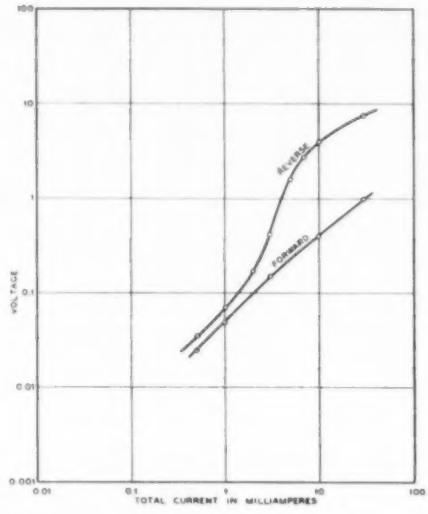

Fig. 5. Forward and reverse curves for a 2 mm diameter plated Sb spot on p-type Ge.

saturation currents are attributed to variations in the state of the surface after etching and also to differences in the adhesion of the various electrodeposits on Ge. In general, the poorer the adhesion the higher the saturation current. The silver deposits on Ge had the poorest adhesion of all and one of the highest saturation currents. Plated 2 mm diameter Sb contacts on n-type Ge were ohmic up to the highest current passed through the contact, 200 ma.

When the results with Sb were obtained, it was thought that perhaps all the metals in groups VA and VIA of the periodic table would behave the same way. Initial tests with Bi and Te in fact did give nearly ohmic contacts to n-type Ge. After the Bi and Te plating solutions were purified by electrolysis, however, both metals produced rectifying contacts on n-type Ge as shown in Fig. 4.

An interesting effect was observed with nickel plating on Ge when the solution was at room temperature. The Ni deposit often curled up at the edges a short time after plating and attached to the Ni were large pieces of Ge. There is a certain amount of hydrogen codeposited with Ni which produces a stress in the deposit. Since the adhesion between electroplated Ni and Ge is good, the stress in the deposited Ni is transmitted to the Ge. The stress apparently is sufficient to crack the Ge under the Ni and the peeling is actually due to this rupture in the Ge. The effect was eliminated when a hot (~60°C) Ni plating solution was used. An increase in the plating solution temperature presumably decreases the amount of codeposited hydrogen in the Ni which reduces the stress transmitted to the Ge under the deposit.

Antimony, the only metal found to give rectifying plated contacts on p-type Ge, was plated from a fluoborate solution. It was prepared by dissolving 6 g of technical grade antimony fluoride in 100 ml of solution containing 10 g of fluoboric acid. As made up, the solution produced Sb-plated spots which were ohmic on both n- and p-type Ge. After electrolytic solution purification, the antimony deposits on n-type Ge remained ohmic but those on p-type Ge became rectifying. Figure 5 shows the forward and reverse voltage-current curves for a 2 mm diameter plated Sb spot on p-type Ge. This represents the first time a rectifying characteristic has been obtained by electroplating a metal contact on p-type Ge. The saturation current in the blocking direction probably could be lowered by the use of plating solutions made from very pure materials. Schmidt (7) reports that a lithium pressure contact on p-type Ge is rectifying. This is attributed to the diffusion of donor lithium atoms into the Ge which converts the surface region to n-type.

Silicon

Metals electroplated on polished Si using ordinary plating techniques have poor adhesion and the deposits usually blister. Wurst and Borneman (4) plated small metal dots on Si using the jet electroplating technique and reported good adhesion. Using their pretreatment procedures and plating solutions, metal electroplated on polished Si specimens with about 2 cm^2 surface area always blistered. The poor adhesion is attributed to a surface oxide layer which cannot be reduced cathodically in aqueous solutions prior to metal deposition as it is on Ge. Archer (10) has estimated the oxide layer thickness on Si after etching to be about 10Å or 2 to 3 atom layers. To improve the adhesion between plated metal and Si, the oxide film must be removed or at least reduced in thickness. Silicon dioxide is soluble in both strong alkaline solutions and HF.

One method which has been found effective in improving the adhesion considerably is to subject the Si to a brief etch in a hot concentrated potassium or sodium hydroxide solution prior to metal plating in a hot cyanide plating bath. Hot, strongly alkaline solutions attack Si vigorously. The Si is transferred quickly from the hot alkaline solution to the plating bath without rinsing and with current on as the Si enters the plating solution. By not rinsing the Si, the corroding effect of the hot alkaline solution continues

until metal deposition begins. By this process, metal plates over at most a monolayer of oxide, and in some places there is direct contact between plated metal and semiconductor.

Another method which gives adherent Ni deposits on Si makes use of a Ni plating bath containing HF. The Si is allowed to soak in the plating solution for about 1 min before the plating current is started. Hydrofluoric acid dissolves silicon dioxide, but the surface may not be clean since there is some evidence that the fluoride simply replaces the oxide on the surface (11). Whatever the mechanism, the adhesion of a subsequent Ni deposit is greatly improved by this procedure. A Ni plating solution developed for plating Ni on Mg (12) was found to be satisfactory: HF (48%) 78 cc/l, citric acid 30 g/l, basic nickel carbonate 130 g/l, wetting agent (sodium lauryl sulfate) 20 drops/l.

Six metals were plated on chemically polished Si using one of the preplating procedures just described. Results are summarized in Table I. The plating solutions used were of standard composition. A "strike" plating technique improved the adhesion of Cu and Zn deposits but not the others. The high initial current density in Cu and Zn plating was reduced after a few seconds to deposit the bulk of the metal. Copper deposits were the most adherent, while Zn gave the poorest results by comparison. The test for adhesion consisted simply of cutting through the deposit by scratching with a sharp object. Even Zn plating, however, did not show signs of the blistering which is common when metals are deposited on Si by ordinary procedures.

The electrical properties of these metal contacts on n- and p-type Si are also given in Table I. These results were obtained with metal spots 1 mm in diameter. Qualitatively they agree with those reported by Wurst and Borneman (4) except for Cu and In on n-type Si, which gave opposite results.

Effect of Semiconductor Electrode

The semiconducting properties of Ge and Si have not been a factor in the electroplating results discussed thus far. Brattain and Garrett (13) have shown that holes are required to carry out anodic processes on semiconductors and electrons are necessary for cathodic reactions. An adequate supply of electrons are present at the surface of n-type semiconductors, under cathodic bias, since they are the majority current carrier. Relatively few electrons are available in p-type Si. If the surface of p-type material is abraded, additional electrons become available at the surface due to a large increase in the generation-recombination rate of hole-electron pairs. A light of high intensity directed at the Si will also raise the minority carrier concentration at the surface. The comparatively few electrons at the surface of chemically polished p-type semiconductors exposed to subdued room light are depleted in a cathodic reaction at very low current densities. This surface depletion of electrons results in a space charge region in the semiconductor. It can be thought of as a concentration polarization of electrons in the semiconductor. Attempts to increase the cathode current by applying more voltage to the cell merely result in increasing the depth of the space charge region in the semiconductor. The current barrier at the surface of the semiconductor eventually breaks down, allowing more current to flow, if the applied voltage is high enough.

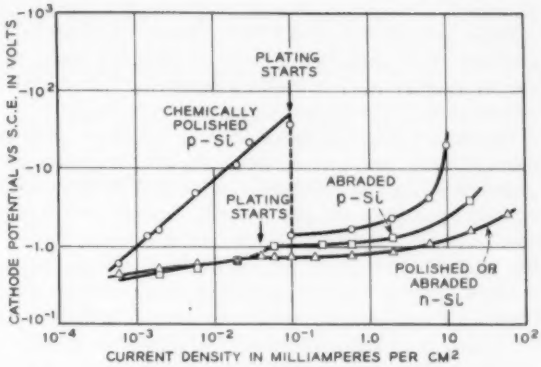

Fig. 6. Cathode potential-current density curves for Ni plating on abraded and polished n- and p-type Si.

An example of what may be encountered in attempting to plate metals on chemically polished p-type semiconductors is illustrated in Fig. 6. It is a log-log plot of the cathode potential vs. current density of 1Ω cm n- and 12Ω cm p-type Si with abraded and polished surfaces in a Ni plating solution. These data were obtained by increasing the current in steps. The current was held constant at each setting and the electrode potential measured when it appeared to reach a steady state. The plating bath was a standard "cold" Ni solution containing nickel chloride, ammonium chloride, and boric acid. Below about 0.1 ma/cm², the cathode reaction is the discharge of hydrogen ions. The E_c-i curves for abraded and polished n-type Si are identical. An abraded

Table I. Metals electroplated on Si with good adhesion and their electrical properties as contacts

Metal	Solution type	Current density, ma/cm²	Relative adhesion	Electrical properties of contact	
				n-Si	p-Si
Cu	Cyanide	200-75	Very good	Ohmic*	Rectifying
Au	Cyanide	15	Good	Rectifying	Ohmic
Ni	Fluoride	40	Good	Rectifying	Rectifying
In	Cyanide	30	Fair	Rectifying*	Rectifying
Sn	Stannate	20	Fair	Ohmic	Rectifying
Zn	Cyanide	100-30	Poor	Ohmic	Rectifying

* Result different from Wurst and Borneman.

p-type Si electrode has about the same E_c-i curve as n-type up to the current density where Ni starts depositing. The potential difference between the two curves is attributed to a small rectifying barrier between plated Ni and the abraded p-type Si.

Polished p-type Si deviates from the other curves even at very low current densities. The experiment was carried out in subdued room light. Most of the voltage applied to the plating cell appears across the space-charge region in the Si. As shown in Fig. 6, the cathode potential can reach as much as 50 v without plating any Ni.[3] At the critical cathode potential (the value is different for each Si electrode), Ni begins to deposit. The start of Ni plating is probably coincident with a local breakdown of the potential barrier at the surface of the Si. The cathode potential drops slowly as Ni covers the Si. The drop in cathode potential at a constant current density is attributed to hole injection by the electroplated Ni contact on the Si. This collapses the space-charge region which reduces the potential drop in the semiconductor.

If the plating solution is capable of corroding the Si, even at a moderate rate, the large polarization effect inside polished p-type Si made cathodic is not observed. This is due to the fact that excess holes and electrons are produced at the surface of Si whenever it is corroded (14). Both strong alkaline and acid fluoride plating solutions will etch Si. The number of electrons produced at the surface in these solutions in the etching process is sufficient to carry out cathode reactions up to current densities where metal deposition begins without surface depletion. Germanium is corroded to some degree in most aerated aqueous solution (15) so that the "internal" polarization effect may not be observed with polished p-type Ge.

Summary and Conclusions

Oxide films and chemical polishing residues on Ge are cathodically reduced in plating solutions prior to metal deposition if the potential at which metal starts depositing is more negative than that required to reduce the surface films. Cyanide plating solutions are usually preferred for this reason. All electroplated metal contacts except Sb gave rectifying contacts on n-type Ge and ohmic contacts on p-type Ge. Antimony behaved just the opposite.

Oxide films on Si are not reduced cathodically in aqueous solutions. When special preplating techniques are used, the adhesion of electrodeposits on Si is improved considerably. Plating solutions that corrode Si serve a double purpose: (*a*) they remove or reduce the oxide layer thickness prior to metal deposition, and (*b*) they prevent the formation of a large polarization effect due to electron depletion inside the Si.

[3] In one experiment, more than 200 v had to be applied to the plating cell before Ni would deposit on polished p-type Si.

Acknowledgments

The author wishes to acknowledge the help received from H. E. Haring and W. A. Sunder in the work on germanium and to G. H. Peranteau for his assistance with the study of contacts on silicon. Thanks are also due to U. B. Thomas for his comments and discussion of the work.

Manuscript received March 30, 1959. This paper was prepared for delivery before the Ottawa Meeting, Sept. 28-Oct. 2, 1958.

Any discussion of this paper will appear in a Discussion Section to be published in the June 1960 JOURNAL.

REFERENCES

1. R. Bray, Purdue University Report, p. 27, Sept. (1950).
2. J. H. Tiley and R. A. Williams, *Proc. Inst. Radio Eng.*, **41**, 1706 (1953).
3. E. H. Borneman, R. F. Schwarz, and J. J. Stickler, *J. Appl. Phys.*, **26**, 1021 (1955).
4. E. C. Wurst and E. H. Borneman, *ibid.*, **28**, 235 (1957).
5. H. B. Linford and D. O. Feder, *Plating*, **45**, 349 (1958).
6. D. R. Turner, *This Journal*, **103**, 252 (1956).
7. P. F. Schmidt, Private communication.
8. H. Harbaugh and F. C. Mathers, *Trans. Electrochem. Soc.*, **64**, 293 (1933).
9. F. C. Mathers and H. L. Turner, *ibid.*, **54**, 293 (1928).
10. R. J. Archer, Private communication.
11. M. M. Atalla, E. Tannenbaum, and E. J. Scheibner, *Bell System Tech. J.*, **38**, 749 (1959).
12. H. K. DeLong, U. S. Pat. No. 2, 728, 720, December 1955.
13. W. H. Brattain and C. G. B. Garrett, *Bell System Tech. J.*, **34**, 129 (1955).
14. D. R. Turner, work to be published.
15. W. W. Harvey and H. C. Gatos, *This Journal*, **105**, 654 (1958).

On the Research and Development of Electron Emitting Substances for Gas Discharges

D. M. Speros

Lamp Research Laboratory, Lamp Development Department, General Electric Company, Cleveland, Ohio

ABSTRACT

Criteria for the stability and chemical behavior of electron emitting substances in gas discharges are obtained by means of thermodynamics. Theoretical analysis is supplemented by means of experimental methods intended for the study of processes at elevated temperatures, such as thermogravimetry and differential thermal analysis. The application of the above permits some insight into the processes of formation, activation, and detrition of electron emitting compositions, guiding the development of a number of improved cathodes.

The purpose of this work was to develop cathodes meeting the requirements of new gas discharge devices. To effect this, a better understanding of the fundamentals involved was necessary. Therefore, a major portion of this work was devoted to the chemical and thermochemical aspects of electron emitting substances, which are but poorly understood at present.

The concern of the theoretical part is to evaluate a degree of relative stability for these materials (with respect to dissociation, sublimation, chemical interaction, physical state, and sputtering) and to predict the processes expected during their history, (such as formation, activation or reduction, and normal detrition) without extended experimentation of a trial and error nature. This part of the work forms an extension or generalization of the thermochemical calculations of Rittner (1) which were concerned primarily with the reduction reaction of the oxide cathode. From the chemical point of view, thermodynamic considerations are obvious in many of their aspects; however, since they appear to be of general usefulness in cathode research, they are outlined in this paper.

The chemical processes occurring in cathodes belong to the realm of solid-state chemistry. Therefore, experimental methods designed for the study of reacting solids were applied to supplement the theoretical analysis and provide information when thermodynamic and kinetic data were lacking.

Procedure

Theoretical basis.—A cathode system is defined as one consisting of α moles of substance A, β moles of substance B, γ moles of substance C, etc., and is represented as follows:

$$A_\alpha B_\beta C_\gamma \ldots .$$

A binary system $A_\alpha B$, where α is the number of moles of A per one mole of B, is for the purpose at hand a sufficient approximation to a large number of actual cathodes. For example, $A_\alpha B$ could represent a common form of the oxide cathode for A = BaO and B = SrO; for A = La and B = B, the boride cathode; for A = Th and B = W, the thoriated cathode, and so on.

The process of formation in each case is as follows:

$$\alpha A(c) + B(c) \rightarrow A_\alpha B(c) \qquad [1]$$

which involves a free energy change:

$$\Delta F = F_{A_\alpha B(c)} - \alpha F_{A(c)} - F_{B(c)} = \Delta H - T\Delta S \qquad [2]$$

As already implied in the above examples, Eq. [1] may represent a chemical reaction, the formation of a solid solution, a process of adsorption, or a combination of more than one of these processes. Since at a temperature T:

$$\Delta F = \Delta F^\circ + RT \ln \frac{A_\alpha B(c)}{A(c)^\alpha B(c)}$$

and at equilibrium $\Delta F = 0$ and

$$\ln \frac{A_\alpha B(c)}{A(c)^\alpha B(c)} = \ln K = -\frac{\Delta F^\circ}{RT}$$

the standard free energy change for the formation of $A_\alpha B$ from its components αA and B was used as a quantitative criterion for the stability of electron emitting substances $A_\alpha B$ with respect to dissociation.

In nearly all cases of interest the vapor pressure of one of the components, B, and of the compound $A_\alpha B$ is negligible in comparison to that of the component A. Therefore, the process of sublimation proceeds for all practical purposes as follows

$$A_\alpha B(c) \rightarrow \alpha A(g) + B(c) \qquad [3]$$

The accompanying free energy change is

$$\Delta F_2 = \alpha F_{A(g)} + F_{B(c)} - F_{A_\alpha B(c)} \qquad [4]$$

The process of sublimation of pure A and the corresponding free energy change are as follows

$$\alpha A(c) \rightarrow \alpha A(g) \qquad [5]$$

$$\Delta F_1 = \alpha F_{A(g)} - \alpha F_{A(c)} \qquad [6]$$

Since obviously:

$$\Delta F_1 - \Delta F_2 = \Delta F \qquad [7]$$

Table I. The $\Delta F^\circ = f(T)$ relations for a number of processes of interest

Process	$\Delta F^\circ = f(T)$	T range of applicability
$CaO\ (c) + SiO_2\ (c) \rightarrow CaSiO_3\ (c)$	$-21{,}300 + 0.12T$*	298-1483
$SrO\ (c) + SiO_2\ (c) \rightarrow SrSiO_3\ (c)$	$-23{,}000 + 0.9T$	298-1600
$BaO\ (c) + SiO_2\ (c) \rightarrow BaSiO_3\ (c)$	$-26{,}800 + 0.1T$*	298-1600
$BaO\ (c) + Al_2O_3\ (c) \rightarrow BaAl_2O_4\ (c)$	$-24{,}500 + 0.3T$	298-2100
$BaO\ (c) + MoO_3\ (c) \rightarrow BaMoO_4\ (c)$	$-59{,}900 + 0.3T$	298-1068
$CaO\ (c) + WO_3\ (c) \rightarrow CaWO_4\ (c)$	$-40{,}600 + 0.6T$	298-M.P.
$SrO\ (c) + WO_3\ (c) \rightarrow SrWO_4\ (c)$	$-58{,}300 + 0.6T$	298-M.P.
$BaO\ (c) + WO_3\ (c) \rightarrow BaWO_4\ (c)$	$-74{,}300 + 0.6T$	298-M.P.

* Available in this form in the literature (2).

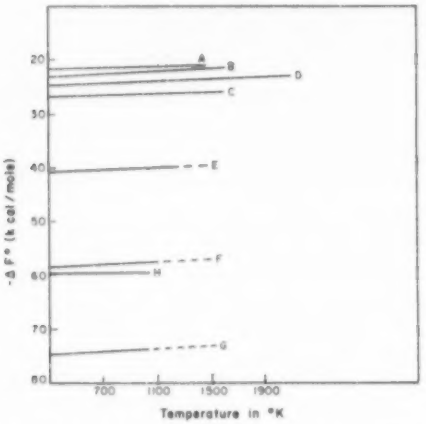

Fig. 1. Standard free energy change as a function of temperature for the formation of some interoxide compounds from the oxides: A, $CaSiO_3$; B, $SrSiO_3$; C, $BaSiO_3$; D, $BaAl_2O_4$; E, $CaWO_4$; F, $SrWO_4$; G, $BaWO_4$; H, $BaMoO_4$.

the free energy change ΔF for the formation of A_aB from its components aA and B is also useful in determining the comparative stability with respect to sublimation of each component A from its combination with a given component B.

The standard free energy change as a function of temperature is shown in Table I for a number of processes of interest which lead to the formation of interoxide compounds.[1] These were evaluated using data in references (2) and (3); since however these calculations involved, in some instances, estimates of entropy and heat capacity values, they are to be considered accurate only in their relative magnitude. These $\Delta F^\circ = f(T)$ functions are plotted in Fig. 1. In accordance with the above, the lower the $\Delta F^\circ = f(T)$ relation for a given compound in this figure, the more stable the compound with respect to dissociation and sublimation.

A third area in which the considerations leading to Fig. 1 are of importance is that of chemical interaction between A_aB and other substances with which it may come in contact. Since all systems tend toward a state of minimum free energy, all substances as shown in Fig. 1 will be thermodynamically unstable in the presence of the free oxides of substances below them in the $\Delta F^\circ = f(T)$ diagram. Further, since in most instances each A may tend to form a number of different combinations with B, an interoxide compound in Fig. 1 will be unstable in the presence of another one if the change of the free energy for their interaction is favorable. Finally, interoxide systems may combine to form a solid solution or compound such as, for example, $Ca_2Al_2SiO_7$.

These considerations also govern the interaction between a component of A or B and a third reagent. In general it can be shown that their combination increases their stability toward chemical attack. For example, it will be seen that $BaO \cdot Al_2O_3$ (or $BaAl_2O_4$) is, for all practical purposes, completely inert in the presence of tungsten, while BaO is not.

If the relative amounts of the components of an emission material are known, the above are useful for the understanding of the nature of cathode coatings and of the interface composition between the coating and the supporting electrode.

Not much is known about the quantitative aspects of sputtering of composite surfaces. However, the process represented by

$$x(\text{solid}) \rightarrow x(\text{gas})$$

will involve the same amount of energy regardless of the path the process follows, the efficiency involved, or the agent causing it. Therefore, from basic considerations alone it can be expected that the separation of an atom or molecule from the surface will involve, as one factor at least, the energy of sublimation regardless of whether this "sublimation" is achieved thermally or by ionic bombardment. Thus it is not surprising that important recent studies on sputtering (4) have succeeded in interrelating, empirically at least, this phenomenon with the heat of sublimation, among other factors. Therefore the criterion ΔF, used for the stability with respect to sublimation, dissociation, and chemical reactivity was used also for the stability with respect to sputtering as the best alternative at the present state of knowledge.

The physical state of A_aB as a function of temperature, the nature of the combination A_aB as a function of a and temperature, and an estimate of the magnitude of the thermodynamic quantities involved were obtained from the study of the appropriate phase diagram.

The application of the above considerations to actual systems involves the well-known limitations of thermodynamics. The experimental work indicated,

[1] The oxides that combine to form these substances do not differ enough in their acidic character to justify the term "oxygen salts" nor do they exist in such a loose combination as to correspond to "mixed oxides." The term "interoxides" is proposed to define this class of materials.

however, that the activation energy and diffusion barriers were of lesser magnitude than should have been expected from solid-state reactions. Therefore, these limitations were of lesser importance than would have otherwise been the case.

Experimental Methods

The awareness of the importance of the thermochemical history of the electron emitting materials led to the application, in this work, of thermal methods of experimental investigation such as thermogravimetric analysis (T.G.A.), and differential thermal analysis (D.T.A.)

The basis for the application of these methods is as follows: It has been shown in the previous section that if A and B will form a combination A_xB such as to increase the stability of A, the sign of ΔF for the process of this combination will be negative.

Since the entropy change for processes in the solid state is small,[2] then

$$\Delta F \cong \Delta H$$

If the change in heat content ΔH is unknown, the next best thing is to determine its sign. By means of D.T.A., the temperature range at which the process takes place, the exothermic or endothermic nature of the process, as well as a very approximate magnitude of ΔH are determined.

This method was also used in order to obtain an indication of the rates at which the thermodynamically predicted processes take place.

Phase diagrams and thermodynamic data for the binary sytems A_xB of interest are few; for the ternary systems resulting from the processes exemplified by Eq. [8], below, are virtually nonexistent. Hence, once the A_xB system was evaluated, D.T.A. provided the means of determining whether the process of Eq. [8] produced a system of increased stability.

The difficulties of interpretation of D.T.A. records can often become formidable when a complex process, such as that of the activation of an emission material, is being studied. Other methods such as x-ray diffraction, mass spectroscopy, microscopy, and T.G.A. were then applied in conjunction with D.T.A.

The maximum temperature attainable by the conventional D.T.A. apparatus used was 1500°C.[3] Therefore, approximate melting point determinations of compounds melting at higher temperatures were performed in inert atmospheres inside a tungsten wound furnace. The temperature was determined by means of a calibrated micropyrometer focused at a "blackbody" cavity formed by a tungsten container into which a small crystal of the compound was placed.

The thermionic behavior of selected materials was examined by means of high vacuum diodes for academic purposes; since it is unknown whether thermionic or secondary processes predominate in a given gas discharge, greater reliance was placed on results obtained by studying the breakdown voltage and the cathode drop in the actual gas discharges for which these cathodes were intended.

Interoxide Systems As Electron Emitting Substances

Interoxide systems $(M_xO_y)_\alpha \cdot (R_zO_w)$, where M_xO_y represents an "emissive" oxide, BaO for instance, and R_zO_w a refractory oxide such as Al_2O_3, if used as such, form poor lamp cathodes even if $\alpha > 1$. Their behavior as cathodes however improves appreciably if an excess of the emissive metal M is introduced. This was done by chemically reducing part of the M_xO_y component as follows:

$$(M_xO_y)_\alpha \cdot (R_zO_w) + \beta R \rightarrow$$

$$\left(\beta \frac{wx}{zy}\right) M \cdot \left(\alpha - \beta \frac{w}{zy}\right) M_xO_y \cdot \left(\frac{\beta}{z} + 1\right) R_zO_w \quad [8]$$

where the left hand side of the equation represents the emission mixture while the right hand side represents the activated cathode. The reducing agent R used was the same, in each case, as the R of the refractory oxide. This was done in order to obtain, after activation, the simplest possible chemical species hence the easiest to study.

The type of cathode thus produced was controlled by adjusting the following variables: (*a*) selection of the interoxide system; (*b*) selection of the reducing agent; (c) amount of the reducing agent; (*d*) state of subdivision of the reducing agent.

In cases where it was desirable that the reduction reaction proceed in a short time, a potent reducing agent (1)[4] in fine powder form was mixed with the powder of the interoxide substance. In the other extreme, the reducing agent was alloyed with the cathode support.

It may be noted that, in all cases, the process of activation, being a chemical reaction in the solid state, does not involve evolution of gases (see below, Process of Activation), nor does it necessitate any particular atmosphere or lack of it for its progress. If the composition of the interoxide system is such that $\alpha \leqq 1$, the emission mixture is stable in the atmosphere for extended periods of time as shown in Fig. 2. Finally, the reduction in volume of the emission mixture upon activation is much less than if, for instance, it had involved the decomposition of carbonates, a helpful fact, as it will be seen when the system is used in conjunction with a refractory metal sponge or compact.

The electron emitting behavior of interoxide systems in lamps parallels that found in this work and by others (5, 6) by means of measurements of the thermionic emission constants of interoxide systems consisting of BaO and a number of refractory oxides. An inspection of these results brings out the possibility that the value of the work function ϕ, or more precisely the slope of the Richardson plots, is approximately the same and in the vicinity of 1.6 e.v. at 750°-850°C regardless of the refractory oxide (Al_2O_3 or ZrO_2, etc.) and, except at the two extremes of

[2] This is also true for the evaluation of stability with respect to sublimation, since the difference $\Delta F_1 - \Delta F_2$ cancels out the large increase of entropy on sublimation of αA.

[3] For substances containing excess barium, the D.T.A. apparatus could not be used above 950°-1000°C because of severe chemical attack on the Pt-Pt:13% Rh thermocouples.

[4] In general, however, it should be remembered that now the ΔF reduction = $\Delta F_R + (\Delta F'' - \Delta F')$ where ΔF_R is the free energy of reduction of M_xO_y to M and R_zO_w, and $\Delta F''$, $\Delta F'$ are the free energies of formation from the oxides of the final and original interoxide substances, respectively.

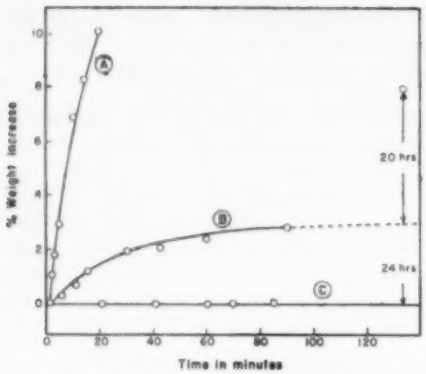

Fig. 2. Weight gain of cathode materials on exposure to air of relative humidity as stated. A, BaO; relative humidity: 70%; B, 0.76 $BaO \cdot BaAl_2O_4$; relative humidity: 80%; C, $BaAl_2O_4$; relative humidity: 80%.

composition, regardless of the BaO content of the interoxide system. In this work the emission coatings were applied on cathodes made of molybdenum, tungsten, and nickel; hence to this extent this value of ϕ is independent of the cathode base. Furthermore, the value of A in the Richardson equation

$$i = AT^2 e^{-e\phi/kT}$$

seems dependent on the amount of Ba present in excess of the stoichiometric formulas for the interoxide system, being very small for the pure substances and increasing with the Ba content.

This evidence points to the hypothesis that the work function in interoxide systems is determined by the nature of the emissive sites involved (BaO-Ba in this case, see also below, Process of Activation) while the saturated current density is determined by the number of these sites per unit area.

If the above is true, then the role of the refractory component is simply to increase the stability of the BaO-Ba emissive sites, as explained, and to increase the amount of Ba that may be combined with the BaO-refractory oxide matrix, as will be explained.

Preparation of Starting Materials

Interoxide substances usually are prepared by heating a mixture of alkaline earth carbonates or oxalates, nitrates, sulfates, etc., with the oxides, hydrates, or other compounds of the refractory component to the point of melting.

In this work the interoxide substances of interest were prepared by the direct combination of the two oxides in the solid state,

$$\alpha M_xO_y + R_zO_w \xrightarrow{\text{heat}} (M_xO_y)_\alpha \cdot (R_zO_w) \qquad [9]$$

In most instances the reactions proceeded at relatively low-temperature ranges and rather short reaction times as shown in the D.T.A. records of Fig. 3. At a heating rate of 15°C/min, it is seen that $BaAl_2O_4$ is formed between 400° and 500°C; $BaZrO_3$ between 200° and 800°C; and $BaThO_3$ between 200° and 900°C. The over-all effect is exothermic. It is interesting to note that in all three cases depicted the reactions proceed in three main stages although these stages may occur at different temperature ranges

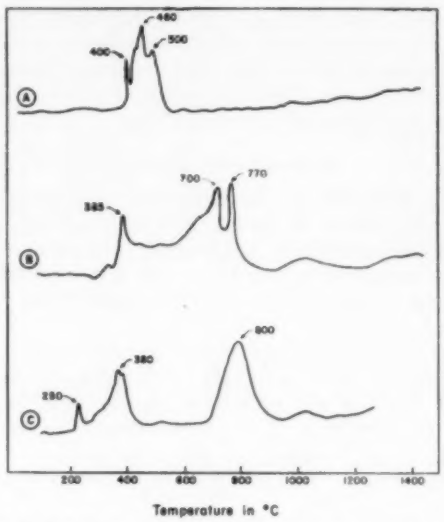

Fig. 3. D.T.A. curves for the formation of some interoxide systems from their component oxides.

(A) $BaO(c) + Al_2O_3(c) \rightarrow BaAl_2O_4(c)$
(B) $BaO(c) + ZrO_2(c) \rightarrow BaZrO_3(c)$
(C) $BaO(c) + ThO_2(c) \rightarrow BaThO_3(c)$

in each case. The reaction leading to the formation of $BaThO_3$ does not proceed to completion in the 50 min of heating as shown, but the other two apparently do proceed to completion: if the aluminate or zirconate samples are taken out of the apparatus after the last stage, reground, replaced in the apparatus, and heated again, no evidence of further reaction is observed. Melting point determinations, chemical analysis, and x-ray diffraction data confirm this to the extent that published data are available. X-ray powder pattern data have been obtained for $BaAl_2O_4$ prepared as described above, which is presented in Table II compared with the data in A.S.T.M. card No. 2-0545. It is seen that the A.S.T.M. intensity values,[5] with the exception of the intensity of the principal line at $d = 3.17$, are approximately twice those determined[6] in this work. As the value assigned to all intensities is relative to that of the principal line (which is assigned the value of 100), we believe, as suggested by Dr. Addamiano, that the values given by the A.S.T.M. card for $BaAl_2O_4$ are higher than the actual ones by a constant factor because of film saturation by the principal line reflection.

Preparation of Cathodes

The interoxide substance is ground and mixed with the powder of the reducing agent. Then, depending on the particular intended application, the mixture is either suspended in a comparatively volatile organic liquid such as butyl acetate, or used as the dry powder. The liquid suspensions may be used for coatings by dipping, spraying, or painting in the usual manner.

The dry powder may be used to provide very thin coatings of the mixture on the electrodes or to form dispersions in refractory metal compacts (or sponges). In connection with the former use it has

[5] Obtained from photographic film recordings.

[6] By means of a Geiger counter detector.

Table II. X-ray diffraction data of $BaAl_2O_4$

This work		ASTM	
d-spacings	Intensities	d-spacings	Intensities
4.57	35		
		4.56	80
4.18	15	4.06	20
4.05	5		
3.75	7	3.17	100
3.16	100		
2.62	39	2.62	80
2.51	6	2.51	20
		2.46	10
		2.26	20
2.25	30	2.24	70
2.20	18	2.20	20
		2.19	10
2.01	25	2.01	60
1.98	21	1.977	20
		1.951	10
1.71	11	1.71	20
1.68	18	1.68	30
1.64	5	1.64	20
1.595	29	1.594	60
1.577	13	1.577	30
1.508	18	1.507	40
		1.477	10
		1.465	10
		1.428	10
		1.395	20
1.392	8	1.389	10
		1.351	35
1.350	14		
1.307	8	1.307	20
		1.279	30
1.276	12		
1.253	7		
1.243	11		
1.227	7		
1.207	14		
1.123	6		
1.112	7		
1.102	6		
1.066	4		
1.010	10		
0.9868	9		
0.9212	6		
0.8385	6		
0.8183	8		
0.7991	5		
0.7968	5		

been found that some of these mixtures, for instance, that of $BaAl_2O_4$ and Al, will adhere to clean metals if the mixture contains a slight excess of BaO or $BaCO_3$ (see below, Chemical Processes). For some uses a thin coating, visible to the naked eye only by direct comparison of the coated and uncoated portions of the electrode, is sufficient to provide desirable performance.

In connection with the latter use the interoxide substance and its reducing agent are mixed in powder form with a chemically inert (see below) refractory metal powder, usually tungsten, the latter being in large excess, as for example 9:1 by weight, for one of the applications reported here. The resulting mixture is pressed without benefit of binders, lubricants, or other additives into compacts of the desired shape and dimensions. A pressure of 6000 kg/cm^2 is sufficient for simple shapes such as that of a short cylinder. The compacts then are placed in refractory firing boats and fired at a temperature of

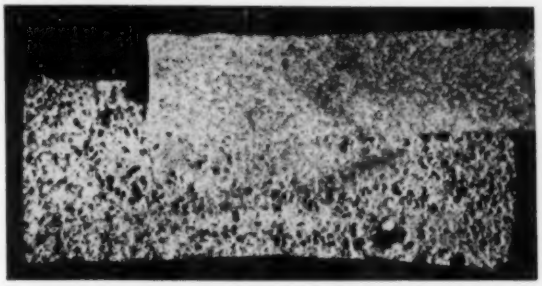

Fig. 4. Photomicrograph of cross section of pellet cathode bottom attached by means of spot welding to the tungsten electrode shown at the top. (Specimen and photomicrograph by K.S.G. Pertwee of Large Lamp Department.)

1050°C in dry hydrogen or an inert atmosphere for at least 20 min. This treatment causes the compacts to sinter into hard, porous pellets of a density range of 8.5 to 9.5 g/cm^3. If the tungsten content is more than approximately 60% by weight, the resistance of the pellets is very low; therefore it may be spot welded directly on a metal lead to form one type of cathode as shown in Fig. 4.

The purpose of the above procedure is primarily to sinter the tungsten particles; for, as will be seen, the activation process involves lower temperatures and shorter times than those mentioned above. The resulting structure is quite similar to cathodes already reported (7), the basic difference being that, due to the choice of $\alpha \leqq 1$ for the interoxide system and to the incorporation of R, the activation is independent of the tungsten sponge which serves simply as a physical support (see below, Chemical Processes).

After activation the coatings obtained from liquid suspensions and the thin dry powder coatings are unstable in the ordinary atmosphere; the sintered tungsten compacts however are stable even if stored for several weeks under saturated humidity conditions (see below, Chemical Processes).

The Process of Activation

The D.T.A. records of Fig. 5 indicate that Eq. [8] describes in reality a complex, multistage process.

From a practical point of view the low temperatures and short times[7] of "activation" are convenient in that the cathodes become activated while lamps are being processed in ovens.

From the theoretical point of view it is interesting to note that the similarities observed in the reactions of formation of the interoxide compounds, Fig. 2, have a parallel in their reactions of reduction. These consist of two main processes: a low-temperature sharp exothermic reaction and a process at higher temperature proceeding at a slower rate and having a hump-like appearance. An increase in β (Eq. [8]) causes an increase in the height and area of the peaks as shown in Fig. 5A. Both processes decrease in intensity and are displaced toward higher temperatures as α is decreased to the extent of necessitating longer time intervals for their completion than indicated by Fig. 5. Finally for $\alpha < 1$ the low-tem-

[7] The D.T.A. experiments were performed in argon at atmospheric pressure at a heating rate of approximately 15°C/min.

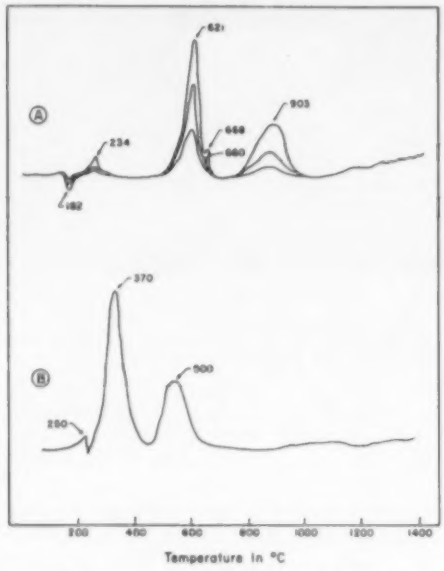

Fig. 5. D.T.A. curves for the reduction (activation) processes
(A) $1.76BaO \cdot 1Al_2O_3$ + various amounts of Al
(B) $9BaO \cdot 1ZrO_2 + 2.3Zr \rightarrow 3.3(1.33BaO \cdot 1ZrO_2 \cdot 1.39Ba)$

perature process begins to become endothermic while the higher temperature hump has still an exothermic appearance.

Repetition of the runs using various proportions of reactants, x-ray diffraction studies, mass spectroscopic work, and chemical analyses were of assistance for the interpretation of the records of Fig. 5 as follows.

At approximately 160°C the small amount of water adsorbed by the powders begins to separate causing the endothermic peak at 186°C on the record for the aluminate case. As the water vapor diffuses out of the sample it attacks the reducing metal it encounters causing the formation of refractory oxide and hydrogen. This exothermic process occurs in the aluminate near 280°C. In the zirconate case this reaction begins at a lower temperature to the extent of balancing the endothermic effect of the desorption of water.

The main reduction reactions then follow peaking at 370° and 620°C for the zirconate and aluminate, respectively. In the case of the aluminate, when the temperature attains the value of 660°C, the melting point of aluminum, the remaining quantity of unreacted aluminum melts, impregnates the sample, and reacts causing the small exothermic peak at 668°C. The area corresponding to the peak at 620°C where aluminum is presumed still solid is far larger than that at 668°C. As this is also the case in the zirconate-zirconium reaction, it may be concluded that the reactions are capable of proceeding in the solid state and it is not necessary to assume the formation of (reducing metal)-(barium) eutectic compositions, which are liquid at the reaction temperatures, in order to explain the progress of these reactions in the short reaction times and low temperatures observed.

The reduction reaction is always followed by a slower exothermic process appearing as a hump on the D.T.A. records. Neither this process nor the unexpectedly exothermic behavior[8] of the peaks attributed to the main reduction reaction have been completely understood to date; however, work in progress has permitted interesting glimpses into their nature which may be summarized as follows.

When the reduction reaction begins, the reducing metal, which is present in excess at the particle interface with the interoxide compound, will reduce a larger quantity of barium oxide than that intended by Eq. [8]. Soon a gradient will be established across the reaction front which in the case of $(BaO)_x(Al_2O_3)$-Al reaction, for instance, involves the series: Al .... Al_2O_3 .... $BaO \cdot 6Al_2O_3$ .... $BaO \cdot Al_2O_3$ .... $3BaO \cdot Al_2O_3$ with the quantity of barium produced increasing in the same order as that of aluminum oxide. As shown in the reactions of formation in Fig. 3, the interdiffusion rate of these species is appreciable and a series of exothermic reactions are thermodynamically predictable to take place; as for example,

$$5Al_2O_3 + BaO \cdot Al_2O_3 \rightarrow BaO \cdot 6Al_2O_3$$

Since these reactions depend on the diffusion of molecules bulkier than Al or Al_xBa_y, they would manifest themselves on the D.T.A. record as humps rather than as sharper peaks as the reduction reaction does.

It is suspected that the above explains the hump process only in part and that this process, as well as that causing the sharper peak at lower temperatures, also involves the exothermic interaction between the Ba formed by the reduction reaction and the resulting interoxide substance. Thus, for instance, the 0.31 g of Ba that is theoretically produced by 1 g of a mixture of $BaAl_2O_4$ and Al according to

$$BaAl_2O_4 + 0.4Al \rightarrow 1.2(0.34BaO \cdot 1Al_2O_3 \cdot 0.5Ba)^9 \quad [10]$$

is not detected by means of x-ray diffraction techniques; hence it does not exist in the elementary crystalline state. This is confirmed by thermogravimetric experiments using a Chevenard thermobalance. Except for a weight loss of approximately 1.8% between 70° and 300°C, which has previously been shown to be due to the evolution of water and hydrogen, there was no other significant weight change up to 1050°C, the maximum temperature attainable by the apparatus used. The experiments were performed in a flow of purified argon (600 cc/min) at atmospheric pressure, using 1-g samples of powder consisting of the mixture shown by the left hand side of Eq. [10]. On the average, the sample was at a temperature above 710°C, the melting point of Ba, for at least 2 hr.

In order to overcome the limitations imposed by the inability to perform these experiments in vacuum, and also in order to obtain an indication of the

[8] Thermochemical calculations show most of these reactions to be slightly endothermic within the limits of uncertainty of the available data.

[9] In addition to Eq. [10], the following give specific examples involving actual cathodes.

$$BaZrO_3 + 0.25Zr \rightarrow 1.25(0.4BaO \cdot 1ZrO_2 \cdot 0.4Ba) \quad [11]$$

$$BaThO_3 + 0.2Th \rightarrow 1.2(0.5BaO \cdot 1ThO_2 \cdot 0.33Ba) \quad [12]$$

nature of the apparent combination between barium and the interoxide system, the thermogravimetric experiments were repeated in a flow of hydrogen instead of argon. The behavior in the 70°C range was nearly the same as in the case of argon; however, an increase in weight was observed at 650° to 700°C because of the formation of barium hydride. This permitted the estimation of a maximum for the heat of the combination Ba-X as follows:

$$Ba - X(c) \rightarrow Ba(c) + X(c) \quad \Delta H = ? \quad \Delta F = ? \quad [13]$$

where ΔH is the quantity to be estimated. This process is the sum of

$$Ba - X(c) + H_2(g) \rightarrow BaH_2(c) + X(c)$$

$$\Delta H_1 = ? \quad \Delta F_1 = ? \quad [14]$$

and

$$BaH_2(c) \rightarrow Ba(c) + H_2(g) \quad \Delta H_2 = +40.9 \; \Delta F_2 = ? \quad [15]$$

therefore $\Delta H = \Delta H_1 + 40.9$ and $\Delta F_1 + \Delta F_2 = \Delta F$.

Reaction [14] proceeds spontaneously and to an appreciable extent even if the flow of H_2 is stopped. Hence $\Delta F_1 \leqq 0$ and therefore $\Delta F \leqq \Delta F_2$ or $\Delta H - T\Delta S \leqq 40.9 - T\Delta S_2$. Since ΔS refers to a reaction involving solids only, it will be small; ΔS_2 refers to a reaction resulting in a gaseous product and will therefore have a larger positive value. Hence $\Delta S_2 > \Delta S$ and therefore $\Delta H \leqq 40.9$ kcal/mole, thus establishing an upper limit for Ba — X.

Subject to further verification this evidence indicates that at least a part of the barium formed is not in a "free" state. This contributes to the explanation of Fig. 5 and the stability of the postulated Ba-BaO-refractory oxide electron emitting sites.

Chemical Processes Involving Refractory Sponge Cathodes

It was seen that the reasons for the choice of equimolar proportions for the composition of the starting interoxide materials included stability in air, low temperatures of activation, lack of copious gas evolution during activation, and ease of control of the chemistry involved in their selection, preparation, and activation.

A further reason is their reduced reactivity toward the refractory metal of the cathode support. As the activation of the interoxide substance is controlled by the reducing agent, it is not necessary that further reduction be made to occur; nor is this desirable because this interaction will result in the creation of an interface concentration gradient and its associated problems.

The pairing of the electron emitting materials and metal supports involves the theoretical considerations at the beginning of this paper. Below, these are applied to the pair $BaAl_2O_4$ — W as an example pertinent to this work. This application necessitates the knowledge of the initial and final states of reactants and products. It was shown in the previous section that the exact state of the barium produced by the reduction process, and hence the final state of the products, are in doubt. Therefore, for comparison purposes, the final state of barium will be taken as being gaseous, because this state offers a common basis for the relative evaluation of the pairs of interest.

The vapor pressure of barium produced in a number of processes was evaluated and is given in Table III. Once again, by necessity, estimates of thermo-

Table III. Theoretical vapor pressures of barium produced by a number of processes of interest

Process or reaction	$\log P_{Ba} = f(T)$
$Ba(c) \rightarrow Ba(g)$	$\log P_{Ba} = \frac{-9730}{T} + 7.83$*
$Ba(c) \rightarrow Ba(g)$	$\log P_{Ba} = \frac{-9340}{T} + 7.42$*
$BaO(c) \rightarrow Ba(g) + \frac{1}{2}O_2(g)$	$\log P_{Ba} = \frac{-25{,}750}{T} + 9.62$
$\frac{4}{3}BaO(c) + \frac{1}{3}W(c) \rightarrow Ba(g) + \frac{1}{3}BaWO_4(c)$	$\log P_{Ba} = \frac{-18{,}650}{T} + 6.50 + 0.74 \log T$
$BaAl_2O_4(c) + \frac{2}{3}Al(c) \rightarrow Ba(g) + \frac{4}{3}Al_2O_3(c)$	$\log P_{Ba} = \frac{-14{,}720}{T} + 6.72 + 0.29 \log T$
$BaAl_2O_4(c) + \frac{2}{3}Al(\;) \rightarrow Ba(g) + \frac{4}{3}Al_2O_3(c)$	$\log P_{Ba} = \frac{-14{,}460}{T} + 6.30 + 0.27 \log T$
$2BaO(c) + \frac{1}{3}W(c) \rightarrow Ba(g) + \frac{1}{3}BaWO_4(c)$	$\log P_{Ba} = \frac{-14{,}730}{T} + 6.10 + 0.74 \log T$†
$BaAl_2O_4(c) \rightarrow Ba(g) + \frac{1}{2}O_2(g) + Al_2O_3(c)$	$\log P_{Ba} = \frac{-29{,}200}{T} + 9.66$
$\frac{4}{3}BaAl_2O_4(c) + \frac{1}{3}W(c) \rightarrow Ba(g) + \frac{1}{3}BaWO_4(c) + \frac{4}{3}Al_2O_3(c)$	$\log P_{Ba} = \frac{-25{,}640}{T} + 6.86 + 0.73 \log T$†
$2BaAl_2O_4(c) + \frac{1}{3}W(c) \rightarrow Ba(g) + \frac{1}{3}Ba_3WO_6(c) + 2Al_2O_3(c)$	$\log P_{Ba} = \frac{-25{,}000}{T} + 6.86 + 0.73 \log T$

* Available in this form in the literature (2).
† See also references (8) and (9).

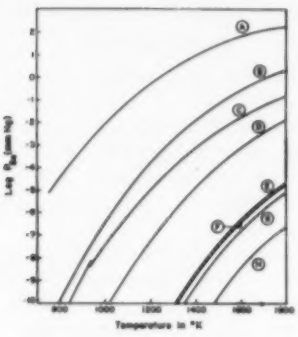

Fig. 6. Logarithm of the theoretical vapor pressure of barium, produced by a number of processes of interest, as a function of temperature.

(A) $Ba(c, l) \rightarrow Ba(g)$

(B) $2BaO(c) + \frac{1}{3} W(c) \rightarrow Ba(g) + \frac{1}{3} Ba_3WO_6(c)$

(C) $BaAl_2O_4(c) + \frac{2}{3} Al(c, l) \rightarrow Ba(g) + \frac{4}{3} Al_2O_3(c)$

(D) $BaO(c) + \frac{1}{3} W(c) \rightarrow Ba(g) + \frac{1}{3} BaWO_4(c)$

(E) $2BaAl_2O_4(c) + \frac{1}{3} W(c) \rightarrow Ba(g) + \frac{1}{3} Ba_3WO_6(c) + 2Al_2O_3(c)$

(F) $BaO(c) \rightarrow Ba(g) + \frac{1}{2} O_2(g)$

(G) $\frac{4}{3} BaAl_2O_4(c) + \frac{1}{3} W(c) \rightarrow Ba(g) + \frac{1}{3} BaWO_4(c) + \frac{4}{3} Al_2O_3(c)$

(H) $BaAl_2O_4 \rightarrow Ba(g) + \frac{1}{2} O_2(g) + Al_2O_3(c)$

chemical data had to be made. Results are plotted in Fig. 6. It is seen that the vapor pressure of barium produced by the reaction between $BaAl_2O_4$ and W resulting in the formation of $Ba_3WO_6(c)$ is comparable to that produced by the thermal decomposition of BaO(c). As is well known with respect to cathode activation, the latter is negligible. The vapor pressure of barium produced by the reaction resulting in the formation of $BaWO_4(c)$ from $BaAl_2O_4$ and W is even less. When these are compared with the vapor pressure of barium produced by the total[10] reduction of $BaAl_2O_4$ by Al it is concluded that the activation of the $BaAl_2O_4$ + 0.4Al + 13.2 W mixture[11] is independent of the tungsten sponge and that the formation of an interface composition of tungstates is unlikely.

The above was confirmed by means of D.T.A. work: no evidence of a reaction was observed on heating finely powdered mixtures of $BaAl_2O_4$ and W up to 1500°C.

In contrast, the reaction between BaO and W and also that between interoxide systems containing BaO in excess of the equimolar composition is thermodynamically favored to nearly the same extent as that between $BaAl_2O_4$ and Al.[12] However, in these cases the role of the tungstate interface becomes apparent. Thus, although the reaction resulting in the formation of Ba_3WO_6 is more favorable than that resulting in the formation of $BaWO_4$, the former is less favorable kinetically since it and the accompanying production of barium depends on the diffusion of the reactants through the $BaWO_4$ interface. Therefore, a pellet cathode of this kind will depend on concentration gradients and hence, delicately, on the cathode temperature, the control of which for directly heated lamp cathodes is not conveniently effected. This is particularly true, of course, in intermittently pulsed discharges where the bulk of the cathode is only slightly above room temperature.

The stability in air after activation of the pellet cathodes containing interoxide materials is interpreted as follows: Upon exposure to the water and carbon dioxide of the atmosphere barium hydroxide and carbonate form on the surface pores of the pellet, with an accompanying large increase in volume of the emission material that has thus been attacked. As these surface pores were already filled with the interoxide substance inasmuch as the activation did not involve any appreciable reduction in volume, the formation of these impervious "plugs" prevents further penetration of vapors and gases and therefore further attack below the surface. If substances such as the usual carbonates had been used for the formation of the pellets, their activation would have been accompanied by a large decrease in volume making the pellets more susceptible to atmospheric attack. The above constitutes an additional reason for the choice of interoxide systems for the pellet cathodes.

[10] Used here as a limiting case; the vapor pressure of Ba from the actual activating process used (Eq. [9]) is substantially higher, $BaAl_2O_4$ and $BaO \cdot 6Al_2O_3$ being the end products rather than Al_2O_3.

[11] Usually employed to manufacture the compacts.

[12] The theoretical vapor pressure of Ba from the reaction between BaO and W resulting in the formation of Ba_3WO_6 is nearly two orders of magnitude higher than determined experimentally (9), either because the enthalpy estimated in this work for the formation of Ba_3WO_6 from its component oxides is too high or because, as shown in this section, the Ba formed by the reduction reaction becomes at least partly bound into the interoxide lattice.

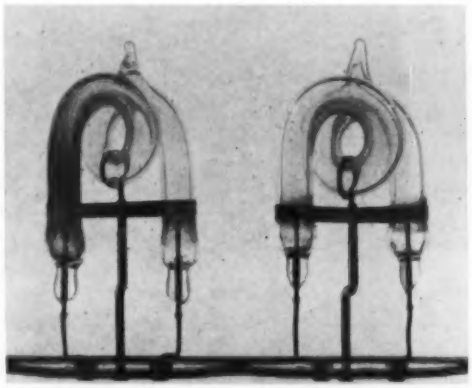

Fig. 7. Left: Standard electronic flashtube after 2500 flashes (near end of life). Minimum average breakdown voltage: 400 v. Right: Lamp identical to that above but using emission materials shown by Eq. [11] (thin film application on tungsten electrode) after 70,000 flashes. Minimum breakdown voltage constant at 285 ±5 v. Both lamps were operated at 125 watt-sec (or Joules) per flash.

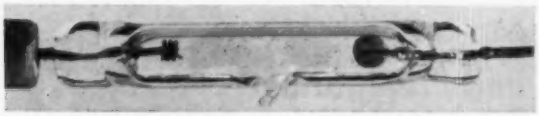

Fig. 8. A new type of repetitive electronic flashtube (used, for instance, for stroboscopic purposes) using pellet cathode of emission materials shown by Eqs. [10] or [11] or [12]. The life of these tubes is several million flashes.

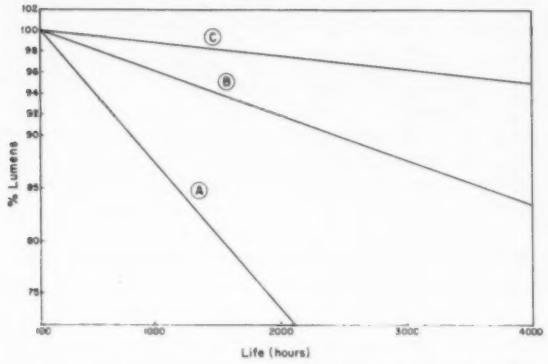

Fig. 9. Maintenance (in per cent of lumen output at 100 hr) vs. life in hours, of: A, standard 400-w high-pressure mercury discharge lamp; B, same as A, but with electron emitting materials as shown by Eqs. [12] or [13] (from liquid suspension); C, same as B, but with modified electrodes.

After manufacture into lamps, the pellet surface is reactivated either thermally or by sputtering. The ease with which this can be accomplished indicates that the attack, even after severe exposure, was very superficial. In the case of thermal reactivation, the formation of tungstates may be expected on the surface. D.T.A. experiments show that barium carbonate and W react at a high rate at 760°C (and slower well below this temperature). T. G. A. work with several interoxide pellets in each experiment failed to detect any weight loss (due to the accompanying evolution of CO) thereby confirming the above results of lamp behavior. This indicates that the formation of tungstates is insignificant. It may become significant, however, when the dry thin coatings mentioned earlier are used on a tungsten base. It will be recalled that these thin coatings adhere tenaciously to the tungsten base and provide good cathode performance if a slight excess of BaO or $BaCO_3$ is introduced. Probably the formation of tungstates to an extent of forming a number of "anchoring" sites but not to the extent of forming an interface could account for this.

Performance Characteristics

In addition to the requirement of ease of manufacture and use already mentioned, lamp cathodes must meet certain standards of performance. These are long life, low breakdown or starting voltage of the lamp, good lamp efficiency (number of lumens output per watt input), and good lamp "maintenance."

Improvements in performance obtained by the use of various forms of interoxide cathodes as described in this paper are shown in the examples of Fig. 7, 8, and 9.

Acknowledgments

The writer is indebted to Drs. J. S. Saby, J. M. Lafferty, V. L. Stout, and Mr. D. E. Elmendorf of this company for their encouragement and discussions. He is also indebted to Mr. R. L. Woodhouse for performing the D.T.A. runs, to Dr. E. G. Zubler for mass spectroscopic work, to Dr. R. P. Taylor for chemical analyses, and for the x-ray diffraction studies to Miss J. R. Cooper and Dr. A. Addamiano, all of this laboratory. For the T.G.A. runs, indebtedness is expressed to Dr. R. C. Griffis of Lamp Metals & Components Department and to Messrs. S. L. Slomski and E. C. Martt of Photo Lamp and Large Lamp Departments, respectively, for tests on lamp performance and general assistance. For discussions on various matters associated with this paper and critical reading of the manuscript, thanks are tendered to Drs. M. D. Gibbons, L. V. McCarty, A. E. Newkirk, H. A. Liebhafsky, T. A. Vanderslice, and J. E. White of this company and E. S. Rittner of Philips Research Laboratories.

Manuscript received March 16, 1959.

Any discussion of this paper will appear in a Discussion Section to be published in the June 1960 JOURNAL.

REFERENCES

1. E. S. Rittner, *Philips Research Repts.*, **8**, 184 (1953).
2. O. Kubaschewski and E. U. Evans, "Metallurgical Thermochemistry," John Wiley & Sons, Inc., New York (1956).
3. F. D. Rossini, *et al.*, National Bureau of Standards, Circ. 500 (1952).
4. G. K. Wehner, *Phys. Rev.*, **102**, 690 (1956); **108**, 35 (1957).
5. D. A. Wright, *British J. Appl. Phys.*, **5**, 391 (1954).
6. H. Huber and J. Freytag, *LeVide*, **54**, 310 (1954).
7. P. P. Coppola and R. C. Hughes, *Proc. IRE*, **44**, 351 (1956).
8. E. S. Rittner, W. C. Rutledge, and R H. Ahlert, *J. Appl. Phys.*, **28**, 1468 (1957).
9. W. C. Rutledge and E. S. Rittner, *ibid.*, **28**, 167 (1957).

The Calcium Silicate Mn + Pb Phosphor Phase Relationships and Preparation

D. E. Harrison and Mary V. Hoffman

Lamp Wire & Phosphors Department, General Electric Company, Cleveland, Ohio

ABSTRACT

Phase relations were examined in the vicinity of $CaSiO_3$ in the system to pseudowollastonite inversion temperature. Addition of $MnSiO_3$ to (Ca,Pb) $CaSiO_3$-$MnSiO_3$-$PbSiO_3$. Lead solid solutions in $CaSiO_3$ lower the wollastonite SiO_3ss markedly lowers the solubility of lead in (Ca,Mn,Pb)SiO_3ss and causes a change in structure from pseudowollastonite to wollastonite. Application of the phase data is used to demonstrate how the synthesis technique can be varied to produce major differences in particle size of the phosphor.

The properties of the $CaSiO_3$:Mn + Pb phosphor are described by Froelich (1), Merrill and Schulman (2), Schulman, Ginther, and Evans (3) and Fonda and Froelich (4). Various synthesis techniques are described by Steadman (5), Schulman (6), and Froelich (7). Phase data pertinent to the phosphor composition are limited. Glasser (8) recently re-examined the system $CaSiO_3$-$MnSiO_3$ and, in general, he confirmed the earlier results of Voos (9), although differing in many details. No data are reported in either the binary system $PbSiO_3$-$CaSiO_3$ or the ternary system $CaSiO_3$-$PbSiO_3$-$MnSiO_3$.

The object of this study was to examine the pertinent phase relationships in the vicinity of $CaSiO_3$ composition and in particular to determine the extent of the solubility of lead in $CaSiO_3$ and its effect on the inversion temperature. Phase data were used as a basis for the interpretation of the reactions which occur during synthesis of the $CaSiO_3$:Mn + Pb phosphor.

Experimental Procedure

The raw materials used for phosphor synthesis were Mallinckrodt Special Bulky silicic acid, silicic acid prepared from tetraethylorthosilicate, and reagent grade $PbSO_4$ and $MnCO_3$. The $CaCO_3$ was prepared by Chemical Products Plant of the General Electric Company. Compositions in the system $CaSiO_3$-$PbSiO_3$ were made from silicic acid prepared by hydrolysis of tetraethylorthosilicate; all other compositions were made with Mallinckrodt silicic acid.

Preparation of compositions and heat treatments.—The ingredients were ground in either an agate or a glass mortar with reagent grade acetone until dry. Calcines were prepared in either platinum or fused silica crucibles at temperatures ranging from 1000° to 1200°C for 3 hr to one month. Ternary compositions were prepared from preformed $CaSiO_3$, $MnSiO_3$, and $PbSiO_3$. The compositions examined are listed in Table I.

Apparatus and techniques.—(*a*) Phase identification was made with a General Electric recording diffractometer using $Cu_{K\alpha}$ radiation ($\lambda = 1.540$Å) filtered with Ni.

(*b*) Microscopic examinations were made with a petrographic microscope.

(*c*) A quench technique was used to examine the solid solution regions by procedures similar to those described by Shepherd, Rankin, and Wright (10). Thermocouples were calibrated using lithium metasilicate (mp 1201°C) and gold (mp 1063°C).

(*d*) Particle size distribution curves of phosphor powders were calculated from settling rates of particles in water by application of Stokes law using the technique of Rabatin and Gale (11).

Results and Discussion

α(Ca,Mn)SiO_3 fluoresces a weak green and β(Ca,Mn)SiO_3 fluoresces a strong orange with cathode ray excitation. Fonda and Froelich showed that Mn-activated wollastonite, the low-temperature form of $CaSiO_3$ called (β), and not pseudowollastonite, the high-temperature modification called (α), could be sensitized to 2537Å radiation by lead. Therefore, β(Ca,Mn,Pb)SiO_3 is the species implied by the notation $CaSiO_3$:Mn + Pb.

Phase Relationships

Preliminary studies showed that in the vicinity of the $CaSiO_3$ composition, the system CaO-MnO-PbO-

Table I. Composition of $CaSiO_3$-$PbSiO_3$-$MnSiO_3$ mixtures

Mole % Sample No.	Composition		
	$CaSiO_3$	$PbSiO_3$	$MnSiO_3$
1	99.5	0.5	—
2	99.0	1.0	—
3	97.0	3.0	—
4	94.0	6.0	—
5	92.0	8.0	—
6	96.5	0.5	3.0
7	96.0	1.0	3.0
8	95.5	1.5	3.0
9	93.5	0.5	6.0
10	93.0	1.0	6.0
11	92.5	1.5	6.0
12	90.5	0.5	9.0
13	90.0	1.0	9.0
14	89.5	1.5	9.0
15	87.5	0.5	12.0
16	87.0	1.0	12.0
17	86.5	1.5	12.0

SiO_2 can be regarded as a 3-component system $CaSiO_3$-$MnSiO_3$-$PbSiO_3$. Consequently, examination of the binary systems $CaSiO_3$-$PbSiO_3$ and $CaSiO_3$-$MnSiO_3$ (after Glasser), and the solid solution region β(Ca,Mn,Pb)SiO_3 provided data necessary to understand many of the reactions which occur during synthesis of the $CaSiO_3$:Mn + Pb phosphor.

A discussion of the pertinent phase data follows:

The inversion temperature of calcium metasilicate.—The literature shows conflicting claims on the temperature of the dimorphic inversion in calcium metasilicate. Voos, for example, reports that the inversion occurs at 1210°C whereas Osborn and Schairer (12) give a value of 1125°C. Our attempts to prepare β-$CaSiO_3$ from $CaCO_3$ and $SiO_2 \cdot XH_2O$ always resulted in a mixture of α- + β-$CaSiO_3$ when fired at temperatures below ca. 1170°C; a sample fired at 1000°C for one month consisted of about 50% α- + 50% β-$CaSiO_3$. At 1180°C or above, only α-calcium silicate formed. α-$CaSiO_3$ will begin very slowly to invert to β-$CaSiO_3$ at 1150°C after several weeks. The data are not conclusive but they indicated that the inversion lies between 1150° and 1180°C.

The system $CaSiO_3$-$MnSiO_3$.—Glasser has recently re-examined the system $CaSiO_3$-$MnSiO_3$ and he is in general agreement with the earlier results of Voos except in many details and the disclosure that the solid solution series extends to 90% $MnSiO_3$ rather than to 100% as reported earlier. He shows that $MnSiO_3$ solid solutions in $CaSiO_3$ raise the inversion temperature to a maximum of 1400°C. The $\alpha \rightleftharpoons \beta$-$CaSiO_3$ inversion temperature was not redetermined in the system $CaSiO_3$-$MnSiO_3$. However, Glasser and Osborn (13) found the $\alpha \rightleftharpoons \beta$-$CaSiO_3$ inversion temperature to occur at 1125°C in the system CaO-Cr_2O_3-SiO_2.

The system $CaSiO_3$-$PbSiO_3$.—Nothing has been reported in the binary system $CaSiO_3$-$PbSiO_3$. The high volatility of Pb limited this investigation to the area around the $CaSiO_3$ composition. Solid-state calcines of preformed $CaSiO_3$ and $PbSiO_3$ were used as starting materials for quench studies. The loss of lead after calcining these mixtures for 6 days at 1050°C is shown in Table II. Since 5 to 7 additional days were required for the samples to reach equilibrium in the quench furnace, further lead losses can be expected, but the magnitudes of these losses were not determined.

The quench data are given in Table III and are shown graphically in Fig. 1. The unusual shape of the two phase area, particularly the flat lower limit, probably reflects the fact that the compositions have shifted from the binary join. Consequently, the phase

Table II. Loss of Pb from $CaSiO_3$-$PbSiO_3$ mixtures

No.	Initial composition Mole % $CaSiO_3$-$PbSiO_3$		Composition after 1050°C/6 days mole % $CaSiO_3$-$PbSiO_3$		Mole % Pb loss
1	99.5	0.5	99.55	0.45	10.0
2	99.0	1.0	99.27	0.73	27.0
3	97.0	3.0	97.22	2.78	7.3
4	94.0	6.0	94.34	5.66	5.7
5	92.0	8.0	92.14	7.86	1.8

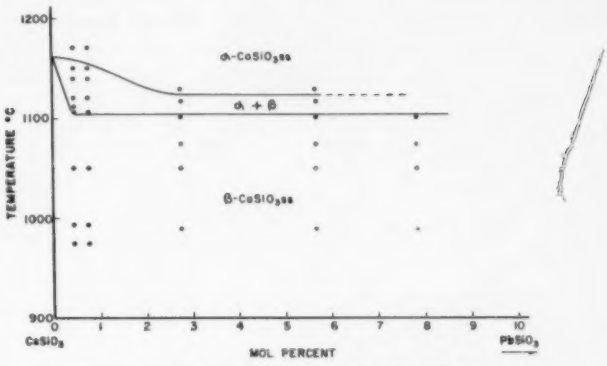

Fig. 1. A portion of the system $CaSiO_3$-$PbSiO_3$

data can be taken only as an approximation of the true equilibrium relationships.

$PbSiO_3$ is soluble in α calcium metasilicate to at least 6 mole % and it lowers the inversion temperature; the addition of 3 mole % $PbSiO_3$ lowers the inversion below 1125°C. Extrapolation of the two-phase area boundaries to pure calcium silicate indicates that the inversion occurs at 1160° ± 10°C.

The (Ca,Mn,Pb)SiO_3 *ss phase region.*—A portion of the plane $CaSiO_3$-$MnSiO_3$-$PbSiO_3$ in the vicinity of $CaSiO_3$ was examined at 1160°C. This temperature was selected because it is near the inversion temperature and also is a practical temperature for phosphor synthesis. Calcines were prepared by heating mixtures of preformed α(Ca,Pb)SiO_3 and $MnSiO_3$ for periods up to three weeks with a thorough grinding every 12 hr.

Lead is much less soluble in β- than in α-$CaSiO_3$ in the presence of $MnSiO_3$. For example, solution of 3 mole % $MnSiO_3$ in α(Ca,Pb)SiO_3 changes it to β(Ca,Pb,Mn)SiO_3 and lowers the Pb solubility from over 6 mole % to less than 1 mole %.

The loss of Pb after various firing times from a typical phosphor composition is shown in Table IV. These data reveal that 8.3% Pb is lost during the formation α(Ca,Pb)SiO_3ss (prepared from PbO + CaO + SiO_2) whereas 33.3% Pb is lost after 4 hr and 53.7% Pb after 16 hr at 1160°C from the reaction of α(Ca,Pb)SiO_3 + $MnSiO_3$ to yield the quaternary composition $\beta(Ca_{0.94-z}Mn_{0.06}Pb_z)SiO_3$. The greater stability of lead in α(Ca,Pb)SiO_3ss than in β(Ca,Mn,Pb)

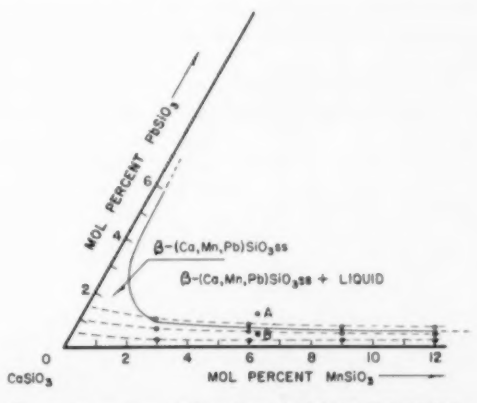

Fig. 2. A portion of the plane $CaSiO_3$-$MnSiO_3$-$PbSiO_3$

Table III. Quench data for the system $CaSiO_3$-$PbSiO_3$

No.	Composition mole % $CaSiO_3$-$PbSiO_3$		Temperature	Phase present
1	99.55	0.45	975	β(Ca, Pb) SiO_3
			994	β(Ca, Pb) SiO_3
			1050	β(Ca, Pb) SiO_3
			1106	β(Ca, Pb) SiO_3 + Trace α(Ca, Pb) SiO_3
			1112	β(Ca, Pb) SiO_3 + α(Ca, Pb) SiO_3
			1121	β(Ca, Pb) SiO_3 + α(Ca, Pb) SiO_3
			1140	β(Ca, Pb) SiO_3 + α(Ca, Pb) SiO_3
			1151	β(Ca, Pb) SiO_3 + α(Ca, Pb) SiO_3
			1165	α(Ca, Pb) SiO_3
2	99.27	0.73	975	β(Ca, Pb) SiO_3
			994	β(Ca, Pb) SiO_3
			1050	β(Ca, Pb) SiO_3
			1106	β(Ca, Pb) SiO_3 + α(Ca, Pb) SiO_3
			1121	β(Ca, Pb) SiO_3 + α(Ca, Pb) SiO_3
			1140	β(Ca, Pb) SiO_3 + α(Ca, Pb) SiO_3
			1151	β(Ca, Pb) SiO_3 + α(Ca, Pb) SiO_3
			1165	α(Ca, Pb) SiO_3
3	97.22	2.78	990	β(Ca, Pb) SiO_3
			1050	β(Ca, Pb) SiO_3
			1075	β(Ca, Pb) SiO_3
			1102	β(Ca, Pb) SiO_3
			1117	β(Ca, Pb) SiO_3 + α(Ca, Pb) SiO_3
			1128	α(Ca, Pb) SiO_3
4	94.34	5.66	990	β(Ca, Pb) SiO_3
			1050	β(Ca, Pb) SiO_3
			1075	β(Ca, Pb) SiO_3
			1102	β(Ca, Pb) SiO_3
			1117	β(Ca, Pb) SiO_3 + α(Ca, Pb) SiO_3
			1128	α(Ca, Pb) SiO_3
5	92.14	7.86	990	β(Ca, Pb) SiO_3
			1050	β(Ca, Pb) SiO_3
			1075	β(Ca, Pb) SiO_3
			1102	β(Ca, Pb) SiO_3

SiO_3ss can be demonstrated qualitatively by a spot test with an acidic solution of KI. α(Ca,Pb)SiO_3ss (Sample B) gave no test for Pb, whereas β(Ca,Mn, Pb)SiO_3 (Sample E) gave a strong test for Pb even after most of the surface Pb had been removed by refiring with NH_4Cl.

The area adjacent to the solid solution region is a liquid plus crystal area. The presence of liquid was detected by quench studies and by its effect on the oxidation state of Mn. Compositions in the crystal plus liquid area had a permanganate pink color and they were sintered into dense agglomerates. In contrast, composition within the solid solution region remained nearly white in body color and did not sinter.

Table IV. Loss of Pb from phosphor composition

Composition	Wt % Pb content	% Pb lost
(A) Batch (CaO + PbO + SiO_2)	1.08	—
(B) 1st Fire, 1140°C/4 hr (Ca, Pb) SiO_3 ss	0.99	8.3
(C) 2nd Fire, 1160°C/4 hr (Ca, Mn, Pb) SiO_3 ss	0.72	33.3
(D) 2nd Fire, 1160°C/ 16 hr (Ca, Mn, Pb) SiO_3 ss	0.50	53.7
(E) 3rd Fire, 1160°C/4 hr + NH_4Cl(Ca, Mn, Pb) SiO_3 ss	0.43	60.2

Because of the volatility of Pb, the quaternary solid solution region reported can be regarded only as a rough approximation to equilibrium conditions. For this reason, the diagram of the plane $CaSiO_3$-$MnSiO_3$-$PbSiO_3$, shown in Fig. 2, has curved dashed lines to indicate the approximate Pb contents.

Preparation of the $CaSiO_3$:Mn + Pb *phosphor*

Synthesis techniques in which all of the components, i.e., CaO+MnO+PbO+SiO_2 are initially fired together require an excess of Pb in order to allow for losses by volatilization. A typical initial composition is indicated in Fig. 2 by point "A" which is in the liquid plus crystal area adjacent to the solid solution region. As the firing progresses the composition gradually shifts to point "B" located within the solid solution region. The metastable liquids formed serve as effective mineralizers, but they promote large particle size and higher oxidation states of Mn. A second firing with NH_4Cl is necessary to remove a surface film of "lead-manganese-silica" which coats the phosphor crystallites.

Certain applications require a phosphor with smaller particle size. In this case it is desirable to avoid formation of metastable liquids. According to the phase data it should be possible to prepare either β(Ca,Mn)SiO_3ss or α(Ca,Pb)SiO_3ss and react each material with either PbO or MnO to form β(Ca,Mn, Pb)SiO_3ss. In this way, metastable liquids are

avoided in the system $CaSiO_3$-$MnSiO_3$-$PbSiO_3$. However, the quaternary solid solution is unstable due to the volatility of lead so that the reaction:

$$\beta(Ca,Mn)SiO_3ss + Pb^{2+} \rightarrow \beta(Ca,Mn,Pb)SiO_3ss \quad [1]$$

cannot be expected to be very successful.

The alternative reaction:

$$\alpha(Ca,Pb)SiO_3ss + Mn^{2+} \rightarrow \beta(Ca,Mn,Pb)SiO_3ss \quad [2]$$

should be more successful due to the greater stability of lead in $\alpha(Ca,Pb)SiO_3ss$ than in $\beta(Ca,Mn,Pb)SiO_3ss$. A sufficiently large excess of Pb can be incorporated initially in $\alpha(Ca,Pb)SiO_3ss$ to allow for losses by volatilization.

Although reaction [2] avoids quaternary liquids, it is still necessary to form $\alpha(Ca,Pb)SiO_3ss$, and low-melting liquids in the system CaO-PbO-SiO_2 cannot be avoided. However, advantage can be taken of the polymorphic inversion from $\alpha(Ca,Pb)SiO_3ss$ to $\beta(Ca,Mn,Pb)SiO_3ss$. Although α- and β-$CaSiO_3$ have about the same densities, a volume change sufficiently large to cause disintegration of agglomerates may be expected in going from $\alpha(Ca,Pb)SiO_3ss$ to $\beta(Ca,Mn,Pb)SiO_3ss$ because of the difference in size between Pb^{2+} and Mn^{2+} ions.

Attempts to prepare $\beta(Ca,Mn,Pb)SiO_3ss$ by reaction [1] did not yield high brightness phosphors since it is not possible to incorporate enough Pb in the phosphor to give sufficiently high absorption for 2537Å.

The preparation of $\beta(Ca,Mn,Pb)SiO_3$ by reaction [2] proved successful. Thus, the preparation of the phosphor involves three steps: (*a*) formation of $\alpha(Ca,Pb)SiO_3ss$, (*b*) formation $\beta(Ca,Pb,Mn)SiO_3ss$, and (*c*) removal of a surface film of "manganese-lead-silica." Each step is discussed in detail.

(*a*) $\alpha(Ca,Pb)SiO_3$ forms metastably below the inversion temperature so that the reaction proceeds rapidly at temperatures between 1100° and 1200°C. The occurrence of metastable liquids accelerates the reaction and it causes the development of large aggregates having diameters between 30 and 100 μ.

(*b*) The formation of $\beta(Ca,Mn,Pb)SiO_3ss$ requires that both MnO + SiO_2 be incorporated into $\alpha(Ca,Pb)SiO_3ss$. Addition of MnO and SiO_2 as $MnSiO_3$ is impractical since three days or more are required for the reaction to reach equilibrium. This result is not surprising since $CaSiO_3$ and $MnSiO_3$ must have about the same lattice energy as evidenced by their extensive solid solution series. If MnO and SiO_2 are mixed with $\alpha(Ca.Pb)SiO_3ss$, $MnSiO_3$ forms more readily than the quaternary solid solution and again the reaction is very sluggish in reaching completion. However, $\beta(Ca,Mn,Pb)SiO_3ss$ can be formed in 2-3 hr at 1160°C by reacting $MnCO_3$ plus $\alpha(Ca,Pb)$ SiO_3:SiO_2. Using this method it is necessary to add sufficient excess silica in the preparation of $\alpha(Ca,Pb)SiO_3ss$ to account for all of the Mn in the quaternary composition.

Silica is not soluble in $\alpha(Ca,Pb)SiO_3$ at concentrations greater than about 1 mole %, although there may be slight solubility below this amount. Only silica which is in contact with α calcium silicate will react with MnO to form $\beta(Ca,Mn,Pb)SiO_3ss$. Isolated

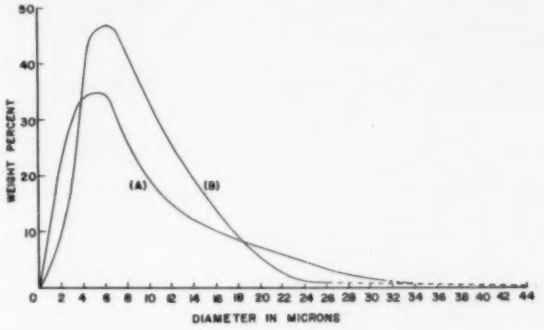

Fig. 3. Particle size distribution curves of $CaSiO_3$:Mn + Pb phosphors. (A) CaO + PbO + MnO + SiO_2 → β(Ca, Pb, Mn) SiO_3 ss; (B) α(Ca, Pb) SiO_3 ss + Mn^{2+} → β(Ca, Pb, Mn) SiO_3 ss.

SiO_2 particles react with MnO to form $MnSiO_3$ which effectively removes Mn from the reaction.

Microscopic examination of samples obtained by quenching after various times clearly revealed the course of the reaction. MnO + SiO_2 diffuse rapidly along grain boundaries of the $\alpha(Ca,Pb)SiO_3$ aggregates. Inversion of $\alpha(Ca,Pb)SiO_3$ begins at the periphery, and as each crystallite of $\alpha(Ca,Pb)SiO_3$ inverts to $\beta(Ca,Mn,Pb)SiO_3$ sufficient contraction occurs to permit the crystallite to separate from the matrix. Thus, this process leads to the disintegration of the aggregates of $\alpha(Ca,Pb)SiO_3$.

(*c*) The Pb which is volatilized from the quaternary solid solution appears to react with excess silica to form a lead silicate film which causes slight sintering. Sintering can be minimized by employing as short a firing time as possible and by using as little excess silica over stoichiometry as practical.

Lead silicate on the surface of the $\beta(Ca,Mn,Pb)SiO_3ss$ crystals also stabilizes higher oxidation states of Mn. Consequently the surface film serves as a filter which considerably lowers the fluorescent brightness of the phosphor. The film may be removed by refiring with NH_4Cl.

The product obtained has substantially smaller particle size than phosphor produced by initially firing together CaO+MnO+PbO+SiO_2. Phosphor prepared by reaction [2] showed less than 1 wt % oversize on 325 mesh sieve whereas conventional material gave 10-15 wt % oversize. Particle size distribution curves are shown in Fig. 3. It is evident that reaction [2] serves to minimize aggregate growth rather than to yield smaller crystallites since either technique yields a maximum of material in the 5 to 7 μ range. The area under curve "A" for material produced by initially firing together CaO+MnO+PbO+SiO_2 represents 85-90 wt % of the total material since 10-15 wt % is greater than 44 μ or 325 mesh. On the other hand, curve "B" for phosphor produced by reaction [2] represents 100 wt % since substantially all of the material is less than 325 mesh. Either technique yields phosphor with the same fluorescent properties.

Acknowledgment

The authors thank E. S. Palik for determining the particle size distributions of phosphor powders.

Manuscript received April 1, 1959. This paper was prepared for delivery before the Philadelphia Meeting, May 3-7, 1959.

Any discussion of this paper will appear in a Discussion Section to be published in the June 1960 JOURNAL.

REFERENCES

1. H. C. Froelich, *J. (and Trans.) Electrochem. Soc.*, **93**, 101 (1948).
2. J. B. Merrill and J. H. Schulman, *J. Opt. Soc. Amer.*, **38**, 471 (1948).
3. J. H. Schulman, R. J. Ginther, and L. W. Evans, *ibid.*, **38**, 817 (1948).
4. G. R. Fonda and H. C. Froelich, *J. (and Trans.) Electrochem. Soc.*, **93**, 114 (1948).
5. A. Steadman, U.S. Pat. 2,299,510, Oct. 20, 1943; *Chem. Abs.*, **37**, 1658[8].
6. J. H. Schulman, U.S. Pat. No. 2,474,193, June 21, 1949; *Chem Abs.*, **43**, 6517g.
7. H. C. Froelich, U.S. Pat. 2,542,322, Feb. 20, 1951; *Chem. Abs.*, **45**, 5027a.
8. F. P. Glasser, Private communications.
9. E. Voos, *Z. Anorg. Allgem. Chem.*, **222**, 213 (1935); E. P. Hall and H. Insley, *J. Am. Ceram. Soc.*, **30**, 63 (1947).
10. E. S. Shepherd, G. A. Rankin, and F. E. Wright, *Am. J. Sci.*, 4th Ser., **28**, 293 (1909).
11. J. G. Rabatin and R. H. Gale, *Anal. Chem.*, **28**, 1314 (1956).
12. E. F. Osborn and J. F. Schairer, *Am. J. Sci.*, **239**, 715 (1941).
13. F. P. Glasser and E. F. Osborn, *J. Am. Ceram. Soc.*, **41**, 358 (1958).

The Dielectric Behavior of Solids Embedded in a Homogeneous Medium

Barlane R. Eichbaum

Product Development Laboratory, International Business Machines Corporation, Poughkeepsie, New York

ABSTRACT

Dielectric constant and tan δ of powdered crystal phases of alumina, quartz, and wollastonite were determined. Since it is very difficult to obtain dielectric measurements of very fine (powdered) crystals, a technique of embedding the solids in a homogeneous medium was used. The relationship between particle shape and volume present in the composite to the dielectric properties of such fine powders was in accord with that indicated by Niesel's theory.

The dielectric properties of large single crystals of inorganic materials can be determined since there is sufficient mass present to use standard measuring techniques. Although large single crystals of many inorganic materials are not available, it would be desirable to determine the dielectric properties of granular or pulverized crystallites in order to study their dielectric contribution in composite mixtures. The object of this research is to present a method for determining the dielectric properties of such fine powdered crystallites.

Niesel proposed a theory to compute dielectric properties of solids embedded in a homogeneous medium (1, 2). This theory considers the volume and particle shape of the crystalline materials embedded in the homogeneous medium. In order to overcome the variations which would be encountered if compressed powders were studied, a technique of embedding inorganic powders in a homogeneous medium was devised and used throughout this investigation.

Theory.—Several theories have been developed to predict dielectric properties of polycrystalline mixtures. A theory developed by Lichtenecker (3) in 1926 gives a good approximation for mixtures having a maximum dielectric constant of 10. In 1935 Bruggeman (4) developed equations for determining dielectric constants of mixtures of materials with crystal shapes approximating spheres or lamellae. Niesel (1, 2) gave a method for calculating both the dielectric constant and loss angle of an aggregate consisting of crystals (assumed to be ellipsoids) mixed with a homogeneous material.

The equations derived by Niesel for the isotropic cases of spheres, lamellae, and long cylinders embedded in a homogeneous medium are as follows:

(*a*) Spheres

$$1 - Vi = \frac{\epsilon i - \epsilon}{\epsilon i - \epsilon a} \sqrt[3]{\frac{\epsilon a}{\epsilon}} \qquad [1]$$

(*b*) Lamellae (randomly oriented)

$$= \frac{3\epsilon a + 2Vi(\epsilon i - \epsilon a)}{3\epsilon i - Vi(\epsilon i - \epsilon a)} \qquad [2]$$

(*c*) Long cylinder (needles)

$$1 - V = \frac{\epsilon i - \epsilon}{\epsilon i - \epsilon a} \frac{(\epsilon i + 5\epsilon a)}{\epsilon i + 5\epsilon} \qquad [3]$$

where ϵi = dielectric constant inside ellipsoid, ϵa = dielectric constant outside ellipsoid, ϵ = resulting dielectric constant, and Vi = volume fraction occupied by ellipsoids.

If δ_1 is the loss angle of the crystal phase and δ_2 that of the medium, then the resulting loss angle δ_{res} is given by

$$\tan \delta_{res} = m_1 \tan \delta_1 + m_2 \tan \delta_2 \qquad [4]$$

If the loss angles of the two ingredients are known it is necessary to determine the values of m_1 and m_2

(energy fractions) which are derived by Niesel to be as follows for the three cases:

(*a*) Spheres

$$m_2 = \frac{(\epsilon_1 - \epsilon)(2\epsilon_2 + \epsilon_1)}{(\epsilon_1 - \epsilon_2)(2\epsilon + \epsilon_1)} \qquad [5]$$

(*b*) Lamellae

$$m_2 = \frac{\dfrac{K_1}{1 + K_1} + 2K_1}{\dfrac{K_{12}}{1 + K_{12}} + 2K_{12}} \qquad [6]$$

(c) Cylinder additions

$$m_2 = \frac{\dfrac{2K_1}{1 + \frac{1}{2}K_1} + K_1}{\dfrac{2K_{12}}{1 + \frac{1}{2}K_{12}} + K_{12}} \qquad [7]$$

where

$$K_1 = \frac{\epsilon_1 - \epsilon}{\epsilon} \qquad [8]$$

$$K_2 = \frac{\epsilon_1 - \epsilon_2}{\epsilon_2} \qquad [9]$$

$$m_1 + m_2 = 1 \qquad [10]$$

and ϵ = dielectric constant of combined phases, ϵ_2 = dielectric constant of glass phase, ϵ_1 = dielectric constant of crystal phase, m_1 = energy fraction of crystal phase, and m_2 = energy fraction of glass phase.

Sample Preparation

In order to test Niesel's theory it was necessary to devise a method of embedding the inorganic crystals in a homogeneous medium; the dielectric properties were then determined. Polystyrene was selected as the homogeneous medium in which to embed the crystals since it has very low loss properties.

Known volumes of five inorganic powders were dispersed in a known volume of polystyrene and carbon tetrachloride solution. This solvent was selected because it has a dielectric constant and tan δ similar to that of polystyrene (5, 6), and, if it should not evaporate completely, little effects would be contributed. The mixtures were completely dried out, then hot pressed into disks having a 1¼ in. diameter and approximately 0.05 in. thick. In all cases the volume of powdered inorganic material does not exceed 65% or the specimen will not be dense, hence, a true evaluation will not be obtained.

The values of dielectric constant and tan δ were determined with the Boonton Q-meter type 160A at 1 megacycle.

Preliminary investigation.—In order to determine the correlation between the theoretical and experimental values for mixtures having known, measured dielectric constant and tan δ, two glasses, Vycor and window glass, were selected for study by embedding in polystyrene. These glasses were ground wet and screened through 100 and 200 mesh sieves prior to combining with polystyrene. The ground glass is considered an isotropic powder material in this case.

Table I. Theoretical and experimental values of dielectric constant and power factor for Vycor glass-polystyrene mixtures

Theoretical

Lamellae			Spheres			Long Cylinder		
Vycor volume, %	ϵ	tan δ	Vycor volume, %	ϵ	tan δ	Vycor volume, %	ϵ	tan δ
0	2.55	0.00022	0	2.55	0.00022	0	2.55	0.00022
10	2.70	0.00030	10.3	2.70	0.00029	10.5	2.70	0.00046
20	2.86	0.00037	21.2	2.86	0.00036	21.0	2.86	0.00050
30	3.02	0.00045	31.4	3.02	0.00043	31.2	3.02	0.00055
40	3.18	0.00051	41.4	3.18	0.00050	41.0	3.18	0.00061
50	3.36	0.00057	52.1	3.36	0.00056	51.8	3.36	0.00064
60	3.53	0.00063	61.7	3.53	0.00062	61.4	3.53	0.00069
70	3.69	0.00068	70.5	3.69	0.00068	70.1	3.69	0.00072
80	3.90	0.00074	81.7	3.90	0.00078	81.5	3.90	0.00077
90	4.09	0.00080	91.5	4.09	0.00079	91.5	4.09	0.00081
100	4.28	0.00084	100	4.28	0.00084	100	4.28	0.00084

Experimental

−200 mesh			−100 mesh		
Vycor volume, %	ϵ	tan δ	Vycor volume, %	ϵ	tan δ
0	2.55	0.00022	0	2.55	0.00022
2.8	2.57	0.00031	4.8	2.57	0.00036
5.5	2.58	0.00039	6.8	2.59	0.00040
9.0	2.62	0.00045	11.3	2.67	0.00047
14.2	2.73	0.00046	18.7	2.83	0.00049
17.7	2.85	0.00048	24.2	2.92	0.00052
26.0	2.91	0.00054	28.9	3.00	0.00054
34.3	3.03	0.00057	37.4	3.12	0.00057
47.1	3.37	0.00065	52.0	3.35	0.00066
58.5	3.55	0.00069	61.6	3.60	0.00068
100	4.28	0.00084	100	4.28	0.00084

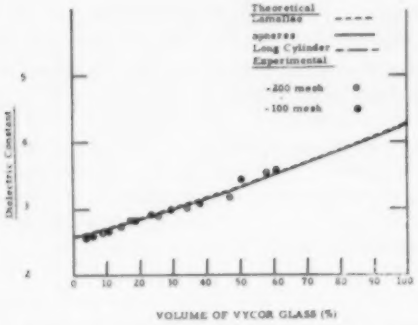

Fig. 1. Volume of Vycor glass on polystyrene vs. dielectric constant and tan δ.

Fig. 2. Photomicrograph of Vycor glass particles. Magnification 1000X.

Two glasses were used because their dielectric properties were quite different and this could be used as a means of verifying the validity of Niesel's equations. Dielectric properties were determined on a square piece of each glass 2 in. by 2 in. by approximately 1/5 in. thick. These glasses were crushed to −100 and −200 mesh grain sizes. Both glasses were investigated using grains of two particle sizes in order to check if the particle size has any effect with either low or high loss glass. Niesel claims that the particle size of the powdered material should have no effect on the results; therefore, it was necessary to substantiate this claim.

Vycor glass-polystyrene mixture.—The two different particle sizes of Vycor glass were embedded in polystyrene. The dielectric properties of the two materials are:

	ϵ	tan δ
Polystyrene	2.55	0.00022
Vycor glass	4.28	0.00084

Since the values for the two end members are known, calculations were made on the basis of lamellar, spherical, and long cylinder (needle) particle shapes in order to determine if the experimental values obtained compare with any of the theoretical curves. Calculated values for the three particle shapes and the experimental value are listed in Table I. All of these values are plotted vs. volume of glass present in Fig. 1.

As can be seen from the graph of Fig. 1, the curves for theoretical dielectric constant are so close together that it is difficult to distinguish between them. The symbols used to denote experimental values for both −100 and −200 mesh sizes follow right in line with the theoretical curves.

Fig. 3. Photomicrograph of window glass particles Magnification 1000X.

The theoretical curves for tan δ on Fig. 1 are easily differentiated. The curve for spherical particles is almost a straight line, whereas that for randomly oriented lamellae has a greater upward curvature, and the curve for randomly oriented needles has a rapid increase which levels off to almost a straight line. Experimental values obtained for both the −100 and −200 mesh particles fall right in line with the long cylinder addition curve. This was not expected because it was assumed that the particles would most closely approach a spherical shape. However, when examined with a petrographic microscope, many of the particles were noted to be a long needle shape as can be seen in the photomicrograph of Fig. 2.

These results were very enlightening, showing that this difference of particle shape has a definite effect, that the particle size difference has no marked effect, and that the experimental and calculated values of both dielectric constant and tan δ vs. volume per cent are almost identical for the case of the long cylinder shaped additions.

Window glass-polystyrene mixtures.—In the experiments using glass-polystyrene mixtures as with the Vycor glass-polystyrene mixtures both −100 and −200 mesh glass grains were embedded in polystyrene for the determination of dielectric properties.

The values of the 100% product in this case at 1 mc and 25°C are;

	ϵ	tan δ
Polystyrene	2.55	0.00022
Window glass	7.95	0.012

The particle shape of this glass (ground) was investigated and assumed to approach a spherical symmetry as can be seen in Fig. 3. Since the particles did not appear to be elongated as many were in the case of Vycor glass, theoretical calculations were performed only for spherical and lamellar particle shapes. Theoretical values obtained for these two shapes vs. volume per cent as well as the experimental values obtained for the two particle sizes are listed in Table II. Curves plotted for theoretical calculations and symbols designating the experimental values are plotted in Fig. 4.

As can be seen in Fig. 4 the lamellar curves for both dielectric constant and tan δ do not approach

Table II. Theoretical and experimental values of dielectric constant and power factor for window glass-polystyrene mixtures

Theoretical

Spheres			Lamellae		
Window glass volume, %	ϵ	tan δ	Window glass volume, %	ϵ	tan δ
0	2.55	0.00022	0	2.55	0.00022
7.5	2.80	0.00116	25	3.66	0.00051
13.2	3.00	0.00194	50	4.92	0.0081
26.5	3.40	0.00340	75	6.30	0.0105
40.8	4.20	0.00549	100	7.95	0.0120
56.4	5.00	0.00733			
72.8	6.00	0.00921			
87.4	7.00	0.01077			
94.2	7.50	0.01140			
100	7.95	0.0120			

Experimental

−200 mesh			−100 mesh		
Window glass volume, %	ϵ	tan δ	Window glass volume, %	ϵ	tan δ
0	2.55	0.00022	0	2.55	0.00022
6.0	2.68	0.0011	6.2	2.68	0.0011
8.2	2.76	0.0015	9.3	2.78	0.0016
12.6	2.88	0.0017	15.5	2.91	0.0024
18.8	3.01	0.0027	21.3	3.18	0.0031
23.7	3.17	0.0033	26.8	3.30	0.0038
27.3	3.32	0.0039	34.5	3.56	0.0048
31.5	3.48	0.0045	42.6	3.96	0.0055
37.6	3.74	0.0052	29.9	4.40	0.0067
47.7	4.31	0.0064	56.7	4.83	0.0076
53.9	4.69	0.0071	100	7.95	0.0120
60.6	5.22	0.0079			
100	7.95	0.0120			

the experimental values, but both the −100 and −200 mesh particle size symbols are very close to the spherical curves. Calculated values of dielectric constant are slightly larger than experimental values, whereas calculated tan δ values are slightly less than experimental values.

However, the curves, being very close, show that the particle shape of the window glass, approaching sphericalness, can be used to make very close approximations to the true experimental values. This helps to substantiate and justify the use of Niesel's theory as does the case for Vycor glass-polystyrene mixtures.

Since the experimental values obtained for the Vycor glass-polystyrene and window glass-polystyrene mixtures so closely approach the theoretical values obtained with Niesel's equations, the same approach is used to determine the 100% volume values for the three crystalline materials, alumina, quartz, and wollastonite.

Dielectric Properties of Alumina, Wollastonite, and Quartz Crystallites

Since Niesel's equations fit the experimental data for the two cases using glasses as the dispersed ingredient, the same technique was used to determine the dielectric properties of the crystal phases of alpha alumina, wollastonite, and low-temperature quartz.

Alumina-polystyrene mixtures.—A very pure grade of fused alumina[1] was used for determining the dielectric properties by embedding in polystyrene. von Hippel (7) determined the dielectric properties of a clear sapphire[2] to be:

$$\epsilon = 8.6 \pm 0.02, \tan \delta = 0.001$$

perpendicular to the optic axis

and

$$\epsilon = 10.55 \pm 0.02, \tan \delta = 0.001$$

parallel to the optic axis

when measured at one megacycle.

This is a single crystal form of alumina and not a powdered form which is randomly oriented.

The alumina grains used in this study appear to have a spherical shape symmetry (Fig. 5). Since these particles appear to be spherical, calculations were made only for spherical shaped particles and not for the other two shapes. Experimental values were first determined for alumina additions up to 61% by volume as shown in Table III. These dielectric constants and power factors are plotted vs. volume per cent of alumina on Fig. 6. Three of the points at volumes of 10.4, 42, and 50.5%, respectively, which fall on a curve drawn through all

[1] Norton's 38900 (−900 mesh) which is alpha alumina and is 99.86% Al_2O_3.

[2] Linde Air Co. alpha alumina.

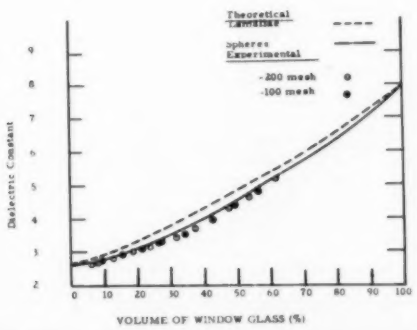

Fig. 4. Volume of window glass in polystyrene vs. dielectric constant and tan δ.

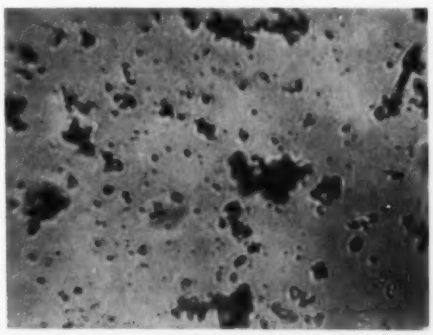

Fig. 5. Photomicrograph of alumina grains. Magnification 1000X.

Table III. Theoretical and experimental values of dielectric constant and power factor for alumina (Norton 38900)-polystyrene mixtures

Experimental					
Alumina volume, %	ϵ	tan δ	Alumina volume, %	ϵ	tan δ
0	2.55	0.00022	0	2.55	0.00022
2.3	2.62	0.00024	10.4*	2.91	0.00027
10.4	2.91	0.00027	25.6	3.55	0.00033
20.9	3.33	0.00031	42.0*	4.36	0.00040
32.0	3.71	0.00036	50.5*	4.82	0.00043
42.0	4.36	0.00040	53.6	5.00	0.00044
50.5	4.82	0.00043	100	8.42	0.00061
61.0	5.29	0.00045			

* Experimental values used to calculate theoretical 100% value.

points, were selected for making calculations of the 100% alumina end point. The calculated values are:

Volume alumina, %	ϵ	tan δ
10.4	8.45	0.00061
42.0	8.42	0.00062
50.5	8.40	0.00060
Avg	8.42	0.00061

With these values other theoretical points were calculated for completing the plot of the theoretical curves on Fig. 6. All theoretical and experimental values are listed in Table III.

As can be seen in Fig. 6 the theoretical curves and symbols for experimental points show good agreement. The dielectric constant and tan δ of these randomly oriented alumina grains approach the values obtained for single crystals by von Hippel.

Quartz-polystyrene mixtures.—Using a very pure grade of low-temperature quartz,[5] which is 99% pure SiO_2, the dielectric constant and tan δ were determined when mixed with polystyrene. Navias (7) determined the average dielectric constant and tan δ of a single crystal of quartz to be

$$\epsilon = 4.44, \tan \delta = 0.00025 \text{ (prism)}$$

$$\epsilon = 4.44, \tan \delta = 0.00024 \text{ (basal)}$$

at 8600 megacycles.

Again, as in the case for alumina, these values are for single crystals and not for fine powders, which

[5] Supplied by Pennsylvania Pulverizing Co.

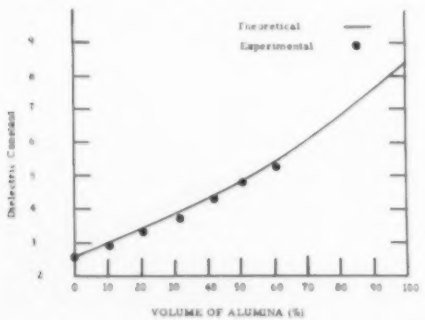

Fig. 6. Volume of alumina in polystyrene vs. dielectric constant and tan δ.

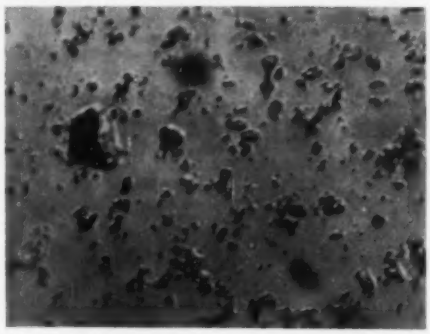

Fig. 7. Photomicrograph of quartz grains. Magnification 1000X.

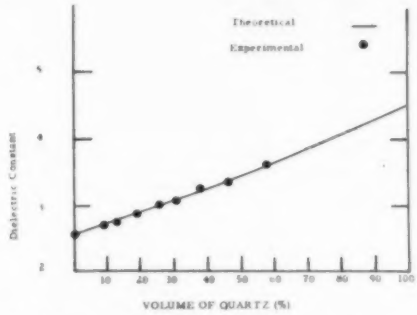

Fig. 8. Volume of quartz in polystyrene vs. dielectric constant and tan δ.

may have similar values regardless of size, but the effects when combined with a continuous phase need to be determined. For the theoretical calculations these quartz grains were considered to be spherical (Fig. 7).

Several experimental values were determined on specimens containing up to 58.3% quartz by volume; these are listed in Table IV. Three sets of values for quartz volumes of 9.6, 25.7, and 58.3% were used for computation to obtain an average dielectric constant of 4.52 and a tan δ of 0.00031 for the quartz grains. Using these values in Niesel's formulas several other theoretical points for quartz volumes up to 100% were calculated and are listed in Table IV. All theo-

Table IV. Theoretical and experimental values of dielectric constant and powder factor for quartz (Pennsylvania Pulverizing Co. —325 mesh)—polystyrene mixtures

Experimental			Theoretical		
Quartz volume, %	ϵ	tan δ	Quartz volume, %	ϵ	tan δ
0	2.55	0.00022	0	2.55	0.00022
9.6	2.71	0.00023	9.6*	2.71	0.00023
13.2	2.76	0.00024	15.7	2.83	0.00024
19.1	2.87	0.00025	21.3	2.90	0.00024
25.7	3.00	0.00025	25.7*	3.01	0.00025
31.0	3.09	0.00026	33.7	3.19	0.00026
38.2	3.26	0.00026	43.2	3.30	0.00026
46.7	3.36	0.00027	52.8	3.49	0.00027
58.3	3.61	0.00028	58.3*	3.61	0.00028
			68.0	3.80	0.00028
			74.6	3.96	0.00029
			86.2	4.20	0.00030
			100	4.52	0.00031

* Experimental values used to calculate theoretical 100% value.

retical and experimental dielectric constant and tan δ values are plotted against volume of quartz on Fig. 8. Both the dielectric constant and tan δ are coincident with the symbols designating the experimental values.

The values of the dielectric properties of these quartz grains are very close to the average values obtained by Navias for single crystals.

Wollastonite-polystyrene mixtures.—Wollastonite has been used successfully as a major ingredient in recently developed low loss insulation. Since no values of the dielectric properties of single crystals of wollastonite are available and synthesis of large wollastonite crystals for measurements would be almost impossible, because pseudo-wollastonite is the stable phase at the high temperature required for synthesis, the values obtained will be considered to approach the average values of a single crystal. The purest commercial grade of wollastonite available[4] was used in this investigation.

The particle shape of C-1 grade wollastonite is shown in Fig. 9. Calculations were made only for long cylinder shape particles in polystyrene because the wollastonite grains are definitely of this shape.

From the several experimental values obtained for the volume of wollastonite in polystyrene listed in Table V three sets of values were selected at 11.0, 24.9, and 62.0% volume for determining the theoretical 100% wollastonite aggregate dielectric properties. The average dielectric constant is 6.15 and the tan δ is 0.00045. Using these values for wollastonite, the theoretical values vs. volume were calculated

[4] Supplied by Godfrey L. Cabot Co.

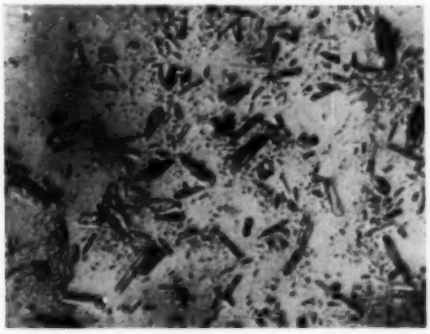

Fig. 9. Photomicrograph of wollastonite grains. Magnification 1000X.

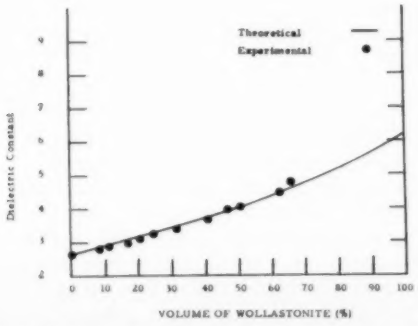

Fig. 10. Volume of wollastonite in polystyrene vs. dielectric constant and tan δ.

Table V. Theoretical and experimental values of dielectric constant and power factor for wollastonite (Godfrey L. Cabot Co. C-1)—polystyrene mixtures

Experimental			Theoretical		
Wollastonite volume, %	ε	tan δ	Wollastonite volume, %	ε	tan δ
0	2.55	0.00022	0	2.55	0.00022
8.5	2.79	0.00024	11.0*	2.84	0.00025
11.0	2.84	0.00025	16.8	3.00	0.00027
16.5	2.98	0.00027	24.9*	3.24	0.00029
20.2	3.08	0.00028	33.0	3.50	0.00031
24.9	3.24	0.00029	47.7	4.00	0.00035
31.7	3.38	0.00030	62.0*	4.50	0.00038
40.2	3.68	0.00033	74.0	5.00	0.00041
46.5	3.99	0.00034	86.8	5.50	0.00043
50.5	4.12	0.00034	100	6.15	0.00045
62.0	4.50	0.00038			
65.8	4.82	0.00038			

* Experimental values used to calculate theoretical 100% value.

and are listed in Table V. These values are plotted on Fig. 10.

Summary

The dielectric properties of solids embedded in a homogeneous medium have been determined with the aid of Niesel's theory which is based on particle shape and volume per cent of the solids. Niesel's theory was first verified by embedding two glasses (one having a high loss and the other a low loss) of 2 specific particle sizes in a homogeneous medium. Since the dielectric properties of both were known (measured) theoretical calculations were made which were almost identical with experimental values on samples with both glasses of 2 different particle sizes. Since such good correlation was observed with these inorganic materials of known dielectric properties the same techniques were used to determine the dielectric properties of alumina, quartz, and wollastonite.

Acknowledgment

The author wishes to acknowledge the U. S. Signal Corps for their sponsorship of this research. He would also like to thank Mr. Sam DiVita, Professor John H. Koenig, Dr. Robert B. Sosman, and Dr. Harold T. Smyth for their assistance and guidance during the course of this research. The author would like to thank Dr. Thomas D. Callinan for his assistance in the preparation of this manuscript.

Manuscript received Sept. 29, 1958. This research was submitted by the author as partial fulfillment for the requirements for his Ph.D. degree at Rutgers University in 1956.

Any discussion of this paper will appear in a Discussion Section to be published in the June 1960 JOURNAL.

REFERENCES

1. W. Niesel, *Ann. Physik*, **6**, [10], 336 (1952).
2. W. Niesel, *ibid.*, **6**, [12], 410 (1953).
3. H. Bruggemann, *ibid.*, **5**, [24], 636 (1935).
4. K. Lichtenecker, *Physik Z.*, **27**, 115 (1926).
5. A. von Hippel, "Dielectric Materials and Applications," pp. 336-362, John Wiley & Sons, New York (1954).
6. *Dielectrics, Trans. Faraday Soc.*, **42A**, 155 (1946).
7. L. Navias, *J. Am. Ceram. Soc.*, **37**, [8], 329 (1954).

Growth of Whiskers by Reduction of Halogenides

H. Wiedersich

Research Laboratories, Westinghouse Electric Corporation, Pittsburgh, Pennsylvania

ABSTRACT

By reduction of $SiCl_4$ with Zn, silicon was produced and similarly by reduction of $FeCl_2$ with H_2, iron. In both cases variations of the growth conditions changed the forms of the crystals from equiaxed into thin, long ones (whiskers). Thermodynamic and kinetic considerations lead to the conclusion that the partial pressure of $SiCl_2$, resp. $FeCl_2$ or HCl determine the growth forms. The hypothesis is suggested that the adsorption of these components makes certain crystallographic plane growth inactive and therefore produces whisker growth.

The phenomenon of filamentary or fibrous growth of metal crystals has been known for more than a hundred years (1). During the past few years these crystals have gained new interest especially due to the discovery that some of them exhibit almost the theoretical strength (2). It became evident that quite a number of different mechanisms are responsible for fibrous growth. Only three basically different categories will be mentioned: (*A*) Growth from the elementary metal: Whiskers grow spontaneous (3) or with applied external pressure (4) from the solid metal or platings. They grow from the root presumably by a dislocation mechanism whereby a stress gradient and/or surface oxidation supplies the necessary energy. (*B*) Growth by reduction of ionic crystals: Compounds inclined to fibrous growth are usually either oxides or sulfides, have a low vapor pressure, and the metal ions have high mobilities in the lattice. The filaments grow from the root. The mechanism suggested by Wagner (5) involves the precipitation of excess metal ions, created by the reduction, at the compound-metal interface. (C) Growth occurs from the vapor phase, either from the elementary vapor (6, 7) or in connection with the reduction of a volatile compound (8-10). The filaments in this group grow from the tip contrary to the two previously mentioned groups.

For growth from the elementary vapor phase, Sears (11) has given a satisfactory theory based on a screw dislocation mechanism. Atoms are adsorbed over the whole surface of the whisker and migrate by surface diffusion to the tip where they attach themselves to a continuous growth step caused by a screw dislocation along the axis of the whisker. Such a whisker should be a perfect crystal apart from one screw dislocation, and its side faces should be atomically smooth.

The present investigation was intended to enlighten the more complex phenomenon of whisker growth by reduction of volatile halides. The following reactions were used:

$$SiCl_4 + 2Zn \rightarrow Si + 2ZnCl_2$$

and

$$FeCl_2 + H_2 \rightarrow Fe + 2HCl$$

which were known to produce whiskers (8-10).

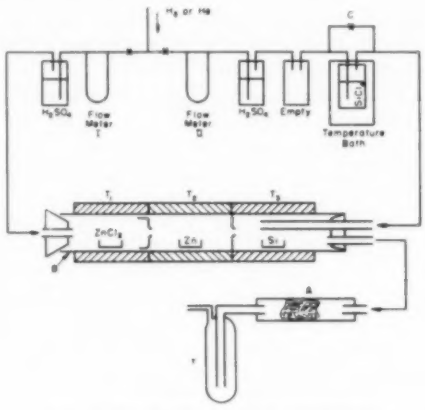

Fig. 1. Experimental setup (schematic)

Experimental

Figure 1 shows schematically the experimental setup for growing silicon crystals. He or H_2, dehumidified by bubbling through concentrated sulfuric acid, was passed through flowmeter I into the left side of the furnace and through flowmeter II and a $SiCl_4$-saturator, which had a bypass C, into the right side of the furnace. The furnace had three separately controlled windings at the positions marked by $ZnCl_2$, Zn, and Si, to provide three different temperature zones for the evaporation of $ZnCl_2$ and Zn, and for the reaction which took place in the zone marked as Si. The interior of the furnace consisted of a Vycor tube with a fixed Vycor baffle between the Zn and Si zones and a removable baffle between the $ZnCl_2$ and Zn zones. There was a short inlet tube for H_2 on the left side and a long one for the H_2-$SiCl_4$ mixture on the right side. The outlet for the gases, on the right side of the tube, leads through chamber A which was filled with glass fibers for the complete removal of $ZnCl_2$, and a trap T immersed in liquid nitrogen to condense the unreacted $SiCl_4$.

The experimental procedure was as follows. The whole tube, B, containing alundum boats filled with $ZnCl_2$ and Zn and an empty boat at the Si location was inserted in the hot furnace to reduce the preheating times and thereby the evaporation of $ZnCl_2$ and Zn before starting the reaction. Then the whole

system was flushed with He before H_2 was introduced. As soon as the furnace was again at the desired temperature the reaction was started by simply closing the bypass C and allowing the $SiCl_4$ vapor to enter the system.

After the run (1 to 4 hr) the bypass C was opened again, the furnace turned off, and the system flushed with He. In order to remove traces of $ZnCl_2$, which precipitated on the grown Si crystals during the cooling period, the boat with the Si crystals was annealed under a vacuum of a few mm Hg at 800°C for an hour. The chemicals used were: Zn (99.99%), $ZnCl_2$(C.P.), and technical $SiCl_4$.

The setup for growing iron crystals was very similar to that described before. The hydrogen was deoxidized by a palladium catalyst and dried by a liquid nitrogen trap. The furnace had a constant temperature throughout. The $SiCl_4$ saturator was omitted, and $FeCl_2 \cdot 4H_2O$ (C.P.) was introduced in place of the $ZnCl_2$ and Zn. In this case the Vycor tube was inserted into the cold furnace, the system connected to the house vacuum, and then heated up to the operating temperature within about 15 min. During this time it was necessary to pass a small flow of hydrogen through the system to prevent condensing of water in the entrance tubes. The water contained in the $FeCl_2$ was practically completely evaporated after the heating-up time, and the flow rates and pressure (1 atm) were adjusted and kept constant throughout the rest of the experiment (6-24 hr).

Results

Silicon.—By controlling the temperature of the temperature bath and the zones T_1 and T_2 of the furnace, the composition of the reacting gases could be controlled. The temperature T_3 of the reaction zone could be fixed independently. The total pressure was practically atmospheric pressure. Table I summarizes the results of the 15 different runs performed. The partial pressures of the different components (indicated by subscripts) in the two entering gases are given by p^*; v_{SiCl_4}, and v_{Zn} are the flow rates of the two different entering gas mixtures. The temperature in the reaction zone is also given. The line before the last states whether whiskers did or did not grow.

All experiments which did not yield whiskers have in common that the initial partial pressure $p^*_{SiCl_4}$ of $SiCl_4$ was comparatively low. The flow rates and the presence or absence of $ZnCl_2$ in the initial mixture do not seem to have an influence. Figure 2 shows silicon whiskers from run XIII. Not all crystals in Fig. 2 can

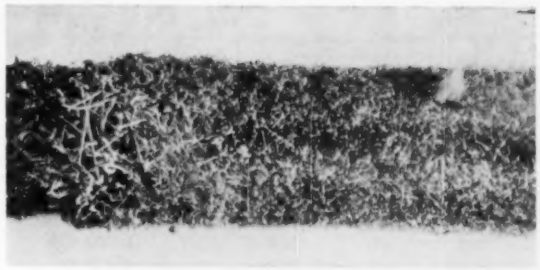

Fig. 2. Silicon whiskers grown in experiment XIII. Magnification 2X before reduction for publication.

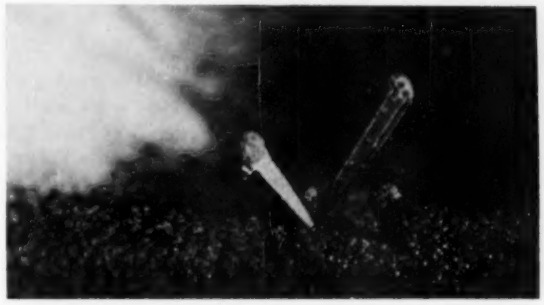

Fig. 3. Silicon crystals grown in experiment X. Magnification 15X before reduction for publication.

be classed as whiskers. Many of those on the left side are not straight and do not have the characteristic smooth surfaces associated with whiskers. However, fine, straight whiskers can be seen. Many of the whiskers, sufficiently large for light microscopic observation, are found to have hexagonal cross section. The diameter of the whiskers ranged from about 5×10^{-5} to 5×10^{-4} cm. Figure 3 shows the types of growth in experiment X. The roughly spherical type of crystals covering the edge of the alundum boat were observed in all experiments which did not yield whiskers but were not observed in those yielding whiskers. Pyramidal crystals were found only in experiment X.

Iron.—Fewer variations in growth conditions were made for iron crystals, since the only aim was to show that the growth mechanism is very much the same as for silicon. Table II summarizes the experiments performed. The symbols used correspond to the ones in Table I. One part of the flow of $H_2(v_1)$ was passed over solid $FeCl_2$ thus converting to the equilibrium mixture of H_2, HCl, and $FeCl_2$ in the presence of solid $FeCl_2$ and Fe. Since the temperature of the furnace was kept constant throughout at $T = 658$°C this mixture had always the composition

Table I. Silicon crystals

Run No.	I	II	III	IV	V, VII, VIII	VI	IX	X	XI, XII	XIII, XIV	XV
$p^*_{SiCl_4}$ [at]	0.077		0.044	0.31	0.31	0.10	0.31	0.31	0.34	0.34	
$v_{SiCl_4} \times 10^5$ [moles/sec]	1.3	2.6	3.9	5.3	5.3	4.1	5.3	5.3	1.1	1.1	0.36
p^*_{Zn} [at]	0.13		0.13	0.13	0.13	0.13	0.29	0.36	0.29	0.29	
$p^*_{ZnCl_2}$ [at]	0.17		0	0	0	0	0	0.41	0	0.28	
$v_{Zn} \times 10^5$ [moles/sec]	1.6	3.2	4.1	4.1	4.1	4.1	5.0	16.1	1.0	1.7	0.55
T, °C	928		928	928	834	834	852	874	830	830	
Whiskers	No		No	Yes	Yes	No	Yes	No	Yes	Yes	
Symbol in Fig. 9	□		■	○	●	△	▲	▽	▼	⌀	

Table II. Iron crystals

Run	A	B	C	G	H	I
v_1 [moles/sec]	10.6×10^{-5}	21.1×10^{-5}	4.9×10^{-5}	10.6×10^{-5}	10.6×10^{-5}	10.6×10^{-5}
v_2 [moles/sec]	10.8×10^{-5}	10.8×10^{-5}	10.8×10^{-5}	21.5×10^{-5}	3.4×10^{-5}	10.8×10^{-5}
$\frac{v_2}{v_1}$	1.02	0.50	2.18	2.04	0.51	1.02
p'_{FeCl_2} [at]	2.85×10^{-3}	4.31×10^{-3}	1.39×10^{-3}	1.50×10^{-3}	4.31×10^{-3}	2.85×10^{-3}
p'_{HCl} [at]	0.082	0.108	0.054	0.053	0.108	0.082
p'_{H_2} [at]	0.915	0.889	0.944	0.945	0.889	0.915
Whiskers	Some	Many	None	None	Many	Some

Values common to all runs: $p^*_{FeCl_2} = 7.25 \times 10^{-3}$, $p^*_{HCl} = 0.156$, $p^*_{H_2} = 0.837$ at; temperature 658°C; $S_{max} = 1.12$; r_{max} (calc.) = 10^{-14} cm/sec; $r_{exp} = 5 \times 10^{-5}$ cm/sec.

$p^*_{HCl} = 0.156$, $p^*_{H_2} = 0.837$, and $p^*_{FeCl_2} = 7.25 \times 10^{-3}$ at. Equilibrium data of Kangro and Peterson (12) and vapor pressure data of Mayer (13) were used to obtain the values of the partial pressures. Into this mixture pure H_2 was introduced with the flow rate v_2.

A decrease of the ratio v_2/v_1 (this means smaller amounts of H_2 get introduced into a given volume of the equilibrium mixture) causes an increase in the tendency to form whiskers. Figure 4 shows the growth resulting from the runs G, I, and H. Above the centers of the boats an iron wire is suspended from which most but not all of the whiskers grew. Small crystals were found, in all experiments, growing on the boats, the wires, and the surrounding Vycor tubes. They were mostly cubes with indications of (110) and (111) planes as shown in Fig. 5. The whiskers as shown in Fig. 6 and 7 frequently had right angle kinks and varied in thickness from about 5×10^{-4} cm to 8×10^{-3} cm. The cross section was usually square or rectangular; a few hexagonal ones were found. Sometimes the cross section decreased toward the tip. Figure 8 shows the tip of a whisker apparently bounded by (100) planes and one (111) plane.

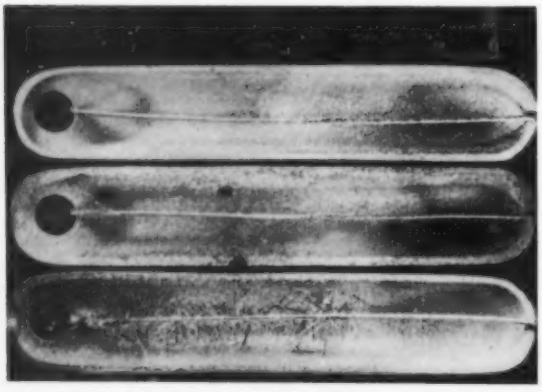

Fig. 4. Iron crystals and whiskers from experiments G (top), I (middle), and H (bottom).

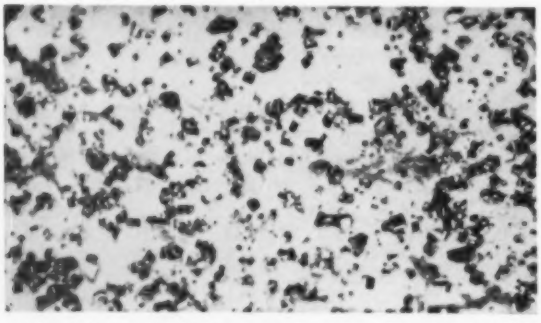

Fig. 5. Iron crystals from experiment C. Magnification 32X before reduction for publication.

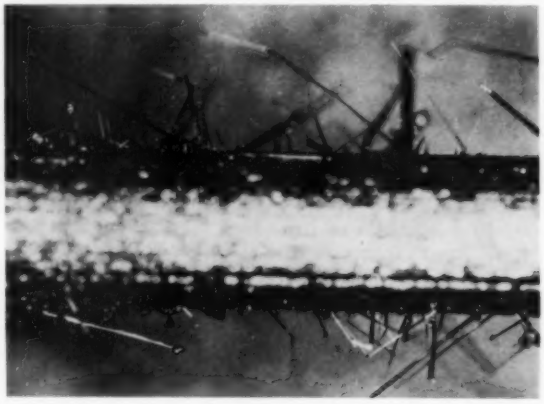

Fig. 6. Iron whiskers from experiment I. Magnification 38X before reduction for publication.

Discussion

There are principally three different processes involved in the growth of the crystals in the present kind of system: (*a*) intermixing of the two incoming

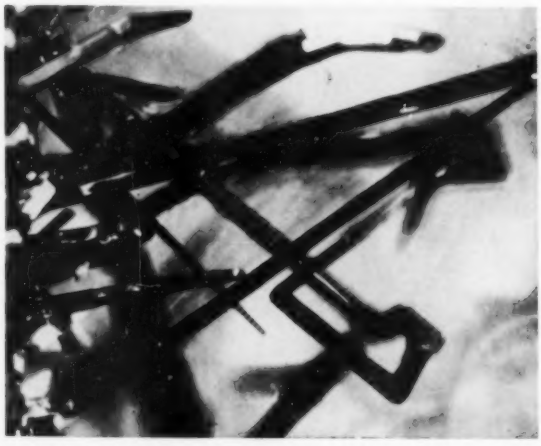

Fig. 7. Iron whiskers from experiment H. Magnification 38X before reduction for publication.

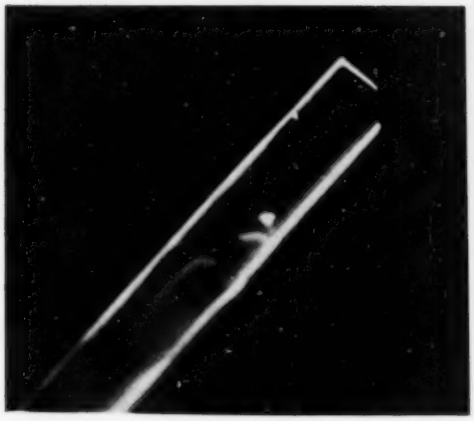

Fig. 8. Tip of an iron whisker. 300X before reduction for publication.

gases by convection and diffusion; (*b*) chemical reactions; and (*c*) precipitation on the growing face of the crystal.

Since no simple way of estimating the intermixing by convection is available, we consider only the process of diffusion. From kinetic gas theory one obtains for the diffusion constant in gases the expression (14)

$$D = \frac{32}{9\pi}\left(\frac{kT}{\pi}\right)^{3/2}\frac{1}{\delta^2 p\sqrt{m}}$$

where k = Boltzmann constant, T = absolute temperature, δ = collision diameter, p = pressure, and m = mass of the molecules. Using reasonable average numbers for these quantities ($T = 1150°K$, $\delta = 3$ Å, $p = 10^6$ dynes/cm^2, $m = 2 \times 10^{-22}$ g); a rough estimate for D is:

$$D = 1.5 \text{ cm}^2/\text{sec}$$

Thus one can expect that for a tube of radius 1 cm complete mixing is achieved in less than 1 sec. This is to be compared with the time the gas mixture remains in the hot part of the reaction zone (≈10 cm), which ranged between 1 and 20 seconds. So the reacting gases are expected to have mixed completely in all experiments, especially since convection is favoring the mixing.

Very little is known about the details of the second of the above mentioned processes, the chemical reaction. We shall asume that it takes place mainly in the gaseous phase and shall try to derive some conclusions about the growth of the crystals which are based on this assumption.

Due to the nature of the experiments it is not possible to derive values of the actual supersaturation S (defined as ratio of the partial pressure in the gas p to the equilibrium pressure p_{equ}) during growth. Yet one can easily obtain an upper limit for S assuming one can apply the ideal gas law.

Silicon.—The main, and probably the exclusive, reaction taking place is

$$SiCl_4 + 2Zn \rightarrow Si + 2ZnCl_2 \qquad [1]$$

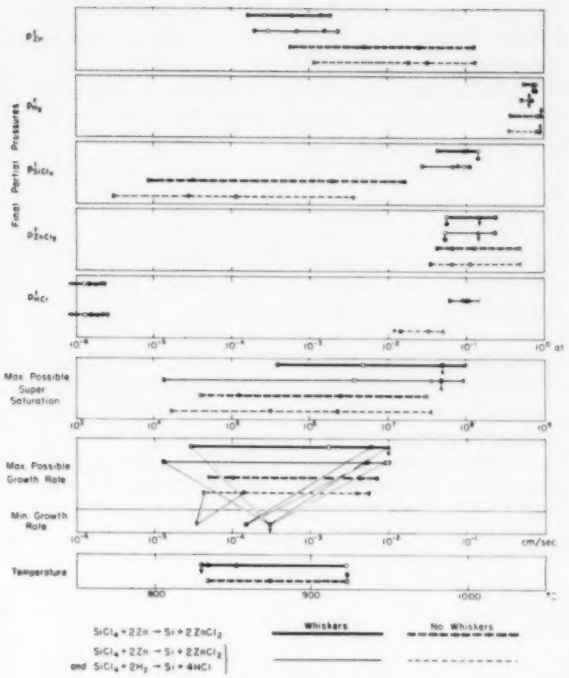

Fig. 9. Range of variables during growth of Si crystals

Preliminary experiments have shown that hydrogen by itself is not able to reduce $SiCl_4$ at the temperatures used even though thermodynamic equilibrium data (15) predict a reaction

$$SiCl_4 + 2H_2 \rightarrow Si + 4HCl \qquad [1a]$$

should yield measurable amounts of Si. In the following it is therefore assumed that only reaction [1] has taken place in the experiments. Yet in Fig. 9 the values obtained by taking in addition [1*a*] into account are added. From Gibbs free energy data given by Kellogg (15) and vapor pressures (14, 16) one obtains the equilibrium constant K^2 [1] in the law of Mass Action for reaction [1]

$$K^2 = \frac{p_{SiCl_4} \times p^2_{Zn}}{p_{Si} \times p^2_{ZnCl_2}} \qquad [2]$$

the p's denote the partial pressures of the chemical Species indicated by subscripts in the gas mixture. A supersaturation $S > 1$ ($S = 1$ means equilibrium between gas and solid phase) is obtained only if the homogeneous reaction in the gas phase is faster than the heterogeneous one of precipitation. The maximum value of S which could be achieved would occur if the first reaction reaches equilibrium before the second has proceeded in any appreciable amount. Taking this into account one derives from [2] in a straight forward way the limits of S:

$$1 \leqq S \leqq \frac{1}{K^2 \times (p_{Si})_{equ}} \frac{p_{SiCl_4} \times p^2_{Zn}}{p^2_{ZnCl_2}} \qquad [3]$$

In case all three components $SiCl_4$, Zn, and $ZnCl_2$ are introduced, one can use on the right side of the Eq. [3] the partial pressures before the reaction since the

[1] The square is used to be in agreement with Kellogg's definitions.

amount reacted in the gas phase to achieve equilibrium is extremely small as long as practically no precipitation has taken place.

In case no $ZnCl_2$ is added, the change in p_{ZnCl_2} due to the reaction has to be taken into account and one obtains:

$$1 \leqq S \leqq \frac{1}{(p_{Si})_{equ}} \sqrt[3]{\frac{p_{SiCl_4} \times p^2_{Zn}}{4K^2}} \qquad [4]$$

Now Eqs. [3] and [4] have to be expressed in terms of the partial pressures p^* in the entering gases. The two gas mixtures characterized by $p^*_{SiCl_4}$ and by p^*_{Zn} and $p^*_{ZnCl_2}$ enter the reaction chamber and mix by convection and interdiffusion. Assuming the diffusion constants are equal (actually they will differ by less than the factor 10) one can obtain the possible upper limit of S in terms of the composition of the entering gases. One volume unit of the final mixture may be composed of "a" units of (Zn, $ZnCl_2$, H_2) and $(1 - a)$ units of ($SiCl_4$, H_2). Then the partial pressures in the final mixture are, neglecting the reaction:

$$p_{SiCl_4} = (1 - a)\, p^*_{SiCl_4}$$

$$p_{Zn} = a\, p^*_{Zn}$$

$$p_{ZnCl_2} = a\, p^*_{ZnCl_2}$$

Inserting these expressions into [3] and [4] and maximizing with respect to "a" gives finally the maximum supersaturations which are possible:

$$S_{max} = \frac{1}{K^2 (p_{Si})_{equ}} \cdot \frac{p^*_{SiCl_4} \times p^{*2}_{Zn}}{p^{*2}_{ZnCl_2}} \qquad [5]$$

$$S_{max} = \frac{0.53}{(p_{Si})_{equ}} \sqrt[3]{\frac{p^*_{SiCl_4} \times p^{*2}_{Zn}}{4K^2}} \qquad [6]$$

The values of S_{max} for the different runs are contained in Fig. 9.

Iron.—Similar considerations lead to

$$S_{max} = \frac{1}{K (p_{Fe})_{equ}} \frac{p^*_{FeCl_2} \times p_i}{p^{*2}_{HCl}} \qquad [7]$$

for the maximum possible supersaturation during the growth of iron crystals. The p^*'s are the partial pressures in the equilibrium mixture entering the reaction chamber, p_i is the partial pressure of the pure H_2 entering (which was always $\simeq 1$ at.), and K is defined as

$$K = \frac{p_{FeCl_2} \times p_{H_2}}{p_{Fe} \times p^2_{HCl}} \qquad [8]$$

The value of $K \times (p_{Fe})_{equ}$ was taken from (12, 13). In all experiments S_{max} was equal to 1.12.

One other set of values was obtained by conventional application of the Law of Mass Action. These are the final partial pressures p' in the gas after complete equilibrium with the precipitated phase is achieved. The values of the p''s for the various components are given in Fig. 9 for silicon and in Table II for iron. These values are a good approximation for the partial pressures in contact with the growing crystals so long as the growth proceeds at low supersaturations.

The following should be mentioned in connection with the third of the previously mentioned processes, the precipitation on the growing face of the crystals. From kinetic gas theory one can obtain the number Z of impacts per unit area of a surface per second:

$$Z = \frac{p}{(2\pi\, mkT)^{1/2}} \qquad [9]$$

where p is the partial pressure of the gas. If one assumes every impinging atom sticks at the place it hits, the rate of linear growth would be

$$r = \frac{Zm}{\rho} \qquad (\rho = \text{density}) \qquad [10]$$

The maximum possible growth rate obtained at the maximum supersaturation, r_{max} (calc), is given in Fig. 9 and in Table II and is compared with a rough estimate of the growth rate r_{exp} obtained from some experiments simply by dividing the length of the longest whiskers by the time the experiment lasted. This assumes that the whiskers have grown at a constant rate throughout the experiment and r_{exp} is therefore an estimate of the lower limit of the maximum growth rates in these experiments. Although r_{max} in several cases is larger than r_{exp}, runs XIII and XIV for silicon and the experiments with iron show clearly that one cannot explain the growth of the whiskers simply by the direct attachment of the impinging atoms at the growing face. One has to take into account a surface diffusion process similar to that proposed by Volmer and Estermann (17).

Discussion of Results

A comparison of the experimental range of the values of the variables which could be critical to the form of growth of the Si crystals is made in Fig. 9 for the two observed growth forms. It should be mentioned that the ends of the lines are not necessarily the actual limits for the occurrence of one or the other type of growth; they give only the range which these variables covered in the performed experiments. The final partial pressure of $SiCl_4$ was $\geqq 4.5 \times 10^{-2}$ ($\geqq 2.8 \times 10^{-2}$) at. for all cases where whiskers grew and $\leqq 1.7 \times 10^{-2}$ ($\leqq 3.8 \times 10^{-3}$) for all other experiments. The limits for the case that H_2 should take part in the reaction are added in parenthesis; then the partial pressures of HCl do also not overlap (they have the limits $\geqq 6.4 \times 10^{-2}$, respectively, $\leqq 5.2 \times 10^{-2}$ at.). All the other variables cover, for both growth forms, nearly the same range, or they overlap to a wide extent. This seems to indicate that the silicon tetrachloride (and/or hydrogen chloride) partial pressure has the main influence on the growth form of the Si crystals.

A similar situation was found for the growth of iron crystals. While temperature, maximum supersaturation, and maximum possible growth rate are identical for all experiments, an increase of the final partial pressures of $FeCl_2$ (1.4×10^{-3} to 4.3×10^{-3} at.) and of HCl (0.05 to 0.11 at.) leads from practically no whisker growth to pronounced whisker growth. The small relative change in the final H_2 partial pressure (0.89 to 0.95 at.) would hardly cause the change in growth form. On the basis of the present

experiments it is not possible to decide whether a high $FeCl_2$ partial pressure or a high HCl partial pressure or the combination of both is necessary for whisker growth.

The final partial pressures are a good approximation for the actual partial pressures of these components in contact with the growing crystal as long as the growth proceeds at relatively low supersaturations. The latter is surely true for the growth of iron ($S \leqq 1.12$). It can be shown that the statement that higher $SiCl_4$ partial pressures are necessary to produce whiskers than to produce equiaxed crystals still holds qualitatively, even if silicon grew at high supersaturations.

The findings suggest the following growth mechanism for silicon and iron whiskers: If the density of certain adsorbed species of molecules ($SiCl_4$, $FeCl_2$, or HCl) exceeds a critical value, a further growth of some crystallographic planes gets suppressed. These planes form the side faces of the whisker [(100) for iron, (112) or (110) for silicon]. The growing tip will usually consist of different kinds of planes and hence be able to attach new atom layers. The growth itself may proceed by a screw dislocation mechanism as suggested by Sears (11) for mercury whiskers, yet the possibility that each new atom layer starts with a surface nucleus could not be ruled out by an estimate of the supersaturation necessary for a high enough surface nucleation rate.

Manuscript received June 24, 1957. This paper was prepared for delivery before the Washington Meeting, May 12-16, 1957.

Any discussion of this paper will appear in a Discussion Section to be published in the June 1960 JOURNAL.

REFERENCES

1. G. Bischof, *Ann. d. Phys. (Poggendorf)*, **60**, 285 (1843).
2. C. Herring and J. K. Galt, *Phys. Rev.*, **85**, 1060 (1952).
3. K. G. Compton, A. Mendizza, and S. M. Arnold, *Corrosion*, **7**, 325 (1951).
4. R. M. Fisher, L. S. Darken, and G. K. Carroll, *Acta. Met.*, **2**, 368 (1954).
5. C. Wagner, *Trans. AIME*, **194**, 214 (1952).
6. G. W. Sears, *Acta Met.*, **1**, 457 (1953).
7. R. V. Coleman and G. W. Sears, *ibid.*, **5**, 131 (1957).
8. E. R. Johnson and Y. A. Amick, *J. Appl. Phys.*, **25**, 1204 (1954).
9. A. W. Cochardt and H. Wiedersich, *Naturwiss.*, **42**, 342 (1955).
10. S. S. Brenner, *Acta Met.*, **4**, 62 (1956).
11. G. W. Sears, *ibid.*, **3**, 361 (1955).
12. W. Kangro and E. Peterson, *Z. anorg. Chem.*, **261**, 157 (1950).
13. C. G. Mayer, U.S. Bur. Min., Techn. Paper 360 (1925).
14. S. Dushman, "Scientific Foundations of Vacuum Technic," John Wiley & Sons, Inc., New York (1949).
15. H. H. Kellogg, *Trans. AIME*, **188**, 862 (1950).
16. Landolt-Börnstein, "Physikalisch-Chemische Tabellen," Springer, Berlin (1923-1936).
17. M. Volmer and J. Estermann, *Z. Physik*, **7**, 13 (1921).

Electrolytic Production of Boron

George T. Miller

Hooker Chemical Corporation, Niagara Falls, New York

ABSTRACT

Elemental boron was produced by the fused salt electrolysis of potassium fluoborate. A study was made of anode and cathode materials of construction, particularly the effect of various grades of graphite as anode material. The effect of additives to the electrolyte (including potassium, aluminum, calcium, vanadium, nickel, Inconel, water, and sulfate ion) on boron yield and purity was investigated. A method of passivating elemental boron was developed.

Isotopic boron-10 was produced under contract with the U. S. Atomic Energy Commission by the Hooker Chemical Corporation, using Commission-owned facilities at Model City, New York. The plant was divided into two phases: isotope enrichment and elemental boron production.

The product of the isotope enrichment phase of the plant was a boron trifluoride-dimethyl ether complex. The designed capacity was 40 kg per month of boron-10. Because crystalline elemental boron was required and the isotopically enriched boron in the complex involved considerable cost of manufacture (over $500/lb), an efficient means of reducing the complex to the elemental form was sought. Fused salt electrolysis was investigated and ultimately employed for this purpose.

During the research and development stage and through the process improvement stage, a number of conclusions were reached and also a number of perplexing questions manifested themselves. This paper reviews some of the conclusions and manifested questions believed to be significant.

Basically, the process investigated was the fused salt electrolysis of potassium fluoborate and potassium chloride (1). Based on electrolyte analyses which disclosed the rate of KF production to be approximately 7-8 times that of boron production on a weight basis and on effluent gas analysis which disclosed an F_2 to Cl_2 weight ratio of approximately 3 to 1, the over-all reaction may be expressed by the following equation.

$$4KBF_4 + 2KCl \rightarrow 4B + 6KF + 5F_2 + Cl_2$$

The electrode processes have not been resolved.

The following factors affected cell design. Elemental fluorine and chlorine are produced at ap-

proximately 800°C. The proportion of potassium fluoride in the melt increases during electrolysis. The boron product is removed in solid form because of its high melting point.

General Description (2, 3)

The cell, as finally designed, consisted of a 23 cm ID x 58 cm deep graphite anode crucible protected on the outside by Inconel or nickel. The crucible was heated by a circumferential electrical resistance heater. A Monel cathode was suspended in the potassium chloride, potassium fluoride, potassium fluoborate melt. A reducing atmosphere was maintained above the melt level to avoid corrosion of the cathode. A current of 550 amp, equivalent to approximately 80 amp/dm^2, was used. To provide for periodic cleaning, the whole cell and furnace was mounted on trunnions to permit turning the cell to a horizontal position.

Normal operation of the process involved the addition of 2.5 kg potassium fluoborate to the molten (750°-800°C) electrolyte of 11.5 kg potassium chloride and potassium fluoride. After placement of the cathode, electrolysis at 550 amp and 5-6 v was effected for 3½ hr. The cathode with adherent product was raised above the electrolyte level and precooled to approximately 400°C by an internal flow of air. The cathode was then removed from the cell and quenched in water to effect rapid removal of the product from the cathode. Product was purified by water and acid leaching of the material after crushing operations. Final drying and packaging consummated the operation.

Materials of Construction (2, 4)

Since the purity of the boron would be dependent to a large extent on the materials of construction, this was selected as the subject of initial research work.

Cathode material was selected from a list of nonferrous metals which did not form borides readily. Further, the material had to retain strength at 900°C. Selection narrowed down to copper. To minimize failure due to grain growth, the cathode was cooled internally with nitrogen or carbon dioxide to control its temperature at about 600°-700°C. The copper cathode was satisfactory except for an erratic life of from about 4 to 12 runs, after which it became porous. Subsequently it was found that a Monel cathode developed a protective coating of a very hard and adherent boride. The Monel cathodes did not require cooling and their life was increased to more than 20 runs. Monel was considered a satisfactory material of construction for the cathode.

Since chlorine and fluorine were liberated at about 800°C, graphite was the only suitable material for the anode. The anode material problem soon reduced itself to the selection of the most suitable grade of graphite (Table I).

Note that fine graphite grain size materially improved the quality of boron product as did decreased porosity of the graphite. The comparatively coarse and porous arc furnace electrode graphite spalled badly, rapidly contaminating the electrolyte. For the same grade, graphite yielded a slightly purer product than carbon in addition to the advantages of better electrical conductivity. The ash content of the graphite affected the purity of the boron product adversely. However, the effect due to ash content was secondary to the effect of density and grain size.

Table I. Effect of anode material

Anode material	Ash in %	Apparent density, g/cc	Average % boron in product
Furnace electrode grade graphite	1.9	1.64	69
Extruded high-purity graphite	0.01	1.65	89
Extruded high-density and purity carbon	0.1	1.70	91
Extruded high-density and purity carbon	0.04	1.72	94
Resin impregnated graphite	1.4	1.85	94
Molded — very fine grained graphite	0.1	1.71	97

The highest density, finest grained material obtainable at the time this research was in progress was National Carbon's ATJ grade of graphite. This material yielded the highest purity product of all anode materials tested. However, this graphite was both expensive and not always in stock. When these factors exerted sufficient weight, a compromise was sought. High-purity stock graphite, such as National's AUC or Great Lakes' HPL-9, was machined to shape and then made essentially impervious by the Graph-I-Tite[1] process. This treatment deposits graphite in the voids. The resultant product is most dense near the surface and progressively less dense toward the center. Initial use of the crucible was approximately comparable to National's ATJ grade, but continued operation was not as satisfactory. This was due to corrosion of the surface of the graphite, thus exposing progressively less dense material. The Graph-I-Tite treated material was better than untreated graphite but not as satisfactory as the high density, fine grained graphite, the choice thus becoming one of economics and availability.

Because external electrical heating was employed, a shell was used to protect the Nichrome wire from corrosive salts passing through the anode wall. Initially this shell was made of nickel, which promptly developed cracks. However, after Virgo[2] treatment (fused salt descaling treatment), nickel did not develop cracks and was most satisfactory. Here again the laws of supply and demand were felt and Inconel was substituted. This resulted in contamination of the boron with products of corrosion of the Inconel shell. Most of these contaminations, especially chromium, could be removed by acid leaching. Although more attention had to be paid to the boron purification steps when using Inconel, availability dictated its use. While conducting corrosion tests in molten electrolyte without an applied potential, it was noted that nickel, Inconel, and Hastalloy-B corroded ap-

[1] Graphite Specialties, Niagara Falls, N. Y.

[2] Registered trade name, Hooker Chemical Corp.

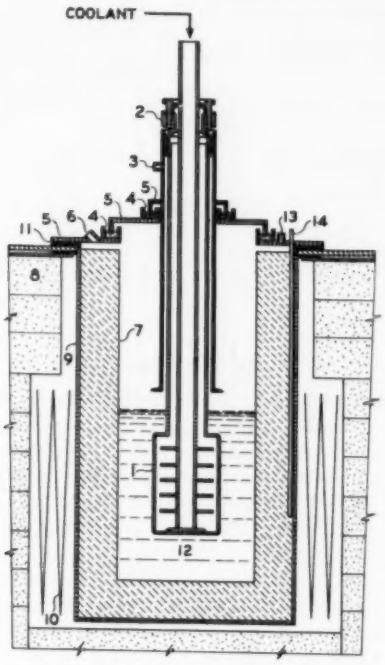

Fig. 1. Electrolytic cell for the production of boron: 1, cathode; 2, quickseal coupling; 3, gas inlet (H_2); 4, salt seal (KCl); 5, cover section; 6, gas outlet; 7, graphite anode; 8, insulating brick; 9, anode shell; 10, heating element; 11, insulating gaskets; 12, cell electrolyte; 13, purge fitting; 14, thermocouple.

preciably only at the liquid-air interface. Under comparable conditions, it was noted that nickel weld rod, ASTM code E3N11, was attacked only slightly.

Cell Design Considerations (2, 3, 4)

Initial laboratory work utilized a hydrogen atmosphere in the cell to minimize oxidation of the graphite. When an inert gas, such as helium, was tried, the copper cathode was rapidly and severely attacked at the electrolyte surface. It soon became evident that chlorine and fluorine liberated in the cell at about 800°C attacked copper vigorously, but HCl and HF did not. The final cathode design is shown in Fig. 1.

Provision was made in this design to concentrate the hydrogen flow at the cathode-electrolyte interface. This proved very effective and permitted satisfactory operation at about 1/3 prior hydrogen flow rates when a nondirected hydrogen flow was used. The cover was sealed by a powdered salt seal ring. This proved an effective and simple technique for control of the cell atmosphere as well as assuring that vent gases would be directed toward the exhaust system. The lack of bolts assured against damage in case of hydrogen failure and a resultant explosion due to air entering the cell. The balance of the structure provided for positioning the cathode above the melt or in the melt, internal cooling, and d-c circuitry. The most desirable temperature control point was found to be in the annular space between the graphite anode and its protective shell.

Table II. Recommended operating details for the electrolytic production of boron

Electrolyte:	70% KCl, 12% KF, 17.8% KBF_4, 0.2% H_2O
Temperature:	750°-800°C
Current:	80 amp/dm²
Voltage:	5-6 v
Power:	55 kwhr/kg
Ampere efficiency:	74%
Cell atmosphere:	H_2 purge directed at electrolyte surface near cathode. Rate: 20 liters/min at 550 amp
Cathode:	Monel
Anode:	High-density, fine grained graphite

Operation (2, 4)

Composition of the electrolyte had a significant effect on yield and/or purity of the boron product (Table II). The first run using a new charge of KCl invariably resulted in poor yield and purity of boron. If the KCl-KF weight ratio was permitted to decrease below approximately 2.5-1, the boron yield decreased. The KCl-KF weight ratio therefore was maintained between 3-1 and 6-1 by partial removal of the electrolyte after a run and replenishing it with KCl.

Purity of the elemental boron was impaired severely when commercial grade KCl was substituted for C.P. grade KCl. A knowledge of the constituent of commercial grade KCl responsible for degrading the boron product was considered desirable in order to effect improvement in purity of normal production. The seemingly obvious approach of determining the foreign material in the product did not yield a solution. Apparently the responsible material entered into side reactions which contaminated the boron product with carbon primarily.

A major difference between technical and C.P. grade KCl is a tenfold difference in the sulfate ion. To ascertain if high sulfate would affect boron purity adversely, 1% of K_2SO_4 in KBF_4 was used. As shown in Table III, it had no apparent adverse effect on the yield or purity of the boron product. The opportunity to explore the effects of bromine was not realized, although the effects of other possible contaminants were investigated.

This work was conducted in three different cells having different grades of graphite. The effect of an additive is thus evidenced by comparing per cent yield and per cent B with product obtained from the same cell without an additive.

Calcium chloride affected the adherence of the product to the electrode causing the deposit to fall out. The purity appeared unaffected. The effect of calcium could be a valuable asset in the design of a continuous cell. Addition of vanadyl sulfate to the electrolyte resulted in decreased purity, apparent decreased yield, and erratic adherence of the product to the cathode.

Aluminum fluoride monohydrate was added in one series of tests and found to yield a dense product of normal yield and purity. Elemental aluminum addition resulted in a slightly higher purity and yield of a very dense product.

The results of drying salts before addition to the melt had given inconclusive results which seemed

Table III. Effect of electrolyte additives

Additive	Concentration in electrolyte		Average % B	Average % yield	Comparison without additive		Cell No.
	g	% by wt			% boron	% yield	
K_2SO_4	25	0.18	95.0	81.5	94.7	75.5	1
$CaCl_2$	100	0.72	93.0	Fell off cathode	92.8	87.8	2
Vanadyl sulfate	66.2	0.47	89.0	48.0	94.7	75.5	1
$AlF_3 \cdot H_2O$	56	0.40	94.7	86.8	95.0	87.0	3
Aluminum	14	0.10	95.5	83.5	94.7	75.5	1
Water	25	0.18	95.8	88.0	94.7	75.5	1
Nickel	38.8	0.28	90.9	73.3	94.7	75.5	1
Inconel	39.2	0.28	88.7	59.2	94.7	75.5	1

to indicate improved yield and purity in the absence of water. It was, therefore, a most surprising result when the addition of 1% water to the KBF, before charging resulted in a high density end product of improved yield and purity. This was probably due to a build-up of potassium oxide in the cell which reduced a tendency toward anode effect, a phenomenon otherwise experienced in the cell at approximately 600 amp. This effect of water addition was experienced by Kroll in his work on titanium (5).

Noncathodic nickel or Inconel was severely attacked during electrolysis resulting in decreased cell performance. It clearly confirmed the adverse cell operation that resulted when the graphite anode crucible was porous, cracked, or corroded through.

The first electrolytic run made on a new charge of KCl and KBF, resulted in a lower yield and purity of product than the second run. By using a partial charge of KBF, and considering the first run as a pre-electrolysis, the yield and purity of subsequent runs could be maintained at acceptable levels. Approximately 30 to 40 runs would be made before total discharge and recharge. The addition of a small quantity of elemental potassium to the pre-electrolysis electrolyte resulted in normal yields and purity of product. Such additions had no discernible effect on subsequent runs. The effect of pre-electrolysis and elemental potassium addition was probably to establish the oxide content referred to under water addition.

Table IV. Effect of drying conditions on purity of boron

Drying conditions	Batch No.	% Boron in dried product: With air purge	With oxygen purge	With argon purge
110°C, 24 hr, no agitation, atmospheric pressure	240	97.0		96.3
	251	97.7		96.8
	213	96.4		94.8
110°C, 1½ hr, agitated, 18 in. vacuum	213	96.4		95.5
100°C, 2.5 hr, agitated, 29 in. vacuum broke vacuum @ 100°C	293	95.3	96.9	
100°C, 2.5 hr, agitated 29 in. vacuum broke vacuum @ 35°C	293	96.2	97.0	
100°C, 24 hr, no agitation, 29 in. vacuum	S-19	94.1	94.4	
100°C, 24 hr, no agitation, atmospheric pressure	S-19	94.0	94.3	

Processing of Cell Product (6)

The product from the electrolytic cell was essentially an agglomerate of boron crystals and electrolyte. To free the boron of soluble impurities, the product was crushed in a rod mill to pass 100 mesh, leached with boiling water and finally boiling HCl. After due washing, rinsing with alcohol, and oven-drying, the product was packaged in polyethylene bags. It was found, when checking analyses for shipping, that the total boron analysis decreased 2-3% after several months' storage. This was traced to boron acting as a getter, adsorbing gases from the air. By drying boron at 100°C in a vacuum oven with an oxygen purge and preferably with agitation for the minimum time needed to effect drying, the boron was passivated. The resultant purity was higher than when dried in an inert atmosphere purged oven (Table IV).

Boron oxide wets elemental boron very well. The observed result of higher boron analysis when using an air or oxygen atmosphere is therefore attributed to a very thin protective film of boron oxide formed on the surface of the boron.

The final product had a size specification of 100% through 100 mesh and 90% through 200 mesh. Approximately 20% passed through 325 mesh and a trace was colloidal. X-ray diffraction demonstrated that the product was mostly crystalline with some scattering due to amorphous material or very fine particle size. When the less than 325 mesh fraction was removed, the remaining material was crystalline.

The purity of the final product was 94-96% boron. Principle impurities were carbon, nickel, chromium, silicon, magnesium, potassium, water, oxygen, and copper.

Acknowledgment

The author wishes to express his appreciation to the U.S. Atomic Energy Commission for permission to deliver this paper, the work discussed having been carried out under USAEC Contract No. AT-(30-1)-1524.

Manuscript received March 23, 1959. This paper was prepared for delivery before the Philadelphia Meeting, May 3-7, 1959.

Any discussion of this paper will appear in a Discussion Section to be published in the June 1960 JOURNAL.

REFERENCES

1. H. S. Cooper (To Walter M. Weil), U.S. Pat. 2,572,-248, Oct. 23, 1951.

2. G. T. Miller, U.S.A.E.C. Report NYO-1265, May 31, 1956.
3. G. T. Miller, U.S.A.E.C. Report HEC-79, April 22, 1957.
4. G. T. Miller, U.S.A.E.C. Report HEC-89, May 7, 1958.
5. W. J. Kroll, *This Journal*, **106**, 8C (1959).
6. G. T. Miller, U.S.A.E.C. Report HEC-88, April 18, 1958

Overvoltage and Catalysis

Paul Rüetschi

Research Center, The Electric Storage Battery Company, Yardley, Pennsylvania

ABSTRACT

Analogies between heterogeneous catalysis on solid-gas interfaces and electrochemical kinetics on solid-liquid interfaces are discussed. The surface potential of a solid-gas interface corresponds to the Galvani potential difference of a solid-liquid interface. These potentials depend to a first approximation linearly on the number of adsorbed potential-determining particles. A corresponding linear variation adsorption energy is explained on the basis of electrostatic or induced interaction between adsorbed particles. This behavior is coherent with a logarithmic dependence of the number of adsorbed particles on the bulk concentration or pressure in the liquid or gaseous phase (Temkin isotherm) and a linear dependence of the activation energy of adsorption on the number of adsorbed particles (Becker-Zeldovich equation). It is shown that the Temkin isotherm corresponds to Nernst's formula for electrode potentials and the Becker-Zeldovich equation to Volmer's equation for the rate of electrochemical reactions, and that these equations follow immediately from the theory of charge-transfer adsorption or electrostatic interaction between (activated) potential-determining species or complexes. This treatment leads to a new interpretation of the charge-transfer coefficient and of the influence of the electronic properties of the electrode material and of specifically adsorbed foreign species on hydrogen overvoltage, oxygen overvoltage, and metal deposition overvoltage.

The kinetics and thermodynamics of electrochemical phenomena at solid-liquid interfaces and of catalytic phenomena at solid-gas interfaces are closely related. It is the object of this paper to point out correspondences between the two fields and to derive the fundamental laws of electrochemical thermodynamics and kinetics, in particular the Nernst equation and the Volmer-Tafel equation, from these considerations.

Adsorption and Interaction

The relation between the number of adsorbed species on a solid-gas or solid-liquid interface and bulk concentration (or pressure) of the adsorbable species is described by isotherms. The Langmuir isotherm is derived on the assumption that adsorption occurs at fixed sites and that the energy of adsorption is independent of the number of particles adsorbed. Fixed site adsorption is, however, unlikely for many reactions proceeding on electrodes and catalysts. The energy of adsorption usually decreases with increasing number of adsorbed particles. The Freundlich isotherm is therefore more likely to be obeyed since it allows for the latter effect. However, very few experimental results suggest a logarithmic decrease of the energy of adsorption with increasing number of adsorbed species, as derived from the Freundlich isotherm. Very often the energy of adsorption decreases nearly linearly with the number of adsorbed particles. Such a behavior is accounted for by the Temkin isotherm. The latter can be derived for intermediate ranges of coverage from a fixed site Langmuir-type isotherm by allowing for a linear variation in adsorption energy (1) and, more generally, for mobile adsorption as follows.

Using Boltzmann statistics, the concentration n_i^* (number of particles per cm^2) of species i in the adsorption zone is given by

$$n_i^* = n_i \exp\left[-(w_i^* - w_i)/kT\right] \qquad [1]$$

where n_i is the corresponding concentration in the bulk, and w_i^* and w_i are the energies of a particle i in the adsorption zone and in the bulk, respectively. Here, we assume the entropies of the (mobile) particle in the adsorption zone to be not much different from the entropy of the particle in the bulk. It is now important to consider that, because of the nonideal behavior of the adsorbed particles, n_i^* and w_i^* are connected by an activity function. For such a function of exponential character (activity coefficient varying exponentially with the concentration n_i^* in the adsorption zone), w_i^* becomes a linear function of n_i^* (2) and, neglecting the variation of the term linear in n_i^* compared with the variation of the term exponential in n_i^*, one obtains from [1]

$$n_i^* \cong a \ln n_i - b \qquad [2]$$

where a and b are constants. Equation [2] is the Temkin isotherm.

A linear decrease of adsorption energy with increasing number of adsorbed particles is widely observed. On the other hand, the surface potential solid-gas of the Galvani potential difference elec-

trode-electrolyte depend approximately linearly on the number of adsorbed particles n_i^*. Boudart (3) and Mignolet (4) have discussed the relation between change in surface potential and change in energy of adsorption for solid-gas interfaces. The adsorption energy was expressed in terms of a charge-transfer process, involving the excitation of an electron of the conduction band into a vacant surface orbital provided by the adsorbed species and the surface. The energy difference $w_i^* - w_i$ becomes then a linear function of the surface potential or the Galvani-potential difference

$$\Delta(w_i^* - w_i) = \alpha z_i e_o \Delta(\phi_i - \phi_{ii}) \qquad [3]$$

where $\Delta(\phi_i - \phi_{ii})$ is the change in surface potential or in Galvani potential difference, $z_i e_o$ the charge of the adsorbed particle i, and α the so-called "structural factor" (5). The latter is a characteristic fraction of the total Galvani potential difference. Experimentally, Boudart finds for adsorption of hydrogen on metals $\alpha \sim \frac{1}{2}$.

It will be shown now that the value of α can be derived from classical electrostatic considerations in a surprisingly simple manner. One can apply the model of a flat-plate electric condenser. For electrochemical interfaces, this model is particularly useful and the capacity of the electric double layer can be determined experimentally. The electrostatic energy content of a charged electric condenser is given by

$$U = \int_o^q V dq = \int_o^v CV dV = \frac{1}{2} CV^2 = \frac{1}{2} qV \qquad [4]$$

where V is the voltage, q the charge, and C the capacity. The energy content per particle with a charge $Z_i e_o$ varies then with the voltage as follows

$$\Delta(V z_i e_o/q) = \frac{1}{2} z_i e_o \Delta V \qquad [5]$$

This equation is identical to [3] since, by correspondence, $\Delta(V z_i e_o/q) = \Delta(w_i^* - w_i)$, and $\Delta V = \Delta(\phi_i - \phi_{ii})$. This means that α must be equal one-half as long as the adsorption capacity C, due to species i, is independent of voltage or charge. For a variable capacity, Eq. [4] must be integrated, taking into account this dependence which would lead to values of α different from one-half.

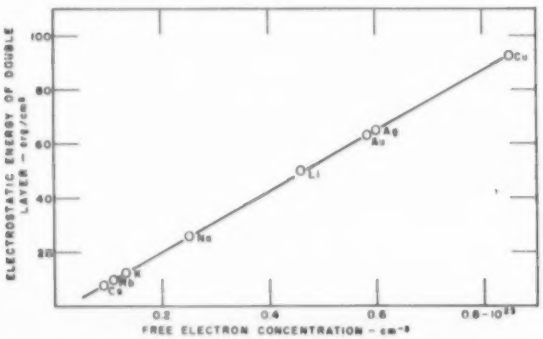

Fig. 1. Electrostatic energy of the double layer on a metal surface against vacuum as a function of free electron concentration.

The interpretation of adsorption on the basis of charge transfer has gained wide acceptance in modern work on catalysis (6, 7). The concepts have been substantiated not only by measurements of changes in work function and contact potential but also by changes in electric resistance (8) and by changes in magnetic behavior (9) of thin solid films during the adsorption process. The surface potential or the Galvani potential difference depends generally on the competitive adsorption of a variety of different species 1, 2, 3—. However, adsorption is generally specific enough to one particular species i such that, at least over limited regions, the variations in adsorption of other species can be neglected. In considering adsorption of the species i on a surface modified by the presence of other species 1, 2, 3— i, the surface potential or the Galvani potential difference, as modified by the presence of these other species, determines according to [3] the adsorption energy of i.

For a bare metal surface against vacuum the electron concentration in the metal is the main parameter characterizing the surface potential barrier. The relation between surface potential and electron concentration becomes evident from Fig. 1. Here, the electrostatic energy of the double layer on a surface against vacuum is plotted against electron concentration.[1] The surface potential (dipole term) is only a relatively small fraction of the total work function (10). Therefore, the work function plays a direct part in the determination of surface potentials and Galvani potential differences only insofar as the dipole term is concerned. However, the dipole term is often a more or less fixed fraction of the total work function.

It has been shown (11) that the energy of cohesion of metals is related to the electron concentration. For alkali metals the energy of sublimation is proportional to $\rho^{2/3}$ where ρ is the free electron concentration. The surface energy is also a function of the electron concentration. According to Breger and Zhukhovitskii (12) the surface energy can be calculated by

$$\sigma = (3\rho/\pi)^{4/3} (\pi h^2/128m) \qquad [6]$$

where h is Planck's constant and m the electronic mass. A recent review on atomic theories of surface energy has been given by Ewald and Juretschke (13). It is known that particularly for solids of the same crystallographic type the surface energy is a fixed fraction of the cohesion energy or heat of sublimation. Since surface potential, cohesion energy, and surface energy are functions of the electron concentration, relations to other quantities depending on electron concentration, e. g., lattice constants, compressibilities, electronic work function (14), are to be expected. For alkali metals one finds, e.g.,

$$L \cong \frac{3}{5} \phi \qquad [7]$$

where L is the sublimation energy and ϕ is the work function (11).

Adsorption energies at zero coverage, calculated on the basis of a charge transfer model, are equally

[1] Data obtained from R. Stratton, *Phil. Mag.*, **44**, 1236 (1957).

related to the electronic properties of the metal. For an ionic bond (and electron transfer from the adsorbed particle to the surface) one has used

$$-(w_i^* - w_i) = \phi - I + e_o^2/4K_o r \qquad [8]$$

where I is the ionization energy, r the image force distance (15), and K_o is the Coulomb's Law constant $= 4\pi e_o$ where e_o is 8.854 x 10^{-12} amp sec volt^{-1} m^{-1}. For formation of a negative ion the signs of ϕ and I reverse. Electronic work function and image force distance depend on electron concentration. Adsorption has also been interpreted successfully strictly on the basis of image forces for electrons and protons of adsorbed species for apparent covalent surface bonds (16). The parameter determining the energy of adsorption is then the distance r between the adsorbed particle and the surface mirror plane. For hydrogen atoms on metals, the following equation has been derived

$$-(w_i^* - w_i) = e_o^2/4K_o r)\,(1 + qa_o^2/2r^2) \qquad [9]$$

where a_o is the Bohr radius. The distance r will vary with lattice parameter and electron concentration. For covalent bonds the Pauling formula has been used

$$-(w_i^* - w_i) = \frac{1}{2}D(M-M) + \frac{1}{2}D(A-A) + 23.06(X_M - X_A)^2 \qquad [10]$$

to calculate adsorption energies (17) at zero coverage. Instead of conventional (chemical) electronegativities, the bond moments of the adsorption bonds must be used. The bond moments depend on electron concentration and work function. Stevenson (18) has suggested that $X_M = 0.355\phi$ could be used in Eq. [10], whereas, according to Gordy and Thomas (19), the true (chemical) Pauling electronegativities are related to the work function as follows: $X_M = 0.44\phi - 0.15$. Heats of adsorption can be calculated for any type of bonding from the charge-transfer complex theory as developed by Mulliken (19-21).

As pointed out, Eqs. [8], [9], and [10] refer to the energy of adsorption at zero coverage. The variation of adsorption energy with coverage is due to interaction between adsorbed particles and can, in many cases, be described by Eqs. [3] and [5].

Rate equations describing the kinetics of heterogeneous reactions have hitherto been formulated often without taking into account the activity of intermediate species or activated complexes. However, Horiuti has pointed out that this is incorrect (2). It has been shown above how electrostatic interaction leads to a linear variation of adsorption energy with coverage.

If adsorption energies vary linearly with the number of adsorbed particles, a similar behavior might be expected for activation energies of adsorption (22). Activated complexes formed at interfaces must in fact be considered as adsorbed species. Hereby it is basically immaterial whether the energy level of the species in the adsorbed "activated" state is higher or lower than in the bulk (23). Activation energies of adsorption are (negative) adsorption energies of the activated complex. The activation energy changes then according to [3] linearly with the number of adsorbed "activated" complexes. Therefore the rate of adsorption depends exponentially on the number of adsorbed particles. Such a behavior is indeed widely observed and has been described by Becker (24) and Zeldovich (25) in the form

$$d\theta/dt = a(1-\theta)\exp(-b\theta) \qquad [11]$$

The variation introduced by the factor $1-\theta$ is to be neglected in comparison with the variation introduced by the exponential term. For mobile adsorption $1-\theta$ loses much of its meaning anyway.

We shall now derive the Volmer-Tafel equation for electrochemical reactions from the theory outlined above. The energy difference between a point at the critical distance X^* from the electrode interface, in the region of the activated complex where the electron transfer takes place, is composed of a constant "chemical" term and a variable electric term, respectively. According to [3] and [5] $w_i^* - w_i$ is a linear function of the Galvani potential difference

$$w_i^* - w_i = \alpha Z_i e_o \Delta(\phi_I - \phi_{II}) + \epsilon^* - \epsilon \qquad [12]$$

where $\epsilon^* - \epsilon$ is the "chemical part" of the activation or adsorption energy. The $\Delta(\phi_I - \phi_{II})$ must be measured with reference to the Galvani potential difference $(\phi_I - \phi_{II})_o$, corresponding to the point where n_i^* becomes zero. At this point the charge of the double layer is due to the foreign inert species only. The current of the electrochemical reaction is simply proportional to the number of activated complexes n_i^*, and using [1] and [12] one obtains

$$i = \nu Z_i e_o n_i^* \delta = \nu Z_i e_o \delta n_i \exp[-\alpha Z_i e_o(\phi_I - \phi_{II})/kT] \cdot \exp\{[\alpha Z_i e_o(\phi_I - \phi_{II})_o - (\epsilon^* - \epsilon)]/kT\} \qquad [13]$$

where ν is a frequency factor and δ the thickness of the reaction zone. The exponential dependence of current on voltage described by [18] is the Volmer equation. Over the regions where the charge of the electrode double layer varies predominantly due to accumulation of reacting species and where $(\phi_I - \phi_{II})_o$ remains constant, $(\phi_I - \phi_{II})$ is a linear function of the charge of the double layer condenser due to n_i^*. This illustrates the analogy between the Becker-Zelovich equation [11] and the Volmer equation [13]. Both rate expressions contain a term exponentially dependent on the number of adsorbed particles n_i^*.

The "transfer coefficient" or "structural factor" α can be determined experimentally from the slope of a Tafel-plot. The model from which α has been derived here is different from the one of Volmer (26), who considered the transport of a charge halfway through an electric field without taking into account the interaction with, or energy increase of the other charges of the double layer condenser. The present derivation of the current-voltage relation is more satisfactory.

In order to define an electrochemical equilibrium, at least two (independent) electrode reactions must proceed at an electrode. The two reactions are to produce electrochemical currents in opposite direction at equal rates. If the final products of one reac-

tion are not identical with the initial reactants of the other reaction, a "mixed electrode potential" is established (27). A true equilibrium is observed when the products of the forward reaction are equal to the reactants of the backward reaction. If for the product 1 and the reactant 2 a rate equation of type [13] is valid, one derives for equilibrium ($i_1 = -i_2$) the Nernst equation. Since ($\phi_I - \phi_{II}$) is a linear function of n_i^*, the Nernst equation has the form of the Temkin isotherm [2].

The general rate equations for heterogeneous reactions contain the Galvani potential difference $\phi_I - \phi_{II}$. It is pointed out here that they can also be formulated in a similar manner using the experimentally measurable Volta potential differences. Galvani potential differences and surface potentials of condensed phases against vacuum are not measurable but could be calculated in principle on the basis of a sufficiently detailed knowledge of the configuration of the nuclei and electrons in the interior and surfaces of the phases (28, 29). The surface potentials are obtained semi-empirically by comparing the chemical potential μ_i of a charged species i in the bulk of the phase with the experimentally measurable real potential (negative work function) of this species. The surface dipole term is usually a small fraction of the total negative work function and is not appreciably altered by electrostatic surface-charge (10). The surface potential of a condensed phase against vacuum or a gas phase and the Galvani potential difference for this interface have the same physical meaning since a gas phase or vacuum has a zero surface potential. The experimentally measurable Volta potential differences are the result of electrostatic excess charges. They can be induced by changes in surface potentials (30-33).

It has sometimes been assumed that the electrochemical interface is composed of several different double layers. However, it seems that electrostatic interaction (or overlap) is so strong that it is better to consider only one over-all dipole barrier. Also, the Galvani potential difference has been split into a dipole term and an ionic term. However, it is difficult to differentiate these two terms since dipoles can be treated as two separate charges. Furthermore the dipole term should be dependent on the ionic term since dipole adsorption and polarization change with field strength. It is preferred here not to make this differentiation.

Potentials of Zero Charge

Potentials of "zero charge," corresponding to a state of maximum interfacial energy and/or a minimum in electrode double layer capacity (37) are of importance for the interpretation of the term $(\phi_I - \phi_{II})_s$ in the rate equation. The electrode potential at which the charge on the electrode is virtually zero has been determined experimentally for conditions where electron transfer can take place more or less completely (ideal reversible electrode) or is practically impossible (ideal polarized electrode). There is conclusive experimental data that the potential of zero charge is different for the two cases (38).

The electrode potential of ideal polarized electrodes is determined by the externally applied voltage like the tension of a metal-dielectric type condenser. Differences in zero-charge potentials of various electrode metals are to a large extent accounted for by differences in work functions (39, 40) and depend therefore on the particular crystalline face exposed (41). A strict linearity between zero charge potentials and work functions could be expected if adsorption of species at the interface would be purely "electrostatic" in nature (42, 43).

The electrode potential of ideal reversible electrodes is determined thermodynamically by the bulk concentrations of potential-determining species. At the potential of zero charge the concentrations are adjusted such that adsorption of negative and positive ions is balanced to produce a maximum interfacial energy. Some experimental evidence has been accumulated (38, 40) showing that potentials of zero charge of ideal reversible electrodes tend to be independent of the electrode material. This would mean that the electrochemical interface behaves analog to a contact metal-metal. For redox potentials where the emf is (theoretically) independent of the nature of the inert electrode, the state of zero charge would be maintained when the inert electrode is exchanged for some other metal. For a metal electrode in a solution of its own ions, a different ion concentration must be provided for each metal to produce the state of zero charge.

Although the difference in zero charge potentials between polarized and reversible electrodes is due to different adsorption characteristics between "specifically adsorbed" and "inert" species, the physical nature of the state of zero charge is the same in both instances, namely, a state of maximum surface energy. Differences in zero charge potentials are related to differences in the closest approach of the various species to the electrode surface. Potential determining or "specifically adsorbed" ions generally can approach the electrode more closely than "inert" ions. The influence of the nature of the species in the electrolyte and their adsorbability is particularly well demonstrated by the *p*H-dependence of zero-charge potentials (44). Electrodes which adsorb hydrogen and establish reversible hydrogen potentials show a variation of zero charge potentials with pH. This shows that potential-determining ions are specifically adsorbed.

It should be pointed out that, in analogy to metal-gas interfaces, some sort of strong adsorption forces must always be expected on electrode surfaces. An independence of zero charge potentials of the electrolyte often simply means that the species of the solvent (H^+ ions or OH^- ions or water dipoles) are adsorbed rather than the solute. There is no clear-cut distinction between the two types of zero charge electrodes. The differentiation is in fact one of degree. The process of strong adsorption generally can be considered as an electrode reaction, forming a surface product. The particles taking part in this reaction must be considered as specifically adsorbed, and the electrode potential varies then approximately logarithmically (according to a Temkin isotherm)

with the bulk concentration of these particles (45, 46).

Application to Problems in Electrode Kinetics

In recent discussions on the mechanism of hydrogen evolution a distinction has been made (47-52) between the so-called Volmer-Tafel (discharge-recombination) mechanism

$$2H^+(aq) + 2e^- \rightarrow 2H(ads)$$

$$H(ads) + H(ads) \rightarrow H_2$$

and the so-called Volmer-Horiuti (ion-atom reaction)

$$H^+(aq) + e^- \rightarrow H(ads)$$

$$H(ads) + H^+(aq) + e^- \rightarrow H_2$$

Without specifying the actual configuration and energetic state of the particular activated complex involved and experimental evidence thereof, these formulations are of little help. Any number of other theoretical reaction routes, like for instance (53)

$$2H^+(aq) + 2H(ads) + 2e^- \rightarrow 2H_2$$

$$H_2 \rightarrow 2H(ads)$$

(which does not require the Volmer discharge step) can be postulated. On the basis of the model developed earlier in this paper the differentiation is unnecessary. The electric double layer contains, on the solution side of the interface, protons in various energetic states corresponding to various stages of discharge, which means that their positive charge is shielded to various degrees by overlapping electrons and by negative ions. These adsorbed protons are mobile, like most species in electrochemical double layers. The adsorption follows a Temkin-isotherm and the adsorption (or activation) energy will vary linearly with the number of adsorbed protons. For an approaching proton the surface then looks energetically uniform, and each proton has statistically the same chance to follow the easiest reaction path, which is simply a charging of the double layer condenser. Because of electrostatic interaction there will be no "bare" spots on the surface. The introduction of the degree of coverage θ or the fraction of free surface $1-\theta$ as a concentration term in the rate equation does not have much meaning. According to the outlined model there is no saturation coverage and the Galvani potential difference keeps increasing more or less linearly (as long as the adsorption capacity is constant) with the number of adsorbed potential-determining ions. This is the reason why the linear relation between logarithm of current and potential prevails to very high rates and why generally no limiting value is reached (54). The metal electrons of the surface are able to be transferred to particles on the solution side over relatively large distances, e.g., during electrochemical reduction of azobenzene on a smooth liquid mercury electrode (55), due to the high electric field at the interface. Recombination of "discharged" protons can occur at various distances as far from the interface as the electron waves can reach (56, 57). The critical distance X^* from the interface where electron transfer takes place may be smaller statistically on one metal than on another. The discharge probability is simply proportional to the number of protons in the double layer.

At this point mention should be made of the stoichiometric numbers ν_i, introduced by Horiuti (58, 59) and commonly defined as number of times the postulated rate-determining step is repeated when the over-all reaction, as represented by the stoichiometric equation, occurs once. In the formulation of Parsons (60) the over-all process requires the formation and decomposition of ν_i activated complexes. Makrides showed from considerations of reaction rates at states close to equilibrium that stoichiometric numbers can take any positive value and are usually equal to the ratio of two small integers (61). If, on the basis of the outlined theory, the activated complex for the hydrogen evolution reaction is assumed to consist of one excited proton only and an electron in the metal, the concentration of activated complexes is immediately given by [1] and [12] and the current-voltage relation by [13]. If the activated complex is considered to consist of two excited protons and two electrons in the metal, one obtains formally the same result since the protons must share the activation energy in equal parts, which can be described alternatively by electrostatic interaction or by the existence of strong resonance between the protons, or by the formation of hydrogen molecule ions. In this manner stoichiometric numbers do not enter the considerations, which is fortunate as can be seen from the recent controversy betwen Horiuti and Bockris (62, 63). From this point of view, the present theory is able to unify various overvoltage theories advanced previously, based on hypothetical existence of atomic hydrogen (64, 65), protons (26), and hydrogen molecule ions (66). The fact that deposition of atomic hydrogen into palladium metal lattice requires a considerable overvoltage would at first suggest that the activated complex consists of single protons rather than molecules. However, on the basis of the present theory strong interaction between adsorbed protons must be present, and with the condenser model all the particles in the interface must actually be included in the activated complex. The interaction between adsorbed particles in the double layer gives also an explanation of the experimentally observed separation factors (67).

It has been shown above that the transfer coefficient α assumes preferably the value $\alpha \cong \frac{1}{2}$. Careful experimental work by Schuldiner (68) on noble metals and noble metal alloys yielded values of α larger than one, or Tafel slopes smaller than 0.058 v at overvoltages below 100 mv. The apparent slope of 0.029 has been explained by the recombination theory of Tafel; however, this explanation is not satisfactory. One must also consider that noble metals have high exchange currents and the backward reaction is of strong influence at low overvoltages. Knorr and co-workers (69) have recently shown that overvoltages below 100 mv on noble metals are

due mainly to diffusion overvoltage of molecular hydrogen.

Bockris and co-workers have developed what they termed "diagnostic criteria" to determine the "rate-controlling step" in hydrogen evolution (70). In deriving their theoretical Tafel slopes they have used $\alpha \cong \frac{1}{2}$ throughout. However, as shown in Eq. [13] α assumes this value only under the special condition that $(\phi_i - \phi_{II})_o$ is constant. The variation in Galvani potential is then due to accumulation of protons only, and the adsorption capacity a constant. The results of the "diagnostic analysis" do not seem to be unambiguous either since on Ni, e.g., electrochemical desorption (71), slow discharge (47) and electrochemical desorption (50) have been named rate determining. The lattice heterogeneity of the electrode surface is not accounted for in the present theory. There are some indications that this heterogeneity is not of primary importance. This is also brought out by MO calculations for adsorption bonds at zero coverage on linear atomic chain models (72).

Some theories have been advanced about electrochemical reduction of water instead of hydrated protons. Usually, it has not been considered that the dissociation equilibrium of water is established with a rate constant of 10^{-5} sec^{-1} and protons are continually produced by this preceding reaction (55, 73). The field effect at the interface can even enhance this reaction rate.

Temkin and Frumkin (74) have suggested that because of the apparent independence of the preexponential factor A in the equation $i = A \exp(-E/RT)$ from the nature of the metal (75), one should expect approximately equal values of the activation energy E for equal current rates i. Generally one should expect a dependence of the frequency factor on the activation energy (76).

In comparing overvoltages of different metals it is necessary to keep the composiiton of the electrolyte the same. This has been taken into account in the work by Rüetschi and Delahay (77) but has not been considered by others (74). Adsorption of anions decreases overvoltage in the sequence $SO_4^{--} < Cl^- < Br^- < I^-$ (43). According to [13] the terms $\epsilon^* - \epsilon$ and $\alpha z_i e_o (\phi_i - \phi_{II})_o$ determine the influence of the electrode material on overvoltage since n_i^* and $\Delta(\phi_i - \phi_{II})$ are constant for a given current. The first term is a measure for the covalent adsorption energy, which can be calculated with [10], omitting electronegativities. Experimental support for a linear relation between covalent adsorption energy and overvoltage has been found (77).

With respect to this conclusion, the present theory gives the same result as considerations of potential energy surfaces according to Horiuti and Polanyi (78). Rüetschi and Delahay used equation [10] without electronegativities to calculate $\epsilon^* - \epsilon$ which is, according to the above argument, the correct procedure. Energetic terms due to polarity of the M-H bond are taken care of by the Galvani potential difference. Bond moments of M-H bonds are anyway quite small. Using bond moments, the last term in Eq. [10] becomes $23.06\ \mu^2$.

Eyring and co-workers (81) have used the value $\mu = 0.46$ for the M-H bond, derived from contact potential measurements by Bosworth (82) for tungsten. However, Mignolet (83) has shown that Bosworth's value is too high. On the basis of Mignolet's results one obtains $\mu = 0.212$ for the tungsten-hydrogen bond and $\mu = 0.183$ for the nickel-hydrogen bond. The moment for the copper-hydrogen bond is even smaller (84). These values show that the contribution of the last term in [10] must be quite small, in the order of one kilocalorie or so. This is the reason why adsorption energies calculated without considering the dipole term agree surprisingly well with experimental results. According to [13] hydrogen overvoltage should generally decrease linearly with covalent adsorption energies $\epsilon^* - \epsilon$ which is in qualitative agreement with Bonhoeffer's experiments (85). The decrease of overvoltage with adsorption energy has recently been derived in a similar manner by Krishtalik (86). It must however be pointed out that exceptions to this rule might be found, since $\epsilon^* - \epsilon$ can contain other terms, e.g., adsorption energies for water.

Various attempts have been made recently to explain an apparent maximum in the curve of overvoltage vs. adsorption energy (50-52), since it had been observed that metals like Mo, Ta, W, Zr, with very high adsorption energies for hydrogen show relatively high values of hydrogen overvoltage. It should be pointed out here that these metals also have an extremely high adsorption energy for other species than hydrogen, e.g., oxygen (and oxygen in water dipoles), and that the experimental hydrogen overvoltage values necessarily refer to somehow oxidized or hydrated surfaces. It is known that cathodic polarization of these metals does not remove the oxide layers completely, which also is related to the fact that these metals cannot be plated out from aqueous solutions. It is pointed out here that hydrogen overvoltage depends not only on the adsorption energy of hydrogen but also on the adsorption characteristics of foreign, inert species, e.g., anions. The influence of the adsorption of foreign inert species which do not take part in the electrode reaction is expressed in [13] by the term $(\phi_i - \phi_{II})_o$. This term is related to the zero charge potentials and electronic work functions.

Since covalent adsorption energies increase according to [10] with the strength of the metallic bond (cohesion energy or sublimation energy) one deduces from [7] a qualitative relation between adsorption energy and electronic work function. On the basis of these considerations Rüetschi and Delahay have explained for the first time the dependence of overvoltage on work function (87), observed empirically by Bockris (47). From equations [6] to [10] it follows that overvoltage can be related to various other electronic properties of the electrode metal, in particular electron concentration, surface energy (88, 89), interatomic distances (90), compressibility (91), cohesion energy (92), melting point (93), and others.

Bockris and Potter (47) had explained the dependence of overvoltage on work function from the fact that the Galvani potential difference of the contact interface between the metal of the reference electrode and the metal of the electrode under investigation changes with the electronic work function of this metal. These authors, and similarly Lorents (91), have not considered that the Galvani potential difference electrode-electrolyte of the reversible hydrogen electrode also changes, in the opposite direction, with the work function of the electrode metal, which becomes apparent from the fact that the (theoretical) hydrogen electrode potential, as measured against a reference electrode, does not depend on the nature of the electrode metal.

Recently, Conway and Bockris (50) have adopted the use of Eqs. [7] and [10] in explaining the relation between electronic work function, adsorption energy, and overvoltage according to Rüetschi and Delahay. However, Conway and Bockris used polar instead of covalent adsorption energies for $\epsilon^* - \epsilon$. Moreover, they used chemical (Pauling) electronegativities for single atoms as given by Gordy and Thomas (94). The present theory shows that the use of large terms of this sort is incorrect, since $\epsilon^* - \epsilon$ is a covalent, chemical term. Any bond moment terms are taken care of energetically by the Galvani potential difference. The present theory is able to account for the influence of specifically adsorbed foreign species, in particular anions, on overvoltage by the term $(\phi_i - \phi_{ii})_e$.

Progress in this direction has been made previously by Frumkin, Iofa, Kabanov, and others (54). The considerations have in general been limited to the diffuse part of the double layer (95), whereby the electric work involved, to transfer a hydrogen ion from the bulk to the outer Helmholtz plane, was separated out. However, electrochemical reactions always involve "specific" adsorption and often high electrolyte concentration, and the diffuse part of the double layer (in which the potential depends logarithmically on the charge) is less important than the compact part. The introduction of the adsorption potential of the outer Helmholtz plane also tends to obscure the pH-dependence of overvoltage. According to Frumkin the overvoltage-current relation can be expressed by (54)

$$\eta = a + (2RT/F) \ln i + \psi_i - (RT/F) \ln H^+$$

if one uses $\alpha = \frac{1}{2}$. Since $\psi_i \cong (RT/F) \ln H^+ +$ constant, one would derive a relative independence of η on pH, which is not supported experimentally. Therefore, it is preferred to use the simple condenser model, which accounts for electrostatic interaction of adsorbed protons.

The slow variation of overvoltage with time during prolonged polarization can be explained by changes in the electrode surface area and by dissolution of hydrogen in the metal. With some metals, embrittlement becomes apparent under these conditions. The penetration of atomic hydrogen into the metal lattice changes the electronic configuration, the electron concentration (96), and the covalent adsorption energy. These changes should be taken into account in the interpretation of experiments with bipolar hydrogen diffusion electrodes (97).

It is easy to derive on the basis of the present theory the general laws for build-up and decay of overvoltage. Since at high polarization the electrode potential is simply proportional to the number of adsorbed potential determining species, overvoltage should increase linearly with time under constant current conditions. This is generally observed. On the other hand, overvoltage should decay, after interruption of the polarizing current, logarithmically with time since one derives from [13]

$$n_i^* \sim dn_i^*/dt \sim d(\phi_i - \phi_{ii})/dt \sim \exp\left[-\alpha z_i e_o (\phi_i - \phi_{ii})/kT\right]$$

The slope of the voltage-log time curve must approximate the (negative) Tafel slope of the voltage-log current plot. It is interesting to note that in 1928 Baars formulated the desorption of hydrogen from electrodes analog to the Becker-Zeldovich equation [11]. This early work of Baars (98) is in complete agreement with the present theory.

The presence of the activated adsorbed species at electrode interfaces becomes evident from many experimental observations. The rate of decay and build-up of overvoltage proves the adsorption capacities involved are usually much larger than normally observed for a double layer with inert or nonspecifically adsorbed particles. If the polarizing current is reversed for a very short period of time and the electrode potential forced down rapidly toward the open-circuit potential and then cut off, the overvoltage recovers considerably before the electrode potential falls slowly to the open-circuit value. For very large surface-area porous electrodes, as used in storage batteries, the amount of gas evolved after interruption of current can actually be measured, and it can be shown that the voltage decreases linearly with the amount of desorbed gas (99), which is a direct support for the condenser-theory. The presence of activated species during metal deposition and dissolution has also been demonstrated by Gerischer (100) with potentiostatic techniques. Phenomena relating to adsorption and electrostatic interaction are particularly pronounced in oxygen overvoltage experiments on oxide electrodes (101).

Manuscript received Sept. 17, 1958. This paper was prepared for delivery before the New York Meeting, April 27-May 1, 1958.

Any discussion of this paper will appear in a Discussion Section to be published in the June 1960 JOURNAL.

REFERENCES

1. B. M. W. Trapnell, "Chemisorption," p. 124, Butterworth Scientific Publications, London (1957).
2. J. Horiuti, *J. Research Inst. Catalysis, Hokkaido Univ.*, **4**, 55 (1956).
3. M. Boudart, *J. Am. Chem. Soc.*, **74**, 3556 (1952).
4. J. C. P. Mignolet, *J. Chem Phys.*, **23**, 753 (1955); *Bull. Soc. Chem. Belg.*, **64**, 126 (1955).
5. J. C. P. Mignolet, *Bull. Soc. Roy. Sci. Liege*, **12**, 422 (1954).
6. G. M. Schwab, *Trans. Faraday Soc.*, **42**, 689 (1946).
7. D. A. Dowden, *J. Chem. Soc.*, **1950**, 242.

8. R. Suhrmann and W. M. H. Sachtler, *Z. Naturforschung*, **9a**, 14 (1954).
9. P. W. Selwood, S. Adler, and T. R. Phillips, *J. Am. Chem. Soc.*, **77**, 1462 (1955).
10. F. Seitz, "The Modern Theory of Solids," p. 398, McGraw Hill Book Co., New York and London (1940).
11. H. Frohlich, "Elektronentheorie der Metalle," pp. 256-285, Verlag Julius Springer, Berlin (1936).
12. N. A. Breger and A. A. Zhukhovitskii, *Zhur. Fiz. Khim.*, **20**, 355 (1956).
13. P. P. Ewald and H. Juretschke, "Structure and Properties of Solid Surfaces," p. 82, University of Chicago Press (1953).
14. S. N. Zadumkin, *Zhur. Fiz. Khim.*, **27**, 502 (1953).
15. J. H. de Boer, "Electron Emission and Adsorption Phenomena," p. 81, McMillan Co., New York (1935).
16. F. E. Bellas, Theory of Adsorption of Gases on Metallic Surfaces, Pennsylvania State Univ., Thesis, June 1956.
17. D. D. Eley, *Discussions Faraday Soc.*, **8**, 34 (1950); *J. Phys. Chem.*, **55**, 1016 (1951).
18. D. P. Stevenson, *J. Chem. Phys.*, **23**, 203 (1955).
19. R. S. Mulliken, *J. Am. Chem Soc.*, **74**, 811 (1952).
20. F. A. Matsen, A. C. Makrides, and N. Hackerman, *J. Chem. Phys.*, **22**, 1800 (1954).
21. R. J. Brodd, *J. Phys. Chem.*, **62**, 54 (1958).
22. S. Glasstone, K. J. Laidler, and H. Eyring, "The Theory of Rate Processes," p. 144, McGraw Hill Book Co., New York and London (1941).
23. J. H. de Boer, "Advances in Catalysis, IX," p. 472, Academic Press Inc., New York (1957).
24. J. Becker, *Trans. Am. Electrochem. Soc.*, **55**, 153 (1929).
25. Y. Zeldovich, *Acta. Physicochim. USSR*, **1**, 449 (1934).
26. T. Erdey-Gruz and M. Volmer, *Z. Physik. Chem.*, **150A**, 203 (1930).
27. C. Wagner and W. Traud, *Z. Elektrochem.*, **44**, 391 (1938).
28. P. Rüetschi, *ibid.*, **60**, 29 (1956).
29. P. Rüetschi, *This Journal*, **104**, 176 (1957).
30. E. Lange, *Z. Phys. Chem. N. F.*, **7**, 96 (1956).
31. C. Herring, "The Atomistic Theory of Metallic Surfaces," American Society for Metals, Cleveland (1952).
32. E. Callen, *Am. J. Phys.*, **25**, 138 (1957).
33. P. Klein and E. Lange, *Z. Elektrochem.*, **43**, 570 (1937).
34. K. Huang and G. Wyllie, *Proc. Phys. Soc.*, **62**, 180 (1948).
35. H. Strehlow, *Z. Elektrochem.*, **56**, 119 (1952).
36. N. S. Hush, *Australian J. Sci. Research*, **A1**, 480 (1948).
37. B. W. Erschler, *Erfolge der Chemie, russ.*, **21**, 237 (1952).
38. H. J. Oel and H. Strehlow, *Z. phys. Chem.*, **4**, 89 (1955).
39. A. N. Frumkin, *Colloid Symposium Annual*, **7**, 89 (1930).
40. P. Rüetschi and P. Delahay, *J. Chem. Phys.*, **23**, 697 (1955).
41. B. S. Krasikov and V. V. Syseva, *Dokl. Akad. Nauk. SSSR*, **114**, 826 (1957).
42. A. Frumkin, *J. Chem. Phys.*, **7**, 552 (1939).
43. A. Frumkin, *Z. Elektrochem.*, **59**, 807, 818 (1955).
44. V. L. Kheifets and B. S. Krasikov, *Zhur. Fiz. Khim.*, **31**, 1992 (1957).
45. K. Esin and M. Markov, *Acta Physicochim. USSR*, **10**, 353 (1939).
46. R. Parsons, "Proc. Second International Congress of Surface Activity," Vol. 3, pp. 38, 45, Academic Press Inc., New York (1957).
47. J. O'M. Bockris and E. C. Potter, *This Journal*, **99**, 199 (1952).
48. K. J. Vetter, *Z. Elektrochem.*, **59**, 435 (1955).
49. H. Gerischer and W. Mekl, *ibid.*, **59**, 1049 (1955).
50. B. E. Conway and J. O'M. Bockris, *J. Chem. Phys.*, **26**, 532 (1957).
51. H. Gerischer, *Z. Phys. Chem., N. F.*, **8**, 137 (1956).
52. R. Parsons, *Trans. Faraday Soc.*, **54**, 1053 (1958).
53. J. Horiuti and T. Nakumura, *Z. Phys. Chem. N. F.*, **11**, 358 (1956).
54. A. N. Frumkin, *Trudy Soveschchaniya Elektrokhim, Akad. Nauk SSSR, Otdel Khim. Nauk*, **1950**, 21 (1953).
55. P. Rüetschi, *Z. Physik Chem.*, **5**, 323 (1955).
56. N. I. Kobozev and N. I. Nekrasov, *Z. Elektrochem.*, **36**, 529 (1930).
57. W. Gutt and D. J. G. Ives, *Chem. Soc.*, **1957**, 344
58. J. Horiuti and M. Ikusima, *Proc. Imp. Acad. Tokyo*, **15**, 39 (1939).
59. J. Horiuti, *J. Research Inst. Catalysis, Hokkaido Univ.*, **1**, 8 (1948).
60. R. Parsons, *Trans. Faraday Soc.*, **47**, 1332 (1951).
61. A. C. Makrides, *This Journal*, **104**, 677 (1957).
62. J. Horiuti and H. Sugawara, *J. Research Inst. Catalysis, Hokkaido Univ.*, **4**, 1 (1956).
63. J. O'M. Bockris and E. C. Potter, *ibid.*, **4**, 50 (1956).
64. J. Tafel, *Z. Phys. Chem*, **A50**, 641 (1905).
65. A. Hickling and F. Salt, *Trans. Faraday Soc.*, **38**, 474 (1942).
66. J. Horiuti, T. Keii, and K. Hirota, *J. Research Inst. Catalysis, Hokkaido Univ.*, **2**, 1 (1951).
67. T. Keii and T. Kodera, *ibid.*, **9**, 105 (1958); J. Horiuti and G. Okamoto, *Sci. Papers Inst. Phys. Chem. Res. Tokyo*, **28**, 231 (1936); H. F. Walton and J. H. Wolfenden, *Trans. Faraday Soc.*, **34**, 436 (1938); M. Anbar and H. Taube, *J. Am. Chem. Soc.*, **78**, 3252 (1956).
68. S. Schuldiner and J. P. Hoare, *J. Phys. Chem.*, **61**, 705 (1957); S. Schuldiner, NRL Reports 5091, March 1958, and 5171, July 1958, Naval Research Lab., Washington, D. C.; J. P. Hoare and S. Schuldiner, *J. Phys. Chem.*, **62**, 229 (1958).
69. M. Breiter, H. Kammermaier, and C. A. Knorr, *Z. Elektrochem.*, **60**, 37 (1956).
70. J. O'M. Bockris, "Modern Aspects of Electrochemistry," p. 180, Butterworths Scientific Publications, Ltd. London (1955).
71. J. O'M. Bockris, *Z. Elektrochem.*, **55**, 105 (1951).
72. I. Yasumori, S. Shida, and K. Nakata, *J. Chem. Soc. Japan*, **73**, 892 (1952); K. Fueki, I. Yasumori, and S. Shida, *ibid.*, **76**, 625 (1955).
73. M. Eigen, *Z. Elektrochem.*, **59**, 986 (1955).
74. M. I. Temkin and A. N. Frumkin, *Zhur. Fiz. Khim.*, **30**, 1885 (1956).
75. J. Horiuti, T. Keii, M. Enyo, and M. Fukuda, *J. Research Inst. Catalysis, Hokkaido Univ.*, **5**, 40 (1957).
76. P. Rüetschi, *Z. Phys. Chem.*, **14**, 277 (1958).
77. P. Rüetschi and P. Delahay, *J. Chem. Phys.*, **23**, 195 (1955).
78. J. Horiuti and A. Polanyi, *Acta Physicochim.*, **2**, 505 (1935).
79. D. D. Eley, *Discussions Faraday Soc.*, **8**, 34 (1950); *J. Phys. Chem.*, **55**, 1016 (1951).
80. D. A. Dowden, *Ind. Eng. Chem.*, **44**, 977 (1952).
81. I. Higuchi, T. Ree, and H. Eyring, *J. Am. Chem. Soc.*, **79**, 1330 (1957).
82. R. C. L. Bosworth, *Proc. Cambridge Phil. Soc.*, **33**, 394 (1937).
83. J. C. P Mignolet, *Rec. Trav. Chim.*, **74**, 685 (1955).
84. F. Bloyaert, L. d'Or, and J. Mignolet, *J. Chem. Phys.*, **25**, 53 (1957).
85. K. Bonhoeffer, *Z. Phys. Chem.*, **A113**, 199 (1924).
86. L. I. Krishtalik, *Zhur. Fiz. Khim.*, **31**, 2403 (1957).
87. P. Rüetschi and P. Delahay, *J. Chem. Phys.*, **23**, 1167 (1955).
88. H. Fischer, *Z. Elektrochem.*, **52**, 111 (1948).
89. G. N. Volkov, *Zhur. Fiz. Khim.*, **29**, 390 (1955).
90. H. Leidheiser, *J. Am. Chem. Soc.*, **71**, 3634 (1949); E. N. Khomutov, *Zhur. Fiz. Khim.*, **24**, 1201 (1950); St. G. Christov and N. A. Pangarov. *Z. Elektrochem.*, **61**, 113 (1957).

91. A. K. Lorents, *Zhur. Fiz. Khim.*, **27**, 317 (1953).
92. N. I. Kobozev, *ibid.*, **24**, 113 (1952).
93. N. Chtani, *Sci. Repts. Research Inst., Tohoku Univ.*, **A8**, 399 (1956).
94. W. Gordy and W. Thomas, *J. Chem. Phys.*, **24**, 439 (1956).
95. D. C. Grahame, *Chem. Revs.* **41**, 441 (1947).
96. K. Guminski, *Bull acad. polon. sci.*, **4**, 227 (1956).
97. A. Frumkin, *Z. Physik. Chem.*, **207**, 321 (1957).
98. E. Baars, *Marburger Sitzungsberichte*, **63**, 214 (1928).
99. A. L. Pittman and G. W. Work, NRL Report 5031, Naval Research Lab., Washington, D. C. (1957).
100. H. Gerischer, *Z. Elektrochem.*, **62**, 256 (1958).
101. P. Rüetschi, R. T. Angstadt, and B. D. Cahan, *This Journal*, **106**, 547 (1959).

On the Conductivity of Dispersions

Robert E. De La Rue[1] and Charles W. Tobias

Department of Chemical Engineering, University of California, Berkeley, California

ABSTRACT

Experiments on suspensions of glass beads in electrolytes indicate that Bruggemann's approximation represents the dependence of effective conductance on volume fraction very satisfactorily when the dispersed phase contains a broad range of particle sizes. Data on narrow size ranges fall in between values predicted by the Maxwell and Bruggemann equations. These findings are consistent with the physical assumptions implicit in both theoretical developments.

Presence of gas bubbles or solid dielectrics[2] in electrolytes causes a drop in conductivity relative to the gas- or solid-free condition. Of major interest is the manner in which the effective conductance of the dispersion depends on the volume fraction of the nonconducting phase. In the present study emphasis is placed on particles of spherical shape occupying less than half the volume of the dispersion. Such dispersions occur frequently in industrial electrolytic processes in which gas evolution takes place at one or both electrodes.

According to Maxwell (1) the effective conductivity K_e of random suspensions of spherical particles of uniform diameter and conductivity K_d in a continuous medium of conductivity K_c is related to the volume fraction f of the dispersed phase as follows:

$$\frac{K_e/K_c - 1}{K_e/K_c + 2} = f\frac{K_d/K_c - 1}{K_d/K_c + 2} \qquad [1]$$

If the conductivity of the dispersed phase $K_d = 0$, Eq. [1] simplifies to:

$$\frac{K_e}{K_c} = \frac{1 - f}{1 + \frac{f}{2}} \qquad [2]$$

Rayleigh's treatment (2) of dispersions of spheres of uniform diameter, where the particles occupy cubic lattice positions, leads to an expression identical to Eq. [2] for the case where $K_d = 0$, and $f \to 0$.

In the derivation by Maxwell the assumption has been made that the average distance between the particles of the discontinuous phase is large enough so that the fields around individual particles are undisturbed by the presence of the other particles. This condition is rigorously satisfied only as $f \to 0$. In Fig. 1 we have plotted the potential field around a spherical nonconducting particle, when at large distances from the particle the potential ψ is a linear function of y only, where y is a vector pointing from left to right. In this case

$$\psi = -(S/r^2 - r_s/r)\sin^2\theta \qquad [3]$$

where r_s is the radius of the sphere, $S = -K(dx/dy)_{r\to\infty}$, a constant, r is the distance from the center of the sphere, θ is the angle between r and y, and K is the conductivity of the continuum.

It is apparent from Fig. 1 that the disturbance in the linear field becomes very small at short distances from the sphere. Therefore, in moderately dilute dispersions Maxwell's equation should be an excellent approximation. However, a concentration of $f = 0.25$ already corresponds to an average distance of 0.6 r_s between spheres, and the interaction of fields around the spheres becomes significant. Equation [1] should then no longer represent the relation between volume fraction and conductivity with acceptable accuracy.

Although, according to theory, Eqs. [1] and [2] are subject to limitations, in the past numerous workers have found that experimental data may be

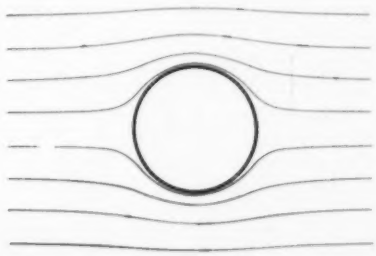

Fig. 1. Potential field around sphere, an insulator, placed in a homogeneous and isotropic conductor. Field is linear at great distances from sphere.

[1] Present address: Stanford Research Institute, Menlo Park, Calif.

[2] Particles exhibiting electronic conduction also may act as insulators, provided the potential gradient in the dispersion is such that the potential difference over a distance corresponding to the largest dimension of the particle in the direction of the field does not exceed the decomposition voltage of the system under consideration.

represented satisfactorily by use of these relations even in moderately concentrated dispersions. Electrical conductivity data obtained on various concentrations of cream in milk were found by Fricke (3) to fit Eq. [2] within experimental error. Eucken (4) reported results of measurements involving the systems water-benzene and water-phenol with KCl and KI, respectively, as solutes. Over the entire range of volume concentrations ($0<f<1$) agreement with Eq. [1] was reported. In a recent review on non-Newtonian fluids Metzner (5) refers to data by Orr and Dalla Valle (6) who measured thermal conductivities[2] of metal shot dispersed in 2% agar gel. Agreement of the experimental data with Eq. [1] within 3% over a large range of volume concentration was again claimed.

Not all investigators found the agreement between the Maxwell-Rayleigh relations and their experimental data satisfactory. Slawinski (7, 8) conducted experimental investigations using enameled metal spheres of approximately 0.5 cm diameter in KCl solutions, in the range of $0.35 < f < 0.6$. His data fitted within 0.4% a curve corresponding to substantially lower effective conductances than would have been predictable by Eq. [2]. This curve corresponded to a relation developed from a physical model in which Slawinski evaluated the integral mean lengths and mean cross sections between spheres arranged in several different lattice orders

$$K_s/K_c=\{1+(f/p)[(1+0.3219p)^2/(1-p)-1]\}^1 \quad [4]$$

where $p = n \cdot f^{n/3}$. Value of parameter n depends on the volume fraction range:

for $0.15 > f$	$n = 0.806$
for $0.15 < f < 0.6$	$n = 0.806 + 0.1333\,f$
for $0.6 < f$	$n = 0.9046$

Data presented by Slawinski for moderate and low volume concentration in random distributions were in far less satisfactory agreement with Eq. [4] than at high concentrations. Unfortunately Slawinski's treatment does not take into account the fundamental principles of the theory of potential, according to which the distribution of potential throughout the conducting medium satisfies the Laplace equation. His equation also contains an adjustable parameter in addition to the volume fraction of the dispersed phase.

More recently Mashovets (9) reported measurements of conductivities of dispersions of glass and hard rubber spheres in $CuSO_4$ solutions where the spheres were fixed in lattice positions. The effective conductances measured were lower than values predictable from Maxwell's equation [2], and by least squares treatment of the data following equation was obtained: $K_s/K_c = 1 - 1.78f + f^2$. Reliability of this equation may be questioned on grounds of lack of adequate description of experiments and failure to indicate reproducibility and confidence limits. It is also doubtful whether the few experimental points taken form an adequate basis for proposal of an empirical equation. Pearce (10) recently presented experimental permittivity values obtained on oil-water emulsions. The data was in good agreement with values calculated by Bruggemann's approximation (11) (see Eq. [6] below). Conductivity measurements on two-dimensional array of metal and bakelite hemispheres submerged in tapwater yielded different results depending on whether the hemispheres occupied lattice positions, or were arranged in a random manner. In the former case Pearce found agreement with Eq. [1], while for random arrangement the Bruggemann approximation seemed to have given a better fit. The two-dimensional model of random arrangement by Pearce, however, does not represent the three-dimensional case accurately enough to base meaningful conclusions on it. Further, Pearce's data on random arrangement of spheres was taken only in the low volume concentration region (up to $f = 0.12$) where, judging from the few experimental points presented in his graphs, the experimental errors may have been comparable to the magnitudes of the possible deviations from Maxwell's or Bruggemann's equations. A comparison of data by the various investigators reveals that the discrepancy between experimental findings is by no means negligible, reaching approximately 10% near $f = 0.5$. Such a large difference in conductivity ratio values cannot be justified on the basis of inherent limitations in the type of measurement. Much rather, one is led to believe that some of the investigators may have taken less caution in defining their systems and in the execution of their experiments than would have been necessary to establish firmly the functional relationship between K_s/K_c and f.

The present work was undertaken with the aim of obtaining data with sufficient confidence in its accuracy to permit the evaluation of the limitations of Maxwell's equation [2] in the range $0 < f < 0.4$. Further, by using a comparatively large range of sizes both in separate fractions and also mixed together within one suspension, it was hoped that differences in conductance behavior between homogeneous and mixed-size dispersions may be detected.

Experimental

Glass beads of excellent shape characteristics[4] were used in the experimental series on spherical nonconducting particles. The beads were separated into size fractions by air elutriation. The diameter range selected for study is given in Table I. Within

[2] Thermal and electrical conductivity of dispersions depend on volume fraction of dispersed phase in an identical manner.

[4] Courtesy Central Research Department of the Minnesota Mining and Manufacturing Co.

Table I

Fraction	Size
	μ
I	49-77
II	107-175
III	175-210
IV	590-840
V*	3100-3400
VI*	6100-6400

VII—Equal volumes of I and VI mixed.
VIII—Equal volumes of fractions I-VI mixed.

* Braun-Knecht-Heimann Co., Catalog No. 13782.

each size range (I-VI) approximately 75% of the beads were within a range of 10% of the mean diameter (Fig. 2a).

The sands[5] were wet-sieved after washing with water and the electrolyte, and only the fraction passing through sieve number 80 and remaining on 100 was used (approximate size range: 0.15-0.175 mm) (Fig. 2b and 2c).

Polystyrene cylinders[6] were cut from fibers of uniform diameter (0.3 mm) to a length of 3 ± 0.3 mm (Fig. 2d).

The specific gravity of the electrolyte was selected to be just slightly below that of the dispersed phase to prevent fast settling. Of the available alternatives, a near saturated solution of $ZnBr_2$ was selected as the continuous phase for the measurements with glass beads and sand. The saturated solution at 20°C has a specific gravity of 2.725 and a conductivity of 0.066 ohm^{-1} cm^{-1}. The specific gravities of the glass beads and of the sand were approximately 2.50 and 2.60, respectively. The density of each size fraction was determined to within unit accuracy in the third decimal figure. For polystyrene cylinders 0.1*N* KCl solution was chosen as the continuous phase.

Conductivity cell.—Following preliminary work with conventional type cells, the main series of measurements were executed with a cylindrical cell (Fig. 3) consisting of two sections, each 2¾-in. long, which could be interconnected by removal of a center electrode. A ¾-in. hole was drilled into Lucite blocks, providing the cylinder sections. Top and bottom electrodes were platinum, surface-welded onto ¼ in. copper plates. Center electrode consisted of a 25 mil platinum plate attached at two sides to ⅛ in. copper bars which served as guides. Sections of the cell were assembled using 1/16 in. Teflon gaskets, and the assembly was held together by bronze studs.

The conventional-type Wheatstone bridge circuit employed in the measurements is illustrated in Fig. 4.

Procedure.—Before each series of measurements the cell was filled with the electrolyte and the cell constants for each cylindrical section determined. Following this, the desired volume fraction of solid phase was weighed on an analytical balance and poured into the cell. The resulting mixture then was stirred with a glass rod for approximately 3 min to remove entrained air. The top electrode was closed and the cell was shaken to insure uniform electrolyte composition and temperature. When the dispersed phase settled below the level of the center electrode, the electrode was closed. Next the resistance of the upper compartment (containing no solids) was

[5] Death Valley Sand or Merck "Sea Sand."

[6] Dow Chemical Company.

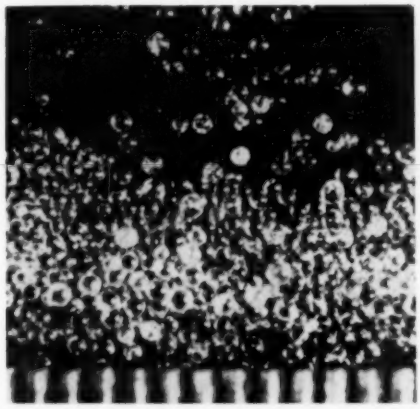

Fig. 2a. Glass spheres, 49-77 μ size fraction

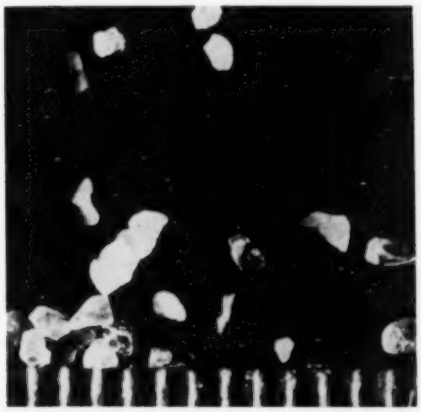

Fig. 2b. "Death Valley Sand", size range 0.15-0.175 mm

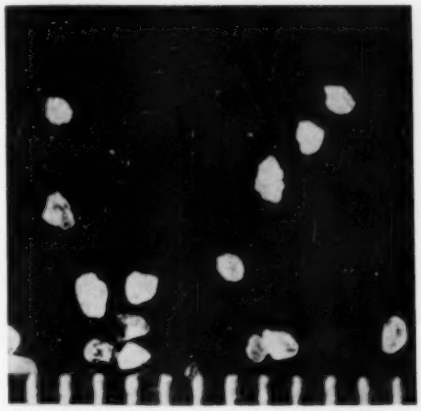

Fig. 2c. " Sea Sand," size range 0.15-0.175 mm

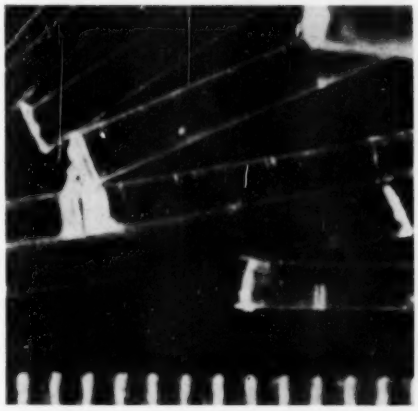

Fig. 2d. Polystyrene cylinders, diameter 0.3 mm, length 3 mm.

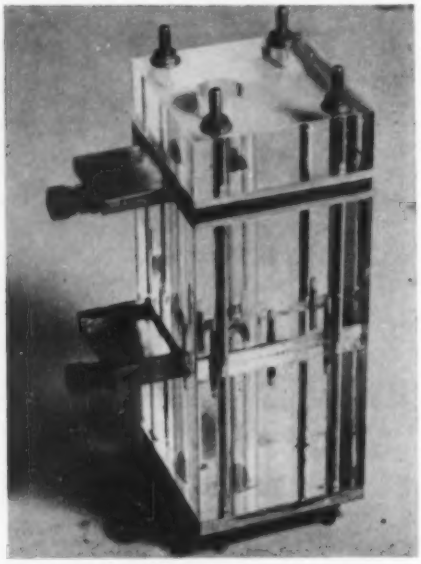

Fig. 3. Assembled conductivity cell, with top and center electrodes in "open" position.

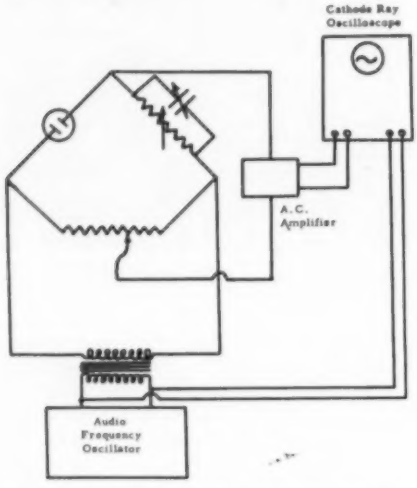

Fig. 4. Schematic diagram of the Wheatstone bridge circuit

measured. The resistance of the lower compartment (containing the known volume fraction of solids) was obtained while the cell was shaken by hand with a rotating, up, down, and sideward motion until a "steady-state" image was obtained on the screen of the cathode-ray oscilloscope. With continued shaking the actual value of the resistance of the dispersions was obtained by adjustment of the slide wire until the image, which was an ellipsoid, would become a line in the vertical gain, the point at which the Wheatstone bridge circuit was balanced.

After the first pair of measurements were completed, to check whether thermal equilibrium existed between the two compartments, the central electrode was opened, and the contents of the compartments thoroughly mixed. Again the solids were allowed to settle into the lower compartment and, after closing the central electrode, conductivity measurement was repeated as described above. In most cases the conductivity ratios obtained by the second pair of measurements were in agreement with those by the first within ±0.2%. If not, the contents of the compartments were again mixed, etc., until the difference between conductivity ratios between two successive measurements was within the limits given above.

Table II. Per cent difference between minimum and maximum values of K_e/K_c measured in three series of runs

f	%
0.1	0.19
0.2	0.17
0.3	1.2
0.4	1.75

To detect any systematic errors such as might be due to weighing and handling of solids, possible imperfect elimination of entrained air, etc., complete series of runs involving measurements at several volume fractions were repeated two or three times. As illustrated in Table II, per cent differences between minimum and maximum values obtained for K_e/K_c at the same volume fractions were only approximately 0.2% at up to f values of 0.2; however at $f = 0.4$ reproducibility was less satisfactory (1.75%).

Data

Figures 5-8 serve to illustrate the results obtained in the 20 series of measurements, each series consisting of four to eight individual measurements of conductivities at approximately evenly spaced volume fractions of solids. On most single- and mixed-size fractions enumerated in Table I and with each sand species and the polystyrene cylinders duplicate measurements were taken. Graphical representation of the data reveals that all the experimental points fall below the line corresponding to Maxwell's equation (Eq. [2]), and this deviation increases with

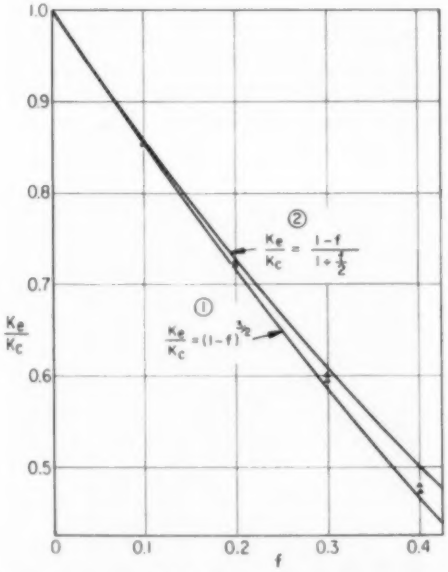

Fig. 5. Dependence of effective conductance on volume fraction of dispersed phase. Size range of spheres: 175-210 μ. ▲, Series I; △, Series II.

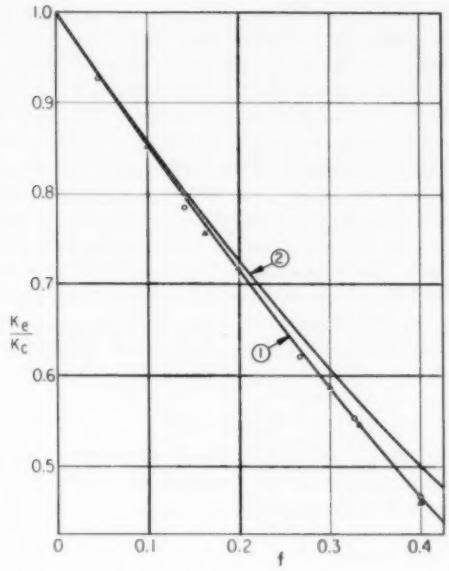

Fig. 6. Dependence of effective conductance on volume fraction of dispersed phase consisting of spherical particles. △, equal weight fractions of size ranges I-VI; ○, equal weight fractions of size ranges I-VI. Curves 1 and 2 as on Fig. 5.

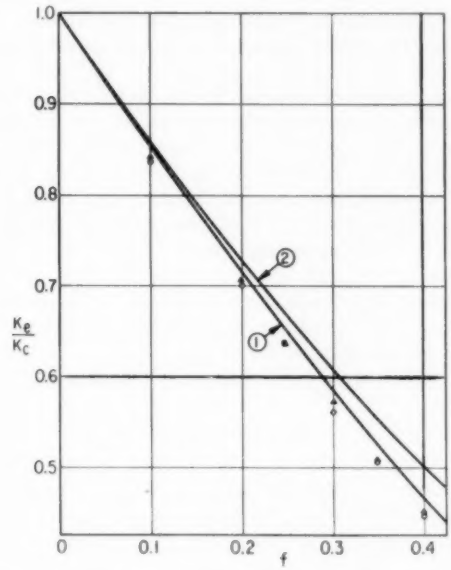

Fig. 7. Dependence of effective conductance on volume fraction of suspended sand. △, "Sea Sand"; ○, "Death Valley Sand." Curves 1 and 2 as on Fig. 5.

volume fraction of the dispersed phase. Further, values of the conductivity ratio on mixed size ranges are slightly but distinctly below the ones obtained on single size ranges. Data on both the polystyrene cylinders and on the two kinds of sands show more substantial differences from Eq. [2] than any on spherical particles.

Best Curves Representing Data

All series were subjected to least squares treatment, using the equation

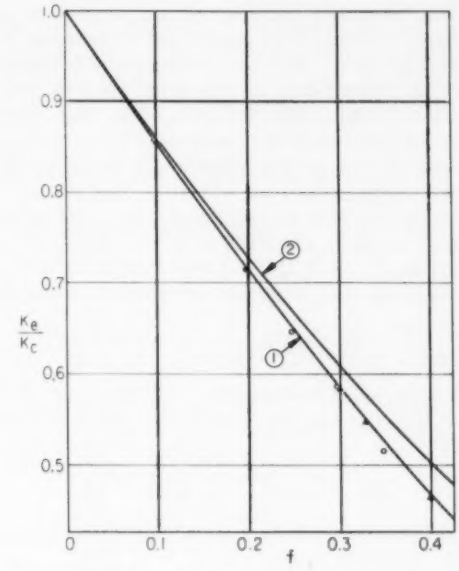

Fig. 8. Dependence of effective conductance on volume fraction of suspended polystyrene cylinders. △, Series I; ○, Series II. Curves 1 and 2 as on Fig. 5.

$$K_e/K_c = X(1-f)^Y \qquad [5]$$

Table III summarizes the least squares values of X and Y. If we assign a value $X' = 1.00$ (which should be satisfied for obvious physical reasons), the modified exponent Y' is obtained. The table also includes the standard deviation S and S'. All coefficients of correlation were greater than 0.998. S and S' are measures of the scatter of data about the curves defined by X, Y, or Y' in units of the ordinate. Twice the standard deviation gives approximately the 95% confidence limits on either side of the curve.

Discussion

While differences between the set of data on single-size fractions and on mixed sizes may be regarded as too small to draw sharp conclusions, the least squares equation representing data on mixed sizes is for all practical purposes identical to the equation proposed on theoretical grounds by Bruggemann (11) in which $Y' = 1.5$ (see Eq. [6] below). That such an agreement for a large diameter range of spherical particles in the dispersed phase confirms reasonable expectations follows from the physical approximations implicit in Bruggemann's mathe-

Table III. Least squares curves representing conductance data in terms of Eq. [5]. X' fixed at 1.00

Dispersed phase	X	Y	S	Y'	S'
I	0.97	1.35	0.010	1.43	0.015
II	0.988	1.47	0.015	1.52	0.014
III	0.998	1.44	0.008	1.45	0.007
IV	0.995	1.45	0.001	1.47	0.002
V	0.988	1.45	0.007	1.48	0.009
VI	0.991	1.48	0.008	1.50	0.008
VII, VIII	0.997	1.50	0.007	1.51	0.007
Death Valley Sand	0.992	1.56	0.005	1.58	0.006
Sea Sand	1.003	1.55	0.010	1.55	0.010
Cylinders	0.994	1.51	0.010	1.53	0.010

matical treatment. If one adds a relatively large spherical particle to a dispersion containing much smaller particles, the disturbance of the field around the large sphere due to the small spheres may be considered negligible. On this basis, the effective conductance of such a system may be evaluated by considering the surroundings of the large sphere as a continuum having an effective conductance K'_e, and apply the Maxwell equation, since the system is "dilute" as far as the large sphere is concerned. The change in K'_e with the volume fraction of the dispersed phase may then be expressed in differential form:

$$dK'_e/df = [-3K'_e/(1-f)][(K'_e-K_d)/(2K'_e+K_d)]$$

Integrating with the boundary conditions $K'_e/K_c = 1$ as $f = 0$ and at the upper limit $K'_e = K_e$, one obtains

$$\frac{K_e/K_c - K_d/K_c}{(K_e/K_c)^{1/3}(1-K_d/K_c)} = 1-f$$

for the case when both phases are conductors, and the Bruggemann equation

$$K_e/K_c = (1-f)^{3/2} \qquad [6]$$

when the dispersed phase is an insulator, or $K_d = 0$. For single sizes or narrow size fractions, the physical conditions necessary for justifying the Bruggemann approximation are not satisfied. Conductivities of such dispersions when $K_d = 0$ must be lower than the value obtained from Maxwell's equation and higher than predicted by Bruggemann's approximation. The series of measurements represented in Table III conform to this qualitatively correct argument.

Size Effect

With the exception of the one series on the 105-177 μ range, where the scatter of data was unusually large, the exponent Y′ shows a slight, gradual increase with particle size. There is no reason why particle size should have any effect on the effective conductance, unless the diameter of the spheres becomes comparable to the dimensions of the vessel containing the dispersion. There is no doubt that the larger exponents found for the size fractions V and VI, respectively, reflect wall effects.

It should be noted that while Maxwell's equation is valid strictly only when the dispersed phase consists of spheres of a single diameter, and of course at that only at very low volume concentrations, Eq. [6], both on the basis of the present experimental results and because of the conditions assumed in the derivation by Bruggemann (11), applies best for random distribution of sizes.

Although the present study was not designed to clarify what effects shapes other than spherical would have on the conductivity ratio K_e/K_c, four series of measurements with sand and two with polystyrene cylinders were also performed. The results as presented in Fig. 7 and 8 and in Table III indicate that Eq. [6] again represents the data fairly well. This agreement however should be viewed with caution. The sand particles used were of "smoothed off" polyhedrical shape for which the approximations incorporated in Eq. [6] may be considered to apply rather well. The "Death Valley Sand" gave slightly lower conductivity ratios than the "Sea Sand" reflecting the more elongated shape of the former (12).

As to the cylinders, Fricke's treatment (13) of the conductivities of prolate spheroids in dilute dispersions yields values close to those one obtains by using Eq. [6]. Therefore at least at low concentrations of the solid, the agreement between the present data and Eq. [6] is not surprising. However, at higher volume fraction of the dispersed phase, there is no adequate theoretical basis by which one can safely generalize the agreement found between the data for cylinders of approximately 10:1 length to diameter ratio and the values predictable from Eq. [6], which has been developed for spheres only.

Conclusions

Experiments of reasonably high precision and reproducibility confirmed expectations based on theory, e.g., that the conductivity of electrolytes is lowered by the presence of randomly distributed spherical nonconductors to a larger extent than predictable from the well-known Maxwell relation. Conductivity data obtained on a large size range of glass spheres in aqueous $ZnBr_2$ solutions aligned closely to curves represented by Eq. [5] with $X = 1.00$ and $1.43 < Y < 1.51$. This form of the equation and the upper limit of the exponent find theoretical support in the approximation first proposed by Bruggemann.

It is recommended that for random dispersions of spherical insulators with a large size-range of spheres, such as occurs in gas-electrolyte emulsions, the Bruggemann equation (Eq. [6]) be used to predict effective conductivity. When the size-range of spheres is narrow it may still be used with about the same or lower probable error than the Maxwell equation, although in that case the Bruggemann equation predicts slightly low values for the effective conductance. For shapes other than spherical Eq. [6] is generally not applicable, particularly not if the particles are greatly elongated or when they contain cavities.

Acknowledgment

The authors wish to express their appreciation to Mr. Eugene J. Fenech for work done on the IBM 650 computer and to Mr. Robert E. Meredith and Dr. Thomas Baron for enlightening discussions.

Manuscript received Feb. 9, 1959. This paper was prepared for delivery before the Cincinnati Meeting, May 1-5, 1955.

Any discussion of this paper will appear in a Discussion Section to be published in the June 1960 JOURNAL.

REFERENCES

1. J. C. Maxwell, "Electricity and Magnetism," Vol. 1, 3rd ed., p. 440, Oxford (1892).
2. Lord Rayleigh, *Phil. Mag.*, **34**, 481 (1892).
3. H. Fricke and S. Morse, *Phys. Rev.*, **25**, 361 (1925).
4. A. Eucken, VDI-Forschungsheft, No. 353 (1932).
5. A. B. Metzner, "Advances in Chemical Engineering," Vol. 1, pp. 121-124, Academic Press, Inc., New York (1956).
6. C. Orr and J. M. Dalla Valla, Chem. Eng. Progr. Symposium Ser. No. 9, **50**, 29 (1954).
7. A. J. Slawinski, *Chim Phys.*, **23**, 710 (1926).

8. *Ibid.*, **26**, 368 (1929).
9. J. P. Mashovets, *J. Appl. Chem.* (*U.S.S.R.*), **24**, 353 (1951).
10. C. A. R. Pearce, *Brit. J. Appl. Phys.*, **6**, 113 (1955).
11. D. A. G. Bruggemann, *Ann. Physik.*, **24**, 636 (1935).
12. R. E. De La Rue, Master's thesis, University of California (1955).
13. H. Fricke, *Phys. Rev.*, **24**, 575 (1903).

Effect of Gas Evolution on Current Distribution and Ohmic Resistance in Electrolyzers

Charles W. Tobias

Department of Chemical Engineering, University of California, Berkeley, California

ABSTRACT

Volume fraction of gases in electrolyzers increases in the direction of net movement of gases, causing a corresponding variation in the ohmic resistance between electrodes. The resulting nonuniformity in current distribution and the increase in over-all resistance is shown to be characterized by a single dimensionless parameter which incorporates the key process variables. The leveling effect of polarization is shown to be significant.

Although the effect of gas holdup in electrolytic cells on the resistance of the electrolyte has long been recognized (1), quantitative interpretation of the effects observed has not been attempted until recent years. Ipatieff, Schischkin, and Jurieff (2) have presented simple calculations relating the total current to volume of gas present in water electrolyzers. Implicit in their treatment is the assumption that the effective resistivity of the electrolyte between the vertical electrodes does not vary in the vertical direction. While this assumption greatly simplifies the physical model, it also deprives the model used by these workers of reality. In addition to neglecting the current density variation caused by differences in gas concentration, these authors expressed the volumetric effect of gas bubbles on conductivity in an erroneous manner.

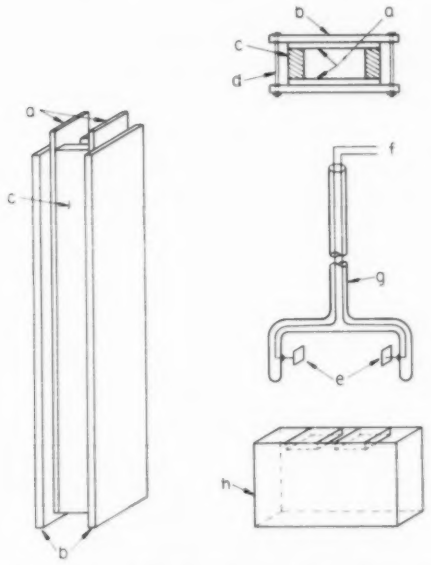

Fig. 1. Experimental cell and conductivity probe used by Baker (2). a, Steel electrodes, 32 x 6 x ⅛ in.; b, Bakelite backing sheets; c, plexiglass separators, 31 x 1 x 1 in.; d, fastening bolts; e, platinized platinum electrodes, 0.5 x 1.0 cm, 7 cm apart; f, shielded leads; g, glass tube, 1 cm OD; h, plexiglass shield fitting over horizontal part of glass tube.

According to measurements of the effective resistance as a function of cell depth (Fig. 1) reported by Baker (3) between parallel electrodes, the volume fraction of gas at a given depth in a given electrolyte is approximately a linear function of current density (Fig. 2). Baker calculated the volume fractions from resistance data obtained by use of a shielded resistivity probe. An experimental plot of the variation of gas volume fraction as a function of distance from cell bottom is shown in Fig. 3.

Current density decrease from bottom to top of a water decomposition model cell was shown by Murakawa and Nagaura (4) by means of direct measurements of branch currents using a "sectioned" electrode (5). Their results conform, at least in a qualitative sense, to expectations based on first principles. When gas evolves along a vertical electrode surface, bubbles ascend under the buoyancy force (and if the electrolyte is in motion, also due to drag forces). The time required for a gas bubble evolved at a point on the surface to reach the surface of the electrolyte will be approximately proportional to the distance of this point from the surface. Consequently the volume fraction of gas in the electrolyte gradually increases with elevation, causing the conductivity of the suspension to diminish along the same direction.

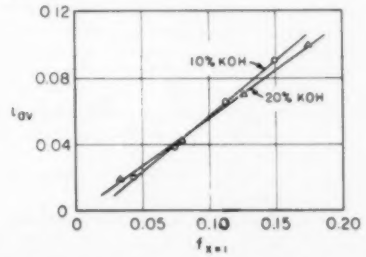

Fig. 2. Volume fraction of gas near the electrolyte surface [from data by Baker (3)].

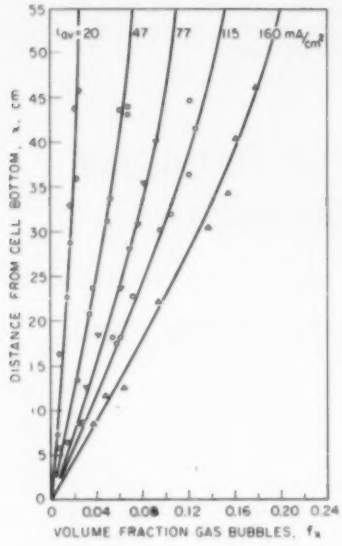

Fig. 3. Experimental volume fractions at different cell depths

The aim of the present work is to establish a theoretical treatment by which the most important design and process variables are combined in functional relationship, quantitatively describing the effect of gas evolution on current distribution and cell voltage. In order to lend clarity and simplicity to the mathematical treatment, certain reasonable physical assumptions must be made, which however should not detract from the general validity of the results.

Nomenclature

- b' — $b'_a - b'_c$
- b'_a, b'_c — anodic and cathodic linear Tafel slopes, ohm cm²
- C — dimensional constant, $RT/PmFs\delta$, cm amp^{-1}
- D — bubble diameter, cm
- E — portion of applied cell voltage that depends on current, $E = E + i_r R_x$, volts
- E_p — current dependent part of polarization voltage, $E_p = b'i_x$
- E_D — constant in "linear" Tafel equation, volts approximately the current-independent part of the cell voltage, or the "decomposition" voltage
- F — Faraday, coulombs/gram equivalent
- f_x — volume fraction of gas in electrolyte at level x, dimensionless
- f_{av} — average volume fraction of gas in cell, dimensionless
- h — height of electrolyte column in cell (with or without gas), cm (Fig. 4)
- I_T — total current passing through cell, amp
- i_x — local current density at level x, amp/cm²
- i_{av} — average current density in cell, amp/cm²
- K — dimensionless parameter $CEh/\rho\delta = RTEh/PmFs\rho\delta^2$
- m — number of Faradays passing through the cell, per mole of gas liberated at both electrodes, g-equivalent/mole
- P — partial pressure of gas liberated at electrodes, atm, $P = P_T - P_v$
- P_T — total pressure (approximated by ambient pressure plus arithmetic mean of hydrostatic pressure in cell)
- P_v — vapor pressure of electrolyte at the operating temperature
- R — gas constant, cm³ atm/°K g mole
- R_e — resistance of gas-free electrolyte between the two electrodes, ohms
- r_x — effective resistance of a 1 cm² prism of electrolyte containing gas bubbles, between the two electrodes at elevation x, ohm cm², $r_x = \rho_x\delta = \rho\delta(1 - f_x)^{-3/2}$
- R_{ett} — total ohmic resistance of electrolyte and gas in cell, ohms
- s — average rising velocity of bubbles, cm/sec
- T — absolute temperature, °K
- u — velocity of a gas bubble, cm/sec
- u_s — steady-state velocity of a gas bubble, cm/sec
- dv_x — volume of gas in volume element $w\delta dx$ of electrolyte at level x, cm³ (Fig. 4)
- w — width of electrodes, cm (Fig. 4)
- X — dimensionless reduced vertical distance, $X = x/h$
- x — vertical distance from bottom of electrodes, cm (Fig. 4)
- δ — electrode separation, cm (Fig. 4)
- θ — time, sec
- μ — $b'/\rho\delta$, polarization parameter, dimensionless
- ν — dynamic viscosity, g cm^{-1} sec^{-1}
- ρ — resistivity of gas-free electrolyte, ohm cm
- ρ_x — resistivity of electrolyte containing gas bubbles at level x, ohm cm
- σ_e, σ_g — density of electrolyte and gas, respectively, g/cm³
- ϕ — cell parameter $\phi = I_T C/w = I_T RT/PmFs\delta w$, dimensionless

Cell Model and Physical Assumptions

The geometry of the cell model is shown in Fig. 4. The following assumptions were made:

1. The electrode on the metal side is equipotential, i.e., there is no "terminal effect."

2. Size distribution of bubbles at all levels is the same, and within the range of current densities this size range and distribution may be regarded as constant.

3. The bubbles assume their steady-state (instantaneous) velocity, u_s, essentially immediately after separation from the surface. It can be shown by the solution of the differential equation from u, the velocity of motion of a gas bubble in the gravitational force field, using Stokes law, that

$$u = u_s[1 - \exp(-18\nu\sigma_e\theta/D^2\sigma g)] \qquad [1]$$

Substitution of reasonable values of the physical constants into Eq. [1] indicates that quasi steady

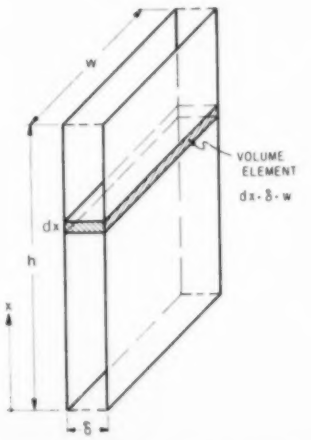

Fig. 4. Model of gas evolution cell

state is reached within 0.01-0.001 sec after release.

4. Velocity of rise is independent of depth. In fact bubbles expand on decrease in hydrostatic pressure. Since the buoyancy force is proportional to D^3 while the drag force is proportional to D^m (where $1<m<2$), ascending bubbles accelerate. In the region of interest velocity of bubbles varies approximately in inverse ratio to the 1/3 to 2/3 power of the pressure; therefore the increase of velocity amounts to only a few per cent, provided the cell depth is not very great. Incorporation of variable velocity into the treatment to be presented, however, would confuse the issue more than it would contribute to the accuracy of the end results.

5. Velocity of rising bubbles is independent of volume concentration of gas. In fact the bubble motion decelerates as the volume concentration of bubbles in the electrolyte increases. Quantitative functional representation of the effect of volume concentration on the departure of velocity from the "free" rate of ascendance however has not been developed so far.[1]

6. Secondary effects on bubble motion, such as those due to coalescence or convection currents in the electrolyte for example, are disregarded.

7. The assumptions under 2-6 above permit the definition of an average velocity, s, at which the gases liberated at the electrodes rise, independent of depth and current density. Within a given electrolyte, however, this velocity depends on pressure, temperature and electrode material.

8. Polarization is linear over the range of current densities occurring within a cell (see Fig. 5). Substitution of a linear relation for a relatively narrow range of current densities has been an accepted technique in treating current distribution problems (6, 7).

9. The flow of current is unidirectional, or at least the curvature of the lines of flow is negligible. It has been shown (6) that for linear geometry this is a good assumption, provided δ/h is small.

[1] Studies by Hanratty, *et al.*, on hindered settling of spherical solids (9) have shown that in the Stokes law region the effective rate of settling may be evaluated if, instead of the density of pure liquid, one substitutes the average density of the suspension (a variable, function of depth), and if one also takes into account the change of effective viscosity with the changing volume concentration. Although the exact functional dependence is more complex, Hanratty's data may be reasonably well represented by $s_x/s_o = (1 - f_x)^4$ when $f_x < 0.35$, where s_o corresponds to the free settling rate, and s_x denotes the actual rate of settling at elevation x.

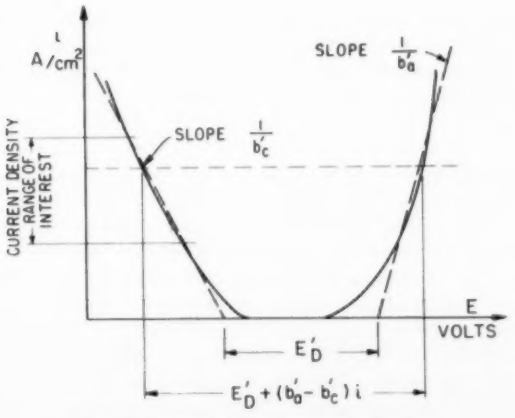

Fig. 5. Linear polarization approximation

Mathematical Treatment

In the steady state, the volume of gas dv_x present in the volume element $w \cdot \delta \cdot dx$ (Fig. 4) is

$$dv_x = (RTwdx/PmFs) \int^x i_x dx \qquad [2]$$

Equation [2] may be derived as follows. The quantity w times the integral equals the total current flowing through the cell between the bottom and level x. This current divided by mF gives the total number of moles of gas produced and, multiplied by RT/P, the total volume of gas produced in the cell per second between the bottom and x. This volume of gas is moving upward a distance of s cm in 1 sec. Therefore, the fraction dx/s of it will be in the given volume element at any given instant of time, and this is the volume dv_x. The volume fraction of gas in the same element is then

$$dv_x/w\delta dx = f_x = C \int^x i_x dx \qquad [3]$$

For a given geometry, P, T, m, and s, C is a constant having the dimensions of length per unit of current. Equation [3] relates the volume fraction of a gas at height x to the total current passing below that level.[2]

As shown by De La Rue and Tobias (8), dependence of the ohmic resistivity ρ_x at level x on the volume fraction of gas is given by the Bruggemann equation

$$\rho_x = \rho(1 - f_x)^{-3/2} \qquad [4]$$

The current-dependent portion of the electrode potentials E_p may be represented by (Fig. 5)

$$E_p = b' i_x \qquad [5]$$

The dependence of potential on current density, resistance, and polarization is then obtained by combination of [4] and [5]

$$E = (b' + r_x)i_x \qquad [6]$$

Note that, in the present application, E is independent of x by virtue of assumption 1 above. The square centimeter resistance r_x is equal to $\rho_x\delta$.

Substitution and rearrangement of [6] yields

$$E/\rho\delta = [\mu + (1 - f_x)^{-3/2}]i_x \qquad [7]$$

The meaning of the polarization parameter μ has been given by Wagner (7) among others.

The differentiation of [3] yields

$$df_x = Ci_x dx \qquad [8]$$

The current density i_x may be eliminated between Eqs. [7] and [8] and the resultant equation integrated

$$(CE/\rho\delta) \int^x dx = \int^{f_x} [\mu + (1 - f_x)^{-3/2}]df_x \qquad [9]$$

[2] Although constant velocity of rise s has been assumed in this derivation, incorporation of velocity dependence on volume fraction of gases as represented, for instance, by the approximation formula in footnote 1, causes no difficulty. Equation [3] transforms to $f_x(1 - f_x)^4 = C\int^x i_x dx$ and the integration of the modified equation repiacing Eq. [9] may be readily accomplished. The resulting form however is implicit in f_x, and does not permit therefore derivation of convenient expressions showing the dependence of key process variables. In the following treatment only the simpler relations involving the constant velocity assumption are presented.

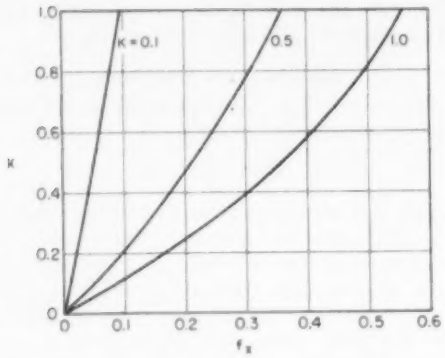

Fig. 6. Volume fraction of gas as a function of reduced height

To obtain a solution in closed form for f_x, let us for the present assign the value $\mu = 0$ (corresponds to constant polarization), and then integrate between the limits given. The solution is

$$f_x = [(KX)^2 + 4KX]/(KX + 2)^2 \qquad [10]$$

where K, the gas effect parameter, and X, dimensionless vertical height, have been introduced to reduce the number of symbols carried. A plot of f_x as a function of X is given in Fig. 6 for $K = 0.1$, 0.5, and 1.0.

Combination of Eqs. [7] and [10] leads to the important relation between local current density and vertical distance

$$i_x = 8K/hc(KX + 2)^2 \qquad [11]$$

Mathematical Results

A number of useful relations may now be derived by simple combinations of the equations derived in the preceding section.

1. The relation between the total current I_T and the current-dependent part of the voltage

$$I_T = i_{av}hw = w\int^h i_x dx = wf_x h/C =$$

$$w(K^2 + 4K)/C(K + 2)^2 \qquad [12]$$

In Fig. 7 the ratio of local to average current density i_x/i_{av} has been plotted by use of Eqs. [11] and [12] for $K = 0.1$, 0.5, and 1.0.

2. Solving [12] for K, we obtain the dependence of K on average current density

$$K = 2[1 - (1 - 1/Chi_{av})^{-1}]^{1/2} - 2 \qquad [13]$$

Equation [13] has been plotted in Fig. 8 The vertical scale is Chi_{av}. Note that for low values of K (<0.15)

$$K \cong Chi_{av} \qquad [14]$$

In this region, K is directly proportional to applied current and depth of cell and, from the definition of C, K is inversely proportional to average velocity of rise of bubbles and to electrode separation.

3. The average effective ohmic resistance of electrolyte R_{eff} relative to gas-free resistance R_e, when the cell depth is the same, is given by

$$R_{eff}/R_e = (K + 2)^2/(K + 4) \qquad [15]$$

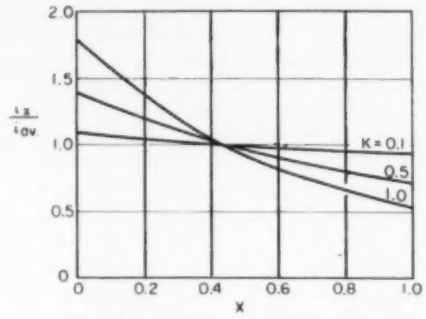

Fig. 7. i_x/i_{av} as a function of reduced height along electrode

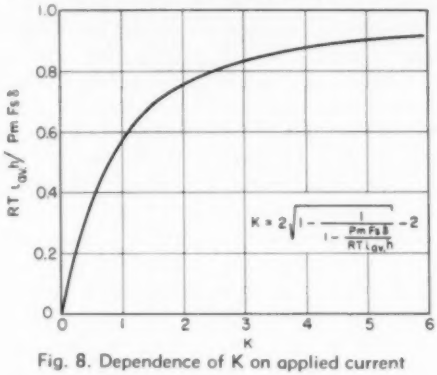

Fig. 8. Dependence of K on applied current

4. The average volume fraction of gases is given by

$$f_{av} = \int^1 f_x dX = K/(K + 2) \qquad [16]$$

Figure 9 illustrates Eqs. [15] and [16], showing that the per cent effect on resistance is greater than the per cent average gas holdup. Figure 10 shows a plot of f_{av} against a dimensionless grouping ϕ including I_T.

Optimal distance of electrodes.—Because of the effect of gas bubbles on the resistivity of electrolyte, setting the electrodes closer together will not result in a proportionate reduction of ohmic voltage drop. As a matter of fact it is easy to realize that bringing them together below a certain distance should result in an increase of voltage drop. (The volume fraction of gas varies in inverse proportion to the electrode separation, while the effective resistance of the dispersion between the electrodes increases more rapidly than does the volume fraction of gas.) For simplicity's sake let us consider only at what average volume fraction f_{av} of gas the effective ohmic resistance will be at a minimum:

$$R_{eff} = A/f_{av}(1 - f_{av})^{3/2} \qquad [17]$$

where all terms not depending on distance have been grouped into a constant A.

Differentiating with respect to f_{av}, and setting the derivative equal to zero, we obtain $f_{av} = 0.4$, i.e., the ohmic resistance will be at its minimum when the electrodes are at such a distance that the average volume fraction of gas between them is 0.4. Although such a high holdup volume seems to be out of the common design and operational range, it should be noted that the ohmic resistance diminishes rather slowly with distance even when $f_{av} > 0.2$. Therefore

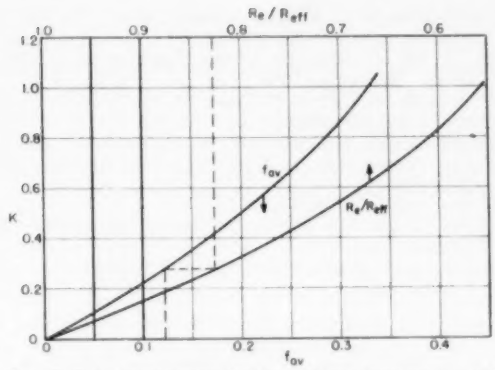

Fig. 9. Relation between holdup-volume fraction f_{av}, effective resistance, and K for gas evolution between plane parallel electrodes.

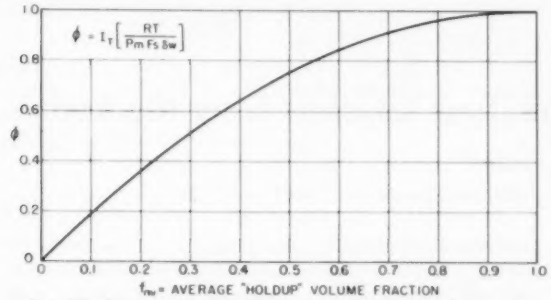

Fig. 10. Average gas holdup as a function of total current

only little can be gained by setting the electrodes closer together than corresponds to $f_{av} = 0.2$.

In attempting to evaluate the effect on the voltage drop of reducing the interelectrode distance, one should keep in mind that in all the developments presented above it has been assumed that the average velocity of gas bubbles is independent of electrode separation. Although for large separations this appears to be a reasonable approximation, it is quite certain that, when the electrodes are so close together, the volume fraction of gas becomes significant, s depends on electrode separation, and the optimal separation will be larger than that corresponding to $f_{av} = 0.4$.

Effect of Polarization

The value $\mu = 0$ has been assigned so far in order to obtain a solution in closed form for the current density distribution, and to show in the manner easiest to follow how the common design and process variable are interrelated.

The relation between X and f_s from the integration of equation [9]

$$KX = \mu f_s + 2(1 - f_s)^{-1/2} - 2 \qquad [18]$$

does not yield an explicit form in f_s and therefore i_s cannot either be expressed in a closed form as a function of X. A reasonable approximation may be obtained however if one replaces[a] the term in Eq. [7] which represents the effect of gas volume fraction on resistance $(1 - f_s)^{-3/2}$ by the first two terms of its binomial expansion $1 + 3/2 f_s$. With this substitution the current density variation as a function of X, K, and μ may be obtained by simple algebraic steps

$$i_s/i_{av} = \frac{3}{2} K[(\mu + 1)^2 + 3KX]^{-1/2}\cdot$$

$$\{[(\mu + 1)^2 + 3K]^{1/2} - (\mu + 1)\}^{-1} \qquad [19]$$

[a] Use of this expression for conditions where $f_{av} > 0.2$ leads to appreciable errors.

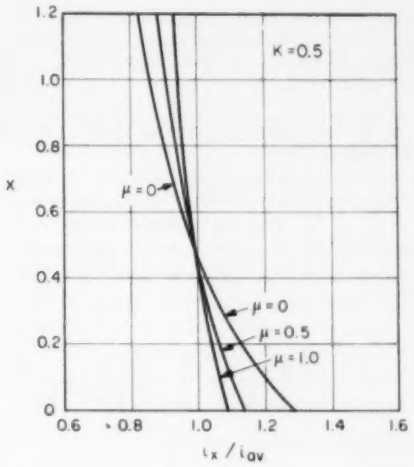

Fig. 11. Leveling effect of polarization on nonuniform current distribution caused by gas evolution.

Figure 11 shows the considerable leveling effect of polarization for a practical range of values of the polarization parameter μ.

When the polarization is strongly dependent on current density and therefore μ is comparable to or larger than unity, the nonuniformity of current distribution is diminished to a significant degree. Under such conditions it is advisable to use Eq. [19] and the correspondingly modified forms of the relations expressing effective resistance, etc.

Note: The fact that the effect of gas evolution on current distribution depends on a single dimensionless parameter should be helpful both in design procedures and when it is desirable to know what effects changes in operational conditions will have.

The foregoing treatment should be regarded as valid only within the physical assumptions made. Therefore, whenever any of the variables (such as size, total current) are changed significantly one must examine whether or not dependent quantities have been affected by phenomena not considered in setting up the physical model. A particularly vulnerable assumption is that relating to the constancy of the average rising velocity of bubbles. Large variations in cell depth or electrode separation will undoubtedly influence s, as will changes in electrode materials. The effect of deceleration of bubble motion due to decrease in bulk density and increase of viscosity cannot be considered quantitatively until further experimental and theoretical developments improve our understanding of the dynamic behavior of suspensions of gases in liquids. The analogy with hindered settling is plausible but not proven. In any case, other factors, such as bulk entrainment of electrolyte and secondary flows caused by descending, relatively gas-free eddies, may so seriously influence bubble motion that conclusions reached by considering the deceleration due to viscosity and density changes alone could be misleading.

The average bubble velocity, s, and its dependence on cell geometry, current density range, and materials used may be established in model experiments. Estimates of s may be obtained by measurement of increase

of electrolyte level due to gas holdup (see Eq. [16]), and the variation of average velocity with total current established by comparing the dependence of K on i_{av} with the values calculated by use of Eqs. [13] and [14].

Manuscript received Feb. 9, 1959. This paper was prepared for delivery before the New York Meeting, April 27-May 1, 1958.

Any discussion of this paper will appear in a Discussion Section to be published in the June 1960 JOURNAL.

REFERENCES

1. V. Engelhardt, "Handbuch der Technischen Elektrochemie," vol. II/I, p. 9, Akademische Verl. M.B.H. 1933).
2. V. V. Ipatieff, V. V. Schischkin, and S. I. Jurieff, *Z. Elektrochem.*, **40**, 713 (1934).
3. W. J. Baker, Master's Thesis, University of California, Berkeley (1951).
4. T. Murakawa and S. Nagaura, *J. Electrochem. Soc. Japan*, **23**, 223, 304 (1955).
5. E. Mantzell, *Z. Elektrochem.*, **39**, 10 (1935).
6. C. W. Tobias and R. Wijsmann, *This Journal*, **100**, 459 (1953).
7. C. Wagner, *ibid.*, **98**, 116 (1951).
8. R. E. De La Rue and C. W. Tobias, *ibid.*, **106**, 827 (1959).
9. T. J. Hanratty and A. Bandukwala, *A.I.Ch.E. Journal*, **3**, 293 (1957).

Technical Note

Preparation and Properties of ZnS-Type Crystals from the Melt

Albrecht G. Fischer[1]

Large Lamp Department, General Electric Company, Nela Park, Cleveland, Ohio

The important semiconducting phosphor materials ZnS, CdS, and ZnSe cannot be melted at normal pressure because they decompose several hundred degrees below their melting points. This tendency is due to the mixed homo-heteropolar nature of their bond. As the diamond lattice requires that the ions be incorporated in a predeformed state and under stress, unstable surfaces result (1, 2).

The first experiments to melt ZnS and CdS in a high-pressure bomb were carried out several decades ago (3), and recently interest has revived in the subject. Accurate values for the melting points and vapor pressures of ZnS and CdS have been reported (4, 5) and a technique of growing crystals of these materials from the melt under high argon pressure has been developed (2, 6).

ZnSe can also be recrystallized from the melt (2). In continuation of earlier work it was found that crucibles of pure graphite and of zirconia can be used. Quartz glass, although rather soft at the melting point of ZnSe, is also suitable as a crucible material since it is not chemically attacked by the melt.

Using a melting point indicator similar to that described in (2) and a Pt-Pt/Rh thermocouple, the melting point of ZnSe has now been determined to be at 1515° ±20°C. $CuGaS_2$ melts at 1280°C.

The vapor pressure at the melting point was determined by a new direct method. A sealed-off evacuated quartz tube filled with ZnSe prefired in vacuum was heated up to the melting point of ZnSe. When the outer pressure in the autoclave was somewhat higher than the decomposition pressure developed in the tube, the walls of the plastic quartz tube were compressed. When, on the other hand, the outer pressure was lower than the inner pressure, the bulb dilated and formed a bubble. In a series of experiments with varying external pressure, it was possible to determine the pressure in the bulb within close limits. In the case of ZnSe it is around 1.8 atm, while it is about 2.5 atm for CdS. This method is also suitable for substances with lower melting points where other glasses have to be used, for instance for certain $A_{III}B_V$ compounds where indirect methods had to be used previously.

The facts that the vapor pressure is comparatively low and that quartz, although already soft at 1500°C, is chemically stable, suggested a new method for the preparation of ZnSe single crystals from the melt. It

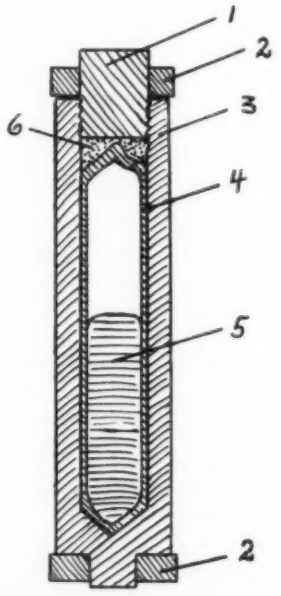

Fig. 1. 1, Graphite stopper; 2, boron nitride rings to prevent electrical shorting of the heater; 3, graphite crucible; 4, quartz bulb; 5, ZnSe or CdS melt; 6, graphite powder.

[1] Present address: RCA Laboratories, Princeton, N. J.

is also suitable for CdS. A quartz tube is filled with ZnSe, heated in vacuum and sealed off. This tube is inserted into a closely fitting thick-walled graphite crucible which can be closed with a plug. The remaining empty space is filled with graphite powder (see Fig. 1). If this assembly is heated up, the softening quartz tube expands, driven by the interior pressure, until the rigid graphite container takes up the mechanical forces and the quartz hull serves merely as a gas-tight lining. The vessel with the molten ZnSe can then be cooled down with any desired temperature gradient in order to crystallize the melt. To prevent devitrification of the quartz it is desirable to use pure graphite with smooth surfaces. Instead of the simple graphite crucible shown in Fig. 1 which has to be destroyed each time a crystal is removed, more elaborately designed vessels can be used which allow disassembly and reassembly.

The method described is expected to find wider application because it allows the growing of large single crystals from the melt in a reproducible way and with simple, inexpensive means; no high-pressure autoclave is needed.

For ZnS or ZnS-rich mixtures, it is better to use high-density zirconia crucibles with stoppers, which are sealed into evacuated, closely fitting quartz tubes and heated in an autoclave. The pressure applied from the outside has to be higher than the decomposition pressure inside. The thermoplastic quartz envelope then forms a gas-tight lining around the ZrO_2 crucible; this permits growing of the crystals in a defined atmosphere and controlling the vacancy equilibrium in the crystals.

It has been found that the pure compounds ZnS, CdS, and ZnSe, or mixtures containing at least about 80% of any one of the constituents, crystallize much more readily than mixtures with lower contents, which have the tendency to stay polycrystalline.

Thermoelectric measurements have shown that undoped ZnSe crystals as well as samples doped with Al and In are n-type, whereas ZnSe crystals doped with Cu or Ag are p-type. The n-type samples are strongly photoconducting, whereas coactivated samples are luminescent.

Solid-state diffusion occurring during the firing of crystals rich in ZnSe or CdS and packed in ZnS powder having the same activator concentration led to spread-band-gap surfaces. This could be observed by a short wave-length shift of the photo- and cathodoluminescence from the interior of the crystals toward their surface. Formation of mixed crystals of ZnSe with ZnTe or GaAs (7) reduces the band gap of ZnSe.

Acknowledgment

It is a pleasure to thank Dr. H. C. Froelich for help with the preparation of this paper.

Manuscript received May 13, 1959.

Any discussion of this paper will appear in a Discussion Section to be published in the June 1960 JOURNAL.

REFERENCES

1. A. Fischer, *Phys. Verh.*, **8**, 204 (1957).
2. A. Fischer, *Z. Naturforschg.*, **13a**, 105 (1958).
3. E. Tiede and A. Schleede, *Ber.*, **53B**, 1717 (1920).
4. A. Addamiano and P. A. Dell, *J. Phys. Chem.*, **61**, 1020 (1957).
5. A. Addamiano, *ibid.*, **61**, 1253 (1957).
6. W. E. Medcalf and R. H. Fahrig, *This Journal*, **105**, 719 (1958).
7. D. N. Nasledov, "Semiconductors and Phosphors," p. 644, Interscience Publishers, Inc., New York (1958).

Technical Review

The Manganese Dioxide Electrode

W. C. Vosburgh

Department of Chemistry, Duke University, Durham, North Carolina

Manganese dioxide has been an important battery reactant since about 1890 when the Zn-MnO_2 cell proposed by Leclanché (1) began to be used in the dry-cell form. Because of the importance of the Leclanché cell and of other uses of MnO_2 a voluminous literature has grown up. A review of the Leclanché cell by Heise and Cahoon (2) was published in 1952 and at the same time reviews of two newer cells with MnO_2 electrodes by Morehouse (3) and Herbert (4). The present review brings together some of the more recent contributions to the structure and properties of MnO_2 and the discharge mechanism of the MnO_2 electrode. Related topics that are not included are the carbon of the Leclanché-cell bobbin, the electrolyte, reactions of the Leclanché cell not closely related to the discharge mechanism, the standard potential and the open-circuit potential of the MnO_2 electrode, and practical features of batteries with MnO_2 electrodes.

Structural Forms of Manganese Dioxide

Reviews of the structure of MnO_2 have been given by Wadsley and Walkley (5) and Brenet (6). Some later contributions have been made by Buser and Graf (7). The large number of more or less differing substances of the approximate composition

MnO_2 (with or without other elements) have been classified as belonging to a relatively few general types which occur naturally. The crystal structures of these have been determined and diagrams of the structures are given in the above references.

The minerals pyrolusite and ramsdellite are MnO_2 with no other element as an essential part of the structure. Ramsdellite in well-crystallized form is rare. Pyrolusite has a more compact crystal structure than ramsdellite (6,8).

Psilomelane is given the type formula $(Ba,H_2O)_2Mn_5O_{10}$ in which the relative amounts of Ba and H_2O are variable (9). The Ba is present as Ba^{++}, and compensation for the charge is made by reduction in the charge of an equivalent number of Mn atoms (9).

The minerals cryptomelane, hollandite, and coronadite are alike except for the additional element present along with the MnO_2, these being K, Ba, and Pb, respectively (10, 11). The type formula is given as KMn_8O_{16}, with K replaceable by other metal atoms, with suitable adjustments of the charge of the Mn.

Lithiophorite and chalcophanite have layer structures in which the MnO_2 forms two layers enclosing other metal ions and water, or hydroxides (12).

Well-crystallized artificial pyrolusite, known also as β-MnO_2, can be prepared. The accepted standard MnO_2 electrode with an acid electrolyte is a β-MnO_2 electrode (13). Well-crystallized ramsdellite has not been prepared, but the artificial material known as γ-MnO_2 and the naturally occurring γ-MnO_2 now usually are considered to be related to ramsdellite (14, 5, 6) although a closer relation of some samples to pyrolusite on the basis of the x-ray diffraction pattern has been pointed out (15). It is suggested (11) that the ramsdellite structure of γ-MnO_2 is partially changed to the more stable pyrolusite structure by as mild a treatment as heating under boiling water. This would make possible a series of disordered intermediate forms. Both natural γ-MnO_2 ores and electrodeposited γ-MnO_2 preparations are used in batteries.

Well-crystallized artificial cryptomelane, or α-MnO_2, has been prepared. Electron microscope photographs of α-MnO_2 showing definite crystal form, are given by McMurdie (16) and Buser, Graff, and Feitknecht (17). In similar photographs of γ-MnO_2 no crystal form can be seen. McMurdie's α-MnO_2 was prepared by the digestion of γ-MnO_2 with NH_4Cl solution either at 100°C or under pressure at 150°C and presumably contained NH_4^+ in its structure. The α-MnO_2 of Buser, Graf, and Feitnecht was prepared with K^+ present.

Electrodeposition of MnO_2 from a bath of $MnSO_4$ and H_2SO_4 gives γ-MnO_2 (14, 6). However, if one of the cations that can take part in the α-MnO_2 structure is present α-MnO_2 may be obtained (18, 19), although Cole, Wadsley, and Walkley (14) obtained γ-MnO_2 in two preparations in which K_2SO_4 was present.

Precipitation processes in which Mn^{++} is oxidized or MnO_4^- reduced (or both) give four different oxides, depending on conditions. The one most commonly formed is γ-MnO_2, but in the presence of K^+ or other similar cations α-MnO_2 or mixtures of α and γ may be formed (14, 20, 21). Some conditions of precipitation give δ-MnO_2 (16), and still other conditions give two forms of a material called manganous manganite (22, 23). As the last name implies, this material contains Mn(II) as well as Mn(IV), and the amount of Mn(II) is variable. Buser, Graf, and Feitknecht (17) showed that δ-MnO_2 and manganous manganite are alike in structure. The crystals are thin plates consisting of two layers of Mn(IV) and O atoms with a variable amount of $Mn(OH)_2$ between the layers. The Mn(II) of the $Mn(OH)_2$ can be replaced by other metals, for example Zn, giving a series of manganites. When the $Mn(OH)_2$ content is small, the material is δ-MnO_2. Compounds $3MnO_2 \cdot Mn(OH)_2 \cdot xH_2O$ and $4MnO_2 \cdot xMn(OH)_2 \cdot 2H_2O$ have been prepared, the latter in well-crystallized form. This preparation indicates that manganous manganite is not a poorly crystallized α-MnO_2 as has been suggested (16,24). Buser and Graf (25) consider that the two forms of manganous manganite are similar in structure to the minerals chalcophanite and lithiophorite, mentioned above. On heating manganous manganite or δ-MnO_2 under water α-MnO_2 is formed if the preparation contains enough K^+, and γ-MnO_2 is formed if the K^+ content is below a certain small minimum (22, 17). Dried δ-MnO_2 containing K^+ was not appreciably converted to α below 300°C (21).

Some Properties of MnO_2

Most of the properties of MnO_2 are well known and need no review here. However, some recent work on certain of the properties should be mentioned.

Changes on heating.—The changes on heating MnO_2 at temperatures between 350° and 450°C serve to show the relative stabilities of the various varieties. Cole, Wadsley, and Walkley (14) represent the changes as follows, most of which they have confirmed. The arrows represent heating at 350° to 450°C except in the one case noted; this

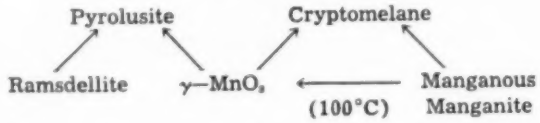

latter change seems to have been carried out only under hot water (17). Pyrolusite, or β-MnO_2, and cryptomelane, or α-MnO_2, are the most stable forms, and of the two α-MnO_2 is much the more stable if it contains K^+ as the additional cation. Whether γ-MnO_2 and manganous manganite are converted to α-MnO_2 or to β-MnO_2 depends on the presence or absence of a suitable cation.

Heating at temperatures of 150° to 350°C affects the properties of γ-MnO_2 (26, 27). The potential of the MnO_2 (that is, the electrode potential when a MnO_2 electrode is made with the material in question, with an ammonium salt electrolyte unless otherwise specified) is decreased by heating. The discharge capacity is also decreased. Combined water is driven off at these temperatures and the

crystal form altered in the direction of increased crystallinity and partial conversion to a pyrolusite structure (11). The decreased discharge capacity may be related to both the decreased water content of the MnO_2 and its change in structure. The electrode potential is determined by the composition of the exterior of the oxide (28). Heating γ-MnO_2 at still lower temperatures, 90° to 140°C, affects the shape of the discharge curve, when electrode potential is plotted against time at constant current (29).

However, when the electrolyte is a solution of HCl and $MnCl_2$ the results are different. Maxwell and Thirsk (21) made electrodes from a number of different MnO_2 preparations, unheated and heated at various temperatures up to 500°C. Heating the MnO_2 either had little effect or caused an increase in the electrode potential, followed by a decrease at the highest temperatures. It is worthy of note also that the various artificial preparations of α-, γ-, and δ-MnO_2 all had electrode potentials higher than artificial β-MnO_2, the differences ranging from 30 to 80 mv.

Surface area.—Measurements of the surface area of MnO_2 by the gas adsorption method have revealed that the area in most cases is very large. For γ-MnO_2 areas of 20-60 m^2/g have been reported (25, 28). This is of the order of 10^5 times the surface of a gram of MnO_2 in the form of a smooth cube. For δ-MnO_2 a surface of 300 m^2/g was found (30), in agreement with the very thin crystal structure proposed for this variety.

The catalytic activity of any one sample of MnO_2 for the decomposition of H_2O_2 is dependent on the surface area, but different samples may differ widely in catalytic activity (5). Variation in the overpotential of similar preparations of electrodeposited MnO_2 electrodes with the temperature and current density of electrodeposition can be explained entirely as caused by variations in surface area (29). However, in general the electrochemical activity of MnO_2 is more dependent on the state of the surface than on the particle size (31).

Ion exchange and isotope exchange.—Manganese oxides, especially when freshly prepared, adsorb a wide variety of cations from solution with liberation of hydrogen ions. This has been considered an exchange adsorption (32), and MnO_2 when hydrated, as most samples are, is a weak acid (33). In the manganous manganites, $4MnO_2 \cdot Mn(OH)_2 \cdot 2H_2O$ and $3MnO_2 \cdot Mn(OH)_2 \cdot xH_2O$, the Mn(II) can be replaced by Zn or various other cations in a reversible ion-exchange reaction (7, 34).

Exchanges between radioactive Mn^{++} and inactive MnO_2 that range from very small to complete have been observed (7). The amount of exchange varies widely with the nature of the MnO_2 and the conditions. With compact lattice structures as in β- and α-MnO_2 and the minerals ramsdellite and chalcophanite exchange of radioactive Mn^{++} takes place only at the surface. There is no diffusion in the lattice. The more open α-MnO_2 structure gives more exchange. Samples of α- and β-MnO_2 having nearly the same surface area per gram gave exchanges of 12% for α and 0.1% for β. In compounds of similar structure and surface area, exchange varies with the amount of disorder. Increase of temperature increases the amount of exchange; a β-MnO_2 that exchanged 2% at room temperature exchanged 15% in a boiling solution (7).

Connected with the ion-exchange property is the observation that each MnO_2 ore or preparation has a characteristic iso-acidic point. This is an electrolyte *p*H of such a value that no change in *p*H takes place when the electrolyte is put in contact with the MnO_2. When MnO_2 is stirred with an electrolyte of higher or lower *p*H than the iso-acidic point the electrolyte *p*H is changed in the direction to approach this point. This change must be taken into account in measuring the change of MnO_2 electrode potential with *p*H. The iso-acidic point is not the same as the isoelectric point which was found to be at the fixed pH 6.5 (35).

Magnetic susceptibility.—The magnetic susceptibilities of a number of manganese dioxides have been measured by Selwood, *et al.* (36). Crystalline pyrolusite is a magnetically concentrated substance; that is, the manganese atoms are so close together that they affect each other magnetically. Artificial γ-MnO_2, a gel form of MnO_2, and Gold Coast and Brazilian ores were found magnetically dilute, indicating a more attenuated structure, in agreement with other data. These have the magnetic behavior expected of a Mn(IV) compound. It was found possible to follow the discharge of a dry cell by measurement of its magnetic behavior, since reduction of Mn(IV) causes an increase in susceptibility.

Conductivity.—It is known that MnO_2 is a semiconductor. Four samples of MnO_2 under high pressure (7×10^6 g/cm^2 or 1×10^5 $lb/in.^2$) gave resistivities of 37-77 ohm-cm (37). Electronic semiconductivity is large when electrons can pass easily from one cation to another. This is the case when ions of one element of different electrical charge occupy equivalent positions in the crystal lattice (38).

Activity.—The term "activity" of a MnO_2 sample is used in describing the practical performance of the material in batteries. Brenet (39) states: "A high activity corresponds practically to the possibility of releasing a maximum quantity of electricity with a maximum potential difference at the cell terminals, over as long a period as possible." This is a tentative definition and he points to the need for a satisfactory method of measuring activity other than by making cells and discharging them. Also, the relation of activity to other properties is not well enough understood.

Lower Oxides of Manganese

The lower oxides and hydroxides of manganese are of interest as possible products of the reduction of MnO_2 in the discharge of the MnO_2 electrode. Two forms of the next lower oxide, Mn_2O_3, have been described and are designated as α- and γ-Mn_2O_3 (40). The more stable is α-Mn_2O_3 which is formed by heating β-MnO_2 to constant weight at 600°C

(41, 40). The less stable oxide, γ-Mn_2O_3, is thought to play a part in the discharge of the MnO_2 electrode (42). It is converted to α-Mn_2O_3 by heating in a vacuum at 500°C or on standing for a year at room temperature (40). The x-ray diffraction pattern of γ-Mn_2O_3 is nearly identical with that of Mn_3O_4, indicating a similarity in structure of these two compounds.

The compound MnOOH occurs as the mineral manganite and can be prepared by oxidation of a Mn(II) salt under carefully controlled conditions. It is a final product of the discharge of the MnO_2 electrode (42-45) and of the reduction of MnO_2 with Mn^{++} at pH 4 to 5 in the absence of Zn^{++} (46). Heating MnOOH at 250° in a vacuum gives γ-Mn_2O_3 (40).

The compound $ZnO \cdot Mn_2O_3$, or $Zn(MnO_2)_2$, which occurs naturally as the mineral hetaerolite, is another final product of the discharge of the Leclanché cell (45, 47) and is formed in the reduction of MnO_2 by Mn^{++} in the presence of Zn^{++} (46). Conditions for its formation in the dry cell have been studied (47). It cannot be the only product of the discharge, or alternatively not a primary product, because its formation would not involve the increase of pH in the bobbin electrolyte that is observed during discharge (44).

All oxides and hydroxides of Mn when heated in air to temperatures in the vicinity of 1000°C are converted to Mn_3O_4, which occurs naturally as the mineral hausmannite.

The compounds MnO and $Mn(OH)_2$ are easily oxidizable by oxygen. It is remarkable that MnO can be oxidized most of the way to Mn_2O_3 before the x-ray diffraction pattern of MnO disappears completely and that of Mn_2O_3 appears (40).

The valence of Mn in some of the lower oxides is a matter on which there is lack of agreement at present. Krishnan and Banerjee (48) measured the magnetic anisotropy of MnOOH and concluded that this compound must be composed of equal parts of Mn(II) and Mn(IV). Brenet (42) prefers to assume only Mn(II) and Mn(IV) in the compounds involved in the MnO_2 electrode reaction. Verwey and de Boer (38) have presented evidence that Mn_3O_4 is composed of Mn(II) and Mn(IV) ions from the electrical conductivity and the crystal structure. On the other hand they presented similar evidence that γ-Mn_2O_3 contains only Mn(III). Since γ-Mn_2O_3 can be prepared by the dehydration of MnOOH in a vacuum at 250°, Mn(III) is suggested for the latter compound, in disagreement with the evidence from magnetic anisotropy. Bhatnagar, *et al.* (41) found a magnetic moment for α-Mn_2O_3 that indicates Mn(III).

The Discharge Mechanism

Early theories.—One of the early theories of the discharge of the MnO_2 electrode was that hydrogen was the primary discharge product, this being subsequently oxidized by the MnO_2. The MnO_2 thus acted as a depolarizer. No definite evidence in favor of this theory has been advanced, and the facts concerning the discharge mechanism can be explained more satisfactorily otherwise.

Another theory involved the formation of Mn^{+++} ions in the electrolyte. Against this is the fact that physical contact between the MnO_2 and the metallic conductor (carbon in the Leclanché cell) is necessary for the effect of the MnO_2 to be detected (49). Also, no appreciable amount of oxidizing substance is found in an NH_4Cl solution digested with MnO_2 (50).

Divers (45) in 1882 explained the polarization of the MnO_2 electrode as the result of the accumulation on the surface of the MnO_2 of the products of the reaction, which he correctly identified as MnOOH and $ZnMn_2O_4$. Divers' explanation of the polarization seems not to have received the attention it deserved. Relatively recent experiments have led to a similar view of the mechanism.

Newer experimental data.—Some of the newer experiments have been carried out on dry cells, but more often special MnO_2 electrodes have been constructed that avoid some of the complications of the dry-cell bobbin. In any case the MnO_2 is brought into intimate contact with either carbon or platinum, by pressure or by electrodeposition of the MnO_2. Except in dry cells, a relatively large volume of electrolyte usually is employed to keep changes in composition small. In what follows it will be assumed that the electrolyte is NH_4Cl solution, with or without added $ZnCl_2$, unless otherwise specified. Potential measurements usually have been made with the help of a reference electrode.

In a dry-cell bobbin an increase in pH takes place on continuous discharge, and a decrease takes place near the zinc electrode. The increase in pH, resulting from the release of NH_3 in the electrode reaction, is partially compensated by the formation of $Zn(NH_3)_2Cl_2$ and other similar complex salts (44). This increase in pH shows that $Zn(MnO_2)_2$ is not the primary product of the discharge of the MnO_2 electrode of the Leclanché cell, as mentioned above.

Even when appreciable pH changes are avoided, or corrections made, the electrode potential of a discharging MnO_2 electrode decreases. The decrease is fairly rapid at first and may be slow later. If the circuit is opened the potential rises fairly rapidly at first, then more and more slowly for a period of days, but does not reattain the initial potential (51). The potential decrease during discharge may be described as a decrease in open-circuit potential combined with a rather large polarization. The growth and decay of this polarization is much slower than in most electrode systems, indicating that it is not simple activation polarization or concentration polarization involving the solution (52, 53). Substitution of other ammonium salts for NH_4Cl makes little or no difference (51) and discharges in 4.4M KOH give much the same results (54).

In the absence of $ZnCl_2$ two products of discharge are observed under most conditions. Mn^{++} is found in solution (55-57) and when the discharge is carried to the point of rapid decrease in potential which terminates the useful part of the discharge an oxide (or oxide mixture) of the composition $MnO_{1.6}$ remains (56, 57). In this solid MnOOH can be recognized by its x-ray diffraction pattern (42).

Analysis of the bobbins of discharged dry cells shows Mn in three forms. Some Mn can be extracted from the bobbin material by a solution of NH_4Cl and $ZnCl_2$ and presumably comes from Mn(II) compounds in the bobbin. The insoluble portion contains both MnOOH and $Zn(MnO_2)_2$. The formation of these products by reduction of MnO_2 accounts quantitatively for the current passed in the discharge (58).

Data on the formation of Mn^{++} as a product of the discharge reveal something of the discharge mechanism. With an electrolyte of H_2SO_4 and $MnSO_4$ it is the only discharge product, other than H_2O (59). At pH 5 in the discharge of γ-MnO_2 electrodeposited on graphite with NH_4Cl or $(NH_4)_2SO_4$ electrolyte, Mn^{++} is formed throughout the discharge. At pH 7.5 or 8 under the same conditions no Mn^{++} is formed in the early part of the discharge (56, 60). The amount of Mn^{++} formed at any one pH is independent of the volume of the electrolyte. The presence of Zn^{++} in the electrolyte reduces the amount of Mn^{++} (61).

Changes in the x-ray diffraction pattern of the oxide during a discharge have been observed (42). Starting with γ-MnO_2, the diffraction patterns indicate an expansion of the crystal lattice as the discharge proceeds. With α-MnO_2 the expansion is not as evident, but is believed to take place. After discharge of a little less than half of the theoretical capacity of the MnO_2 a sudden change in the pattern takes place. The new pattern is that of either γ-Mn_2O_3 or Mn_3O_4 (these being nearly the same), and of the two the γ-Mn_2O_3 is considered the more probable. Finally the pattern of MnOOH appears. When β-MnO_2 is reduced electrolytically only the change to MnOOH is observed.

Interpretation of the experiments.—The slow rate of decay of polarization led Coleman (52) to propose that a solid-state diffusion process is involved. Lower oxide formed on the surface of the MnO_2 is thought to cause the polarization, and a diffusion process operates to remove it (51, 56). This involves the assumption that the composition of the surface of the oxide determines the electrode potential (27, 28). The decay of polarization can then be interpreted as an increase in the available oxygen content of the surface as the result of removal of lower oxide. However, another probable contributing factor is discussed below.

The diffusion process involved in the discharge need not be considered an actual diffusion of Mn and O atoms. The same effect can be attained and electroneutrality preserved within the solid by diffusion of protons and electrons only. Since MnO_2 is a semiconductor we may suppose that electrons can pass through it by being transferred between Mn atoms in different stages of oxidation but at equivalent positions in the crystal lattice (38). Protons can be attached to $O^=$ ions to give OH^- ions. If protons can be transferred from surface OH^- ions to underlying $O^=$ ions and at the same time electrons move from surface Mn ions to underlying ones, the lower oxide on the surface has effectively moved and MnO_2 has moved outward. This should cause the expansion of the MnO_2 lattice that is observed, because Mn^{+3} is larger than Mn^{+4} and OH^- is larger than $O^=$.

The changes taking place during discharge can be explained similarly. To reduce MnO_2 requires electrons for the Mn atoms and protons for attachment to the O atoms. Electrons come from the electrode and with physical contact between electrode and oxide they are available anywhere within the MnO_2. Protons are available from NH_4^+ ions of the electrolyte or from H_2O. The reaction may be considered to take place where the electrons and protons meet, for it may be considered that here the oxide is reduced. Qualitatively, the meeting place can be considered to to be at the surface of the MnO_2 exposed to the solution. One reason for postulating this location is the formation of Mn^{++} in the solution. The indications are that the Mn^{++} is dissolved from a surface oxide by action of the electrolyte (61). The reduction reaction on the surface is followed by reaction of part of the lower oxide to give Mn^{++} and inward diffusion of the remainder.

A somewhat different view is that during the discharge the protons penetrate the oxide and meet the electrons in the interior (42, 57). Some of the reaction must still be considered to be on the surface to explain the formation of Mn^{++} and the growth and decay of polarization in terms of an increase in the amount of lower oxide during current flow and its decrease when the circuit has been opened (62).

To decide between the two suggested locations of the reaction one may ask whether diffusion inward from the surface is fast enough to account for the reduction of MnO_2 during a discharge to an oxide of the composition $MnO_{1.5}$. Some recent experiments in the author's laboratory indicate that it is not, and we must assume with Brenet (42) and Naumann and Fink (57) that protons from the solution can penetrate to the interior of the oxide during a discharge.

There is a disagreement as to the valence of Mn in the solid primary product of the electrode reaction. Brenet (42) points to the instability of Mn^{+3} in solution and to the evidence that the final product, MnOOH, is composed of equal amounts of Mn(II) and Mn(IV), and prefers to assume that Mn^{++} [or $Mn(OH)_2$] within the oxide structure is the primary product. This eventually combines with an equivalent amount of MnO_2 to give MnOOH. Others (55, 56) have assumed the formation of a Mn(III) compound as the first step in the reduction. This may be followed by further reduction to Mn^{++}, especially on the surface, accounting for the large fall in potential during discharge.

There can be little doubt that Mn^{+3} is the first reduction product of Mn^{+4}, because the simultaneous entrance of two electrons into a Mn^{+4} ion is improbable. The question is whether this ion is stable on the surface of, or within, a MnO_2 structure or must be immediately reoxidized or reduced to Mn^{++}. While Mn^{+3} is unstable in solution, some of the Mn(III) complexes are quite stable. This is true, for example, of the pyrophosphate complex, which is soluble and sufficiently stable to be the reaction product in a precise titration (63). The bonds to oxygen joining the Mn to the complex must be somewhat similar to the bonds between Mn and O in the solid oxide.

Because there is a possibility of the stable existence of a Mn(IIII) oxide (or oxyhydroxide) on (or in) the MnO_2 it will be assumed in what follows that this is the primary product of the reduction of MnO_2. The discussion would be little different if $Mn(OH)_2$ were assumed.

The discharge mechanism.—A definite discharge mechanism can be formulated on the basis of the above experiments and conclusions. It is constructed to apply to electrodeposited MnO_2 on a graphite rod, but should be easily adaptable to a bobbin.

When current starts, electrons from the electrode and protons from the solution meet at the surface of the MnO_2 exposed to the solution and also beneath the surface, many of the protons penetrating the crystal lattice of the MnO_2. The electrons are retained by Mn atoms and the protons are attached to $O^=$ ions to form OH^- ions.

$$MnO_2 + H^+ + e^- \rightarrow MnOOH$$

The surface of the MnO_2 is very large, so the true current density is small, and with a concentrated electrolyte the ordinary concentration polarization is small. There is no evidence of appreciable activation polarization. However, as the surface composition changes from largely MnO_2 to one containing much MnOOH the electrode potential decreases. This decrease is slow because the surface is large and because much of the lower oxide is formed beneath the surface. There is in addition a diffusion toward the interior where there is less lower oxide. With γ-MnO_2 the decrease in potential is slower than with α-MnO_2 or with γ-MnO_2 that has been heated (29). It may be concluded that in α-MnO_2 and heated γ-MnO_2 the penetration of the protons is less than in the unheated γ-MnO_2, and consequently the surface gains lower oxide more rapidly.

When enough MnOOH has accumulated on the surface of the MnO_2 further reduction to $Mn(OH)_2$ takes place.

$$MnOOH + H^+ + e^- \rightarrow Mn(OH)_2$$

Then Mn^{++} appears in the electrolyte and as the surface is reduced further giving a larger surface concentration of Mn(II) the potential continues to fall.

The lower oxides on the surface will react with the electrolyte if the composition and *p*H are suitable. At *p*H 5 MnOOH can react.

$$2MnOOH + 2H^+ \rightarrow MnO_2 + Mn^{++} + 2H_2O$$

As the *p*H increases the surface must be further reduced to react appreciably.

$$Mn(OH)_2 + 2H^+ \rightarrow Mn^{++} + 2H_2O$$

These reactions are slow and do not come to equilibrium in short discharges (60). They are not dependent on current flow and continue after the circuit is broken. Therefore, more Mn^{++} is formed in an intermittent discharge than in a continuous one (56).

When after a period of discharge the circuit is broken, the excess lower oxide on the surface decreases fairly rapidly at first and then more and more slowly. Inward diffusion of the lower oxide takes place and if conditions are favorable the oxide also reacts with the electrolyte to give Mn^{++}. The potential therefore rises, but since the MnO_2 as a whole now contains less available oxygen than initially the potential never reattains the initial value.

A discharge terminates with a relatively rapid decrease in potential when the formation of reduction products on the surface is considerably faster than their disposal. What causes this condition is not clear. The only suggestion is that the lattice hardens and protons can no longer penetrate it (57).

Daniel-Bek (64) has presented a different theory to account for the polarization and recovery of the MnO_2 electrode. He observed that the potential of graphite or carbon in contact with NH_4Cl solution is very stable and is less than that of MnO_2. Also, a mixture of MnO_2 and carbon in contact with NH_4Cl solution has a smaller potential than MnO_2 alone. This was also observed by Jennings and Vosburgh (50). MnO_2 in contact with carbon and electrolyte is considered to constitute a short-circuited local cell. Such a cell is like a local cell on a metal surface, but with larger resistance in the electronic portion of the circuit. With the electrode as a whole on open circuit the current in the local cell is small because of polarization, but because of the appreciable resistance between MnO_2 and carbon the potential of the carbon is smaller than that of the MnO_2. Both are smaller than the true open-circuit potential of the MnO_2.

When the MnO_2 electrode is discharged the potential of the carbon decreases more than that of the MnO_2 and its surface (which is of low capacity) is partly discharged. The potential of the carbon determines the measured potential of the electrode as a whole. When the external circuit is broken the carbon must be recharged by the local-cell current before a steady state is reattained.

The theory of Daniel-Bek accounts qualitatively for the polarization and recovery of the MnO_2 electrode and is in accord with the effect on the electrode behavior of variation of the surface area of the carbon. It seems probable that both this and the theory based on the changes in composition of the MnO_2 will need to be taken into account in a complete theory of the MnO_2 electrode process.

A mechanism has been proposed by Cahoon and coworkers (55, 58) that differs somewhat from the one described above. They consider the MnO_2 to be reduced electrochemically directly to Mn^{++} which passes into solution. The Mn^{++} then reacts with MnO_2 to give MnOOH, or with MnO_2 and Zn^{++} to give hetaerolite. This is quite similar to the mechanism of Brenet (42). He considers that the electrochemical reaction is reduction to Mn^{++} within the MnO_2 lattice. The Mn^{++} passes into solution (but not necessarily immediately) and forms $Mn(OH)_2$ which is oxidized to MnOOH. More research is needed to reconcile the different theories that have been proposed.

Acknowledgment

The preparation of this paper was supported in part by the Office of Ordnance Research.

Manuscript received Feb. 25, 1959. This paper was prepared for delivery before the Ottawa Meeting, Sept. 28-Oct. 2, 1958.

Any discussion of this paper will appear in a Discussion Section to be published in the June 1960 JOURNAL.

REFERENCES

1. G. Leclanché, *LeMondes*, **16**, 532 (1868); *Compt. rend.*, **83**, 54 (1876).
2. G. W. Heise and N. C. Cahoon, *This Journal*, **99**, 179C (1952).
3. C. K. Morehouse, *ibid.*, **99**, 187C (1952).
4. W. S. Herbert, *ibid.*, **99**, 190C (1952).
5. A. D. Wadsley and A. Walkley, *Revs. Pure and Appl. Chem. (Australia)*, **1**, 203 (1951).
6. J. Brenet, *Bull. Soc. franc. mineral. et crist.*, **77**, 797 (1954).
7. W. Buser and P. Graf, *Helv. Chim. Acta*, **38**, 810 (1955).
8. A. M. Bystrom, *Acta Chem. Scand.*, **3**, 163 (1949).
9. A. D. Wadsley, *Acta Cryst.*, **6**, 433 (1953).
10. J. W. Gruner, *Am. Mineral.*, **28**, 497 (1943).
11. A. Bystrom and A. M. Bystrom, *Acta Cryst.*, **3**, 146 (1950).
12. A. D. Wadsley, *ibid.*, **5**, 676 (1952), **8**, 165 (1955).
13. W. M. Latimer, "Oxidation Potentials," 2nd ed., p. 238, Prentice-Hall, Inc., New York (1952).
14. W. F. Cole, A. D. Wadsley, and A. Walkley, *Trans. Electrochem. Soc.*, **92**, 133 (1947).
15. P. H. Delano, *Ind. Eng. Chem.*, **42**, 523 (1950).
16. H. F. McMurdie, *Trans. Electrochem. Soc.*, **86**, 313 (1944).
17. W. Buser, P. Graf, and W. Feitknecht, *Helv. Chim. Acta*, **37**, 2322 (1954).
18. S. Okada, I. Uei, and H. Chin, *J. Eletrochem. Soc. Japan*, **15**, 79 (1947).
19. I. Nakajima, *ibid.*, **21**, 369 (1953).
20. G. Butler and H. R. Thirsk, *Acta Cryst.*, **5**, 288 (1952).
21. K. H. Maxwell and H. R. Thirsk, Proc. 6th Meeting Intern. Comm. Electrochem., Thermodynam., and Kinet., **1955**, 390.
22. W. Feitknecht and W. Marti, *Helv. Chim. Acta*, **28**, 129, 149 (1945).
23. A. D. Wadsley, *J. Am. Chem. Soc.*, **72**, 1781 (1950).
24. G. Butler and H. R. Thirsk, *This Journal*, **100**, 297 (1953).
25. W. Buser and P. Graf, *Helv. Chim. Acta*, **38**, 810 (1955).
26. G. Brenet and A. M. Moussard-Briot, *Rev. gen elec.*, **61**, 405 (1952).
27. A. Kozawa and K. Sasaki, *J. Electrochem. Soc., Japan*, **22**, 569 (1954).
28. A. Kozawa, *This Journal*, **106**, 79 (1959).
29. A. Kozawa and W. C. Vosburgh, *ibid.*, **105**, 59 (1958).
30. W. Buser and P. Graf, *Helv. Chim. Acta*, **38**, 830 (1955).
31. J. Brenet and A. Herand, *Compt. rend.*, **230**, 1598 (1950).
32. B. Ghosh, *J. Chem. Soc.*, **1926**, 2605.
33. W. Biltz and O. Rahlfs, *Nachr. Ges. Wiss. Göttingen Geschaft., Mitt., Math-physik. Klasse* **1930**, 189. *Chem. Zentr.*, **102 I**, 45 (1931).
34. P. Jordon, *Helv. Chim. Acta*, **34**, 699 (1951).
35. K. Sasaki, *Mem. Fac. Eng. Nagoya Univ.*, **3**, 81 (1951).
36. P. W. Selwood, R. P. Eischens, M. Ellis, and K. Wethington, *J. Am. Chem. Soc.*, **71**, 3039 (1949).
37. R. Glicksman and C. K. Morehouse, *This Journal*, **103**, 149 (1956).
38. E. J. W. Verwey and J. H. de Boer, *Rec. trav. chim.*, **55**, 531 (1936).
39. J. Brenet, *Proc. Intern. Comm. Electrochem. Thermodynam. and Kinet. 7th Meeting, Lindaw 1955* (Pub. *1957*), p. 299.
40. T. E. Moore, M. Ellis, and P. W. Selwood, *J. Am. Chem. Soc.*, **72**, 856 (1950).
41. S. S. Bhatnagar, A. Cameron, E. H. Harbard, P. L. Kapur, A. King, and Bram Prakash, *J. Chem. Soc.*, **1939**, 1433.
42. J. Brenet, *Proc. Intern. Comm. Electrochem. Thermodynam. and Kinetics. 8th Meeting, Madrid, 1956.*
43. N. C. Cahoon, *Trans. Electrochem. Soc.*, **92**, 159 (1947).
44. N. C. Cahoon and G. W. Heise, *This Journal*, **94**, 218 (1948).
45. E. Divers, *Chem. News*, **46**, 259 (1882).
46. H. F. McMurdie, D. N. Craig, and G. W. Vinal, *Trans. Electrochem. Soc.*, **90**, 509 (1946).
47. L. C. Copeland and F. S. Griffith, *ibid.*, **89**, 495 (1946).
48. K. S. Krishnan and S. Banerjee, *Trans. Faraday Soc.*, **35**, 385 (1939).
49. A. Keller, *Z. Elektrochem.*, **37**, 342 (1931).
50. C. W. Jennings and W. C. Vosburgh, *This Journal*, **99**, 309 (1952).
51. D. T. Ferrell, Jr., and W. C. Vosburgh, *ibid.*, **98**, 334 (1951).
52. J. J. Coleman, *Trans. Electrochem. Soc.*, **90**, 545 (1946).
53. A. M. Chreitzberg, Jr., and W. C. Vosburgh, *This Journal*, **104**, 1 (1957).
54. P. D. Lukovtsev and S. A. Temerin, *Trudy Soveshchaniya Electrokhim. Acad. Nauk S.S.S.R., Otdel. Khim Nauk* **1950**, 494 (1953).
55. N. C. Cahoon, *This Journal*, **99**, 343 (1952).
56. A. M. Chreitzberg, Jr., D. R. Allenson, and W. C. Vosburgh, *ibid.*, **102**, 557 (1955).
57. K. Naumann and W. Fink, *Z. Elektrochem.*, **62**, 114 (1958).
58. N. C. Cahoon, R. S. Johnson, and M. P. Korver, *This Journal*, **105**, 296 (1958).
59. S. Yoshizawa and W. C. Vosburgh, *ibid.*, **104**, 399 (1957).
60. A. Sam, Ph.D. Thesis, Duke University, 1958.
61. W. C. Vosburgh, M. J. Pribble, A. Kozawa, and A. Sam, *This Journal*, **105**, 1 (1958).
62. J. Euler, *Z. Elektrochem.*, **60**, 1056 (1956).
63. J. J. Lingane and R. Karplus, *Ind. Eng. Chem., Anal. Ed.*, **18**, 191 (1946).
64. V. S. Daniel-Bek, *Trudy Soveshchaniya Elektrokhim. Akad. Nauk S.S.S.R., Otdel. Khim Nauk* **1950**, 513 (1953).

Brief Communication

Investigations on the Silver-Zinc Alkaline Storage Battery by the Aid of Radioactive Isotopes

Theodore Z. Palágyi

Central Research Institute for Chemistry, Hungarian Academy of Sciences, Budapest, Hungary

The failure of silver-zinc storage batteries is generally caused by the negative electrode, and less often by the separator or the positive electrode (1, 2). Both silver and zinc have isotopes with suitable hard gamma radiation and half-life of about ¾ year; consequently these isotopes can be used easily for labelling of electrodes. This fact induced us to employ Zn^{65} and Ag^{110} isotopes for the purpose of life tests and for investigating processes taking place during storage of the cells.

Our method was based on the hypothesis that, if Zn^{65} isotope is deposited on one of the negative plates of the cell, then the path of the ions while cycling can be followed by the aid of the radioactive contamination of the surface of the nonlabelled plates. The same principle was used to label with Ag^{110} isotope the positive electrode of experimental cells and to follow the path of the dissolved silver ions.

The experiments were performed with cells of 10 amp-hr nominal capacity. Both the zinc and the silver isotopes were deposited on the electrodes by electrolysis. The quantity of the deposited isotope was controlled partly by measuring the activity change of the electrolysis solution and partly by measuring the activity on the electrode itself, with a cylindrical GM-tube, as well as by the autoradiographic method.

The investigations were performed with cells assembled in three different ways: loosely, normally, and more tightly than normal. Each cell contained only one labelled (positive or negative) plate. After formation, some of the experimental cells were cycled and the others were subjected to storage. One charging-discharging cycle lasted 24 hr. After each tenth cycle a measuring discharge was performed.

As far as possible examinations were performed simultaneously on the cells assembled in the three different ways. The cells were opened after the first 20 cycles and after each 20 subsequent cycles, and the degree of contamination of the individual plates with isotope was examined. Then the electrodes were replaced in the cells and the cycling was continued, with the exception of the tightly assembled cells in which the electrodes could not be replaced.

On the basis of contamination with isotope of the nonlabelled electrodes, our experiments show that the zinc ions dissolved from the labelled negative plate can reach not only the other negative plates but the positive electrodes too. The degree of migration of the zinc ions considerably depends on the mode of building in of the electrodes and on the quantity of the electrolyte; in tightly assembled cells having little electrolyte the migration of the zinc ions is of lower degree. The failure of the loosely assembled cells was usually caused by coming to an end of the reversibility of the negative electrode as well as by the formation of acicular zinc crystals, resulting in short circuit. Failure of the tightly assembled cells was caused rather by the separator losing its insulating properties; moreover, the active material of the positive electrode dissolved and reached the negative electrode. Our investigations with Ag^{110} isotope related to this problem and to the storage of cells are still under way.

Manuscript received May 14, 1959.

Any discussion of this paper will appear in a Discussion Section to be published in the June 1960 JOURNAL.

REFERENCES

1. H. H. Bieber, P. F. Bruins, and H. P. Gregor, *Ind. Eng. Chem.*, **50**, 1273 (1958).
2. E. Zöld and L. Kiss, *Magy. Kém. F.*, **63**, 334 (1957).

THE ELECTROCHEMICAL SOCIETY, INC.

The Electrochemical Society is an international organization of individuals and companies concerned with or interested in Electrochemistry and allied subjects.

The Society is dedicated to the advancement of the theory and practice of Electrochemistry and related subjects, as shown in the following divisions:

Battery	Electro-Organic
Corrosion	Electrothermics and Metallurgy
Electric Insulation	Industrial Electrolytic
Electrodeposition	Theoretical Electrochemistry
Electronics	

Among the means to this end are the holding of meetings for the reading and discussion of professional and scientific papers on these subjects, the publication of such papers, discussions, and communications as may seem appropriate, and cooperation with chemical, electrical, and other scientific and technical societies.

It is an incorporated society without capital stock. The affairs of the Society are managed by a Board of Directors under a Constitution and Bylaws. Officers are nominated by a nominating committee appointed by the Board of Directors and elected by the members.

Direct all general correspondence and inquiries regarding membership to Society headquarters at 1860 Broadway, New York 23, N. Y.

Officers of the Society

President	W. C. GARDINER
Past President	SHERLOCK SWANN, JR.
Vice-President	R. A. SCHAEFER
Vice-President	H. B. LINFORD
Vice-President	F. L. LAQUE
Treasurer	L. I. GILBERTSON
Secretary	I. E. CAMPBELL

Current Affairs

Award of the Palladium Medal to A. N. Frumkin

A. N. Frumkin, 1959 Palladium Medalist

Aleksandr Naumovich Frumkin will receive the fifth impression of the Palladium Medal on October 18, 1959, at the Fall Meeting of The Electrochemical Society to be held in Columbus.

Professor Frumkin is a member of the Academy of Sciences of the U.S.S.R., Professor of Electrochemistry at the University of Moscow (a Chair held for twenty-five years), and Director of the Electrochemical Institute of the U.S.S.R. He is undisputedly the leading figure in electrochemistry at the present time and his influence is felt in practically all fields associated with electrified interfaces. His work has already been recognized by the Soviet Government, who have given him eleven awards between 1931 and 1955.

Frumkin's earliest work (about 1916) concerned the theory of adsorbed layers and equations of state for these films. His most well-known early paper is probably that on the effect of the electrokinetic potential on the concentration of hydroxonium ions in the Helmholtz double layer. He introduced, in this way, the relation between the structure of the electric double layer and the kinetics of reactions at electrified interfaces, a subject to which the major contributions have been made by the Russian school. Work from Frumkin's groups contributed much to the clarification of the nature of the potential of the electrocapillary maximum. Associated studies of the double layer capacity showed for the first time the vital necessity of creating clean surfaces in such studies. Studies of adsorption at the solid-solution interface were attempted (contact angle): this work gave rise to improved insight into the nature of wetting at the solid-solution interface.

The most extensive studies carried out by Frumkin relate to that central electrochemical reaction, the hydrogen evolution reaction, in which the rate-controlling proton discharge reaction on mercury from aqueous acid solutions was established with considerable certainty, and against appreciable opposition.

The theory of mixed electrodes was examined by Frumkin as early as 1941 and these studies contributed much to the understanding of current distribution at corroding materials.

Lastly, it must be pointed out that these very considerable achievements, selected from many others of comparable importance, concern only those contributed by Frumkin and those working under his immediate supervision. As Director of an Institute with about one hundred electrochemists studying fundamental problems (under Frumkin and a number of eminent electrochemists who assist in the supervision of the research), Frumkin has inspired the creation of a great outpouring of electrochemical studies from the Soviet Union, which have multiplied as the large numbers of co-workers who passed through his group fructified the work of other groups, both in research institutes and industry. In this connection, leading contributions have been made to the field of mass transport, corrosion inhibition, hydrogen embrittlement, wetting, flotation and batteries. Of the many electrochemists of international repute who have emanated from Frumkin's laboratory, a few of those best known in the West may be named as: Bagotsky, Burshstein, Erschler, Dolin, Jofa, Kabanov, Kolotyrkin, Levich, Levina, Lukovstev, Slygin, and Temkin.

At the age of sixty five, Frumkin is busily at his

work of directing research in Moscow and in the new Institute of Electrochemical Studies in Siberia. To those who have met him in recent years, it is clear that he is at the height of his powers.—J.O'M.B.

Columbus Meeting, October 18-22, 1959

C. L. Faust

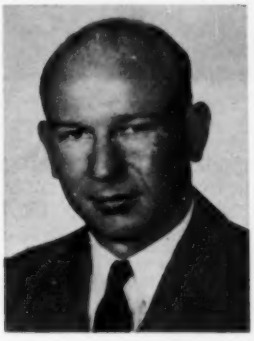

C. A. Snavely

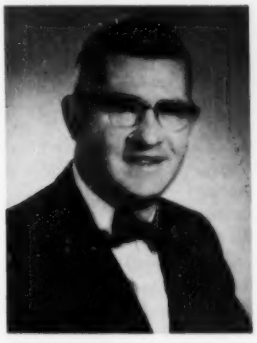

R. W. Hale

L. D. McGraw

The Fall Meeting of The Electrochemical Society will be held in Columbus, Ohio, from October 18 through 22, 1959. Headquarters will be at the Deshler Hilton Hotel with several sessions of the program at the nearby Neil House Hotel. The complete program appeared in the August JOURNAL, pp. 189C-213C.

The Columbus Section Committee arranging for the meeting is under the General Chairmanship of C. L. Faust. Those responsible for particular aspects are: Vice-Chairman and Hotel Arrangements, C. A. Snavely; Finance, R. W. Hale; Registration, L. D. McGraw; Entertainment, J. H. Winkler; Publicity, R. E. Durtschi; Tours, N. H. Keyser; Transportation, E. M. Sherwood; and Ladies' Program, Mrs. F. W. Fink.

Several events are planned for all registrants.

General Mixer

On Monday evening, October 19, an informal buffet supper will be held at Valley Dale Country Ballroom. Cocktails will be served before the buffet, and entertainment is planned for later in the evening. Special buses will leave the headquarters hotel at 5:45 P.M. and return after the entertainment.

Palladium Medal Address

The Palladium Medal Address by Professor A. N. Frumkin, Institute of Electrochemistry, the Academy of Sciences of U.S.S.R., Moscow, is scheduled for Tuesday, October 20, at 4:00 P.M. in the Ballroom, Deshler Hilton Hotel.

Reception and Banquet

The Palladium Medal Award Banquet is scheduled for Tuesday evening, October 20; cocktails will be served from 6:30 to 7:30 P.M. in the Ballroom Foyer. Professor A. N. Frumkin will receive the Award at the banquet.

Informal Buffet

The Wednesday evening feature will begin with cocktails in the Ballroom at 6:30 P.M., followed by a buffet supper and an informal program.

Division Luncheons and Business Meetings

Four Divisions have scheduled luncheon-business meetings at 12:15 P.M. as noted: Battery Division,

Aerial view of Columbus, looking northwest and showing the downtown area and outlying districts. In the background is the LeVeque Lincoln Tower; to the left, the Department of State Building; and, across the Scioto River, the Franklin County Veterans Memorial Building.

J. H. Winkler

R. E. Durtschi

N. H. Keyser

E. M. Sherwood

Tuesday, October 20, in Private Dining Room 10; Electro-Organic Division, Tuesday, October 20, in Room 307; Electrodeposition Division, Wednesday, October 21, in the Spanish Room; Corrosion Division, Thursday, October 22, at the Neil House in Mezzanine Parlor 4.

Plant Trips

Several interesting plant trips are planned for this meeting. Trips are scheduled to Industrial Nucleonics, and the Ohio State University Research Foundation. Also planned are inspection trips through the Battelle Memorial Institute Laboratories in Columbus, and Battelle's Nuclear Research Center located near Columbus.

Detailed information will be available at the registration desk. Please register early in the week for these trips, as attendance will be limited.

Ladies' Program

A program with the entertainment and comfort of the ladies in mind has been arranged.

A morning Coffee Hour at the Ladies' Headquarters, Rm. 212, will be a daily event from 10:00 to 11:00 A.M., except on Wednesday.

On Monday at 12:30 P.M., the ladies will be taken by bus to the Ohio Union on the Ohio State University campus where lunch will be served. After the luncheon, there will be a talk on flower arrangements followed by optional tours of the Ohio Union, the Ohio State Museum, and the Department of Horticulture.

Mrs. F. W. Fink

On Tuesday following a luncheon at 1:00 P.M. at the Columbus Athletic Club, the folk singing of Mrs. Anne Laylin Grimes will be enjoyed.

On Wednesday, October 21, buses will leave the Hotel at 10:00 A.M. to take the ladies to Ilanka's Provincial House, where they will partake of a complimentary brunch. A bus tour to the Ericson Glass Works at Bremen will start from there and occupy most of the afternoon.

Thursday, to top off the ladies' program, at 11:30 A.M. the ladies are invited to an informal sherry party at the home of the Chairman of the Ladies' Program, Mrs. F. W. Fink.

In addition to the preceding program, the ladies are cordially invited to all of the general functions.

Change in Committee Meeting Schedule

The meeting of the Membership Committee will be held on Monday, October 19, at 12:15 P.M., in the Private Sky Room, instead of Wednesday, October 21, at 5:00 P.M. in Private Dining Room 10 as listed in the August issue of the JOURNAL containing the Columbus Program.

Azariah Thomas Lincoln (1868-1958)

In a recent issue of the Journal,[1] it was announced that the Society had received a bequest from the estate of the late Azariah T. Lincoln. Since Professor Lincoln was 89 at the time of his death, March 31, 1958, there are probably very few members of our Society who are familiar with his work and accomplishments. The purpose of this article is to aquaint readers of the JOURNAL with the career of this long-time member (since 1902) of our Society.

Azariah T. Lincoln was a true son of Wisconsin. He was born in the small mining village of Montfort where he received his early schooling. He took County Teachers Examinations and earned successively the third, second, and first grade teacher's certificates.[2] He taught one year in a rural school and then secured a position as principal of a small village school. In order to work for the State Teacher's Certificate, he attended the University of Wisconsin for a year as a special student and again went back to teaching. He then passed the State Board examinations and secured the State Teacher's Certificate. A special interest in geology induced him to return to the university, and he graduated in June 1894 with a major in geology and a minor in chemistry. A position in geology was not available at that time so he returned to teaching. He did, however, spend the summers as an assistant in the chemical laboratory at the university and, as a result, he received a fellowship in chemistry. In his graduate work, he majored in chemistry and minored in mathematics and geology.

In June 1899, Lincoln received the first Ph.D. degree in chemistry ever awarded by the University of Wisconsin. His major professor was Dr. Louis Kahlenberg (1870-1941) who

[1] *This Journal*, **106**, 104C (1959).

[2] H. S. Van Klooster, *Rensselaer Polytech. Inst. Bull., Eng. Sci. Ser.*, No. 65, 1-8 (1951).

was President of our Society in 1930. In the 1890's, there was considerable controversy regarding the Arrhenius Theory of Electrolytic Dissociation and it is not surprising that the two publications resulting from Lincoln's doctoral research are titled "The Dissociative Power of Solvents"[3] and "The Electrical Conductivity of Non-aqueous Solutions."[4] Pyridine and various alcohols and aldehydes were some of the solvents used, and ferric chloride, silver nitrate, and antimony trichloride were among the solutes used. Lincoln concluded that the experimental results ". . . make it apparent that any theory that aims to explain electrical conductivity of solutions in general, must take into consideration the influence of the solvent on the dissolved substance."[4]

Dr. Lincoln's professional contributions were primarily in the field of education. His first position was that of private research assistant to Professor Wilder D. Bancroft at Cornell. He then taught general chemistry at the University of Cincinnati and, from 1903 to 1907, he was instructor and then assistant professor at the University of Illinois where he married Jennette Carpenter. In 1907, Dr. Lincoln joined the staff of Rensselaer Polytechnic Institute and, in his 14 years there, he helped with the organization of a four-year course in chemical engineering and taught various courses including physical chemistry and general chemistry.

A. T. Lincoln

In 1921, Dr. Lincoln accepted a position at Carleton College, Northfield, Minn., and, two years later, he became head of the chemistry department. During his career there, he had the satisfaction of seeing about 45 of his chemistry majors earn the Ph.D. degree in chemistry at 15 different graduate schools.[5] Dr. Lincoln retired in 1939 but continued to reside in Northfield. He established a small business manufacturing plastic shrub and plant markers and a weather-resistant indelible ink.[5] In May 1950, he lectured to the Wisconsin Section of the American Chemical Society on "Researches in Chemistry at the Turn of the Century." Among Dr. Lincoln's list of about 25 publications[2] are the following books: "A Textbook of Physical Chemistry," "General Chemistry," "Laboratory Manual of General Chemistry," and "Exercises in Elementary Quantitative Chemical Analysis."

—M. L. Holt

[3] L. Kahlenberg and A. T. Lincoln, *J. Phys. Chem.*, 3, 12 (1899).
[4] A. T. Lincoln, *ibid.*, 3, 457 (1899).

Power for Outer Space is Featured in Thirteenth Annual Power Sources Conference

More than 1000 representatives of the power sources industry attended the Thirteenth Annual Power Sources Conference at Atlantic City, N. J., on April 28, 29, and 30, 1959. Because much of the material discussed is not readily available elsewhere, a fairly complete summary of the meeting is being given here.

Each year, under the direction of Mr. Arthur F. Daniel, director, and Mr. David Linden, deputy director, Power Sources Division, the U. S. Army Signal R&D Laboratory, Fort Monmouth, N. J., sponsors this conference, at which progress on battery research and development is presented to representatives of government, industry, universities, and foreign governments. Session chairmen during the three-day conference were: Mr. Upton B. Thomas, Bell Telephone Laboratories; Mr. Sidney J. Magrum, Army Research Office; Mr. Arthur F. Daniel, Col. Leon J. D. Rouge, Mr. W. L. Doxey, Mr. David Linden, Mr. Charles H. Clark, Dr. Adolph Fischbach, USASRDL.

The opening paper was given by Mr. Nelson W. Snyder, Advanced Research Projects Agency, who stated that entirely new ideas or new concepts, either based on what is already known in science or what is yet to be discovered, will increase the number of possibilities of power systems for space. Applied scientists in industry and in universities must help in developing new materials, new concepts, new theories, and interpret the voluminous, complex information that is flowing from the pens of fundamental scientists. We are searching for methods to perform tasks that are far beyond our present experience.

During the session on nuclear energy sources, Mr. William Crane, The Martin Co., spoke on the utilization of waste fission products as a source of energy. He reported that, in 1956, the radioisotope sales by the U. S. Atomic Energy Commission amounted to only 16,000 curies, but it is predicted that by 1975 twelve billion curies of fission products, amounting to 50 mw of power, will be lost unless a method is developed to use these products. Practical applications for these waste products can be developed in the next year which will use safely all of the Sr-90 and prometheum produced in today's reactors. A 100 w electrical power unit has been designed that operates at an over-all efficiency of 5% for the conversion of heat to electrical energy. Calculations indicate that such power packs can be built today with the Sr-90 available, in size from 5 to 500 w of electrical energy. The development of a coplanar electron tube has made possible the application of heat directly to the cathode to supply the heat necessary for operation of the tube. This application of heat directly to the cathode avoids the useless cycle of taking the heat generated by the isotope, converting it to electricity, at the loss of 90% of the energy. The direct use of thermal energy minimizes power requirements of equipment and reduces the quantity and cost of the isotopes used. Another and more conventional application of isotopic heat is the use of this thermal energy to winterize equipment for arctic use.

Dr. Emil Kittl, USASRDL, spoke on "Design Considerations for Nuclear Power sources," and the role that thermonuclear batteries will play in filling the existing gap between short-life, high-power-rate chemical batteries and extreme long-life, low-power-rate solar batteries.

Among those who presented papers during the symposium on thermal energy conversion was Mr. A. D. Steele, Minnesota Mining and Manufacturing Co., who reported that ef-

fort is being directed to develop the use of radioisotope heat in conjunction with static energy conversion devices. This device, a thermoelectric generator, operates rather simply. Heat is created by the capture, in a small, cylindrical metal container, of the alpha particle emitted by polonium 210. The semiconductor thermoelectric conversion p- and n-type elements connected in series extend radially away from the fuel container to cold junctions along the inside of the outer shell of the device. A Seebeck electromotive force is generated at the cold junctions of each couple, all of which are connected in series. The outer container serves as the radiator. The experience gained seems to indicate that the joining of thermoelectricity and nuclear energy will be practical.

Dr. Clarence M. Zener, Westinghouse Electric Corp., described a procedure for computing the thermal efficiency of a thermoelectric generator. Based on this procedure and certain design considerations, he believes that thermal efficiencies to 35% will be achieved with a three-stage thermal electric generator within the foreseeable future.

The final speaker during this symposium was Mr. Robert J. Denington, Thompson Products, Inc. He stated that mercury vapor cycle engines operating at 1200°F are particularly light in weight and will be less than 10 lb/kw output for plants larger than 200 kw without shielding. Increasing temperatures for the mercury engine or using a rubidium cycle engine at 1800°F or above would make 7 lb/kw attainable, and lightweight radiator designs would yield a similar result.

The afternoon session on the first day was devoted to solar energy sources. Mr. George Hunrath, USASRDL, discussed in detail the investigation of a solar energy conversion system utilizing the silicon p-n junction type photovoltaic cell, and electrochemical storage batteries for possible use in space vehicles. It is seen that a blocking diode is necessary to prevent any parallel groups of cells which are on the dark side of the satellite from loading down the illuminated groups and to prevent the battery from discharging into the groups of cells when the satellite is in the dark region of the orbit. The transmission losses through clear and sandblasted windows, intended for use as protective covers of solar cells, were determined. Results indicate a 6.5% loss through a clear window and a 20% loss through a sandblasted window. Data show that, as the cell temperature increases above 25°C (reference point), there is a loss in cell voltage at the rate of 1.9 mv/°C. There is also a loss in output power at the rate of 0.48%/°C. This latter figure has been found to vary somewhat with different cells. Conclusions drawn from a radiation damage study show that the only radiations which produced observable damage were 2 mev electrons, 20 mev protons, and 40 mev alpha particles. The total flux required to reduce the output of the cell to 75% of its initial value was very high.

Mr. Joseph J. Loferski, Radio Corp. of America, reported on a program designed to investigate potentially better semiconductor materials for p-n junction photovoltaic solar cells. The work has been concentrated on GaAs, with some parallel work continuing in InP. The maximum efficiency (ratio of output electrical power to input solar power) actually attained in GaAs cells lies between 5 and 6% for cells whose area is a few tenths of a square centimeter.

Mr. William Cherry, USASRDL, followed Mr. Loferski and discussed large area solar cells and stated that silicon, by far the most developed cell to date, is being produced in large quantities with efficiencies of 10% and greater with areas of 2 cm^2. Some individual cells have shown efficiencies in excess of 14% and it is anticipated that eventually production quantities of 15% efficient cells will become available. The solar converter of the future might be described as a "photovoltaic rug" and measure several square feet in area. An insulating substrate, such as spun glass or plastic, would have plated metallic contacts around each end. First an n-type semiconductor base material a few microns thick is evaporated, sprayed, or painted on the surface with appropriate masking, making contact to one of the metallic contacts but not the other. Next, a p-type film is laid down over the n-film, but this time contact is made to the opposite metallic film only. To improve carrier collection efficiency and reduce series resistance, ohmic contact strips must be made to the p-type or solar exposed surface. Holes drilled through the end metallic films and fasteners used in conjunction with metallic shorting bars enable the connection of the "rugs" in series and/or parallel. Such a system can be rolled for ease of transportation or ejecting into outer space, then spread out on the ground, on roofs, or above the atmosphere.

Dr. M. E. Lasser, Philco Corp., reported that recent studies on photogalvanic batteries indicate that both the method of preparation of Ag—Ag halide electrodes and the composition of the adjacent electrolyte are the major factors determining the rate of recombination of the photochemical reaction products. Under the optimum conditions found thus far, photogalvanic currents equivalent to quantum yields of 2 to 5% could be obtained. Experimental cells consisted of one bare Pt electrode and one thin Pt sheet covered with solidified melts of AgCl or AgBr about 5 to 20 μ thick immersed in a solution of 0.01M Fe^{++} +0.001M Fe^{+3} in 0.1M HCl or HBr, repsectively. Upon illumination, the Pt-AgCl or Pt-AgBr electrodes behave like Ag electrodes provided that proper care is taken in the electrode preparation to reduce the porosity of the melt and to avoid undesirable impurities.

The final speaker on the first day was Dr. Maria Telkes, Curtiss-Wright

Brief Communications

The JOURNAL accepts short technical reports having unusual importance or timely interest, where speed of publication is a consideration. The communication may summarize results of important research justifying announcement before such time as a more detailed manuscript can be published. Consideration also will be given to reports of significant unfinished research which the author cannot pursue further, but the results of which are of potential use to others. Comments on papers already published in the JOURNAL should be reserved for the Discussion Section published biannually.

Submit communications in triplicate, typewritten double-spaced, to the Editor, Journal of The Electrochemical Society, 1860 Broadway, New York 23, N. Y.

Corp., who discussed the collection and concentration of solar energy for thermal applications, and reported that "selective black" coatings have been developed recently which absorb the rays of the sun, but are completely transparent or reflective in the range longer than 2.5 μ. In this way, thermal re-radiation can be diminished. Flat-plate solar heat collectors have been constructed and evaluated for heating water. These collectors use black plates with water circulating pipes attached to them, contained in a well-insulated box and covered by glass panes. One glass pane of the best quality "water white" glass reflects about 8%, absorbs 2%, and transmits 90% solar energy at optimum incidence. Recently developed plastics containing fluorine, such as trithene or teslar, transmit 95% solar radiation. Considerable work has been carried out with spherical parabolic reflectors. Practical concentration ratios in excess of 10,000 can be obtained, approaching a theoretical possible efficiency of 60 to 70%.

Secondary batteries were discussed at the opening session on the second day. Using cathodes consisting of porous nickel or cadmium plaques, Dr. Von Dohren, Accumulatoren Fabrik A. G., was able to determine the dependence of the rate of oxygen reduction on the oxygen pressure and the applied potential. In all experiments, an immobilized electrolyte was used and the temperature was kept constant. At constant potential, a linear relationship of the rate of oxygen reduction with pressure was found in the pressure range of 2 to 7 kg/cm^2. At constant pressure, the O_2 reduction rate increases, when more negative cathodic potentials are applied. Electrodes containing cadmium show distinct steps in the rate of O_2 reduction at the $Cd/Cd(OH)_2$ potential, which is due to a compact layer-formation of cadmium hydroxide. With electrodes containing both cadmium and nickel, the method used by Dr. Von Dohren allows a discrimination between the different fractions of the effective surfaces of both components at which the reduction takes place. Electrodes containing metallic cadmium will furnish the necessary electrons for the O_2 reduction on its own, forming $Cd(OH)_2$ in equivalent amounts, and for this reaction no external current is necessary.

Mr. A. W. Speyers, Vitro Laboratories, stated that three types of alkaline battery testers have been developed successfully. One of these testers is designed for field use to indicate the state-of-charge of either the type BB401/U or the BB406/U nickel cadmium battery. Initially, these batteries are discharged at a fixed rate, for a period of 24 sec, followed by a controlled charge for 84 sec, and then a 12-sec discharge. The rated discharge voltage of the BB401/U is 28 v, while the BB406/U is 20 v. Tests on the BB401/U battery indicate the optimum currents are 10 amp discharge and 5 amp charge in order to detect batteries that are not 100% charged.

Notice to Members and Subscribers
(Re Changes of Address)

To insure receipt of each issue of the JOURNAL, please be sure to give us your old address, as well as your new one, when you move. Our records are filed by states and cities, not by individual names. The Post Office does not forward magazines.

Dr. Herbert Hunger, USASRDL, opened the afternoon session on fuel cell batteries. He gave a general review of the status of fuel cells, and pointed out their potentialities and the variety of their problems. According to Dr. Hunger, a broad area of application both military and industrial is open for the continuously fed battery or fuel cell, ranging from portable electrical power sources to space sources, and its commercial applications seem to be closer than ever before.

Dr. G. E. Evans, National Carbon Co. Research Laboratories, stated that progress in electrode preparation can be summarized by pointing out that present fuel cells show better voltage-current curves at atmospheric pressure than was achieved a year ago at 150 psig. Another major breakthrough has been the improvement in low-temperature performance. Cells have been produced which yield useful power down to about 20°C, so that batteries can now heat themselves from normal room temperature up to the preferred range of 50° to 70°C. The open circuit voltage for recent cells is about 1.1 v compared to a voltage of 0.5 v at 40 ma/cm^2 a year ago.

The redox cell appears to be close to practical exploitation for military applications in the near future, and later for commercial applications, according to Dr. Max L. Feldman, General Electric Co. A cell system was operated continuously for a period of 16 days in various modes of discharge and charge. The maximum power was slightly over 100 w, although the voltage efficiency was rather poor due to the high internal resistance of the cells.

A second redox type of fuel cell battery was reported on by Dr. M. Eisenberg, Lockheed Aircraft Corp. Dr. Eisenberg stated that, on the basis of theoretical kinetic considerations, three fundamental criteria are given for the selection of suitable redox couples and of their combinations for the design of electrochemical fuel cells: 1. couples should have a large difference in their respective equilibrium potential values; 2. each of the redox couples should have an inherently high exchange current density, i_o, in order to minimize chemical polarization losses; 3. the couples (and the supporting electrolyte systems) should have large ionic diffusion coefficients, and low kinematic viscosities to enable the achievement of high rates of mass transfer for a given cell geometry and mode of convection. Under these conditions, the desirable high limiting current densities and low concentration polarization values should be obtained.

At the morning session on the final day, primary batteries were discussed. Mr. John Hovendon, USASRDL, reported on a program involving the battery fabrication and testing facilities of four members of the battery industry and the test facilities at USASRDL. The objectives of this program are to ascertain the present "state of the art" and the individual company's capability regarding the manufacture of paper-lined dry cell batteries; and to obtain characteristic performance data of sufficient magnitude to permit a sound statistical analysis and evaluation to support subsequent adoption of this structure as a standard item for military procurement. At USASRDL, it was found that the average capacity retention for all batteries tested after three months' storage at 113°F—50% R. H. is 93%; after twelve months' storage at 70°F —50% R. H., capacity retention is 89%. Additional study must be applied to the Leclanché system in order to realize its full capacity, but there is little doubt that, within a short time, the shelf life of this battery will be quoted as three to five years with 90% capacity maintenance.

The next paper was presented by Mr. John Paulson, Ray-O-Vac Co., who spoke of the development of a BA-2270/U battery of the Leclanché type in which a flat cell construction was employed. Current work has been directed toward the construc-

tion of test lots of this battery on a pilot line scale. This battery is made up from multiple-cell strips which are accordion-folded and assembled into one stack to form the completed battery. The A-section cells are all connected in parallel to give a nominal 1.5 v. The B-section cells are in series, the section having 45- and 90-v taps. The A-section anodes are connected in parallel by means of a ribbon of metal foil. The mix cakes for the A and B_1 sections are tamped, while the much thinner cakes for the B_2 section are formed by coating the wet mix onto a woven supporting screen. Initial capacities in both the A and B sections are 8+ hr. An accelerated shelf test is conducted at 113°F for one month at which time the battery is tested at —40°F. Results of this test indicate capacities to around 60% of initial.

Mr. R. Glicksman, Radio Corp. of America, discussed a research and development program to develop improved primary batteries utilizing organic compounds as the active electrode components. Of the various heterocyclic nitro compounds studied, the nitropyridines appear to be the most promising. In general, it was found that nitropyridine compounds operate at potentials 0.05-0.15 v higher than their corresponding nitrobenzene derivatives and have comparable electrode efficiencies. When these heterocyclic nitro compounds are coupled with a magnesium anode, dry cells can be made which have higher cell operating voltages than the magnesium-nitrobenzene cells. In addition, the favorable half-cell potential discharge curve of compounds such as 4-nitropyridine in NaOH electrolyte indicates the possibility of using these cathode materials with a zinc anode to form a practical dry cell couple.

The final session of the three-day conference was devoted to high-rate batteries. Mr. Charles E. Bowland, Gulton Industries, discussed the development of a battery voltage regulator that can be used with high-rate batteries that is a transistorized package to work in conjunction with batteries to maintain a fairly constant line voltage over a wide range of input voltages and temperature, while being subjected to shock and vibration. With a battery supply voltage that drops off as much as 20-30%, outputs can be maintained within ±2% of nominal. The output of the battery is connected to the voltage regulator which is in series with the load. As the output voltage begins to decay from nominal, a sensing circuit, composed of temperature-stabilized Zener diodes, detects this change and sends an error signal to the regulator which adds voltage to the output, reducing the error to zero. This approach has proved extremely successful and has given the battery a considerably longer useful life. Extremely efficient, values in excess of 90% are standard with power levels up to 115 w.

Mr. Kenneth R. Scribner, Eastman Kodak Co., discussed the subject of ammonia chemistry and outlined the ammonia battery concept in general. Due to the lack of available literature, Eastman Kodak has been conducting its own research program in the field of ammonia chemistry necessary to a battery development program. The choice of electrochemical constituents which will produce a practical battery in the ammonia system is as wide, if not wider, as that in the aqueous system. Combinations of constituents and variations in the mechanical parameters of cell construction, such as salt concentration, type of separators, and others, have allowed the assembly of a variety of batteries differing widely in their size, configuration, and rate of discharge.

The concluding results of the reliability program for Battery BA-472-( )/U were given by Mr. Nicholas Wilburn, USASRDL. The modified test to failure program conducted for this battery has many advantages. Its total cost was relatively low. Each component of the battery has large environmental safety factors to provide for emergencies where the specified environmental stresses may be exceeded; and the use of qualified components in other batteries leads to the ideal situation where each succeeding reliability program, involving a given basic design, becomes simpler, less costly, and faster to perform. These demonstrated advantages lend much support to the selection of the modified test-to-failure concept for the development of reliable batteries or any other missile component.

Mr. Martin Klein, USASRDL, made the first public disclosure of the principles of a device for the movement of electrolyte in automatically activated batteries by pressure differential. This device is applicable for all reserve-type batteries using liquid electrolyte. The development of these devices is expected to overcome the present problems of weight and volume, low heater efficiency, and permit optimum operation of extremely high electrolyte velocity. In principle, the proposed devices will have all of the characteristics of the ideal automatic activating device. In the new device, the electrolyte is maintained in the reservoir under the pressurized inert gas, and activation is accomplished by opening an electrolyte path to the battery either manually or remotely by an electrically activated diaphragm. The electrolyte will then be pushed down uniformly by the expanding gas into the battery. The electrolyte velocity will be dependent upon the size of the orifice, the ratio of the initial gas and electrolyte volume, and upon the initial gas pressure. Either slow or

Manuscripts and Abstracts for Spring 1960 Meeting

Papers are now being solicited for the Spring Meeting of the Society, to be held at the Lasalle Hotel in Chicago, Ill., May 1, 2, 3, 4, and 5, 1960. Technical sessions probably will be scheduled on Electric Insulation (including a Symposium on "Electrolytic Capacitors"), Electronics (including Luminescence and Semiconductors), Electrothermics and Metallurgy (including a symposium on "High-Purity Vanadium" and a round table on "Methods of Reducing Iron Ores"), Industrial Electrolytics, and Theoretical Electrochemistry.

To be considered for this meeting, triplicate copies of abstracts (*not exceeding 75 words in length*) must be received at Society Headquarters, 1860 Broadway, New York 23, N. Y., *not later than January 4, 1960. Please indicate on abstract for which Division's symposium the paper is to be scheduled, and underline the name of the author who will present the paper.* Complete manuscripts should be sent in triplicate to the Managing Editor of the JOURNAL at the same address.

* * *

The Fall 1960 Meeting will be held in Houston, Texas, October 9, 10, 11, 12, and 13, 1960, at the Shamrock Hotel. Sessions will be announced in a later issue.

rapid activation should be possible. The geometrical shape of the reservoir will have practically no effect on the operation of the system. One method for heating these batteries is to place the heating elements for activating the battery directly in the electrolyte where all of the heat may be absorbed by the electrolyte.

Mr. C. F. Gerhan, Willard Storage Battery Division, stated that the inherent advantages of the zinc-silver oxide battery can be expanded by providing the basic battery with an automatically activating device. This device can incorporate a low-pressure system which will rapidly and uniformly fill the battery, changing it from a completely dormant state to a fully active state in less than one tenth of a second. Low-pressure batteries held in ambient temperatures of 160°F over a period of a year show less loss in voltage or capacity at high discharge rates than similar batteries contained in atmospheric pressure. Activation characteristics were not materially changed during this stand.

The final speaker of the three-day session was Dr. D. T. Ferrell, American Machine and Foundry Co., who discussed chemically heated batteries. In the chemically heated battery, all of the heat is introduced via the electrolyte, and no attempt is made to heat the battery pack directly. The electrolyte is heated as it passes through a heat exchanger interposed between the electrolyte reservoir and the battery pack. The heat exchanger is simply a length of copper tubing surrounded by a chemical heat powder. The heat powder is ignited by electric matches which, with a series wired thermostat, are connected in parallel with the activating squibs. At temperatures where heat is required, the thermostat is closed and the heat powder is ignited simultaneously with the activating squibs. The electrolyte passes through the hot copper tubing and is heated sufficiently to bring the battery pack to operating temperature. At temperatures where heat is not required, the thermostat is open and the heat powder is not ignited. Several batteries have been designed to employ this method of heating and some are in production. Two of these battery types each weigh 12 lb and occupy a volume of 186 cu in., deliver 5 amp-hr at 28 ± 4 v and are tapped at 7 v. Design discharge current is 20 amp; satisfactory performance is obtained from 5 to 60 amp. Over the temperature range from −65° to +165°F, activation occurs within 6 sec. Another battery is now under development to demonstrate the feasibility of 1-sec activation at −40°F.

Division News

E & M Round Table on Methods of Reducing Iron Ores, Spring 1960

The Electrothermics and Metallurgy Division of the Society proposes to hold a round-table conference on the timely subject "Methods of Reducing Iron Ores" at the Spring 1960 Meeting of the Society to be held in Chicago, May 1-5. The purpose of the conference is to compare the various nonelectric methods of reducing typical iron ores with one another, and with electric smelting methods.

The conference will consist of:

1. A number of formal papers, each one by a specialist in one particular type of reduction
2. A general discussion of the subject.

R. R. Rogers, Mines Branch, Dept. of Mines & Technical Surveys, 552 Booth St., Ottawa, Ont., Canada, would be glad to receive suggestions as to the types of iron ore to be discussed, the types of reduction which should be covered in the formal papers, and specialists who would be qualified to discuss these particular types of reduction.

E & M Symposium on High-Purity Vanadium, Spring 1960

Papers on the subject "High-Purity Vanadium—Its Preparation, Properties, and Alloys" are being solicited by the Electrothermics and Metallurgy Division of the Society for a symposium, under the Co-Chairmanship of D. J. Hansen and M. Schussler of Union Carbide Metals Co., at the Spring Meeting of the Society in Chicago, May 1-5, 1960.

Topics on which contributions will be welcomed include:

- Resources of Vanadium Minerals—Domestic and Foreign
- Mining and Beneficiation of Vanadium Minerals
- Techniques for Reduction to High-Purity Metal
- Consolidation and Fabrication Techniques
- Properties of Alloys Based on High-Purity Vanadium
- Applications for Ductile Vanadium and Its Alloys.

Availability of ductile vanadium has stimulated exploratory work on its properties and potential uses in many laboratories. If enough of this information is presented at the symposium to warrant separate publication, the Division will sponsor preparation of a booklet containing the papers and discussion.

Titles, authors' names, and abstracts in triplicate (*not exceeding 75 words*) must be received at Society Headquarters, 1860 Broadway, New York 23, N. Y., *by January 4, 1960*. Abstracts should bear the notation "For Vanadium Symposium, Spring 1960," and the name of the author who will present the paper should be underlined. Complete manuscripts, ready for publication in all details, must be given to the Symposium Chairman immediately following presentation.

E & M Symposium on Rhenium, Spring 1960

The Electrothermics and Metallurgy Division is inviting papers on various aspects of rhenium technology to be combined into a symposium for the Spring Meeting in Chicago, May 1-5, 1960. Bruce W. Gonser of Battelle Memorial Institute is Chairman of this symposium.

Although emphasis may be given to the extractive and physical metallurgy of rhenium, a broader coverage is planned. In particular, papers are desired that cover recent investigations on properties, alloys, and development of applications.

Rhenium is relatively expensive, but in recent years excellent sources of supply have been developed which are far in excess of current consumption. Some excellent and unique properties indicate that more rhenium could be used advantageously if it were better known.

Titles, authors' names, and abstracts in triplicate (*not exceeding 75 words*) must be received at Society Headquarters, 1860 Broadway, New York 23, N. Y., *by January 4, 1960*. Abstracts should bear the notation "For Rhenium Symposium, Spring 1960," and the name of the author who will present the paper should be underlined. Complete manuscripts, ready for publication in all details, must be given to the Symposium Chairman immediately following presentation.

Officers of Local Sections of The Electrochemical Society

Council of Local Sections (1959-1960)
K. S. Willson, Chairman
3785 W. 33 St., Cleveland 9, Ohio
A. J. Cornish, Vice-Chairman
J. C. White, Secretary
C. A. Hampel† (1958-1960)
M. F. Quaely† (1959-1961)

Boston (Spring 1959-1960)
H. C. Gatos, Chairman
Lincoln Lab., Mass. Institute of Technology, Lexington 73, Mass.
H. H. Homer, Vice-Chairman
H. L. Creamer, Treasurer
Charles Levy* (1959-1960)
L. B. Rogers* (1958-1960)

Chicago (Spring 1959-1960)
J. Kuderna, Chairman
Automatic Electric Co., Northlake, Ill.
J. Miller, Vice-Chairman
R. Wehrmann, Treasurer
R. Chelton, Secretary
E. L. Koehler*
C. A. Hampel*

Cleveland (Spring 1959-1960)
F. A. Shirland, Chairman
Harshaw Chemical Co., 1945 E. 97 St., Cleveland 6, Ohio
R. A. Powers, Vice-Chairman
R. C. Griffis, Treasurer
J. F. Yeager, Secretary

Columbus (Fall 1958-1959)
F. W. Fink, Acting Chairman
Corrosion Research Div., Battelle Memorial Institute, Columbus 1, Ohio
R. W. Hale, Sec.-Treas.
C. A. Snavely*

Detroit (Spring 1959-1960)
A. E. Remick, Chairman
Dept. of Chemistry, Wayne State University, Detroit 2, Mich.
Manuel Shaw, 1st Vice-Chairman
J. P. Hoare, 2nd Vice-Chairman
S. E. Beacom, Sec-Treas.
Frank Passal*
Henry Brown*

†Council Representative on Board of Directors.
* Representative on Council of Local Sections.

India (Spring 1959-1960)
M. S. Thacker, Chairman
Council of Scientific & Industrial Research, Old Mill Rd., New Delhi 2, India
A. Jogarao, Vice-Chairman
N. R. Srinivasan, Vice-Chairman
S. Krishnamurthy, Sec.-Treas.

Indianapolis (Spring 1959-1960)
A. M. Max, Chairman
5640 Guilford Ave., Indianapolis 20, Ind.
R. R. Haberecht, Vice-Chairman
T. C. O'Nan, Sec.-Treas.
J. M. Booe*
F. C. Mathers*

Midland (Spring 1959-1960)
R. S. Karpiuk, Chairman
4608 Bristol Court, Midland, Mich.
M. R. Bothwell, Vice-Chairman
D. Chapin, Sec.-Treas.
P. F. George*

Mohawk-Hudson (Spring 1959-1960)
W. H. Smith, Chairman
Metallurgy & Ceramics Research Dept., General Electric Co., P. O. Box 1088, Schenectady, N. Y.
D. A. Vermilyea, Vice-Chairman
R. J. Stamets, Sec.-Treas.
W. E. Tragert*
J. R. Rairden*

New York Metropolitan (Spring 1959-1960)
Frances S. Lang, Chairman
Box 263, Whitehouse Station, N. J.
P. L. Howard, Vice-Chairman
R. A. Glicksman, Sec.-Treas.
M. F. Quaely*
A. C. Loonam*

Niagara Falls (Spring 1958-1959)
Karl Kunkel, Chairman
Hooker Chemical Corp.
Buffalo Ave. & 47 St.,
Niagara Falls, N. Y.
S. W. Scott, Vice-Chairman
D. J. Hansen, Sec.-Treas.

Ontario-Quebec (Spring 1958-1959)
John Convey, Honorary Chairman
H. A. Timm, Chairman
Dominion Magnesium Ltd., Haley, Ont., Canada
L. G. Henry, Vice-Chairman (Membership)
R. P. Bailey, Sec.-Treas.
L. G. Henry* (1957-1959)

Pacific Northwest (Spring 1958-Oct. 1959)
H. J. Wittrock, Chairman
Kaiser Aluminum & Chemical Corp., Spokane 69, Wash.
G. C. Ware, Vice-Chairman
Lawrence Young, Sec.-Treas.

Philadelphia (Spring 1959-1960)
G. W. Bodamer, Chairman
Rohm & Haas Co., 5000 Richmond St., Philadelphia 37, Pa.
K. A. Krieger, Vice-Chairman
A. A. Ware, Treasurer
H. C. Mandell, Jr., Secretary

Pittsburgh (Spring 1958-1959)
E. H. Phelps, Chairman
Applied Research Lab., U. S. Steel Corp., Pittsburgh, Pa.
J. W. Faust, Jr., Vice-Chairman
W. E. Haupin, Sec-Treas.
J. J. Stokes, Jr.*
A. J. Cornish*

San Francisco (Spring 1959-1960)
R. A. Zimmerly, Chairman
Columbia-Geneva Steel Div., U. S. Steel Corp., Pittsburg, Calif.
R. E. DeLaRue, Jr., Vice-Chairman
S. H. Dreisbach, Treasurer
H. F. Stout, Secretary
R. F. Bechtold* (1959-1961)
Morris Feinleib* (1959-1960)

Southern California-Nevada (Spring 1959-1960)
M. Schwartz, Chairman
3017 Oakhurst Ave., Los Angeles 34, Calif.
M. E. Carlisle, Vice-Chairman
G. A. Larchian, Sec.-Treas.
W. M. Hetherington*

Washington-Baltimore (Spring 1959-1960)
David Schlain, Chairman
P. O. Box 348, College Park, Md.
Jerome Kruger, Vice-Chairman
Sigmund Schuldiner, Treasurer
R. J. Brodd, Secretary
J. C. White*
Ralph Roberts*

Officers of Divisions of the Society

Battery (Fall 1958-1960)
J. C. White, Chairman
4205 Woodberry St., University Park, Hyattsville, Md.
E. J. Ritchie, Vice-Chairman
C. H. Clark, Sec.-Treas.

Corrosion (Fall 1958-1959)
M. A. Streicher, Chairman
1206 Winstead Rd., Mayfield, Wilmington, Del.
R. T. Foley, Vice-Chairman
Milton Stern, Sec.-Treas.

Electric Insulation
(Spring 1959-1960)
A. J. Sherburne, Chairman
1770 Wendell Ave., Schenectady, N. Y.
T. D. Callinan, Vice-Chairman
C. C. Houtz, Sec.-Treas.

Electrodeposition (Fall 1958-1960)
Abner Brenner, Chairman
National Bureau of Standards, Washington 25, D. C.
D. G. Foulke, Vice-Chairman
D. R. Turner, Sec.-Treas.

Electronics (Spring 1959-1961)
M. F. Quaely, Chairman
88 Mt. Hebron Rd., Montclair, N. J.
J. S. Prener, Vice-Chairman
(Luminescence)
P. H. Keck, Vice-Chairman
(Semiconductors)
A. E. Martin, Vice-Chairman
(General Electronics)
A. E. Hardy, Sec.-Treas.

Electro-Organic (Fall 1958-1960)
Garrett Thiessen, Chairman
408 N. 10 St., Monmouth, Ill.
Milton Allen, Vice-Chairman
R. A. Day, Jr., Sec.-Treas.

Electrothermics and Metallurgy
(Spring 1959-1961)
G. M. Butler, Chairman
Carborundum Co., Buffalo Ave., Niagara Falls, N. Y.
J. H. Westbrook, Vice-Chairman
E. M. Sherwood, Vice-Chairman
L. H. Juel, Sec.-Treas.

Industrial Electrolytic
(Spring 1958-1959)
J. C. Cole, Chairman
Diamond Alkali Co., Union Commerce Bldg., Cleveland 14, Ohio
W. D. Sherrow, Vice-Chairman
B. F. Bechtold, Sec.-Treas.

Theoretical Electrochemistry
(Spring 1959-1960)
C. W. Tobias, Chairman
Dept. of Chemistry & Chemical Engineering, University of California, Berkeley, Calif.
Ralph Roberts, Vice-Chairman
L. G. Longsworth, Sec.-Treas.

Personals

Ricardo O. Bach, formerly with the Central Research Labs. of the American Smelting & Refining Co. in South Plainfield, N. J., has become director of the Inorganic Products Division of the Research Dept. of the Lithium Corp. of America in Minneapolis, Minn.

Frank E. Swindells recently was appointed manager of research for photosensitive devices and chemical research for the Electronic Tube Division of Allen B. Du Mont Labs., Inc., Clifton, N. J. In his new post, Dr. Swindells will have responsibility for research and development of multiplier phototubes, image intensifiers and converters, image dissectors, and other electro-optical transducers. In addition, he will direct chemical research. He had managed chemical research for Du Mont prior to his new appointment with emphasis on transparent and black background screen phosphors.

Herbert Bandes, of Arthur D. Little, Inc., Cambridge, Mass., has been transferred to San Francisco as director of research in the company's Western Division laboratories. Dr. Bandes will help to develop closer relations with the West Coast's growing electronic industries. He has had considerable experience in the field of solid state chemistry, with emphasis on semiconductors. His most recent project was helping to plan a crystal-growing facility for Air Force-Cambridge Research Center. He was Chairman of the Electronics Division of the Society in 1957-1959, and this month he would have assumed the duties of Secretary of the Boston Section.

R. F. Rolsten has accepted a position as research chemist at the Anaheim Laboratories of the U. S. Borax Research Corp., Calif. Dr. Rolsten previously was employed at the Explosives Dept., Du Pont Experimental Station, Wilmington, Del.

N. R. Srinivasan has returned to India from the U.S.S.R. and resumed his duties at the Bhilai Steel Plant, Bhilai.

J. Vaid has joined Jay Engineering Works, Calcutta, as research and development engineer.

T. L. Rama Char has been nominated as a member of the Electroplating Sectional Committee of the Indian Standards Institution, New Delhi, on behalf of the Indian Institute of Science, Bangalore.

Ivar J. Moltke-Hansen

Ivar J. Moltke-Hansen of Brusseis, Belgium, long-time member of the Society, died on June 20, 1959, at the age of 84.

Mr. Moltke-Hansen, a Norwegian subject, studied electrochemistry in Berlin-Charlottenberg, Germany, and practiced for a few years in the United States of America. He settled permanently in Brussels in 1922. He never forgot his American friends although he had the opportunity to return to the United States only once in the last 50 years.

Mr. Moltke-Hansen joined The Electrochemical Society, for which he always had the deepest attachment, in January 1903 and was made an Emeritus Member in October 1940.

He leaves behind his wife, whom he married in 1907, three sons, a daughter, and two grandchildren.

Guy Hastings Fetterley

Guy Hastings Fetterley, Chippawa, Ont., Canada, died on July 5, 1959. He was 46 years old.

He was born in Toronto, Ont., the son of J. B. Fetterley and the late Mrs. J. B. Fetterley. He grew up in St. Catharines and attended high school in that city.

Mr. Fetterley graduated from the University of Toronto with a B.A.Sc. degree in chemical engineering in the year 1935 and joined the Research and Development Dept. of Norton Co. in Chippawa on May 20 of that year. He had resided in Chippawa since that time.

At Norton Co., Guy was active in a number of developments which have since become of considerable commercial importance. He devised a test procedure for electrical grade fused

magnesia (Magnorite) which has been in use for many years and is now known as the Fetterley test. He was also instrumental in standardizing boron carbide molding powder and designed a small plant for the production of this material.

During World War II, Guy was in active charge of a project for the Manhattan District Corps of Engineers which finally developed the Fetterley process for the manufacture of elemental boron.

Other projects in which Guy had been actively interested included silicon carbide heating elements (hot rods), silicon carbide grain for lightning arresters, and boron nitride.

Although his training was in chemical engineering, Guy's background and interest in electronics led him far into the field of engineering physics. More recently, he had been concerned with the theory of abrasives and, at the time of his death, he was pursuing investigations into such problems as impact and wear. He also was interested in the electronic applications of silicon carbide crystals.

He had been awarded several patents and had published numerous scientific papers. He was a Regional Editor of the JOURNAL and a contributing editor to the book "High-Temperature Technology."

In addition to The Electrochemical Society, which he joined in October 1942, he was an active member of the Chemical Institute of Canada and one

G. H. Fetterley

of the founders of the Niagara local section, the American Association for the Advancement of Science, the Association of Professional Engineers, the Society for Engineering Education, the Institute of Radio Engineers, the American Ceramic Society, and the local section of the Optical Society of America. His wide interests led to his serving on a number of standing committees and ranged all the way from weight lifting to spectroscopy and "ham" radio.

At the time of his death, Guy was a Section Head in the Research and Development Dept. in charge of the engineering physics and crystallographic groups.

Surviving are his wife, Mabel Louise McCalla, whom he married in 1936; one son, Norman Guy McCalla; and his father, J. B. Fetterley of St. Catharines, Ontario.

G. R. Finlay

Book Reviews

Physical Chemistry of High Polymers, by Maurice L. Huggins. Published by John Wiley & Sons, Inc., New York City, 1958. xiii + 175 pages; $6.50.

According to the author, this book is based on notes prepared for a series of lectures to university students on the physical chemistry of high polymers and the structure of molecules, especially proteins. It is therefore intended as an outline of the subject at an intermediate level. The author specifically disclaims for the book both objectivity and comprehensiveness, since he has emphasized both his own works and his own views. Nevertheless, it is a very good outline at the indicated level, containing much formulation of basic principles and many speculative suggestions.

The book cannot be used as a text, since many derivations are missing or sketchy. "It can be shown that..." occurs quite frequently, as indeed it would during the course of a lecture. Also, there is nothing much on experimentation, other than a two-page section in the chapter on structure of corpuscular proteins. No time is spent discussing actual synthesis or fabrication of ultimate products, and there is no discussion of the experimentation leading to the data cited in the text.

There is a brief introductory section on nomenclature and classification followed by a chapter on polymerization, stressing the kinetic approach. The next two chapters cover composition and configuration of chains, and are followed by three chapters on thermodynamics of polymer solutions. Brief discussions of viscosity, plastic flow, and elasticity are then followed by several well-illustrated chapters discussing the structure of various synthetic and natural polymers.

H. W. Salzberg

The Structure of Electrolytic Solutions. Edited by Walter J. Hamer. Published by John Wiley & Sons, Inc., New York, and Chapman & Hall, Ltd., London, 1959. xii + 441 pages; $18.50.

This volume, based on a symposium held by The Electrochemical Society in May 1957, contains 27 chapters written by 42 authors. The Editor and his staff have done an excellent job in obtaining uniformity in length and style of the chapters. Also, while the same topics are sometimes discussed in two or more chapters, there is no real repetition because of the different viewpoints. The book is well printed and bound, and there are very few errors, of proofreading at least. It is not a beginner's book, but presupposes a very good knowledge of the physical chemistry of solutions. The modern status of knowledge and research in this difficult field, and the available experimental methods of attack, are presented by experts in each domain. There are contributions from several countries, an exception being the U.S.S.R.

To quote from H. S. Frank and P. T. Thompson, Chapter 8: "There can be little doubt that the theory of Debye and Hückel gives a complete and correct account of activity coefficients and heats of dilution in ionic solutions which are sufficiently dilute. . . . After thirty years no one has yet succeeded in . . . modifying . . . the theory . . . to give an exact account . . . in real solutions without employing parameters which not only are empirical but also take on numerical values which are often markedly peculiar." Nevertheless, serious attempts have been made to develop a theory for more concentrated solutions, and they are reviewed and discussed here. G. Scatchard, E. Glueckauf, Frank, and Thompson discuss the electrical interactions and solvation effects, as well as the statistical contribution to the activity coefficient, the last three authors considering the Bjerrum cube root region theoretically important but in somewhat different fashion. Chemical interactions (ion pairs, incomplete dissociation, complexes, chelates) are discussed in other chapters.

The structure of water and ice, and the behavior of H and OH ions, are discussed by M. Eigen and L. DeMaeyer. Heats of dilution are reviewed by E. Lange. Topics of other chapters include the use of Raman spectra, utlraviolet spectrophotometry in the investigation of dissociation constants and complex ions,

June 1960 Discussion Section

A Discussion Section, covering papers published in the July—December 1959 JOURNALS, is scheduled for publication in the June 1960 issue. Any discussion which did not reach the Editor in time for inclusion in the December 1959 Discussion Section will be included in the June 1960 issue.

Those who plan to contribute remarks for this Discussion Section should submit their comments or questions in triplicate to the Managing Editor of the JOURNAL, 1860 Broadway, New York 23, N. Y., *not later than March 1, 1959*. All discussion will be forwarded to the author(s) for reply before being printed in the JOURNAL.

diffusion measurements including thermal diffusion (Soret effect), ionic vibration potentials, investigation of NH_3-H_2O mixtures by high field conductance, high-temperature isopiestic measurements, use of anion exchange in studying complexes. Possible new methods of study are mentioned, such as nuclear magnetic resonance, which was a very new tool in 1957. There is special consideration of incomplete dissociation in concentrated strong acids, the case of HSO_4^-, methanol-water solutions of acids, solutions of polyelectrolytes. The last two chapters deal with the theory of melting, and with the evidence for complexes in melts.

One is impressed by the resurgence of ideas which all but disappeared from the literature many years ago. The old textbooks listed ions like $MgCl^+$, $NaSO_4^-$; spectrophotometry and cryoscopy measured degrees of hydration (and on occasion there was not enough water in the solution); an unsuccessful cube-root law was developed by Ghosh, a temporarily successful one (for log f) by Bjerrum. Some of these things have come back, of course in a different context. Many years ago, it was stated that, if certain salts were not fully ionized, then the radicals in the molecule had the same absorption spectrum as the ions. In the present volume, C. W. Davies considers $NiSO_4$ to have a dissociation constant of only 0.004; J. F. Duncan and D. L. Kepert find no shift in absorption spectrum with change of Ni and SO_4 ratio or concentration.

C. V. King

News Items

Journal of ECS Microfilmed

The Electrochemical Society announces that an agreement has been entered into with University Microfilms, Inc., Ann Arbor, Mich., for the microfilming of all volumes of the TRANSACTIONS and JOURNAL of the Society.

This consists of 15 reels and covers Vol. 1-104 (1902-1957), and positive microfilm copies of all these volumes sell for $375.00. When reels are sold separately for any of these volumes, the price is $25.00 each.

Subsequent volumes of the JOURNAL will be on separate reels. Vol. 105 (1958) is now available for $3.10.

One of the most pressing problems faced by libraries is that of providing adequate space for their publications. Microfilm editions are one solution to this problem.

Inquiries concerning purchase should be addressed to University Microfilms, Inc., 313 N. First St., Ann Arbor, Mich.

New ECS Sustaining Member

Tung-Sol Electric Inc., Newark, N. J., recently became a Sustaining Member of The Electrochemical Society.

A. K. Graham Awarded Highest Scientific Honor of AES

The American Electroplaters' Society, Inc., at its Golden Jubilee Convention and Industrial Finishing Exposition, including the Fifth International Conference on Electrodeposition and Metal Finishing, held in Detroit, Mich., June 15-19, 1959, named Dr. A. Kenneth Graham of Jenkintown, Pa., president of Graham, Savage & Associates of that city, as the second winner of the AES Scientific Achievement Award, the society's highest scientific honor. Dr. Abner Brenner of the National Bureau of Standards was Chairman of the Selection Committee.

Also in attendance at the meeting was Dr. William Blum who, as the first winner of the Award, delivered the first "William Blum Lecture" at the Opening Session of the Fifth International Conference on Electrodeposition and Metal Finishing in the Statler-Hilton Grand Ballroom.

Dr. Graham, like Dr. Blum, earned selection by his "decade-plus" accomplishments in advancing the theory and practice of electroplating, metal finishing, and allied arts; in raising the quality of its processes and products; and in enhancing the dignity and status of the profession. He was nominated for the Award by the Philadelphia Branch, AES's second oldest chartered Branch that in 1960 will be celebrating its own Golden Anniversary.

Dr. Graham will deliver the second "William Blum Lecture" at the AES's Annual Convention to be held in Los Angeles in 1960. He will receive a scroll, a $500.00 honorarium, and other attendant honors.

Providing Liquid Refrigerants to Research Workers

The National Bureau of Standards, Washington, D. C., has found that liquefied gases can be commercially procured and then transported over long distances at a cost comparable to the expense involved in conducting a liquefaction operation. Such an approach to procurement places liquefied gases within the reach of all research groups, even those previously hindered from undertaking low-temperature projects because they lacked immediate access to liquefaction facilities. The Bureau itself uses this method to supply liquid refrigerants to research workers in its Free Radicals Research Program. Procurement, along with storage, handling, transfer, and delivery, is conducted by a specially trained staff to free scientists for essential research. Such centralized handling has also proved economical, accelerating research and greatly reducing gas losses.

Announcements from Publishers

"Investigation of Methods of Producing Single Crystals of Non-Metallic Ferromagnetic Substances, Final Report," J. Koenig, Clevite Research Center, for Air

Force Cambridge Research Center, Aug. 1957. Report P131631,* 25 pages; $1.50.

"A Theoretical Study of the Electronic Structure of Transition-Metal Complexes," Aug. 1956. AEC Report ISC-830,* 118 pages; $2.75.

"Transport Numbers and Ion Mobilities in the Fused Salt KCl-$PbCl_2$," Dec. 1957. AEC Report ISC-944,* 79 pages; $2.25.

"Hydrofluoric Acid Decladding of Zirconium-Clad Power Reactor Fuel Elements," 1958. AEC Report ORNL-2460,* 17 pages; 75 cents.

"Determination of Oxygen in Lithium Metal," 1958. AEC Report ORNL-2570,* 10 pages; 50 cents.

"Plating of Beryllium-Copper Components for Electrical Applications (Gold and Silver)," Nov. 1957. AEC Report LA-2229,* 55 pages; $1.50.

"Hydriding of Zirconium and Uranium in Organic Coolants," Nov. 1958. AEC Report HW-58146,* 19 pages; 75 cents.

"Dissolution of Sintered Thorium-Uranium Oxide Fuel in Nitric Acid-Fluoride Solutions," no date. AEC Report ORNL-2519,* 22 pages; 75 cents.

"Ion-Exchange Separation of Metals by a Single-Pass Method," June 1958. AEC Report ISC-1056,* 41 pages; $1.25.

"The Recovery of Uranium and Plutonium from Stainless Steel Sulfate Decladding Solutions by Ion Exchange," no date. AEC Report ORNL-2592,* 29 pages; $1.00.

"The Recovery of Uranium from Sulfate Solutions by Solvent Extraction with Tributyl Phosphate," no date. AEC Report ORNL-2615,* 15 pages; 50 cents.

"Summary of Progress in Unclassified Areas of Reactor Technology," Oct. 1958. AEC Report CEND-0005-RS-41,* 14 pages; 75 cents.

* Order from Office of Technical Services, U. S. Dept. of Commerce, Washington 25, D. C.

"Relation of Wettability by Aqueous Solutions to the Surface Constitution of Low-Energy Solids," M. K. Bernett and W. A. Zisman, Naval Research Lab., Oct. 1958. Report PB 151048,* 12 pages; 50 cents.

"Simple Electrometer Employing an Electrified, Nonconducting Fiber," D. A. McCaig and B. Vonnegut, Arthur D. Little, Inc., for the Office of Naval Research, Feb. 1957. Report PB 131731,* 23 pages; 75 cents.

"The Zinc-Silver Oxide Cell Low Temperature Operation without Auxiliary Heating," L. A. Denison, W. J. Pauli, and G. R. Snyder, Diamond Ordnance Fuze Labs., Ordnance Corps, U. S. Army, Dec. 1957. Report PB 131787,* 34 pages; 75 cents.

"Problems of Corrosion and the Protection of Metals"

Listed below is the translated Table of Contents of the book entitled "Problems of Corrosion and the Protection of Metals" ("Problemy Korrozii i Zaschity Metallov"). The 270-page book, available only in Russian, can be purchased for $2.00 from the Four Continent Book Corp., 822 Broadway, New York 3, N. Y. It is the transaction of the Fifth All-Union Conference on the Corrosion and Protection of Metals held at the Institute of Physical Chemistry, Academy of Sciences, U.S.S.R., in Moscow, June 23-25, 1954. It was published by the Academy of Sciences U.S.S.R. Press, Moscow, 1956.

Contents

Introduction ... 3
I. L. Rozenfeld. Georgii Vladimirovich Akimov—Founder of the Study of Structural Corrosion of Metals ... 5
N. D. Tomashov. The Theory of Metallic Corrosion and Methods of Developing Corrosion Resistant Alloys ... 17
V. P. Batrakov. Electrode Processes during Metallic Corrosion in Oxidizing Media ... 46
N. D. Tomashov and G. P. Chernova. The Increase of the Resistance of the Passive State of Stainless Steels ... 68
L. I. Antropov. The Effect of Additives on Metallic Corrosion in Acidic Media ... 79
A. Ya. Shatlov. The Effect of pH on the Corrosion Stability of the Stationary Potentials of Metals ... 86
Z. A. Iofa and L. D. Shebaeva. An Investigation of the Corrosion of Iron —Pairs of Halogen Acids by Means of Tagged Atoms ... 96
L. K. Lenin. The Role of Colloidal-Chemical Effects during Metallic Corrosion in Salt Solutions ... 107
V. F. Negreev. The Corrosion of Steel by the Sea ... 115
A. S. Afanac'ev and E. N. Chankova. The Oxidized Surface of Steel as a Cathode ... 126
N. N. Balashova and N. D. Tomashov. Beryllium Hydroxide—A Corrosion Inhibitor for Iron ... 136
A. I. Glukhova and G. V. Akimov. The Effect of Temperature on the Corrosion of Stainless Steels in Hydrochloric Acid and Nitric Acid and in Mixtures of the Two ... 142
V. V. Andreeva and A. I. Glukhova. The Effect of the Surface Treatment of Stainless Steel on Its Chemical Stability ... 150
A. F. Lunev. On the Theory of Protective Device and Cathodic Protection of Underground Installations from Corrosion ... 160
I. N. Frantsevich, V. S. Chernovol, I. S. Gerenrot, N. A. Pilipenko, and L. N. Yagupol'skaya. The Complex Electroprotection of the Dashava-Kiev Gas Pipeline from Corrosion ... 173
N. D. Tomashov and Iu. N. Mikhailovskii. On the Kinetics of Electrode Processes during Metallic Corrosion in Soil ... 190
G. V. Akimov, G. B. Clark, and N. I. Isaev. An Investigation of the Behavior of Protective Films on Aluminum in Various Solutions by Means of Resistance and Capacity Measurements ... 209
P. V. Shchigolev. The Corrosion and Electrochemical Stability of Anodized Aluminum ... 227
E. N. Paleolog, G. V. Akimov, N. D. Tomashov, and K. S. Korotkova. The Effect of Protective Films on the Corrosion and Electrochemical Behavior of Magnesium ... 237
M. A. Timonova. The Protection of Magnesium Alloys by Inorganic Films 255
Decisions of the Conference ... 268

"Gas-Recoil Fast Neutron Spectrometer," R. E. Benenson, Wright Air Development Center, U. S. Air Force, June 1958. Report PB 151187,* 36 pages; $1.00.

"Silver Oxide-Zinc Alkaline Storage Batteries: Effect of Float and Normal Charges on Capacity and Related Characteristics," C. P. Wales, U. S. Naval Research Lab., Aug. 1958. Report PB 131925,* 36 pages; $1.00.

"Final Report on Solid Electrolyte Battery Systems," D. M. Smith, Sprague Electric Co., for the Signal Corps, U. S. Army, no date. Report PB 131796,* 280 pages; $4.00.

"The Preparation of Transistor Grade Silicon from Silane or Analogous Compounds," H. C. Kelly, T. J. Flynn, C. W. Davis, and S. Johnson, Metal Hydrides Inc., for Air Research and Development Command, U. S. Air Force, Aug. 1957. Report PB 131875,* 72 pages; $2.00.

* Order from Office of Technical Services, U. S. Dept. of Commerce, Washington 25, D. C.

"A Cadmium Sulfide Solar Generator," D. A. Hammond, F. A. Shirland, and R. J. Baughman, Harshaw Chemical Co., for Wright Air Development Center, U. S. Air Force, Dec. 1957. Report PB 151276,* 135 pages; $2.75.

"Investigation of Various Metal Protective Coatings on the Gum Formation and Oxidation Stability of Gasoline," V. O. Hatch, Aberdeen Proving Ground, U. S. Army Ordnance Corps, June 1957. Report PB 131738,* 35 pages; $1.00.

"Selection and Evaluation of Rare and Unusual Metals for Application to Advanced Weapons Systems," B. Love, Research Chemicals, Inc., for Wright Air Development Center, U. S. Air Force, June 1958. Report PB 151311,* 85 pages; $3.00.

"Organic Polymers Containing Aluminum and Titanium," R. L. Frank, A. A. Baldoni, and T. R. Patterson, Jr., Morton Chemical Co., for Air Force Office of Scientific Research, Jan. 1958. Report PB 131753,* 12 pages; 50 cents.

"Reference Index of the Current Protective Coatings Specifications," Ordnance Tank-Automotive Command, Detroit Arsenal, U. S. Army, no date. Report PB 151166,* 159 pages; $3.00.

"Methods of Determining Surface Roughness," M. K. Testerman, University of Arkansas for Wright Air Development Center, U. S. Air Force, June 1958. Report PB 151268,* 48 pages; $1.25.

"Chemical Resistance and Thermal Stability of Fluorocarbon Elastomer," A. Wilson, C. B. Griffis, and J. C. Montermoso, U. S. Army, Dec. 1957. Report PB 131942,* 23 pages; 75 cents.

"Interactions between Four Volatile Corrosion Inhibitors," R. L. LeMar, Rock Island Arsenal, U. S. Army, Dec. 1957. Report PB 151010,* 42 pages; $1.25.

"Rocket Exhaust Corrosion Simulator," F. B. Cramer, Rocketdyne, North American Aviation, Inc., for Wright Air Development Center, U. S. Air Force, Aug. 1957. Report PB 151273,* 138 pages; $2.75.

Since 1861
AMES has been making these
SILVER SALTS
to YOUR specifications

Silver Nitrate
Silver Cyanide
Silver Chloride
Silver Sulfate
Monovalent Silver Oxide
Divalent Silver Oxide

And now for your Battery
Silver Flour
and
for powder metallurgy
Nodular Silver

M. AMES CHEMICAL WORKS, INC.
17-19 Rogers Street
Glen Falls, New York
Phone 2-4394

ELECTRO-CHEMIST–RESEARCH

Outstanding research opportunity in metal finishing for physical chemist with advanced degree. Good academic background in kinetics and thermodynamics as well as physical and electro-chemistry preferred for research in aluminum oxidation, electro-chemical processes, and anodizing, plating, and bonderizing metal. Direct replies indicating education, experience, and salary requirements to

General Employment Manager
REYNOLDS METALS COMPANY
Richmond, Virginia

Expanding the Frontiers of Space Technology in

ELECTRO-CHEMISTRY

■ Solid state activities in electrochemistry at Lockheed play a highly important role in overcoming challenging problems in test, materials research, metallurgy and other related fields.

Special emphasis is directed to the development of high-energy batteries and fuel cells, and related fuel research in electrode reaction kinetics and materials synthesis by electrochemical methods and vacuum deposition. In the solution of complex electrochemical problems, Lockheed's scientists and engineers develop products that will serve both government and commercial use.

ENGINEERS AND SCIENTISTS

The advanced nature of Lockheed's projects in electrochemistry provides an excellent opportunity for high level scientists and engineers to advance their professional status and offer an ideal environment for working conditions. If you are experienced in electrochemistry or work related to the above areas, you are invited to share in the future of a company that has a history of continual progress and play an important individual role in the development of the nation's space technology. Write: Research and Development Staff, Dept. I-26, 962 W. El Camino Real, Sunnyvale, California. U.S. citizenship required.

Lockheed

MISSILES AND SPACE DIVISION

Systems Manager for the Navy POLARIS FBM; DISCOVERER, SENTRY and MIDAS; Army KINGFISHER, Air Force Q-5 and X-7

SUNNYVALE, PALO ALTO, VAN NUYS, SANTA CRUZ, SANTA MARIA, CALIFORNIA
CAPE CANAVERAL, FLORIDA
ALAMOGORDO, NEW MEXICO • HAWAII

"The Effects of Gamma Irradiation on Acrylonitrile-Butadiene Copolymers," J. A. Parker, F. F. Bentley, E. A. Peterson, and D. Hale, Wright Air Development Center, U. S. Air Force, Sept. 1958. Report PB 151261,* 110 pages; $2.50.

"The Evaluation and Adaptation of the Bromination Technique of Determining Oxygen in Metals," L. A. Keyser and C. D. Houston, Wright Air Development Center, U. S. Air Force, Aug. 1958. Report PB 151250,* 31 pages; $1.00.

"Electrical Generation of Oxygen: Literature Survey," R. D. Nelson, R. Tubbs, W. Sullivan, D. Buchanan, and A. B. Garrett, Ohio State University, for Wright Air Development Center, U. S. Air Force, Aug. 1958. Report PB 151-260,* 111 pages; $2.50.

"Contractile Properties of Polyelectrolytes," W. Budd and J. Mikula, Frankford Arsenal, U. S. Army Ordnance Corps, Oct. 1957. Report PB 131939,* 23 pages; 75 cents.

"Bibliography of Unclassified NRL Formal Reports Numbers 1000 to 5000," Volume PB 151428,* 131 pages; $2.75.

"Organic Silicon Compounds (Kremniyorganicheskiye Soedineniya)," K. A. Andrianov, State Scientific Technical Publishing House for Chemical Literature, Moscow, 1955; translated by the Technical Documents Liaison Office, U. S. Air Force. Volume 59-11239,* 920 pages; $10.00.

* Order from Office of Technical Services, U. S. Dept. of Commerce, Washington 25, D. C.

Employment Situations

Positions Available

Engineers (Aeronautical, Electrical, Electronic, Industrial, General, Mechanical, and Power Plant), **Electronic Scientists, Metallurgists, Physicists, Technologists**—Vacancies exist for professional personnel in the above positions. Starting salaries range from $4490 per annum to $10,130 per annum. The Naval Air Material Center is currently engaged in an extensive program of aeronautical research, development, experimentation, and test operations for the advancement of Naval aviation. Experimental work is also being conducted in the guided missile field. Personnel are needed for work on projects involving modification, overhauling, and testing of aeronautical equipment, materials, accessories, power plants, launching and arresting devices, and for modification and structural testing of aircraft. Also, for work involving the basic design of catapults, launchers, arresting gear and their component parts; test and development work at shore stations and on board U. S. Navy ships; evaluation of new equipment and establishment of performance parameters, and applied research on the many problems relevant to this field.

Interested persons should file an Application for Federal Employment, Standard Form 57, with the Industrial Relations Dept., Naval Air Material Center, Naval Base, Philadelphia 12, Pa. Applications may be obtained from the above address, or information as to where they are available may be obtained from any first or second class post office.

Advertiser's Index

American Brass Company 242C
M. Ames Chemical Works, Inc. 257C
Bell Telephone Laboratories, Inc. 239C
E. I. du Pont de Nemours & Company (Inc.) 241C
Enthone, Incorporated ..... Cover 4
Great Lakes Carbon Corp., Electrode Division ..... Cover 2
Keithley Instruments, Inc. 236C
Lockheed Missiles & Space Division 258C
Reynolds Metals Company 257C
Sylvania Electric Products Inc. 237C
Westinghouse Research Laboratories 258C

CHEMISTS — METALLURGISTS
BS — MS — PHD

To study dissolution of intermetallic compounds, reaction mechanisms and develop etches for investigation of crystal perfection and microstructure. Study special etching problems on semiconductor materials. Experience and training in surface chemistry desirable but not essential. Send resume to

M. F. McConkey
Industrial Relations — Dept. 819

WESTINGHOUSE RESEARCH LABORATORIES

Beulah Road, Churchill Borough
Pittsburgh 35, Pennsylvania

Monographs of The Electrochemical Society

ECS Series

The following are books developed and sponsored by The Electrochemical Society and published by John Wiley & Sons, Inc., 440 Fourth Ave. New York 16, N. Y. Members of The Electrochemical Society can receive a 33 1/3% discount by ordering volumes from Society Headquarters, 1860 Broadway, New York 23, N. Y. Book and invoice will be mailed by John Wiley & Sons. Nonmembers (including subscribers) should order direct from Wiley.

Corrosion Handbook. Edited by Herbert H. Uhlig. Published 1948, 1188 pages, **$16.00**

Modern Electroplating. Edited by Allen G. Gray. Published 1953, 563 pages, **$8.50**

Abstracts of the Literature on Semiconducting and Luminescent Materials and Their Applications. Compiled by Battelle Memorial Institute.

Vol. I, 1953 Issue—published 1955, 169 pages, **$5.00** (soft cover)

Vol. II, 1954 Issue—published 1955, 200 pages, **$5.00** (soft cover)

Vol. III, 1955 Issue—Edited by E. Paskell; published 1957, 322 pages, **$10.00** (hard cover)

Vol. IV, 1956 Issue—Edited by E. Paskell; published 1959, 456 pages, **$12.00** (hard cover)

Electrochemistry in Biology and Medicine. Edited by Theodore Shedlovsky. Published 1955, 369 pages, **$11.50**

Vapor Plating (The Formation of Metallic and Refractory Coatings by Vapor Deposition), by C. F. Powell, I. E. Campbell, and B. W. Gonser. Published 1955, 158 pages, **$5.50**

High-Temperature Technology (Materials, Methods, and Measurements). Edited by I. E. Campbell. Published 1956, 526 pages, **$15.00**

Stress Corrosion Cracking and Embrittlement. Edited by W. D. Robertson. Published 1956, 202 pages, **$7.50**

Arcs in Inert Atmospheres and Vacuum. Edited by W. E. Kuhn. Published 1956, 188 pages, **$7.50**
(Papers Presented at the Symposium on Arcs in Inert Atmospheres and Vacuum of the Electrothermics and Metallurgy Division of The Electrochemical Society, April 30 and May 1, 1956, San Francisco, Calif.)

Technology of Columbium (Niobium). Edited by B. W. Gonser and E. M. Sherwood. Published 1958, 120 pages, **$7.00**
(Papers Presented at the Symposium on Columbium—Niobium of the Electrothermics and Metallurgy Division of The Electrochemical Society, May 15 and 16, 1958, Washington, D. C.)

The Structure of Electrolytic Solutions. Edited by Walter J. Hamer. Published 1959, 441 pages, **$18.50**
(Based on a Symposium held in Washington, D. C., in May 1957, sponsored by The Electrochemical Society, New York, and The National Science Foundation, Washington, D. C.)

Vacuum Metallurgy

Vacuum Metallurgy, third printing, 1958. Edited by J. M. Blocher, Jr.; 216 pages; **$5.00,** less a 20% discount to ECS members only. Available from Electrochemical Society Headquarters, 1860 Broadway, New York 23, N. Y.

(Papers Presented at the Vacuum Metallurgy Symposium of the Electrothermics and Metallurgy Division of The Electrochemical Society held in Boston, Mass., October 6 and 7, 1954)

The Electrochemical Society

Patron Members

Aluminum Co. of Canada, Ltd.,
Montreal, Que., Canada
International Nickel Co., Inc.,
New York, N. Y.
Olin Mathieson Chemical Corp.,
Niagara Falls, N. Y.
Industrial Chemicals Div., Research
and Development Dept.
Union Carbide Corp.
Divisions:
Union Carbide Metals Co.,
New York, N. Y.
National Carbon Co., New York, N. Y.
Westinghouse Electric Corp., Pittsburgh, Pa.

Sustaining Members

Air Reduction Co., Inc.,
New York, N. Y.
Ajax Electro Metallurgical Corp.,
Philadelphia, Pa.
Allen-Bradley Co., Milwaukee, Wis.
Allied Chemical & Dye Corp.
General Chemical Div., Morristown, N. J.
Solvay Process Div., Syracuse, N. Y.
(3 memberships)
Allied Research Products, Inc.,
Detroit, Mich.
Alloy Steel Products Co., Inc., Linden, N. J.
Aluminum Co. of America,
New Kensington, Pa.
American Machine & Foundry Co.,
Raleigh, N. C.
American Metal Climax, Inc.,
New York, N. Y.
American Potash & Chemical Corp.,
Los Angeles, Calif. (2 memberships)
American Zinc Co. of Illinois,
East St. Louis, Ill.
American Zinc, Lead & Smelting Co.,
St. Louis, Mo.
American Zinc Oxide Co., Columbus, Ohio
M. Ames Chemical Works, Inc.,
Glens Falls, N. Y.
Auto City Plating Company Foundation,
Detroit, Mich.
Basic Inc., Maple Grove, Ohio
Bell Telephone Laboratories, Inc.,
New York, N. Y. (2 memberships)
Bethlehem Steel Co., Bethlehem, Pa.
(2 memberships)
Boeing Airplane Co., Seattle, Wash.
Burgess Battery Co., Freeport, Ill.
(4 memberships)
C & D Batteries, Inc., Conshohocken, Pa.
Canadian Industries Ltd., Montreal, Que.,
Canada
Carborundum Co., Niagara Falls, N. Y.
Catalyst Research Corp., Baltimore, Md.
Chrysler Corp., Detroit, Mich.
Ciba Pharmaceutical Products, Inc., Summit,
N. J.
Columbian Carbon Co., New York, N. Y.
Columbia-Southern Chemical Corp.,
Pittsburgh, Pa.
Consolidated Mining & Smelting Co. of
Canada, Ltd., Trail, B. C., Canada
(2 memberships)
Continental Can Co., Inc., Chicago, Ill.
Cooper Metallurgical Associates, Cleveland,
Ohio
Corning Glass Works, Corning, N. Y.
Crane Co., Chicago, Ill.
Diamond Alkali Co., Painesville, Ohio
(2 memberships)
Dow Chemical Co., Midland, Mich.
Wilbur B. Driver Co., Newark, N. J.
(2 memberships)
E. I. du Pont de Nemours & Co., Inc.,
Wilmington, Del.
Eagle-Picher Co., Chemical Div., Joplin, Mo.
Eastman Kodak Co., Rochester, N. Y.
Electric Auto-Lite Co., Toledo, Ohio
Electric Storage Battery Co.,
Philadelphia, Pa.
Englehard Industries, Inc., Newark, N. J.
(2 memberships)
The Eppley Laboratory, Inc., Newport, R. I.
(2 memberships)
Erie Resistor Corp., Erie, Pa.
Exmet Corp., Tuckahoe, N.Y.
Fairchild Semiconductor Corp., Palo Alto,
Calif.
Federal Telecommunication Laboratories,
Nutley, N. J.
Food Machinery & Chemical Corp.
Becco Chemical Div., Buffalo, N. Y.
Westvaco Chlor-Alkali Div., South
Charleston, W. Va.
Foote Mineral Co., Paoli, Pa.
Ford Motor Co., Dearborn, Mich.
General Electric Co., Schenectady, N. Y.
Chemistry & Chemical Engineering
Component, General Engineering
Laboratory
Chemistry Research Dept.
General Physics Research Dept.
Metallurgy & Ceramics Research Dept.

(Sustaining Members cont'd)

General Motors Corp.
Brown-Lipe-Chapin Div., Syracuse, N. Y. (2 memberships)
Guide Lamp Div., Anderson, Ind.
Research Laboratories Div., Detroit, Mich.
General Transistor Corp., Jamaica, N. Y.
Gillette Safety Razor Co., Boston, Mass.
Gould-National Batteries, Inc., Depew, N. Y.
Grace Electronic Chemicals, Inc., Baltimore, Md.
Great Lakes Carbon Corp., New York, N. Y.
Hanson-Van Winkle-Munning Co., Matawan, N. J. (3 memberships)
Harshaw Chemical Co., Cleveland, Ohio (2 memberships)
Hercules Powder Co., Wilmington, Del.
Hill Cross Co., Inc., New York, N. Y.
Hoffman Electronics Corp., Evanston, Ill.
Hooker Chemical Corp., Niagara Falls, N. Y. (3 memberships)
Houdaille Industries, Inc., Detroit, Mich.
Hughes Aircraft Co., Culver City, Calif.
International Business Machines Corp., Poughkeepsie, N. Y.
International Minerals & Chemical Corp., Chicago, Ill.
Jones & Laughlin Steel Corp., Pittsburgh, Pa.
K. W. Battery Co., Skokie, Ill.
Kaiser Aluminum & Chemical Corp.
Chemical Research Dept., Permanente, Calif.
Div. of Metallurgical Research, Spokane, Wash.
Kennecott Copper Corp., New York, N. Y.
Keokuk Electro-Metals Co., Keokuk, Iowa
Libbey-Owens-Ford Glass Co., Toledo, Ohio
P. R. Mallory & Co., Indianapolis, Ind.
McGean Chemical Co., Cleveland, Ohio
Merck & Co., Inc., Rahway, N. J.
Metal & Thermit Corp., Detroit, Mich.
Minnesota Mining & Manufacturing Co., St. Paul, Minn.
Monsanto Chemical Co., St. Louis, Mo.
Motorola, Inc., Chicago, Ill.
National Cash Register Co., Dayton, Ohio
National Lead Co., New York, N. Y.
National Research Corp., Cambridge, Mass.
National Steel Corp., Weirton, W. Va.
New York Air Brake Co., Vacuum Equipment Div., Camden, N. J.
Northern Electric Co., Montreal, Que., Canada
Norton Co., Worcester, Mass.
Olin Mathieson Chemical Corp., Niagara Falls, N. Y.
High Energy Fuels Organization (2 memberships)
Pennsalt Chemicals Corp., Philadelphia, Pa.
Phelps Dodge Refining Corp., Maspeth, N. Y.
Philco Corp., Philadelphia, Pa.
Philips Laboratories, Inc., Irvington-on-Hudson, N. Y.
Pittsburgh Metallurgical Co., Inc., Niagara Falls, N. Y.
Poor & Co., Promat Div., Waukegan, Ill.
Potash Co. of America, Carlsbad, N. Mex.
Radio Corp. of America, Harrison, N. J.
Ray-O-Vac Co., Madison, Wis.
Raytheon Manufacturing Co., Waltham, Mass.
Reynolds Metals Co., Richmond, Va. (2 memberships)
Rheem Semiconductor Corp., Mountain View, Calif.
Schering Corporation, Bloomfield, N. J.
Shawinigan Chemicals Ltd., Montreal, Que., Canada
Speer Carbon Co.
International Graphite & Electrode Div., St. Marys, Pa. (2 memberships)
Sprague Electric Co., North Adams, Mass.
Stackpole Carbon Co., St. Marys, Pa.
Stauffer Chemical Co., New York, N. Y.
Sumner Chemical Co., Div. of Miles Laboratories, Inc., Elkhart, Ind.
Sylvania Electric Products Inc., Bayside, N. Y. (2 memberships)
Tennessee Products & Chemical Corp., Nashville, Tenn.
Texas Instruments, Inc., Dallas, Texas
Metals & Controls Div., Attleboro, Mass.
Three Point Four Corp., Yonkers, N. Y.
Titanium Metals Corp. of America, Henderson, Nev.
Tung-Sol Electric Inc., Newark, N. J.
Udylite Corp., Detroit, Mich. (4 memberships)
Universal-Cyclops Steel Corp., Bridgeville, Pa.
Upjohn Co., Kalamazoo, Mich.
Victor Chemical Works, Chicago, Ill.
Western Electric Co., Inc., Chicago, Ill.
Wyandotte Chemicals Corp., Wyandotte, Mich.
Yardney Electric Corp., New York, N. Y.

Preserve that fresh metal surface... *for less than 1 1/2¢ per 100 sq. ft.*

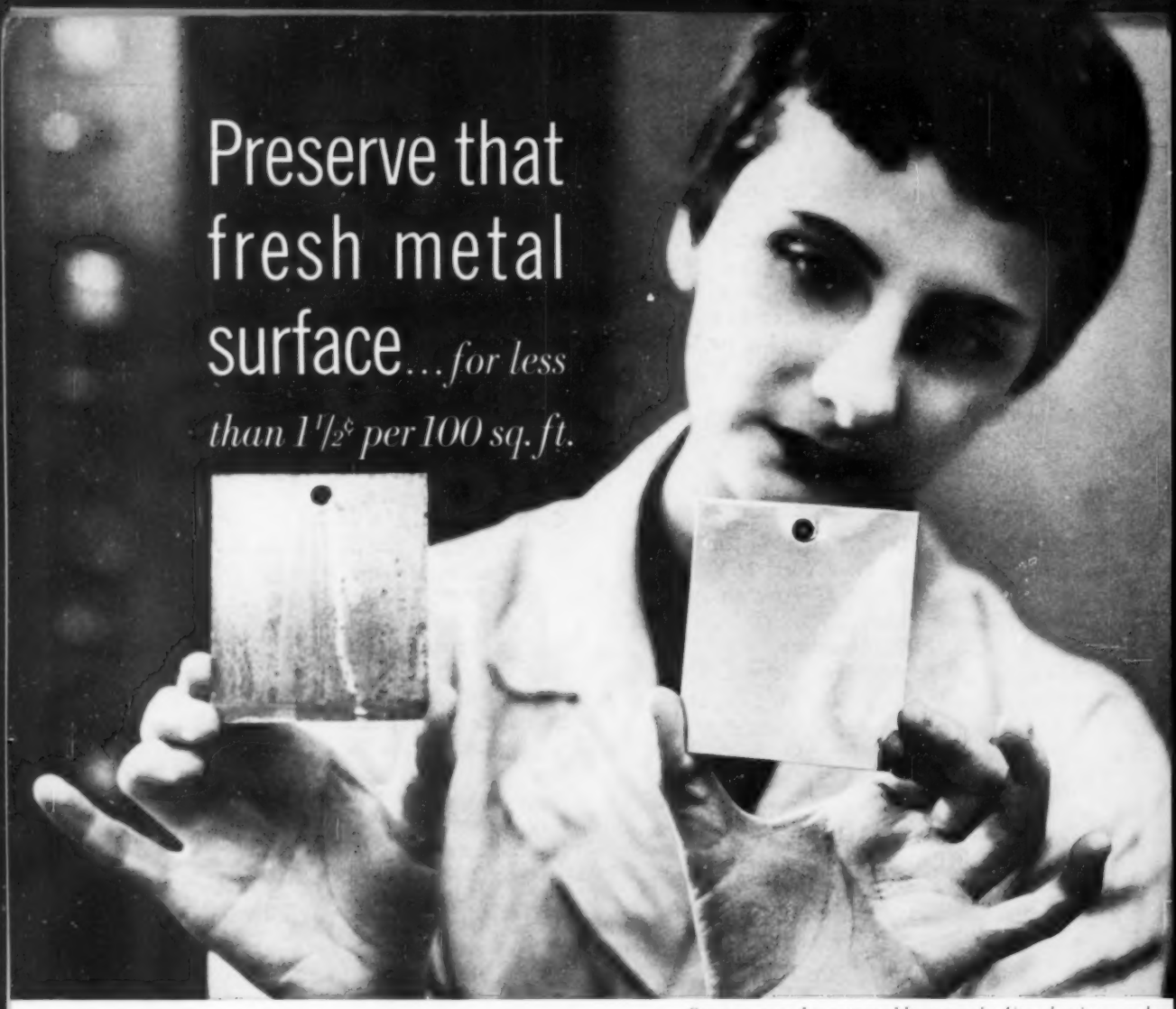

Compare treated vs untreated brass panels. After cleaning, panel on right was rinsed in Entek 45 rinse; panel on left, in standard hot water rinse. Then panels were exposed to 100% humidity at 100° F. for 100 hours. Note how Entek 45 preserves "that fresh metal surfac

From Enthonics research come Enthone Enteks, a new series of rinse water additives which coat metal surfaces with an "invisible shield" against the atmosphere. Entek 45 assures faster drying, eliminates water spots and provides lasting corrosion protection to all metals. Entek CU-55 prevents tarnishing and spotting out of copper and brass even under tropical humidity conditions.

By adding Entek 45 to your final hot water rinse, you can prevent white salt corrosion of zinc and aluminum, prevent yellowing of nickel plate, prevent tarnishing of copper and brass, prevent black spots on cadmium plate.

By treating copper and brass goods or copper or brass plated items with Entek CU-55 you can prevent tarnishing, green salt formation, spotting-out and pit corrosion under high humidity storage conditions.

Entek protection lasts for months, yet costs less than 1½¢ per 100 sq. ft. to treat your parts, less than ½¢ per gallon to make up an Entek 45 solution!

Entek 45 produces an invisible, water-repellent organic film on the metal surface which sheds water rapidly and promotes stain-free drying. This same film acts as an invisible barrier between the metal and the moisture and oxygen in the air.

Entek CU-55 reacts with copper and copper alloys to form an invisible layer which has many times the corrosion resistance of bare copper and brass. Additionally, this layer has better solderability and improves adhesion of lacquers and enamels.

Write today for complete literature on both of these products to Enthone, Inc., 442 Elm Street, New Haven, Connecticut.

ASARCO

ANOTHER PRODUCT OF *Enthonics* RESEARCH

ENTHONE

A Subsidiary of American Smelting and Refining Company